ALFRED-WEGENER-INSTITUT
HELMHOLTZ-ZENTRUM FÜR POLAR- UND MEERESFORSCHUNG

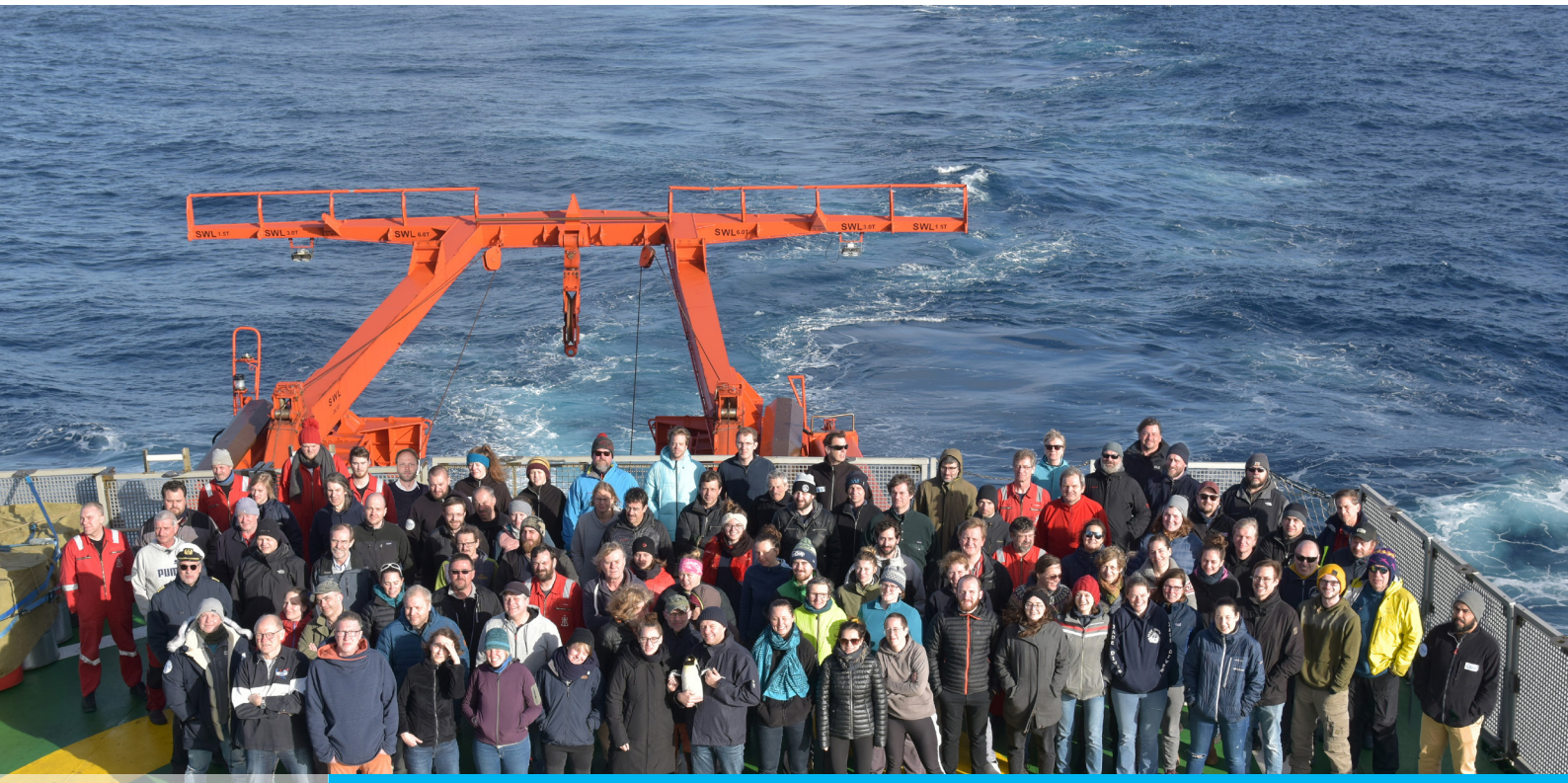

755
2021

Berichte
zur Polar- und Meeresforschung
Reports on Polar and Marine Research

The Expedition PS124 of the Research Vessel POLARSTERN to the southern Weddell Sea in 2021

Edited by
Hartmut H. Hellmer and Moritz Holtappels
with contributions of the participants

HELMHOLTZ

Die Berichte zur Polar- und Meeresforschung werden vom Alfred-Wegener-Institut, Helmholtz-Zentrum für Polar- und Meeresforschung (AWI) in Bremerhaven, Deutschland, in Fortsetzung der vormaligen Berichte zur Polarforschung herausgegeben. Sie erscheinen in unregelmäßiger Abfolge.

Die Berichte zur Polar- und Meeresforschung enthalten Darstellungen und Ergebnisse der vom AWI selbst oder mit seiner Unterstützung durchgeführten Forschungsarbeiten in den Polargebieten und in den Meeren.

Die Publikationen umfassen Expeditionsberichte der vom AWI betriebenen Schiffe, Flugzeuge und Stationen, Forschungsergebnisse (inkl. Dissertationen) des Instituts und des Archivs für deutsche Polarforschung, sowie Abstracts und Proceedings von nationalen und internationalen Tagungen und Workshops des AWI.

Die Beiträge geben nicht notwendigerweise die Auffassung des AWI wider.

Herausgeber
Dr. Horst Bornemann

Redaktionelle Bearbeitung und Layout
Susan Amir Sawadkuhi
Birgit Reimann

Alfred-Wegener-Institut
Helmholtz-Zentrum für Polar- und Meeresforschung
Am Handelshafen 12
27570 Bremerhaven
Germany

www.awi.de
www.awi.de/reports

Der Erstautor bzw. herausgebende Autor eines Bandes der Berichte zur Polar- und Meeresforschung versichert, dass er über alle Rechte am Werk verfügt und überträgt sämtliche Rechte auch im Namen seiner Koautoren an das AWI. Ein einfaches Nutzungsrecht verbleibt, wenn nicht anders angegeben, beim Autor (bei den Autoren). Das AWI beansprucht die Publikation der eingereichten Manuskripte über sein Repositorium ePIC (electronic Publication Information Center, s. Innenseite am Rückdeckel) mit optionalem print-on-demand.

The Reports on Polar and Marine Research are issued by the Alfred Wegener Institute, Helmholtz Centre for Polar and Marine Research (AWI) in Bremerhaven, Germany, succeeding the former Reports on Polar Research. They are published at irregular intervals.

The Reports on Polar and Marine Research contain presentations and results of research activities in polar regions and in the seas either carried out by the AWI or with its support.

Publications comprise expedition reports of the ships, aircrafts, and stations operated by the AWI, research results (incl. dissertations) of the Institute and the Archiv für deutsche Polarforschung, as well as abstracts and proceedings of national and international conferences and workshops of the AWI.

The papers contained in the Reports do not necessarily reflect the opinion of the AWI.

Editor
Dr. Horst Bornemann

Editorial editing and layout
Susan Amir Sawadkuhi
Birgit Reimann

Alfred-Wegener-Institut
Helmholtz-Zentrum für Polar- und Meeresforschung
Am Handelshafen 12
27570 Bremerhaven
Germany

www.awi.de
www.awi.de/en/reports

The first or editing author of an issue of Reports on Polar and Marine Research ensures that he possesses all rights of the opus, and transfers all rights to the AWI, including those associated with the co-authors. The non-exclusive right of use (einfaches Nutzungsrecht) remains with the author unless stated otherwise. The AWI reserves the right to publish the submitted articles in its repository ePIC (electronic Publication Information Center, see inside page of verso) with the option to "print-on-demand".

Titel: Expeditionsteilnehmer der PS124 (COSMUS) Expedition auf dem Helicopter-Deck der Polarstern (Foto: Ralph Timmermann, Alfred-Wegener-Institut, Helmholtz-Zentrum für Polar- und Meeresforschung)

Cover: Expedition participants of the PS124 (COSMUS) Expedition on the Helicopter Deck of Polarstern (Photo: Ralph Timmermann, Alfred Wegener Institute, Helmholtz Centre for Polar and Marine Research)

The Expedition PS124 of the Research Vessel POLARSTERN to the southern Weddell Sea in 2021

Edited by
Hartmut H. Hellmer and Moritz Holtappels
with contributions of the participants

Please cite or link this publication using the identifiers

https://hdl.handle.net/10013/epic.32df6a8a-6fae-46d5-a081-5fa10d0305a9
https://doi.org/10.48433/BzPM_0755_2021

ISSN 1866-3192

PS124

Continental Shelf Multidisciplinary Flux Study (COSMUS)

3 February 2021 – 30 March 2021
Stanley – Stanley

Chief scientist
Hartmut H. Hellmer

Coordinator
Ingo Schewe

Contents

1. ÜBERBLICK UND FAHRTVERLAUF

Hartmut H. Hellmer[1], Moritz Holtappels[1] DE.AWI

Der Fahrtabschnitt PS124 mit dem Titel ‚Continental Shelf Multidisciplinary Flux Study (COSMUS)' begann pandemiebedingt für die Teilnehmer der Wissenschaft und der Besatzungen von Schiff und Flugzeug am 16. Januar 2021 mit einer 14-tägigen Quarantäne in einem Bremerhavener Hotel. Nach einer Woche der völligen Isolation, einer weiteren mit hotelinterner Kontakterlaubnis zu allen Mitreisenden und nach drei negativen PCR-Tests, brachten fünf Busse alle Teilnehmer – ohne Ausnahme – am Nachmittag des 31. Januar 2021 zu einem eigens für diesen Abend geöffneten Terminal des Hamburger Airports. Von dort startete um 21:12 Uhr der längste Flug in der Geschichte der Lufthansa – ein Nonstopflug von Hamburg nach Mount Pleasant, dem britischen Militärflughafen auf den Falkland Islands (Abb. 1.1). Trotz starken Gegenwindes landeten wir dort nach 13.452 Kilometern und einer Flugzeit von 15 Stunden und 45 Minuten am 1. Februar 2021 um 9:15 Uhr Ortszeit. Beim Landeanflug war jedoch die Freude groß, unser Zuhause der kommenden 8 ½ Wochen, *Polarstern*, in der Bucht vor Stanley schon von oben sehen zu können.

Nach dem Ankerlichten vor Stanley (Falkland Islands) am Nachmittag des 3. Februars 2021 wurden zwischen 56° S und 57,5° S drei BSH-Floats ausgelegt. Danach steuerte *Polarstern* direkt den nördlichen Bereich des Filchner-Trogs (südöstliches Weddellmeer) an (Abb. 1.2), um nach einer Teststation im offenen Weddellmeer (70° 25‘ S, 30° W) am 10. Februar mit der Aufnahme einer Schallquellen-Verankerung die Untersuchungen im Rahmen des COSMUS Projektes zu beginnen. Dabei galt es, die in den Jahren 2013 bis 2014 (FOS, Filchner Outflow System, PS82), 2015 bis 2016 (FROSN, Filchner Outflow System Now, PS96) und 2018 (FROST, Filchner Outflow System Tomorrow, PS111) durchgeführten ozeanographischen Messungen fortzuführen und mit biologischen und bio-geochemischen Untersuchungen zum Kohlenstoffkreislauf zu verbinden. Durch eine strukturierte Stationsabfolge gelang es, den multidisziplinären Ansatz der Reise konsequent umzusetzen. Dabei wurde die Tageszeit (8 bis 18 Uhr) vornehmlich dafür genutzt, Verankerungs-, Driftfallen- und Lander-Operationen durchzuführen, während in den Abend- und Nachtstunden CTD-Profile gefahren, Wasser- und Sedimentproben genommen, das OFOBS (Ocean Floor Observation and Bathymetry System) auf vordefinierten Strecken geschleppt und der Meeresboden vermessen wurde. Der eingespielte Stationsablauf konnte jedoch nicht verhindern, dass einige Tage an wissenschaftlicher Zeit durch eine ungewöhnlich stabile Tiefdruckrinne verloren gingen, die immer wieder für die Arbeit behindernde Stürme und Schneetreiben sorgte. Eine gewollte Abweichung von der geplanten Expeditionsroute stellte die Umrundung des am 26. Februar 2021 vom Brunt-Schelfeis gekalbten Eisbergs A74 dar. In der neu gebildeten Passage wurde der bis zu dem Zeitpunkt bewährte Stationsablauf an drei Stationen fortgesetzt. Beendet wurden die Arbeiten im Bereich des Filchner-Trogs am 16. März 2021 mit der Auslegung einer Schallquellen-Verankerung in der Nähe des Stancomb-Wills-Gletschers.

Durch eine erneute Verschlechterung der Wetterverhältnisse an der *Neumayer-Station III* musste ein Großteil der wissenschaftlichen Arbeiten frühzeitig beendet werden. Durch die Aufnahme von Fracht an der Station mussten die Container der COSMUS Reise rechtzeitig gepackt, geschlossen und gestaut sowie die Labore aufgeräumt werden. Am Nachmittag des 17. März erreichte *Polarstern* den Nordanleger der Station, nachdem ein 1 km breiter

Gürtel kompakten Meereises durchbrochen worden war. Das frühe Anlegen erlaubte den Arbeitsgruppen Meereisphysik und Physikalische Ozeanographie auf dem Festeis der Atkabucht noch Arbeiten durchzuführen während sich die übrigen Teilnehmer zum ersten Mal auf der Reise an ‚Land' die Füße vertreten konnten. Die Ladearbeiten begannen am 18. März in der Frühe und endeten durch heranrückendes Meereis bedingt frühzeitig am Abend des 19. März. Die dadurch ‚gewonnenen' Tage wurden genutzt, um eine weitere ozeanographische Verankerung aufzunehmen und eine erste Verankerung für biogeochemische Messungen im zentralen Weddellmeer (69° S, 27° W) auszulegen. Nach Umrundung der South Orkney Inseln, einer ruhigen Überquerung der Drake Passage und der Auslegung von zwei weiteren BSH-Floats zwischen 57,4° S und 55° S, erreichte *Polarstern* Stanley am 30. März 2021 um 9 Uhr (Abb. 1.2).

Wissenschaftlicher Hintergrund

Der Kontinentalschelf des südlichen Weddellmeeres (WS) ist einer der größten des antarktischen Kontinents. Er ist teilweise bedeckt durch das ausgedehnte Filchner-Ronne-Schelfeis und ist ein Hotspot für die Meereisproduktion im Winter, wobei ca. 5 Sverdrup an Tiefen- und Bodenwasser vom Schelf in die Tiefe exportiert werden. Im Sommer vergrößern sich die Polynjas entlang der Schelfeiskante zu großen zusammenhängenden Freiwasserflächen, die eine hohe saisonale Primärproduktion aufweisen. Letztere versorgt ein Ökosystem, welches durch eine artenreiche benthische Fauna mit erhöhter Biomasse besonders im Osten gekennzeichnet ist. Hier scheinen auch die Abundanzen von Meeressäugern vergleichsweise höher zu sein als zur Ronne-Seite des WS hin. In dieser Schelf-Region fallen Meereisproduktion und Tiefen/Bodenwasserbildung räumlich mit einer erhöhten saisonalen Primärproduktion zusammen. Es wird vermutet, dass die biologische CO_2-Fixierung in den oberen lichtdurchfluteten Wasserschichten, das Absinken von partikulärem organischem Kohlenstoff zum Meeresboden und der Export von Schelfwasser in die Tiefsee eine effektive bio-physikalische Kohlenstoffpumpe bilden, die erheblich zur Abscheidung von CO_2 beitragen könnte. Die Bildung des dichten Schelfwassers verhindert gleichzeitig das Vordringen warmer Wassermassen auf den Schelf und damit ein beschleunigtes Schmelzen an der Basis des Filchner-Ronne-Schelfeises. Sowohl das Schelfeis als auch die flachen Meeressedimente sind potentielle Quellen von Spurenmetallen wie Eisen, deren Konzentrationen im Südozean maßgeblich die Algenblüte regulieren und deren Zufuhr erhöhte Primärproduktionsraten auf dem Schelf erst ermöglichen. Da klimatische Veränderungen für diese Region erwartet werden, ist es notwendig, das Ineinandergreifen dieser physikalischen, geochemischen und biologischen Prozesse zu analysieren sowie deren Bedeutung für globale Phänomene einzuschätzen (Meeresspiegelanstieg, CO_2 Aufnahme).

Als interdisziplinäres Team führten wir deshalb eine umfassende Untersuchung durch, die sich auf die Wärme- und Massentransporte, die gekoppelte Nährstoffdynamik und die biologischen Produktionsbedingungen konzentrierte. Ziel war es, (i) die Möglichkeit einer zukünftigen Erwärmung der Schelfwassermassen und eines erhöhten basalen Schmelzens des Schelfeises zu bewerten, (ii) den Umsatz der biologischen Kohlenstoffpumpe zu quantifizieren und deren Regulierung zu verstehen, und (iii) den Beitrag des antarktischen Kontinentalschelfs für die globalen Kohlenstoff- und Nährstoffbudgets zu bestimmen.

Diese Zielsetzungen waren ein wesentlicher, integrativer Bestandteil der Arbeiten an Bord und erforderten einen holistischen Untersuchungsansatz, der alle Disziplinen an Bord umfasste (Abb 1.3). Neben umfangreichen ozeanographischen und meereisphysikalischen Kenntnissen des Massen- und Wärmetransports (Kapitel 2 – 6) waren Untersuchungen zur Nährstoffverfügbarkeit, insbesondere von Spurenmetallen sowie deren Kontrolle der Primärproduktionsraten und Artenzusammensetzung erforderlich (Kapitel 8 und 9). Untersuchungen zur Aggregatbildung und Sedimentation organischer Partikel (Kapitel 7)

sowie zu den dadurch getriebenen benthischen Umsatzraten und der Zusammensetzung benthischer Gemeinschaften (Kapitel 10 und 11) waren ebenso Bestandteil wie die Erhebungen zur Abundanz von Meeressäugern, insbesondere Weddellrobben, die als Toppredatoren produktive Gebiete des Ökosystems anzeigen (Kapitel 4). Die Untersuchung direkter anthropogener Einflüsse wie die Abundanz von Mikroplastik (Kapitel 12) stellte eine weitere verbindende Komponente dar.

Das Ökosystem und die bio-physikalische Kohlenstoffpumpe im Untersuchungsgebiet sind maßgeblich von zukünftigen Veränderungen der Schelfwassermassen abhängig. Die Untersuchungen einer möglichen Erwärmung der Schelfwassermassen und eines erhöhten basalen Schmelzens des Schelfeises schließen an umfangreiche vorangegangene Studien an, die kontinuierlich unser Wissen über die Bildung und Zirkulation von Wassermassen auf dem Kontinentalschelf erweitert haben. Es hat sich gezeigt, dass im nördlichen Bereich des Filchner-Trogs sehr kaltes Eisschelfwasser (ISW, Ice Shelf Water) aus der Filchner-Ronne-Schelfeis Kaverne auf warmes modifiziertes Tiefenwasser (MWDW, Modified Warm Deep Water) aus dem Weddellwirbel trifft. Durch Vermischung am Kontinentalhang werden sowohl Tiefen- (WSDW, Weddell Sea Deep Water) als auch Bodenwasser (WSBW, Weddell Sea Bottom Water) gebildet (Abb. 1.4). Beide Wassermassen speisen den unteren Zweig der globalen Ozeanzirkulation und sorgen somit für die Belüftung der tiefen Schichten der Weltmeere. Eigene Verankerungsdaten aus den Jahren 2014 – 2018 vom östlichen Hang des Filchner-Trogs (76° S) haben gezeigt, dass im Jahr 2017 ein deutlich wärmerer Einstrom des MWDW über die gesamte Winterperiode andauerte. Norwegische Verankerungsdaten aus dem gleichen Zeitraum zeigen zusätzlich, dass dieses Signal bis 77° S vorgedrungen war. Modellszenarien mit dem Finite Elemente Modell FESOM projektieren klimabedingte Veränderungen der Dichtestruktur an der Schwelle des Filchner-Troges, was zu einem erhöhten Einstrom von MWDW ab Mitte dieses Jahrhunderts führen könnte. Diese Veränderungen würden in ihrem Verlauf die Zirkulation unter dem gesamten Filchner-Ronne-Schelfeis beeinflussen. Sollten sich im Bereich des Filchner-Trogs vergleichbare Dichteänderungen aus den Messungen des letzten Jahrzehnts zeigen, so ließen sich die von den Modellen errechneten Ergebnisse besser in die Klimavorhersage einordnen, und die Wahrscheinlichkeit erhöhter basaler Schmelzraten des Schelfeises als auch ansteigender Einträge von Süßwasser würde sich erhöhen. Letztere haben einen großen Einfluss auf die Struktur der kontinentalen Wassersäule, die Meereisbildung und die gesamte Biologie des oberen Ozeans.

Das Vorkommen dieses relativ warmen Wassers im Zusammenhang mit ablandigen Winden könnte eine Ursache für die immer wiederkehrende Küstenpolynja östlich des Filchner-Trogs sein, in deren Bereich Satellitendaten im Südsommer eine erhöhte Primärproduktion zeigen (Abb. 1.3). Sollte, wie oben vermutet, dieses Gebiet eine Kohlenstoffsenke darstellen und der Kohlenstoff durch Tiefenkonvektion in das nordwärts strömende ISW gelangen, so würde er durch die Tiefen- und Bodenwasserbildung am Kontinentalhang (Abb. 1.4) in den Tiefen des Weltozeans für Jahrhunderte gespeichert werden.

Daher umfasste unser Untersuchungsgebiet auch die kontinentale Schelfkante und den Schelfhang westlich der Schwelle des Filchner-Trogs, um eine erneute Bestandsaufnahme zur Ausbreitung des ISW und der damit verbundenen Bildung von Tiefen- und Bodenwasser und dem weiteren Verlauf der Schelfkantenfront (Antarctic Slope Front) durchzuführen. Das Absinken des ISW in große Tiefen wird in den kommenden Jahren durch zwei Verankerungen an ehemaligen norwegischen Positionen aufgezeichnet werden.

Unsere Arbeit an Bord umfasste folgende Ziele:

- Charakterisierung der antarktischen Schelfkantenfront und Bestimmung des Wassermassenaustauschs über die Kontinentalschelfkante des südlichen Weddellmeeres.

- Charakterisierung der Wassermassen auf dem südlichen WS-Kontinentalschelf und Bestimmung von Schmelzwassergehalt, TCO_2 und Nährstoffkonzentrationen.
- Bewertung der zeitlichen und räumlichen Variabilität der physikalischen Parameter, die zur Bildung der Wassermassen beitragen.
- Spezifizierung der klein- und großräumigen Topographie des Kontinentalschelfs und -hangs.
- Spezifizierung der räumlichen und zeitlichen Skalen der Meereisbildung, -drift und dicke im südlichen WS zur Unterstützung langfristiger Schätzungen des Eisexports und zur Validierung von Modellen und Satellitenprodukten.
- Bestimmung des Flusses von Makro- und Mikronährstoffen aus den Sedimenten des Schelfs in die Wassersäule und ihres Potenzials zur Düngung der HNLC-Gewässer.
- Bestimmung der Primärproduktion und ihrer Kontrolle durch Licht, Durchmischungstiefe, Nährstoffe und TCO_2.
- Bestimmung der Nährstoff- und TCO_2-Verarmung als Reaktion auf die Primärproduktion und den Atmosphären-Ozean-Austausch (Eisbedeckung).
- Bestimmung der Sedimentation von organischem Kohlenstoff und dessen Kontrolle durch Primärproduktion, Artenzusammensetzung, Aggregation und Zooplankton.
- Bestimmung benthischer Mineralisierungsraten durch Messung benthischer Sauerstoffaufnahme.
- Bestimmung der Abundanz, Biomasse und Diversität der benthischen Fauna auf dem Schelf und an der Schelfkante in Abhängigkeit von der Verfügbarkeit von organischem Kohlenstoff, dem Substrat des Meeresbodens und dem bodennahen Strömungsregime.

Eine genauere Beschreibung der Abläufe sowie vorläufige Ergebnisse aus den einzelnen Arbeitsbereichen erfolgen in den Kapiteln 2 bis 12. Diese werden erweitert um das Kapitel 13, das sich mit drei Projekten befasst, die sich spontan durch besondere Beobachtungen vor Ort ergaben und in weitere interdisziplinäre Zusammenarbeiten mündeten.

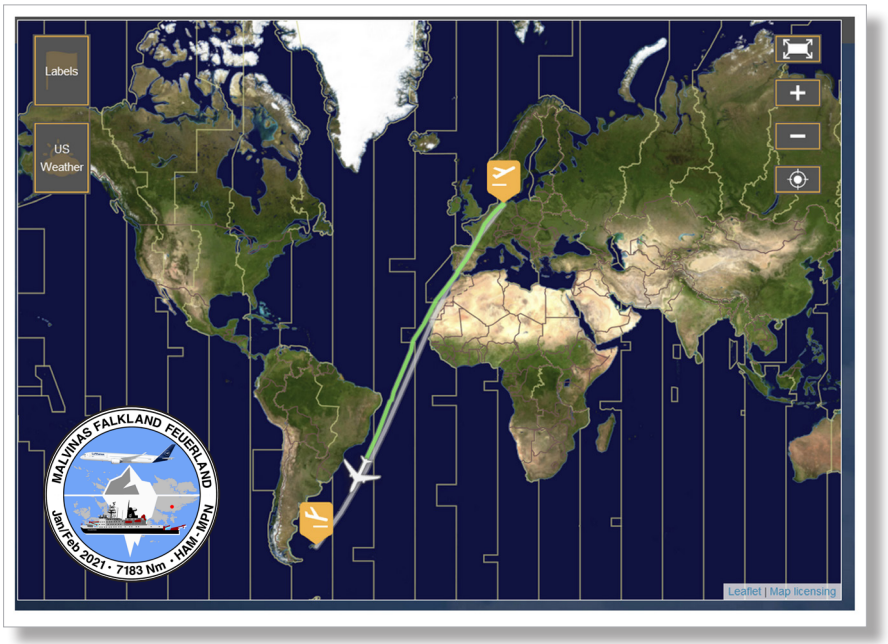

Abb.1.1: Flugstrecke von LH2574 von Hamburg (31.01.2021) nach Mount Pleasant (01.02.2021)
Fig.1.1: Flight track of LH2574 from Hamburg (31-01-2021) to Mount Pleasant (01-02-2021)

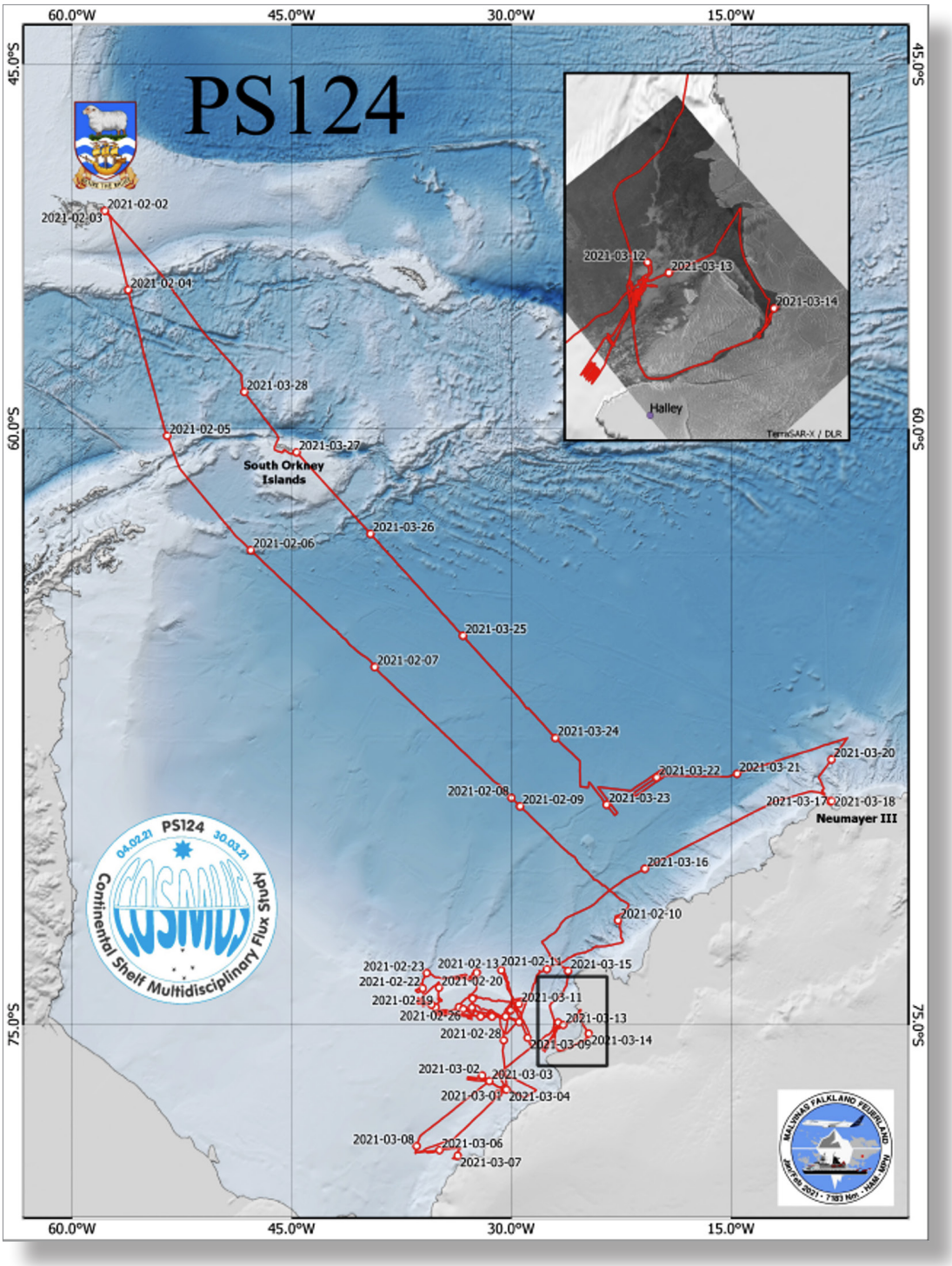

Abb.1.2: Route der Expedition PS124 von Stanley (03.02.2021) nach Stanley (30.03.2021) mit Stopps im südöstlichen Weddellmeer und an der Neumayer-Station III; siehe https://doi.pangaea. de/10.1594/PANGAEA.933473 für eine Darstellung des master tracks in Verbindung mit der Stationsliste der Expedition PS124 (Abb: I Nasis)

Fig.1.2: Route of expedition PS124 from Stanley (03-02-2021) to Stanley (30-03-2021) via the southeastern Weddell Sea and the Neumayer III Station; see https://doi.pangaea.de/10.1594/ PANGAEA.933473 to display the master track in conjunction with the station list for expedition PS124 (Courtesy: I Nasis)

SUMMARY AND ITINERARY

Due to the COVID-19 pandemic the expedition PS124 named ‘Continental Shelf Multi-disciplinary Flux Study (COSMUS)’ started for the scientific party as well as crews of ship and aircraft on 16 January 2021 with a 14-days quarantine at a hotel in Bremerhaven. After one week of total isolation, followed by another one with just allowing contact to the PS124-participants inside the hotel and three negative PCR-tests, five busses carried all members – without exception – to Hamburg Airport, where a terminal was opened only for PS124 in the afternoon of 31 January 2021. From here, the longest long-distant flight in Lufthansa history took off at 21:12 h local time with destination Mount Pleasant, the UK military base on Falkland Islands (Fig.1.1). Despite strong head winds, we had a soft touch-down at 9:15 h local time after 13,342 kilometres and 15 hours and 45 minutes in the air. During the flight approach, we were happy to see our ‘home’ for the next 8.5 weeks, *Polarstern*, already waiting in the bay of Stanley.

Having raised the anchor in the bay of Stanley in the afternoon of 3 February 2021, three floats of the Federal Office for Maritime Traffic and Hydrology (BSH) were deployed between 56° S and 57.5° S. Afterwards, *Polarstern*, steamed directly to the northern Filchner Trough region (southeastern Weddell Sea; Fig. 1.2). After a test station in the open Weddell Sea (70° 25‘ S, 30° W), the field work proposed in the framework of the COSMUS project started with the recovery of a sound-source mooring on 10 February. The work was a continuation of the oceanographic studies carried out in austral summers 2013 – 2014 (FOS, Filchner Outflow System, PS82), 2015 – 2016 (FROSN, Filchner Outflow System Now, PS96), and 2018 (FROST, Filchner Outflow System Tomorrow, PS111), extended to include also biological, and bio-geochemical studies. Due to a well-structured station schedule, we were able to implement the multi-disciplinary approach of the COSMUS cruise. We used daytime (8 am to 6 pm) mainly for mooring, drifting trap, and Lander operations while night time was reserved for CTD (Conductivity-Temperature-Depth) profiling, water and sediment sampling, towing the Ocean Floor Observation and Bathymetry System (OFOBS) on pre-defined tracks, and bathymetry surveys. Despite a rigorous schedule, we lost days at sea due to the unusual existence of a quasi-permanent low-pressure trough to the north, which continuously delivered storms and snow showers to the area. A deviation from the original plan was the circumnavigation of the new iceberg calved from the Brunt Ice Shelf on 26 February 2021. The established station schedule continued at three stations covering the passage from north to south. Work in the Filchner Trough area ended on 16 March 2021 with the deployment of a sound-source mooring near the Stancomb-Wills-Glacier.

As the onboard meteorologist predicted another storm system at the *Neumayer Station III*, we stopped major parts of our scientific programme in good time. For the loading of additional cargo from *Neumayer Station III* our containers had to be packed, closed and stowed, and the laboratories cleaned. After breaking through a 1 km wide compact sea ice belt, *Polarstern* reached the northern ‘pier’ of the station in the afternoon of 17 March so that the sea ice physics and physical oceanography teams were able to study the fast ice of Atka Bay. The rest of the cruise participants welcomed first steps on the Antarctic ‘main land’. The loading of cargo started in the early morning of 18 March and ended in the late afternoon of 19 March, due to the advance of a compact sea ice field. We used the time gained by the early departure

for the recovery of a nearby mooring, despite increasing winds and higher wave crests, and for moving to a new position for the deployment of a biogeochemistry mooring in the central Weddell Sea (69° S, 27° W). After the circumnavigation of the South Orkney Islands, a calm crossing of Drake Passage, and the deployment of two more BSH floats between 57.4° S und 55° S, *Polarstern* arrived at Stanley on 30 March 2021 at 9 am (Fig. 1.2).

Scientific Background

The continental shelf of the southern Weddell Sea (WS) is one of the largest of the Antarctic continent. It is partially covered by the extensive Filchner-Ronne Ice Shelf and is a hotspot for sea ice production in winter, with about 5 Sverdrup of deep and bottom water exported from the shelf to the deep sea. In summer, polynyas along the ice shelf edge increase in size to form large contiguous areas of open water with high seasonal primary production. The latter supports an ecosystem characterized by a rich benthic fauna with increased biomass especially in the east. Here, the Filchner Trough area supports a relatively higher abundance of marine mammals compared to the Ronne side of the Weddell Sea. In this region, sea ice production and deep/bottom water formation coincide spatially with a high seasonal primary production. Biological CO_2 fixation in the upper water column, sinking of particulate organic carbon to the seafloor, and export of shelf water to the deep sea are assumed to form an effective bio-physical carbon pump that could contribute significantly to CO_2 sequestration. At the same time, the formation of cold, dense water hinders the penetration of warm water masses onto the continental shelf, thus prevents accelerated melting at the base of the Filchner-Ronne Ice Shelf. The ice shelf itself and the shallow marine sediments are potential sources of trace metals such as iron, which regulate algae blooms in the Southern Ocean and would enable a high primary production on the continental shelf. Since climate changes are also expected for this region, it is necessary to analyse the interdependence of these physical, geochemical, and biological processes and to assess their significance for global phenomena such as sea-level rise and CO_2 sequestration.

As an interdisciplinary team, we therefore planned a comprehensive investigation focused on the ocean heat and mass transport, the coupled nutrient dynamics, and the conditions for biological production in this region. The aim was to (i) assess the potential for future warming of the shelf waters and related ice shelf basal melting, (ii) quantify the turnover of the biological carbon pump and understand its regulation, and (iii) determine the Antarctic continental shelf's contribution to global carbon and nutrient budgets.

These objectives were an essential, integrative part of the work on board and required a holistic investigation approach involving all disciplines on board (Fig 1.3). In addition to the extensive oceanographic and sea ice physics knowledge of mass and heat transport (Chapters 2 – 6), investigations on the availability of nutrient, especially trace metals, and their control on primary production rates and species composition were required (Chapters 8 and 9). Studies of aggregate formation and sedimentation of organic particles (Chapter 7) as well as of the benthic turnover rates and composition of benthic communities driven by these processes (Chapters 10 and 11) were included, as were surveys on the abundance of marine mammals, especially Weddell seals, which are top predators indicating productive areas of the ecosystem (Chapter 4). The study of direct anthropogenic impact such as microplastic abundance (Chapter 12) provided another unifying component.

The ecosystem and the bio-physical carbon pump in the study area are significantly dependent on future changes in the related water masses. The investigation of a possible warming of the shelf water masses and the subsequent basal melting of the Filchner-Ronne Ice Shelf is based on extensive previous studies that are continuously expanding our understanding of the formation and circulation of water masses on the continental shelf. It was found that the northern part of the Filchner Trough is the location where super-cooled Ice Shelf Water

(ISW) from underneath the Filchner-Ronne Ice Shelf encounters modified Warm Deep Water (MWDW) originating from the rim of the Weddell Gyre. The mixing of both water masses at the continental shelf break forms Weddell Sea Deep Water (WSDW) and Weddell Sea Bottom Water (WSBW) (Fig. 1.4). Both waters contribute to the lower limb of the global thermohaline circulation and, thus, ventilate the bottom layers of the World Ocean. AWI mooring records from 2014 – 2018 from the eastern slope of the Filchner Trough at 76° S reveal an exceptionally warm and prolonged flow of MWDW toward the Filchner Ice Shelf in 2017. Norwegian mooring data from the same period documents this event as far south as 77° S. Model projections with the Finite Element Model FESOM show that the density structure at the sill of the Filchner Trough might change such that, starting in the second half of this century, 'unmodified' WDW might enter the trough continuously with severe consequences for the whole circulation beneath Filchner-Ronne Ice Shelf. If our observations near the sill show similar density changes, our model results should be suitable to increase credibility in terms of (1) climate change projections for this remote region, (2) enhanced basal melt rates, and (3) increased fresh water fluxes. Fresh water fluxes substantially impact water column stability, sea ice formation, and upper ocean biology on the continental shelf and beyond.

The appearance of relatively warm water combined with offshore winds could favour a recurrent coastal polynya east of the Filchner Trough, where satellite data generally show high primary productivity during austral summer (Fig. 1.3). If this area is a carbon sink, as hypothesised above, and deep convection entrains the carbon into the northward-flowing ISW, the formation of deep and bottom waters at the continental slope (Fig. 1.4) would export the carbon to be stored in the deep global ocean for centuries.

Thus, our research area also covered the continental shelf break and the slope west of the Filchner Trough sill. The region is awaiting a new inventory of the spreading of ISW and related deep and bottom water formation, and the westward continuation of the Antarctic Slope Front. The sinking of the ISW to greater depths will be monitored again at two previous Norwegian mooring sites.

In summary, our work on board included the following objectives:

- Characterize the Antarctic Slope Front and determine the water mass exchange across the continental shelf break of the southern WS.
- Characterize the water masses on the southern WS continental shelf and determine glacial melt water content, TCO_2 and nutrient concentrations.
- Assess the temporal and spatial variability of the physical parameters contributing to the formation of the water masses.
- Specify the small and large-scale bathymetric setting of the continental shelf and slope.
- Specify the spatial and temporal scales of sea ice formation, drift, and thickness in the southern WS to support long-term estimates of ice export and validation of models and satellite products.
- Determine the flux of macro- and micronutrients from shelf and slope sediments into the water column and their potential to fertilise HNLC waters.
- Determine the primary production and its control by light, mixing depth, nutrients and TCO_2.
- Determine nutrient and TCO_2 depletion in response to primary production and air-sea exchange (ice-cover).

- Determine the downward flux of organic carbon and its controls by primary production, species composition, aggregation and zooplankton grazing.
- Determine benthic mineralisation and turnover by measuring benthic oxygen uptake.
- Determine the abundance, biomass and diversity of benthic fauna on the shelf and the shelf break in relation to organic carbon availability, seafloor substrate, and near-bottom currents

A more detailed description of work and preliminary results of the different groups will follow in Chapters 1 – 12. They are complemented by the additional Chapter 13, which covers three projects, all initiated spontaneously from unforeseen observations in the field and resulted in further interdisciplinary collaborations.

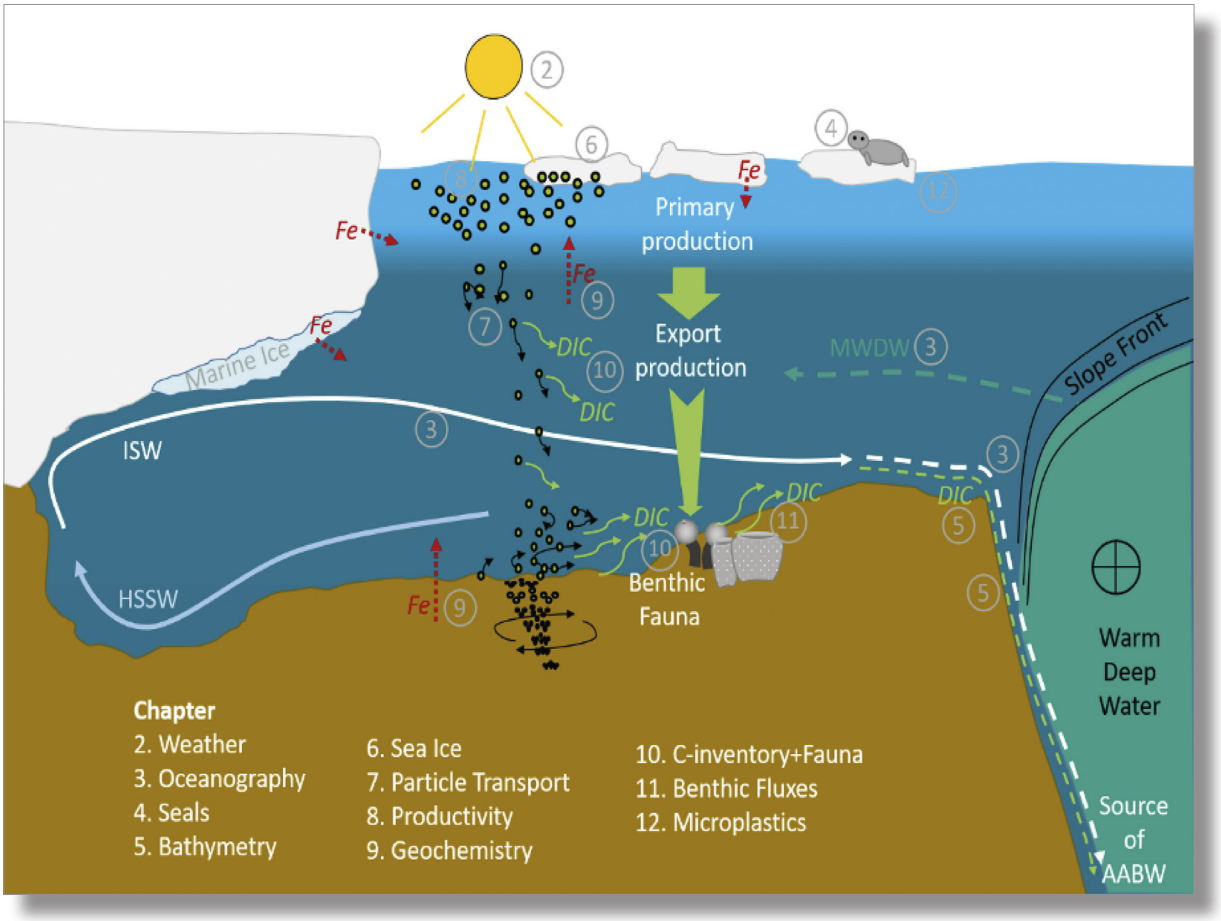

Abb. 1.3: Schematische Darstellung des Untersuchungsgebietes bestehend aus Kontinentalschelf, Filchner-Ronne-Schelfeis, charakteristischen Wassermassen und deren Zirkulation, überlagert mit den wesentlichen Prozessen und Transportwegen des Kohlenstoffkreislaufes und der Nährstoffverteilung; die Arbeiten der verschiedenen Disziplinen an Bord sind über die Kapitelnummern verortet.

Fig. 1.3: Schematic representation of the study area consisting of continental shelf, Filchner-Ronne Ice Shelf, characteristic water masses and their circulation, overlaid with the main processes and transport pathways of the carbon cycle and nutrient distribution; the work of the various disciplines on board is represented by chapter numbers.

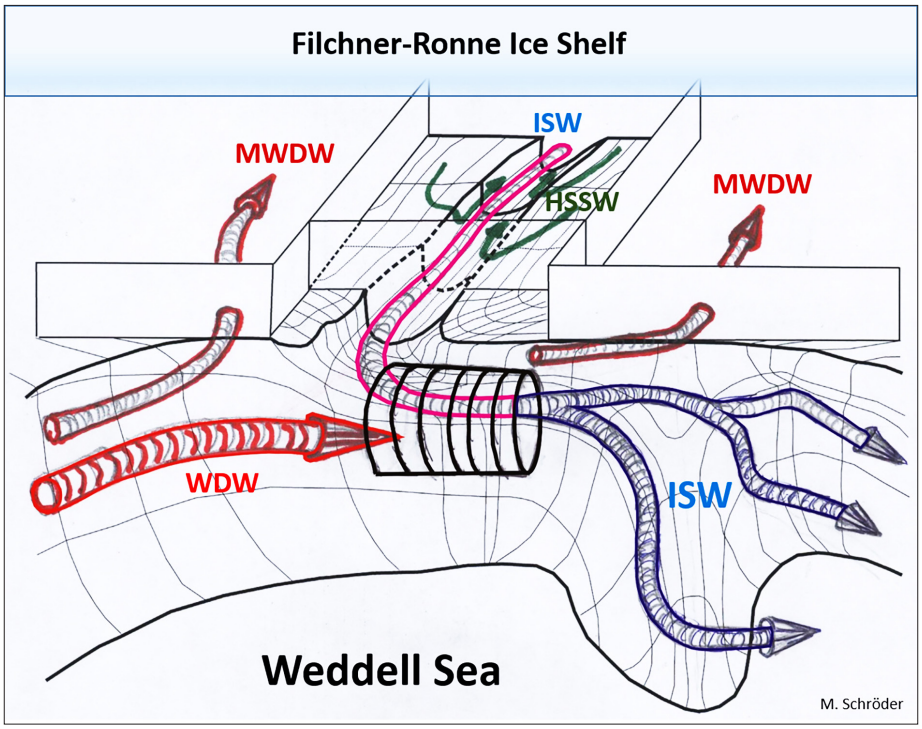

Abb. 1.4: Schematische Darstellung der charakteristischen Wassermassen des südlichen Weddellmeers und ihrer Ausbreitung und Vermischung im Bereich des Filchner-Trogs und Kontinentalhanges, Filchner-Ronne-Schelfeis im Hintergrund, das Weddellmeer im Vordergrund; WDW – Warm Deep Water, MWDW – Modified Warm Deep Water, ISW – Ice Shelf Water, HSSW – High Salinity Shelf Water

Fig. 1.4: Schematic presentation of the characteristic water masses in the southern Weddell Sea together with spreading pathways and mixing in the northern Filchner Trough and at the continental slope, Filchner-Ronne Ice Shelf in the back and Weddell Sea in the front; WDW - Warm Deep Water, MWDW – Modified Warm Deep Water, ISW – Ice Shelf Water, HSSW – High Salinity Shelf Water

2. WEATHER CONDITIONS DURING PS124

Steffen Schröter[1], Christian Rohleder[1], [1]DE.DWD
Frank Otte[2]

Weather and cruise history during COSMUS Expedition PS124

The main purpose of cruise PS124 was to explore the sea areas in the eastern and southeastern Weddell Sea, the nature of the seafloor there, the exploration of the underwater fauna, as well as the tagging of Weddell seals. In addition, the overwinterers and the summer team were picked up from *Neumayer Station III* in the second half of March.

The cruise started on 03 February 2021 from Stanley. *Polarstern* crossed the Drake Passage, she then continued towards the research area, where the ship arrived on 10 February 2021. A number of 58 flight operations with a total of 108 flights were carried out by Heliservice. This included over 90 flight hours with a block time of 106 hours. Altogether there were 287 landings on ice floes, the ice shelf or on *Polarstern*. The flying weather was temporarily challenging due to persistent low pressure phases. However, the pilots handled the repeatedly predicted and thus expected bad weather events very routinely. A total of 71 flight weather reports were prepared, which gave the pilot team the best possible meteorological preparation for the flight.

In addition, 114 standard weather forecast reports were prepared for ship command and science.

The research took place between 73 and 78 degrees south latitude. Furthermore, an iceberg (A 74) the size of London broke off at the Brunt Ice Shelf in late February. *Polarstern* was in close proximity and the opportunity was taken to take samples between the iceberg and the ice shelf. This was done between 12 and 14 March 2021. Subsequently, the ship headed for Atka Bay at *Neumayer Station III*, which was reached on 17 March 2021.

The ice shelf edge was then left again on 19 March 2021. From there, a westerly course was set back to the northern Weddell Sea. Here, a last station with research work took place on 24 March 2021. Afterwards *Polarstern* went on a direct way back to Stanley.

Stanley – Weddell Sea

On 02 February 2021 refueling work took place in the bay off Stanley in a phase of weaker winds of 5-6 Bft from the west. On 03 Febuary 2021 *Polarstern* left the Blanco Bay off Stanley one day earlier than planned to avoid the bad weather due to expected stormy winds and the associated strong swell in Drake Passage. In the process, we found ourselves between the subtropical high-pressure zone extending from the Pacific to the southern Atlantic and a more extensive low over the Weddell Sea in supply of quite humid air from westerly directions. Winds of 7-8 Bft were predominant.

In Drake Passage, winds intensified to 8-9 Bft and significant wave heights reached 4-5 m. On 04 February 2021 the weather situation changed very little for the time being. The wind weakened temporarily to 5 Bft to increase again to 7 Bft in the afternoon. The significant wave height decreased to 3 m. On 05 February 2021 a small high-pressure area approached from the west and finally reached the cruising area in the northwestern Weddell Sea. The wind

speed decreased to 3-4 Bft with a wave height of 1.5 m. This weather condition continued until 09 February 2021. When *Polarstern* arrived at the research area, a station with test operation of the scientific instruments was inserted at about 73° 30'S 032° 30'W.

Research area in the southeastern Weddell Sea

On 10 February 2021 a low pressure system was slowly approaching from the west. The southwest wind increased to 5 Bft. A slight lability could be observed in layers close to the ground, which is why light snow showers occurred repeatedly. The research work and the helicopter operations were nearly not affected.

On 11 February 2021 the low moved eastward over the research area of *Polarstern*. The wind shifted from north to east freshening slightly. Quite humid air was brought in so that temporarily deep stratus clouds occurred in connection with light snowfall. Gradually a certain routine was established in the flight operations. First, the ice team was usually taken to floes in the vicinity of the ship, followed by the seal team either to the same floe or to another more suitable one. The following day a weak intermediate high with 4 Bft easterly winds followed the low. In the afternoon a more powerful storm with its occlusion front approached from the northwest so that in the evening 8-9 Bft from the northeast occurred with the onset of snowfall.

On 13 February 2021 the ship steamed directly into the core of the low, so that variable winds around 3 Bft prevailed. In addition, a certain amount of drizzle could be observed in the precipitation, which led to the assumption of strong icing.

On 14 February 2021 we were on the southeastern flank of the weakening storm low with easterly to northeasterly winds of 5-6 Bft. Snow continued to fall intermittently on this day, partly still mixed with drizzle. Flight operations were cancelled due to the weather forecast.

The low moved slowly eastward on 15 February 2021, so that the wind shifted to the southeast while weakening. The next day, with variable winds of 1-2 Bft, a new intermediate high pressure followed from the west. The sun set for 2-3 hours at this time but it did not get really dark during the whole night.

On 17 February 2021 a small low pressure system moved to the east north of *Polarstern* directly replacing the intermediate high. Due to the low, light snowfalls occurred repeatedly in the research area, about 74° 00'S 035° 00'W, in the eastern Weddell Sea. The next two days a rather indifferent weather situation followed. Smaller disturbances embedded in the basic current led to repeated spells of bad weather.

On 20 February 2021 the ship came under the influence of a powerful low pressure system approaching from the northwest. The easterly wind picked up and reached 7-8 Bft. Combined with snowfall there were intermittent snow drifts and poor visibility. No flight movements were possible on this day.

On 21 February 2021 the wind weakened to 5-6 Bft but snow still fell in some areas. In the precipitation on this day a certain amount of freezing drizzle was also visible and flight plans were hindered as a result.

On 22 February 2021 a more extensive low-pressure complex was located in the north. Again and again smaller ground troughs passed determining the weather this day with snow showers and increasing southeasterly winds to 7 Bft. The bad weather areas, however, were limited to quite a small area.

On 23 February 2021 a trough of low pressure formed from the complex in the north to the southeastern Weddell Sea. With weak circulating winds, snow repeatedly fell with poor visibility. This trough of low pressure remained in the research area until 26 February 2021.

On 27 February 2021 a small intermediate high pressure system reached the area from the west but quite humid air continued to be brought in from the southeast. The wind force was 4 Bft. Smaller disturbances destabilized the air mass again and again causing shower-like snowfall. This situation continued on the following day.

On 01 March 2021 a low pressure system moved in from the northwest. The wind picked up to 6 Bft during the day blowing from northeast to east. From this low a new trough of low pressure formed extending into the southeastern Weddell Sea again.

With easterly winds between 4 and 6 Bft, snowfall and snow showers occurred temporarily until 05 March 2021 on the way to the southernmost point of the cruise which was located at about 77° 20'S 036° 00'W.

On 06 March 2021 a strong depression formed north of *Polarstern*. Southeasterly winds reached 3-4 Bft increasing to 8-9 Bft in the course of the day with a northeasterly turn and snow began to fall again. The low moved southwestward past the research area so that on 07 March 2021 a northeast wind continued to blow at 7-8 Bft. Occasional snowfall occurred. The following day a storm low slowly developed over the Bransfield Strait which subsequently moved to the southeast and with its frontal system determined the weather in the eastern Weddell Sea from the afternoon on. The wind decreased to 5-6 Bft for the time being. Due to the expected gale force winds near the coastline, the ship's command decided to weather further to the northwest at about 74° 30'S 030° 00'W where the wind reached about 7-8 Bft on 09 March 2021. Snow fell temporarily during this period.

On 10 March 2021 the unsettled weather continued and in the afternoon the wind shifted to north to northwest weakening to 5-6 Bft.

On 11 March 2021 the former storm low was located southwest of the research area and slowly dissipated. At the same time a low-pressure complex formed again in the northwest and approached slowly. With winds around 5 Bft the air mass was stratified quite unstably, resulting in repeated snow showers. Due to the weather forecast, it was decided to weather a bit further to the west on this day. In the evening, a northeast turn of the wind was recorded.

On 12 March 2021 the ground pressure gradient intensified, so that the northeast to east wind increased to 8-9 Bft. Snow began to fall and blowing snow occurred over icy surfaces. The next day, when the course approached the iceberg A74, a low pressure trough formed from the low pressure complex in the north, which extended into the southeastern Weddell Sea. Briefly, the wind shifted to the north and decreased to 4 Bft. In the afternoon it increased to 6-7 Bft and turned to the east again. At the ice shelf edge 8 Bft occurred. This resulted in heavy blowing snow, which significantly hindered a flight operation.

This weather condition persisted until 15 March 2021, but the wind gradually decreased to about 4 Bft in the gap between the iceberg and the ice shelf edge. In the afternoon of the 15th, the wind shifted to south to southwest.

On 16 March 2021 this weather continued on its way to Atka Bay.

On 17 March 2021 a high-pressure bridge formed extending from the South Atlantic to Antarctica. Relatively cold and moist air close to the ground was brought in from the southeast with quite weak winds of 2-3 Bft. Particularly in the morning hours sea smoke formed above open water which then spread over the ice like fog.

On 18 March 2021, *Polarstern* finally arrived at the northern jetty to *Neumayer Station III* under high pressure. A low-pressure area slowly approached from the northwest causing the ground pressure gradient to intensify again and the easterly wind to increase to 5 Bft.

On 19 March 2021 the Atka Bay was left and the sailing area was between a high pressure area in the south and a low pressure area in the northwest. Snow fell temporarily with an easterly wind of 4-5 Bft.

The low developed into an extensive complex by 20 March 2021 and winds increased to 7-8 Bft. In addition, snow continued to fall occasionally. The original plan of a mooring deployment at 66° 00'S 000° 00'W was revised and the scientific party selected an alternate position in the Weddell Sea. The sea state increased from 2-3 m to 3-4 m as the operation progressed.

On 21 March 2021 a slight inter-high influence prevailed. With a sea state of still 2-3 m, the wind blew with 5-6 Bft from east to southeast.

On the further way to the west, *Polarstern* came under the influence of a stormy low pressure system on 22 March 2021, which slowly passed the ship to the east. Easterly winds gradually increased to 8-9 Bft and significant seas increased to 4-5 m.

On 23 March 2021 the storm low was located in the northeast and an area of high pressure followed from the west. Winds decreased to 6 Bft with decreasing wave heights to 2-3 m in the evening. Next day the wind shifted to the south and the mooring was deployed at the alternate position of 69° 00'S 027° 00'W.

Weddell Sea – Stanley

On 25 March 2021 the voyage was continued to the northwest and we slowly entered a high pressure area. The wind continued to blow from the south with 5-6 Bft.

On 26 March 2021, *Polarstern* stayed in the high center where variable winds prevailed for the time being. During the course of the day the wind settled to the northeast.

The high slowly moved eastward and the waters around the South Orkney Islands on the western flank of this high were reached on 27 March 2021. The wind was blowing in the lee of the islands with 3-4 Bft from the north. In addition, a swell of 2-3 m was recorded. The islands were passed to the west and due to guard rail effects the wind temporarily increased to 6-7 Bft.

In the Drake Passage, a small, strong low approached from the west on 28 March 2021. This low was passed through and the wind temporarily decreased to 2-3 Bft. In the process, the direction of the wind changed from northeast to southwest. The air mass was very humid so that it was temporarily misty or even foggy. In addition, widespread rain or drizzle fell. The swell on this day was 2-3 m.

Finally, on 29 March 2021, we were on the southwestern flank of the depression and the wind increased to 7-8 Bft. In addition, the significant wave height increased to 5 m in the morning, but decreased to 2-3 m during the day. Northwest of the Falkland Islands was an area of high pressure which was slowly approached.

In the evening of the 29 March, 3-4 Bft were still reached. The high pressure slowly moved eastward, so that the wind changed to north to northwest in the night of 30 March 2021. In the morning of this day *Polarstern* finally reached the bay off Port Stanley and the voyage came to an end. A small ground trough moved from west to east during the day and caused the wind to increase again to 6-7 Bft, occasionally 8 Bft.

Fig. 2.1 and 2.2 display the weather conditions over the course of the expedition PS124.

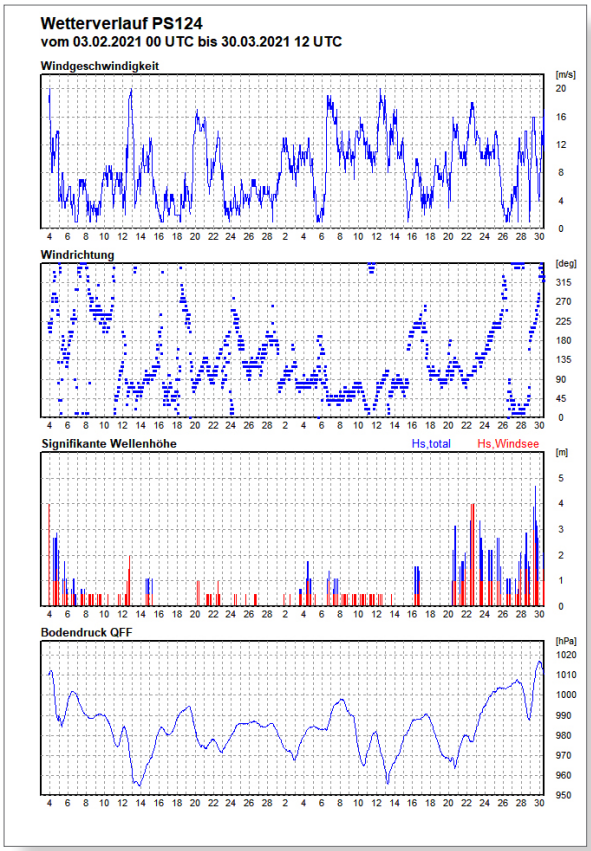

Fig 2.1:
Wind speed, wind direction, wave height and bottom pressure during PS124

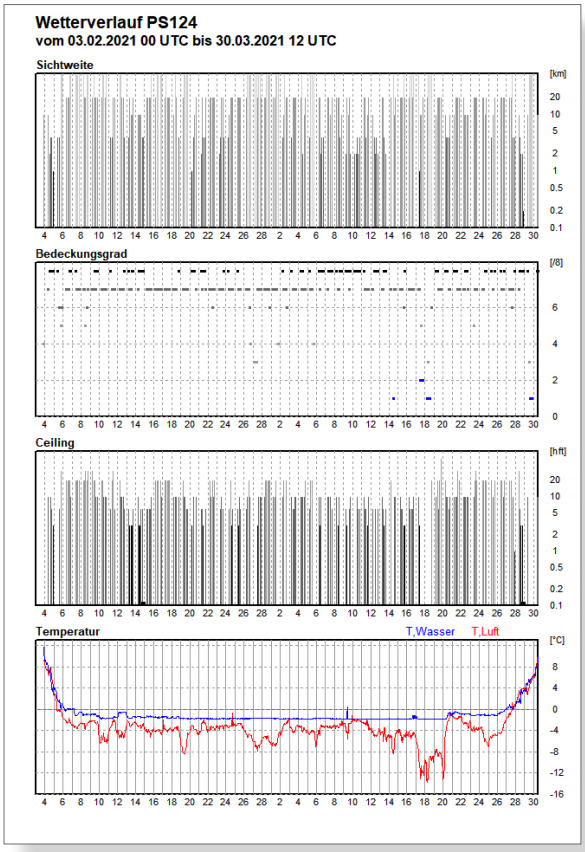

Fig. 2.2:
Visibility, cloud cover, ceiling and temperature in air and in water during PS124

3. OCEANOGRAPHIC CONDITIONS AND DISTRIBUTION OF OCEANIC TRACE GASES NEAR THE SILL OF FILCHNER TROUGH, SOUTHERN WEDDELL SEA

Markus Janout[1], Elin Darelius[2], Hartmut H. Hellmer[1], Yannik Hinse[4], Herve LeGoff[3], Matthias Monsees[1], Svein Østerhus[5], Elena Schall[1], Stefanie Spiesecke[1], Ralph Timmermann[1], Sandra Tippenhauer[1], Mathias van Caspel[1], Lucie Vignes[3], Olaf Boebel[1] (not on board)

[1]DE.AWI
[2]NO.UIB
[3]FR.LOCEAN.UPMC
[4]DE.UNI-Bremen
[5]NO.NORCE

Grant No. AWI_PS124_03

Outline

The southern Weddell Sea's wide continental shelf is characterized by cold and dense waters, which protect the vast Filchner-Ronne Ice Shelf (FRIS) from the impact of warm waters from the deep Weddell Sea. In contrast to other Antarctic ice shelves, basal melt rates at FRIS are still comparatively low. The main oceanographic aspects evolve around the outflow of cold Ice Shelf Water (ISW) and the inflow of modified Warm Deep Water (mWDW), which is regulated by the Antarctic Slope Front at the continental slope north of Filchner Trough. The oceanographic parameters such as temperature, salinity, and currents, needed to address the objectives, were collected by shipboard sampling techniques and autonomous devices such as floats and oceanographic moorings.

Objectives and methods

The Filchner Trough in the southeastern Weddell Sea is the main conduit for northward flowing Ice Shelf Water, defined by temperatures below the surface freezing point. ISW originates from High Salinity Shelf Water (HSSW), formed on the continental shelf in front of Ronne Ice Shelf, and carries the glacial melt from FRIS. The ISW pathway within the trough varies on seasonal time scales with flow out of the Filchner Ice Shelf cavity occurring on the western slope only during late summer/early fall (Darelius & Sallee 2018). On its way to the continental shelf break, ISW encounters a seasonal inflow of modified Warm Deep Water, flowing along the eastern slope of the trough towards the ice shelf front (Ryan et al. 2017, 2020). ISW dominates the bottom layer at the trough's sill where a mixing with open ocean waters forms the deep and bottom waters of the Weddell Sea, the former being the precursor of Antarctic Bottom Water, thus one of the main contributors to the lower branch of the global thermohaline circulation (Foldvik et al. 2004). Projections based on the output of our coupled sea ice–ocean-ice shelf models (BRIOS and FESOM) indicate that in the near future the density of HSSW and, thus, of ISW at the Filchner Trough sill might decrease such that unmodified Warm Deep Water (WDW) can enter the trough and penetrate into the deep FRIS cavity (Hellmer et al. 2012, 2017). The presence of WDW underneath FRIS, similar to the ice shelves fringing the Amundsen Sea to date, is bound to cause a dramatic increase in basal melting. The latter changes ice shelf thickness, reduces the buttressing effect of bottom topography and ultimately influences the

dynamics of the ice streams draining the West and East Antarctic Ice Sheets (Timmermann and Goeller 2017). The resulting fresh water input will have a profound impact on the structure of the shelf water column, the sea ice cover, the formation of deep and bottom waters, and melting at the base of ice shelves located downstream (Timmermann and Hellmer 2013).

This expedition is closely connected to our ongoing monitoring of hydrographic properties beneath the Filchner Ice Shelf in the framework of the Filchner Ice Shelf Project (FISP). The fieldwork was designed to (a) extend existing data sets from the southern Weddell Sea continental shelf, necessary for the initialization and validation of our coupled ice shelf-ice sheet models, and (b) build-up a reference data set to identify changes within the ocean/ice shelf/sheet system, expected to occur due to climate change.

Some general objectives of this project include:

- to specify the controls on slope front dynamics and flow of water masses of open ocean origin onto the southern Weddell Sea continental shelf;
- to determine the temporal variability of the hydrography and tracer distribution in the Filchner Trough with regard to ISW outflow, AABW formation, and southward propagation of mWDW;
- to identify temporal variability by means of mooring observations;
- to provide a comprehensive dataset for numerical model validation and initialization of coupled ocean-ice shelf-ice sheet models.

Specifically we aim:

- to determine the characteristics and dynamics of the slope current in the southern Weddell Sea;
- to monitor the flow of mWDW onto the southern Weddell Sea continental shelf;
- to identify ISW pathways within and out of the Filchner Trough and along the continental slope.

The combination of ship-, seal- and sea ice-based CTD casts combined with long-term moorings in the Filchner Trough and beneath the Filchner Ice Shelf aims at describing the present physical environment in the southern Weddell Sea, and to monitor its variability and possible trends. Tracer observations will help to quantify:

- AABW formation (transient trace gases [CFCs] to identify transit time scales and formation rates), and
- interannual variability by comparison with previous expeditions (e.g., PS96 in 2015/2016 and PS111 in 2018).

Work at sea

Physical Oceanography (shipboard and underway measurements)

Oceanographic work during PS124 included a variety of measurement techniques such as shipboard CTD/LADCP stations, mooring operations, autonomous float deployments, and underway measurements of currents, surface temperature and salinity. During the expedition, we carried out a total of 84 CTD casts to survey the hydrographic properties of the focused region (Fig. 3.1, see Table 3.1 for CTD stations). The CTD/Rosette was operated using the standard SeaBird SBE911plus setup, equipped with double sensors for temperature, salinity,

and oxygen and one sensor each for pressure, substance fluorescence Chl *a*, and beam transmission. In addition, 24 12-liter OTE bottles for water sampling were attached. An altimeter was mounted to monitor the distance to the seafloor. In addition, a high precision thermometer (SBE35, sn77/sw6345) and a stand-alone, internally recording, battery-powered Underwater Vision Profiler (UVP, see Chapter 7) were mounted on the rosette. Serial numbers as well as sensor web IDs are provided in Table 3.2. Salinity samples were measured with the Optimare Precision Salinometer for post-cruise calibration of the conductivity sensors.

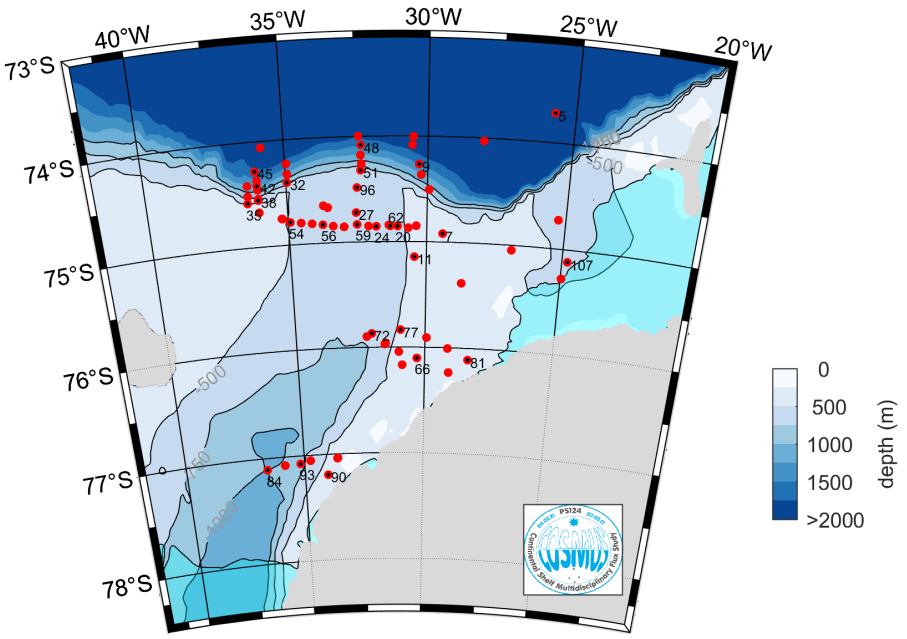

Fig. 3.1: Map of PS124 CTD stations (red dots); the bathymetry (Schaffer et al. 2016) is shown in colors, 500, 750 and 1,000 m-isobaths are marked with black contours. The numbers close to the stations marked with a small black dot refer to CTD stations listed in the first column of Table 3.1, i.e. "5" indicates the location of "PS124_5".

Tab. 3.1: PS124 CTD station list including LADCP profiles and the number of samples taken for Helium and CFC analyses

Station	Date	Time	Latitude [°S]	Longitude [°W]	Water depth [m]	max. Pr. [dbar]	LADCP profile	Helium samples	CFC samples
PS124_5-2	2021-02-08	12:21	-70.418	-30.002	4436	4527		3	3
PS124_5-4	2021-02-08	19:48	-70.418	-29.997	992	1001			
PS124_6-2	2021-02-11	02:02	-73.719	-25.714	3143	3197	2	11	11
PS124_7-4	2021-02-11	19:17	-74.028	-28.074	2465	2495	3		
PS124_8-5	2021-02-12	12:18	-74.921	-29.421	380	380	4	8	6
PS124_8-9	2021-02-12	17:48	-74.920	-29.424	172	202	5		
PS124_9-1	2021-02-13	06:36	-74.003	-30.504	2138	2163	6	8	8
PS124_10-1	2021-02-13	12:49	-74.083	-30.538	1898	1923	7	6	6
PS124_11-1	2021-02-13	16:37	-74.265	-30.303	1502	1513	8	7	7
PS124_11-4	2021-02-13	22:48	-74.364	-30.227	1210	1222	9		

Station	Date	Time	Latitude [°S]	Longitude [°W]	Water depth [m]	max. Pr. [dbar]	LADCP profile	Helium samples	CFC samples
PS124_13-1	2021-02-14	01:24	-74.505	-29.939	874	875	10		
PS124_16-2	2021-02-14	15:46	-75.143	-30.447	435	430	11	7	7
PS124_20-1	2021-02-15	19:12	-74.850	-30.385	435	441	12	8	8
PS124_21-1	2021-02-15	20:55	-74.869	-30.672	477	472	13		
PS124_22-2	2021-02-16	10:36	-74.853	-31.061	551	554	14		
PS124_24-1	2021-02-16	12:08	-74.843	-31.376	575	578	15	5	5
PS124_26-2	2021-02-16	17:58	-74.855	-31.831	607	610	17	7	7
PS124_26-6	2021-02-16	21:24	-74.855	-31.831	636	144			
PS124_27-2	2021-02-17	12:04	-74.851	-32.111	591	589	18	7	7
PS124_30-1	2021-02-17	17:15	-74.852	-32.991	569	572	20		
PS124_31-1	2021-02-18	06:22	-74.721	-32.547	578	580	21	6	6
PS124_32-1	2021-02-18	23:35	-74.747	-35.225	93	91			
PS124_33-1	2021-02-19	00:26	-74.749	-35.199	482	482	22	7	7
PS124_34-1	2021-02-20	09:24	-74.407	-34.959	830	837	23		
PS124_35-1	2021-02-20	11:07	-74.328	-34.938	1202	1208	25		
PS124_36-1	2021-02-20	13:15	-74.229	-34.952	1601	1616	27		9
PS124_37-1	2021-02-20	18:44	-74.580	-36.403	381	409	28	6	6
PS124_38-1	2021-02-21	14:09	-74.512	-36.378	820	826	30		7
PS124_40-1	2021-02-21	17:22	-74.673	-36.014	414	413	31	6	6
PS124_41-1	2021-02-21	19:52	-74.556	-36.019	493	494	32	7	
PS124_42-1	2021-02-21	21:26	-74.544	-36.015	582	585	33		
PS124_43-1	2021-02-21	23:14	-74.459	-36.008	1030	1039	34	6	6
PS124_44-1	2021-02-22	01:03	-74.422	-36.026	1197	1209	35		
PS124_45-2	2021-02-22	05:56	-74.367	-36.017	1406	1420	36	6	7
PS124_46-1	2021-02-22	14:42	-74.415	-36.371	1209	1218	38		7
PS124_47-1	2021-02-22	22:38	-74.281	-36.067	1663	1688	39	8	8
PS124_48-1	2021-02-23	10:16	-74.060	-35.800	1965	2008	40	7	7
PS124_49-2	2021-02-24	09:15	-73.997	-32.417	1790	1812	41		
PS124_50-1	2021-02-24	12:25	-74.082	-32.335	1532	1544	42		
PS124_51-1	2021-02-24	17:03	-74.177	-32.347	1197	1203	45		
PS124_52-1	2021-02-24	19:24	-74.260	-32.327	899	901	46		
PS124_53-1	2021-02-24	22:15	-74.321	-32.358	630	628	47		
PS124_54-2	2021-02-25	06:24	-74.665	-33.560	86	83			
PS124_54-3	2021-02-25	07:21	-74.666	-33.564	556	571	48	7	7
PS124_55-1	2021-02-25	20:18	-74.786	-34.929	495	497	49	6	7
PS124_56-1	2021-02-25	22:09	-74.798	-34.539	527	523	50		11
PS124_57-1	2021-02-25	23:51	-74.811	-34.147	537	535	51	5	
PS124_58-1	2021-02-26	01:35	-74.825	-33.759	546	548	52	4	5
PS124_59-1	2021-02-26	03:10	-74.842	-33.388	555	557	53		7
PS124_60-1	2021-02-26	04:56	-74.853	-33.001	575	577	54		
PS124_61-1	2021-02-26	08:38	-74.833	-32.524	567	570	55		
PS124_62-1	2021-02-26	14:05	-74.645	-33.715	589	329			

Station	Date	Time	Latitude [°S]	Longitude [°W]	Water depth [m]	max. Pr. [dbar]	LADCP profile	Helium samples	CFC samples
PS124_64-1	2021-02-27	07:32	-74.851	-31.062	551	553	56		
PS124_65-2	2021-02-27	11:48	-74.852	-31.329	584	583	57		
PS124_66-1	2021-02-27	14:06	-74.854	-31.830	603	606	58		
PS124_68-2	2021-02-28	22:18	-76.103	-30.304	471	77			
PS124_68-3	2021-02-28	23:10	-76.103	-30.310	447	448	60	7	7
PS124_72-1	2021-03-01	16:54	-75.962	-31.527	594	596	62	7	7
PS124_74-2	2021-03-02	14:21	-75.898	-32.257	762	354			
PS124_76-1	2021-03-02	20:03	-75.869	-32.062	715	708	63	8	10
PS124_77-3	2021-03-03	14:39	-75.970	-31.561	596	596	64		
PS124_78-1	2021-03-03	18:37	-76.043	-31.018	451	452	65	8	6
PS124_80-1	2021-03-04	18:20	-75.835	-30.951	458	453	66	6	5
PS124_81-1	2021-03-04	21:12	-75.908	-29.941	473	478	67		7
PS124_82-1	2021-03-05	00:03	-76.007	-29.115	388	384	68	7	5
PS124_83-1	2021-03-05	02:24	-76.110	-28.305	339	340	69	4	4
PS124_84-1	2021-03-05	04:30	-76.234	-29.054	308	307	70	5	5
PS124_86-1	2021-03-05	12:01	-76.168	-30.884	430	432	71		
PS124_88-1	2021-03-05	21:57	-77.108	-36.586	1064	1074	72	7	8
PS124_90-3	2021-03-06	16:16	-77.037	-33.588	382	132			
PS124_90-4	2021-03-06	16:40	-77.041	-33.601	359	359	73		7
PS124_91-2	2021-03-07	09:07	-77.193	-34.024	455	450	74		
PS124_93-1	2021-03-07	15:42	-77.051	-34.741	775	87	75		
PS124_93-2	2021-03-07	16:22	-77.050	-34.743	744	749	76		12
PS124_95-1	2021-03-08	03:47	-77.075	-35.171	891	899	77		
PS124_96-1	2021-03-08	05:48	-77.080	-35.826	1023	1026	78		
PS124_98-1	2021-03-09	05:51	-75.385	-28.674	436	432	79		11
PS124_100-1	2021-03-10	05:57	-74.484	-32.499	633	631	80		
PS124_107-1	2021-03-11	21:59	-75.047	-26.884	278	272	81		
PS124_109-1	2021-03-13	15:13	-74.726	-25.273	626	623	82		
PS124_110-1	2021-03-13	19:29	-75.114	-24.796	553	550	83		
PS124_111-1	2021-03-14	00:57	-75.277	-24.967	637	61	85		
PS124_111-2	2021-03-14	01:33	-75.277	-24.967	608	611	86		
PS124_117-1	2021-03-24	06:24	-69.000	-26.998	4718	4772			

Tab. 3.2: Sensors attached to the CTD

Sensor	SN	SW ID
SBE9/Pressure	937	
SBE3plus (primary)	5101	5849
SBE4c (primary)	3238	5866
SBE5 pump (secondary)	5254	–
SBE3plus (secondary)	5112	4119

Sensor	SN	SW ID
SBE4c (secondary)	3570	4121
SBE5 pump (secondary)	4317	5889
SBE43-1 (primary)	4016	7695
SBE43-1 (secondary)	4019	7696
Transmissometer, CStar	1198	4126
Fluorometer, EcoFLR	1853	4125
Altimeter	51533	4122
UVP	202	7913
SBE35	0077	6345

To meet our objectives and advance the understanding of the ocean circulation in this region, we aligned CTD stations (Fig. 3.1) in transects

1. normal to the Filchner Trough axis,
2. across the Filchner Trough sill, and
3. across the slope front and down the continental slope

in order to investigate pathways of ISW/WSBW. To increase the temporal and spatial CTD coverage, a total of 10 seals were tagged to 'operate' on the ice-covered southwestern continental shelf during the austral winter months (see Chapter 4). Current profiles were collected with the LADCP (Lowered Acoustic Doppler Current Profiler) system. The LADCP, mounted on the CTD/Rosette, consisted of two RDI Workhorse 300 kHz ADCPs in a master (downward looking, SN23293) and slave (upward looking, SN23292) configuration. The ADCPs were mounted so far that all 24 bottles on the rosette could be used for water sampling. The LADCP was operated with the LADCP tool V1.7b from GEOMAR using the settings and commands displayed in Table 3.3. The PC time was synchronized with the ship's NTP server directly (server 192.168.20.3), using the "Net Time Server"-programme (the spired trial version), which needed to be started in order to perform the synchronization. LADCP data was processed using the GEOMAR LADCP processing Version 3, August 2019. This routine required data input from the shipboard ADCP and the CTD. The latter was provided using a data conversion programme called prladcp. The prladcp opens Seabird processing and initiates the steps datcnv, celltm, binavg and trans. The resulting file has an 1-second resolution. Furthermore, the processing requires input of a CTD data file with a resolution of 1 dbar, which is provided by the "ManageCTD"-programme running on the CTD-computer. The "Seasave"-programme used for acquiring the CTD casts was modified to save the NMEA navigational data string during the cast.

Tab. 3.3: Configuration file for the LADCP during PS124

LADCP
base_path=C:\ladcp\scripts\..\
network_path=L:\scientists\PS124\ladcp\
cruise_id=PS124
up_installed=1
down_installed=1

LADCP

erase_button=enabled
download_files=all

ntp_server=192.168.20.3
[Master-Commands]
mode_15=1
ambiguity_velocity=250
bin_number=20
bin_length=1000
blank_after_transmit=0
broadband=1
sensor_source=0111101
coordinate_transformation=00111
flow_control=11101
pings_per_ensemble=1
time_between_pings=0
time_per_ensemble=1.2
master_slave=1
wait_ensembles_before_sync=0
master_slave_when_to_sync=011
wait_time_before_sync=5500
power_output=255
[Slave-Commands]
mode_15=1
ambiguity_velocity=250
bin_number=20
bin_length=1000
blank_after_transmit=0
broadband=1
sensor_source=0111101
coordinate_transformation=00111
flow_control=11101
pings_per_ensemble=1
time_between_pings=0
time_per_ensemble=1.2
master_slave=2
master_slave_when_to_sync=011
wait_time_before_start_without_sync=200
power_output=255

Tab. 3.4: Configuration file for the SADCP during PS12

SADCP

```
; Restore factory default settings in the ADCP
cr1

; set the data collection baud rate to 9600 bps,
; no parity, one stop bit, 8 data bits
; NOTE:  VmDas sends baud rate change command after all other commands in
; this file, so that it is not made permanent by a CK command.
cb411

; Set for narrowband single-ping profile mode (NP), 80 (NN), 4 meter bins (NS),
; 4 meter blanking distance (NF)
WP000
NP001
NN080
NS0400
NF0400
;WV390 (default)

; Disable single-ping bottom track (BP),
BP000

; output velocity, correlation, echo intensity, percent good
ND111100000

; Ping as fast as possible
TP000000

; Since VmDas uses manual pinging, TE is ignored by the ADCP
; and should not be set.
;TE0000000

; Set to calculate speed-of-sound, no depth sensor, external synchro heading
; sensor,  pitch or roll being used, no salinity sensor, use internal transducer
; temperature sensor
EZ1011101

; Output beam data (rotations are done in software)
EX00000

; Set transducer misalignment (hundredths of degrees).
; Ignored here but set in VmDAS options.
;EA00000

; Set transducer depth (decimeters)
ED00110

; Set Salinity (ppt)
ES35

;set external triggering and output trigger; no trigger
CX0,0

;set external triggering and output trigger
;CX1,3

; save this setup to non-volatile memory in the ADCP
CK
```

Underway current profiles of the upper ~200 m were collected with *Polarstern's* Ocean Surveyor 150 kHz (RD-Instruments) shipboard (S)ADCP. The SADCP was operated using the settings given in Table 3.4. For protection against sea ice, the Ocean Surveyor is mounted behind a window, flooded with water, in the ship's hull. When steaming through ice, air accumulates inside the window over time, which compromises the data quality. During PS124 the air was periodically released by the laboratory electrician. The data from the SADCP was merged online with the corresponding navigation data (i.e., the vessel's GPS system) and stored on the hard disk using the programme VMDAS. Pitch, roll, and heading information were converted from NMEA. Current velocities were recorded in beam coordinates to allow corrections during post processing. Processing during the cruise was conducted using GEOMAR SADCP software (OSSI19). Final data processing and quality control will be done at AWI after the field campaign.

Underway temperature and salinity are measured with a thermosalinograph, consisting of two SBE21 SeaCAT with an additional external thermometer SBE38 for minimum thermal contamination from the ship. The two systems are operated in parallel on the same seawater intake. The pumped system is equipped with a flow meter and set to pump 60 L/min. Position and time information is added via NMEA telegram. The system is located in the ship's keel with the water intake at about 11-m depth, depending on the ship's draft. During PS124, the system was running continuously and was only switched off for short maintenance and cleaning. Salinity samples were episodically collected to calibrate the conductivity cell, depending on the sea-ice conditions. On average, samples were taken every other week and analyzed with an Optimare Precision Salinometer on board by the ship's laboratory-electrician. The sensors are usually operated for one full season (about half a year, depending on the expedition schedule) and changed during time in port in Bremerhaven. After post-cruise calibration of sensors, the data are processed and calibrated by Fielax GmbH and stored in the PANGAEA data repository.

A SBE37 Seabird CTD (microcat) was installed on the OFOBS (Chapter 11) in order to record temperature and salinity along the imaging transects. More details are provided in Chapter 13.

Oceanographic moorings

Moorings are major tools to monitor ocean climate and study trends and variability in water mass properties. PS124 carried out a total of 40 mooring operations (Table 3.5). 22 moorings were deployed, and 16 were successfully recovered. Two recoveries failed (P3 and AWI256-2) likely related to corrosion on the acoustic releasers. Mooring operations were carried out in cooperation with LOCEAN (Paris), NORCE (Bergen), and University Bergen and were focused on the central parts of the Southeast Weddell Sea circulation system. The target circulation features include the inflow of mWDW and outflow of ISW across the Filchner Sill (LOCEAN and NORCE), the Antarctic Slope Front dynamics at the continental slope (University of Bergen), and the ISW export down the continental slope at 36° W and the seasonal mWDW inflow at 76° S (AWI). The time series at 76° S was initiated in 2014 and, following the successful recovery of the three moorings deployed during PS111, now provides a 7-year record of water mass properties. The three-mooring-array at 76° S was amended by a fourth mooring deployed in the deeper part of Filchner Trough as a western extension. All moorings are designed to remain at a safe distance below the surface of at least 200 m in order to minimize the iceberg impact risk.

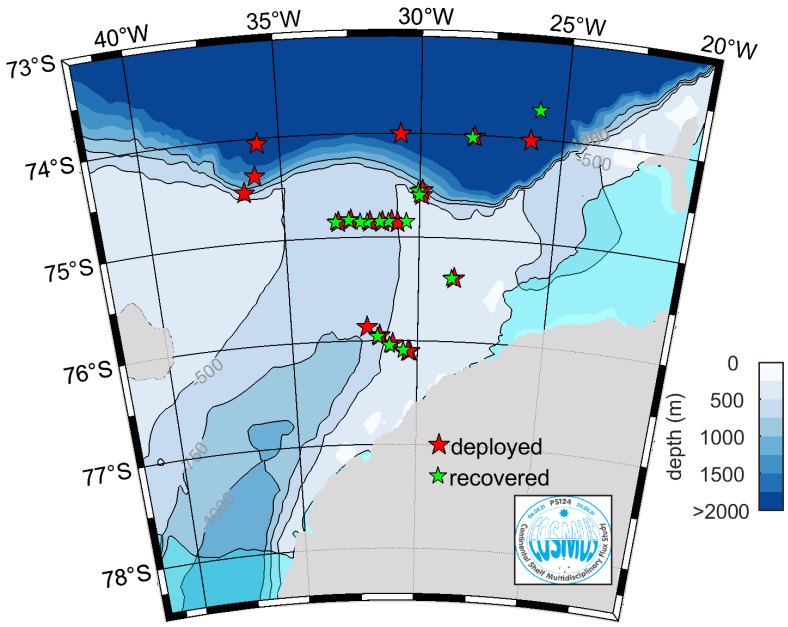

Fig. 3.2: Map of recovered (green stars) and deployed (red stars) moorings; the bathymetry (Schaffer et al. 2016) is shown in colors, 500, 750, and 1,000 m-isobaths are marked with black contours.

Tab. 3.5: List of deployed and recovered moorings during PS124

Mooring	Station	DateTime	Latitude	Longitude	Depth [m]	Comment
AWI-255-2	PS124_06-3	2021-02-11 06:47	73°43.24‘S	25°46.33‘W	3200	recovered
P6	PS124_07-1	2021-02-11 13:55	74°01.23‘S	28°04.45‘W	2545	recovered
SWS-06-01	PS124_07-2	2021-02-11 17:40	74°00.90’S	28°06.28’W	2535	deployed
SWS-05-01	PS124_09-2	2021-02-13 11:50	74°00.29’S	30°41.89’W	2143	deployed
M3	PS124_14-1	2021-02-14 07:08	74°33.00’S	29°55.05‘W	687	recovered
M6	PS124_15-1	2021-02-14 10:00	74°35.83‘S	29°55.65‘W	536	recovered
P4	PS124_18-1	2021-02-15 12:13	74°51.14‘S	30°22.73‘W	463	recovered
P3	PS124_22-1	2021-02-16 07:29	74°51.09‘S	30°43.09‘W	490	rec. failed
P1	PS124_23-1	2021-02-16 09:56	74°51.08‘S	31°03.54‘W	559	recovered
P2	PS124_24-2	2021-02-16 13:45	74°50,94‘S	31°22.80‘W	602	recovered

Mooring	Station	DateTime	Latitude	Longitude	Depth [m]	Comment
S-2018-E	PS124_25-1	2021-02-16 15:34	74°51.26‘S	31°50.17‘W	635	recovered
S2-2017-E	PS124_27-1	2021-02-17 11:25	74°51.02‘S	32°05.84‘W	614	recovered
S2-2018-C	PS124_28-1	2021-02-17 14:12	74°50.09‘S	32°30.79‘W	600	recovered
S2-2018-W	PS124_29-1	2021-02-17 15:48	74°51.13’S	33°00.78’W	595	recovered
P7	PS124_39-1	2021-02-21 15:58	74°30.94’S	36°22.79’W	814	deployed
SWS-W2	PS124_45-7	2021-02-22 13:31	74°21.88’S	35°57.16’W	1444	deployed
SWS-D1	PS124_48-2	2021-02-23 13:44	74°03.13’S	35°46.50’W	2096	deployed
AWI-256-2	PS124_49-1	2021-02-24 08:52	73° 59.74‘S	32°21.90‘W	1835	rec. failed
S2-2021-W	PS124_60-2	2021-02-26 07:31	74°51.19’S	33°00.06’W	600	deployed
S2-2021-C	PS124_61-2	2021-02-26 10:18	74°49.97’S	32°32.56’W	600	deployed
P1	PS124_64-2	2021-02-27 09:18	74°50.87’S	31°01.33’W	560	deployed
P2	PS124_65-1	2021-02-27 11:21	74°51.25’S	31°22.72’W	607	deployed
S2-2021-E	PS124_66-2	2021-02-27 15:31	74°51.20’S	31°49.85’W	631	deployed
WetCam-Fish	PS124_67-2	2021-02-28 08:45	74°51.66’S	30°48.54’W	523	deployed
AWI-252-3	PS124_69-1	2021-03-01 12:21	76°05.54‘S	30°28.14‘W	457	recovered
AWI-253-3	PS124_70-1	2021-03-01 14:06	76°02.74‘S	31°01.42‘W	471	recovered
AWI-254-3	PS124_72-9	2021-03-02 08:44	75°57.68‘S	31°29.79‘W	606	recovered
AWI-263-1	PS124_73-1	2021-03-02 11:43	75°51.95’S	31°59.66’W	735	deployed
AWI-253-4	PS124_75-1	2021-03-02 17:48	76°03.11‘S	30°59.60‘W	453	deployed
AWI-254-4	PS124_77-4	2021-03-03 16:12	75°57.68‘S	31°30.41‘W	606	deployed
254-4R SWS-03-01	PS124_77-2	2021-03-03 13:53	75°57.37’S	31°30.52’W	610	deployed
AWI-252-4	PS124_79-2	2021-03-04 10:10	76°06.01’S	30°18.00’W	469	deployed

Mooring	Station	DateTime	Latitude	Longitude	Depth [m]	Comment
AWI-252-4R	PS124_79-3	2021-03-04 14:28	76°06.15'S	30°22.07'W	478	deployed
Lotus 56	PS124_87-1	2021-03-05 17:35	76°52.76'S	33°51.69'W	573	deployed
Lotus 57	PS124_89-1	2021-03-06 13:10	77°00.48'S	34°02.91'W	487	deployed
Lotus 58	PS124_89-2	2021-03-06 13:30	77°01.11'S	33°49.57'W	440	deployed
Lotus 64	PS124_89-3	2021-03-06 13:46	77°01.75'S	33°39.05'W	399	deployed
P5	PS124_98-3	2021-03-09 08:20	75°23.50'S	28°38.43'W	446	recovered
M6	PS124_99-1	2021-03-09 16:42	74°35.69'S	29°55.01'W	548	deployed
M3	PS124_102-1	2021-03-11 09:02	74°33.01'S	29° 54.63'W	761	deployed
P5	PS124_106-1	2021-03-11 17:26	75°23.39'S	28° 38.20'W	455	deployed
SWS-07-1	PS124_115-2	2021-03-15 15:23	74°00.93'S	26°07.80'W	2864	deployed
AWI-244-6	PS124_116-1	2021-03-20 16:16	69°00,30'S	07°01.61'W	2973	recovered
BGC-1	PS124_117-2	2021-03-24 13:14	69°00.07'S	27°00.07'W	4717	deployed

Nevertheless, upper-ocean measurements are urgently needed to understand the role of stratification and upper ocean dynamics relative to advective processes in this region as well as to document the seasonal mixed layer evolution, which is particularly important for biological studies. In order to accomplish these measurements, we deployed two newly-designed pipe-moorings as upper-ocean extensions of the AWI252- and AWI254-moorings. The pipe-moorings each consist of 13 five-meter-long segments of PVC-piping (30 cm diameter, Fig. 3.3). The segments are connected to provide a closed rigid tube, which is supposed to withstand the impact of an iceberg. The tube includes buoyancy and oceanographic instruments and is designed to minimize the risk of entanglement. Sufficient throughflow to the instruments is ensured by holes in the pipes. In addition to standard CTD and temperature sensors, the upper part of pipe-mooring AWI252-R is equipped with a SBE19plusV2 CTD, which additionally carries fluorescence, light, and oxygen sensors. The goal of this deployment is to generate, at least, a one year-long cycle of mixed layer evolution and spring and summer bloom dynamics in collaboration with the group Benthos Pelagic Processes (Chapter 10).

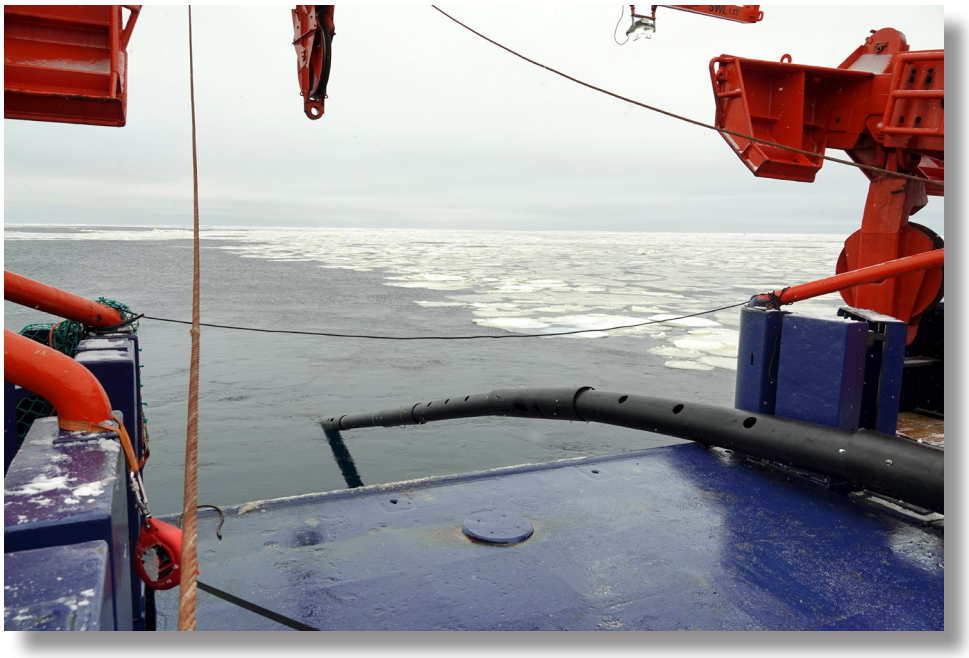

Fig.3.3: The tube during the deployment of mooring AWI252-R (Photo R. Timmermann)

The BGC-mooring was the last deployment during PS124, and results from a multi-disciplinary initiative across various AWI-sections to quantify the different components of the carbon budget throughout a full year. Besides basic oceanographic instruments, the mooring carries a suite of biogeochemical sensors, an autonomous water sampler, an underwater vision profiler, and two sediment traps. Deteriorating weather conditions during this late time in the season shifted the deployment from the original location near Maud Rise on the Prime Meridian to the central Weddell Sea. The top of the mooring is only 40 m below the surface to allow for the necessary biogeochemical measurements within the mixed layer. However, in contrast to the 'iceberg-rich' southern Weddell Sea, the iceberg risk was considered comparatively low at this new site.

Following the unexpected finding of large numbers of fish nests discovered with the towed camera system (OFOBS, Chapter 11), an ad-hoc mooring (Wetcam-Fishnests) was designed to install cameras above the seafloor to monitor the development of the fish nests. The mooring consists of two cameras programmed to record images every 6 hours for up to 2 years. The cameras are mounted directly on the acoustic releasers approximately 3 m above the seafloor. Just above that, an Aquadopp current meter and an SBE37 CTD were installed to record standard oceanographic parameters.

In order to observe the southward extent of the mWDW-inflow, four LoTUS (Long Term Underwater System) buoys, developed by J. Kuttenkueler at KTH, Sweden, were deployed on the continental shelf east of the Filchner Trough at 77° S. The buoys measure the temperature about 1 m above the bottom at hourly intervals, and they are set to release their anchor and surface on 2 February 2023. Deployment details are given in Table 3.5.

Three sound source-moorings were deployed along 74° S (Fig. 3.4, Table 3.6). These moorings carry Webb-sound sources facilitating under-ice positioning of RAFOS APEX floats as will be discussed below. A complete list of mooring schematics and deployed instruments is archived at AWI.

Tab. 3.6: Deployment of sound sources during PS124

Mooring/ SoSo site	SN	Water depth [m]	Latitude	Longitude	Deploy-ment date/time	Sound source depth [m]	Schedule [UTC] time	Comments
SWS-06	W0023	2536	74°00.903' S	028°06.280' W	2021-02-11 17:40	721	12:51:00	1st sweep 2021-02-12
SWS-05	W0058	2143	74°00.290' S	030°41.887' W	2021-02-13 11:50	718	12:29:30	1st sweep 2021-02-14
SWS-07	W0057	2864	74°00.929' S	026°07.796' W	2021-03-15 15:23	792	13:09:45	1st sweep 2021-03-16

Autonomous floats

During PS124, we deployed a total of 6 Argo floats (type APEX), produced by Teledyne Webb Research, USA. All floats had been appropriated by AWI and are equipped with identical sensor suits. They feature an adjustable Ice Sensing Algorithm, ISA, set to –1.65°C between 40 and 10 dbar, with a surfacing response delayed by 1 profile. Interim data storage internally saves all profiles that could not be transmitted in real-time due to ISA-triggered aborts of surfacing attempts and transmits these profiles during ice-free conditions. RAFOS technology is used for under ice tracking. For data transmission Iridium Rudics is used. The floats were set up for the novel park & drift behavior, by using the APEX new mission sequencing option. The idea is to keep floats grounded during their parking phases throughout their first year of deployment, minimizing their drift, resulting in quasi-stationary CTD casts every 10 days. To this end, floats were launched in waters of around 1,000-m depth with the float's drift depth set to 2,000 m. After this initial year, floats are programmed to change mission parameters automatically, in particular the parking depth to 800 m, and start drifting for the remainder of their mission. This is necessary as floats will be launched in the southern Weddell Sea, where they reside more or less permanently underneath sea ice. The floats hence need to be swept northwards out of the interior Weddell Sea in order to reach open waters to facilitate uploading the stored data via satellite communication. Float acceptance tests were first performed onboard *Polarstern* on 2021-02-03 by starting the float self-test routing via Sail-Loop and terminal programme. All floats completed the self-test successfully. After completion of the self-test, floats were put to sleep. For deployment, all but the first float (8880) were placed in a bucket filled with water after starting the float by magnet sweep. Floats were deployed between 70 and 90 minutes after the start of the PRELUD phase. The deployment positions are plotted in Fig. 3.4 (with float serial numbers given as 3-digit bold numbers). Float identification information is given in Table 3.7, sorted by time of deployment.

In addition to the APEX floats, we deployed 5 NKE floats for the Bundesamt für Schiffahrt und Hydrographie (BSH, Hamburg) as a contribution to the Argo Float Programme. The floats were launched in the Antarctic Circumpolar Current during the transits across Drake Passage. Prior to deployment, the floats were activated following the standard protocol and subsequently launched from the rear starboard side of the ship at a reduced cruising speed of 3–5 kn. Deployment dates and positions are provided in Table 3.8.

Tab. 3.7: Ice resilient APEX float deployments in 2021 during PS124

AWI-ID	S/N	IMEI	WMO ID	Magnet sweep @ (ping time)	Deployed @	Time Start to Launch [min]	Orientation after deployment	Deployment Latitude	Deployment Longitude	ice [%]	Water Depth [m]	Station No	Station No of CTD
PS124_1	8880	300125061818140	7900973	2021-02-05 17:22	2021 02 05 18:32	70	flat	61°18.496'S -61.3083	52°40.018'W -52.6670	0	1188	PS124-4	none
PS124_2	8881	300125061810160	7900974	2021-03-11 09:08	2021-03-11 10:46	98	rightens	74°31.698'S -74.5283	29°07.034'W -29.1172	20	1310	PS124-103	none
PS124_3	8882	300125061813150	7900975	2021-03-11 09:47	2021-03-11 11:14	87	rightens	74°34.091'S -74.5682	29°11.714'W -29.1952	50	1159	PS124-104	none
PS124_4	8883	300125061329720	7900976	2021-03-11 10:15	2021-03-11 11:49	94	rightens	74°37.174'S -74.6196	29°24.210'W -29.4035	50	877	PS124-105	none
PS124_5	8884	300125061817240	7900977	2021-03-15 05:09	2021-03-15 06:28	79	upright	74°39.460'S -74.6577	27°22.178'W -27.3696	90	880	PS124-113-1	none
PS124_6	8885	300125061328710	7900978	2021-03-15 05:37	2021-03-15 06:49	72	flat	74°36.831'S -74.6138	27°16.984'W -27.2831	90	1149	PS124-114-1	none

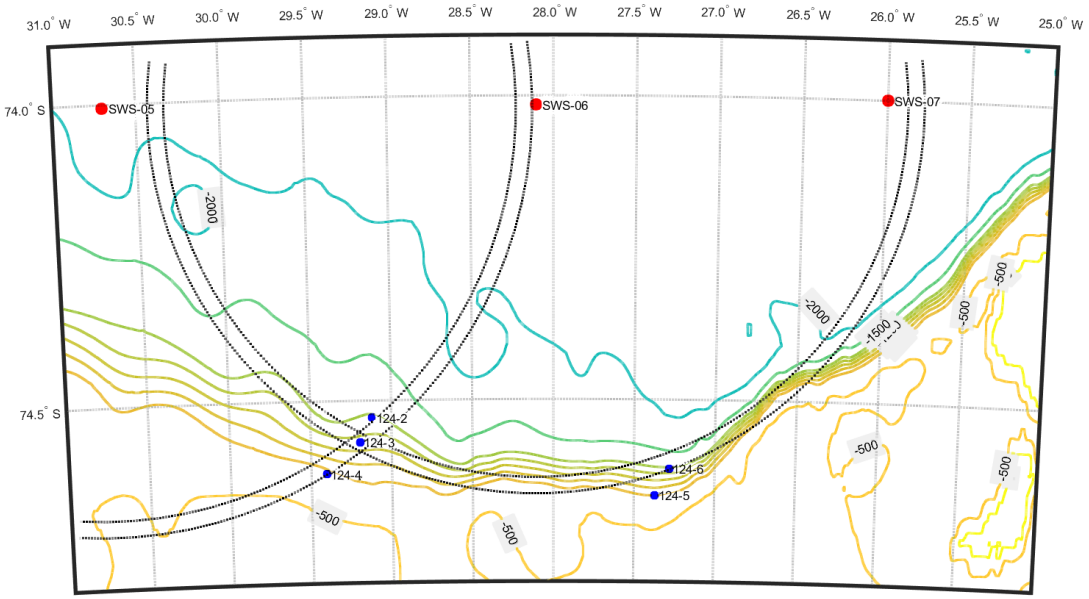

Fig. 3.4: Map of the southeastern Weddell Sea with labelled topographic contours (yellow to green); contours at 500, 800, 900, 1,000, 1,100, 1,200 and 2,000 m; red dots: locations of sound sources deployed during PS124; blue dots: locations of ice resilient Argo floats; the area within the intersection of pairs of dotted circles around SWS-05 and SWS-06 exemplifies the RAFOS tracking precision assuming a ±1 second uncertainty in RAFOS signal time of arrivals.

Tab. 3.8: NKE BSH-float deployments in 2021 during PS124

Station	SN	Deployment time	Latitude	Longitude
PS124_1-1	AI2600-20DE016	04.02.2021 16:28	55°56.233‘S	055°43.892‘W
PS124_2-1	AI2600-20DE015	04.02.2021 20:33	56°48.574‘S	055°19.436‘W
PS124_3-1	AI2600-20DE014	04.02.2021 23:36	57°29.686‘S	055°01.375‘W
PS124_118-1	AI2600-20DE007	28.03.2021 20:02	57°23.990‘S	049°36.941‘W
PS124_119-1	AI2600-20DE008	29.03.2021 11:39	55°01.164‘S	053°00.610‘W

In the afternoon of 17 March 2021, prior to the *Neumayer III*-cargo operations, we visited one landfast ice station in Atka Bay, in collaboration with the sea ice group (Chapter 6). During the station, we deployed a landfast ice-tethered buoy through a 3-m-deep (2 m fast ice, 1 m snow) drillhole located at 70.623° S, 7.842° W. The water depth at this location is 220 m, based on the pressure measurements from a SBE37 CTD, which we manually lowered to the seafloor. The system manufactured by Pacific Gyre includes two SBE37 CTDs (215 m and 110 m depth) and one SBE39 temperature sensor (40 m depth), which are attached to an inductive cable connected to a top buoy. The buoy contains telemetry and sends data from the sensors via Iridium to the Pacific Gyre data portal. The system was placed next to an ice mass balance buoy, deployed by the sea-ice physics team and is expected to contribute to the understanding of the ocean circulation and sea ice-ocean interaction in Atka Bay.

Tracer Oceanography

About 540 water samples for noble gases (^{3}He, ^{4}He, and Ne) and CFC-12 plus SF_6 have been retrieved with the CTD-water-sampler (Niskin bottles) system on regular hydrographic stations (see Table 3.1 for sample numbers). The bottles were closed by stainless steel springs instead of rubber springs. Due to the high volatility and very low concentrations in the water, we took our samples first (i.e., before oxygen, salinity, CO_2, and other sampling). For one noble-gas sample we need 1.5 L (incl. rinsing), for CFCs we need 0.5 L (incl. rinsing). Water samples for helium isotopes and neon are stored in 40 ml gas tight copper tubes, clamped off at both sides. The noble gas samples are to be analyzed at the IUP Bremen noble gas mass spectrometry lab. Water samples for CFC-12/SF_6 measurements are stored in 100 ml glass ampoules, sealed off after a headspace of pure nitrogen was injected. The CFC-12/SF_6 samples will be analyzed also in the CFC-laboratory at the IUP Bremen.

Preliminary and expected results

- The extensive CTD survey combined with the successful mooring recoveries during PS124 will provide crucial information needed to advance our understanding in some of the relevant science questions addressed in the new Helmholtz Research Programme “Changing Earth – Sustaining our Future”, in particular for Subtopics 2.1 (Warming Climates) and 2.3 (Sea level Change). Some of the important aspects and new datasets that will be further detailed below include:
- Improved understanding of the slope front dynamics in the southern Weddell Sea.
- Extension (by three years) of the time series (2013–2018) on the eastern slope of the Filchner Trough based on mooring data from the 76° S-transect.
- Extended information about the temporal variability and strength of the southward flowing mWDW on the eastern slope of the Filchner Trough.
- Improved understanding of the spreading and pathways of ISW in the Filchner Trough and beyond the Filchner Trough sill.

Hydrographic conditions during PS124

The hydrographic conditions in the southeastern Weddell Sea were characterized by near-freezing temperatures, as newly-formed sea ice prevailed throughout the sampling region. We performed several CTD transects in the focus region, in particular oriented across the continental slope in order to observe the dense water outflow from Filchner Trough and the subsequent along-slope propagation of this plume. Furthermore, we occupied one CTD transect along 75° S in order to observe the inflow of mWDW and the outflow of ISW across the 600 m-deep sill, which separates the Filchner Trough from the deep Weddell Sea. Further zonal transects were performed across the eastern slopes of the trough at 76° S and 77° S. This region is episodically impacted by the inflow of mWDW as typically measured by the moorings maintained at 76° S.

The 75° S transect was characterized by cold (–2° C) waters across most of the transect (Fig. 3.5), and the mWDW inflow at the eastern slope. The –1.9° C isotherm, located around a water depth of 300 m, indicates the upper boundary of cold water masses consisting of ISW exported from underneath Filchner Ice Shelf, modified with locally-produced HSSW. Salinities of the cold waters were >34.6 as is typical for this region. The mWDW had temperatures of up to –0.5° C and is a commonly observed feature at this location (Janout et al. 2021). Additional patches of above-freezing temperature (–1.4 to –1.2° C) were measured above the –1.9° C-isotherm, which points to enhanced eddy activity at this location, likely related

to sharp fronts between the different water masses that occupy the region. Smaller areas of mWDW were also found along 76° S, although already at reduced temperatures of –1.3° C, due to mixing with cold ISW along the mWDW's southward propagation (Fig. 3.5).

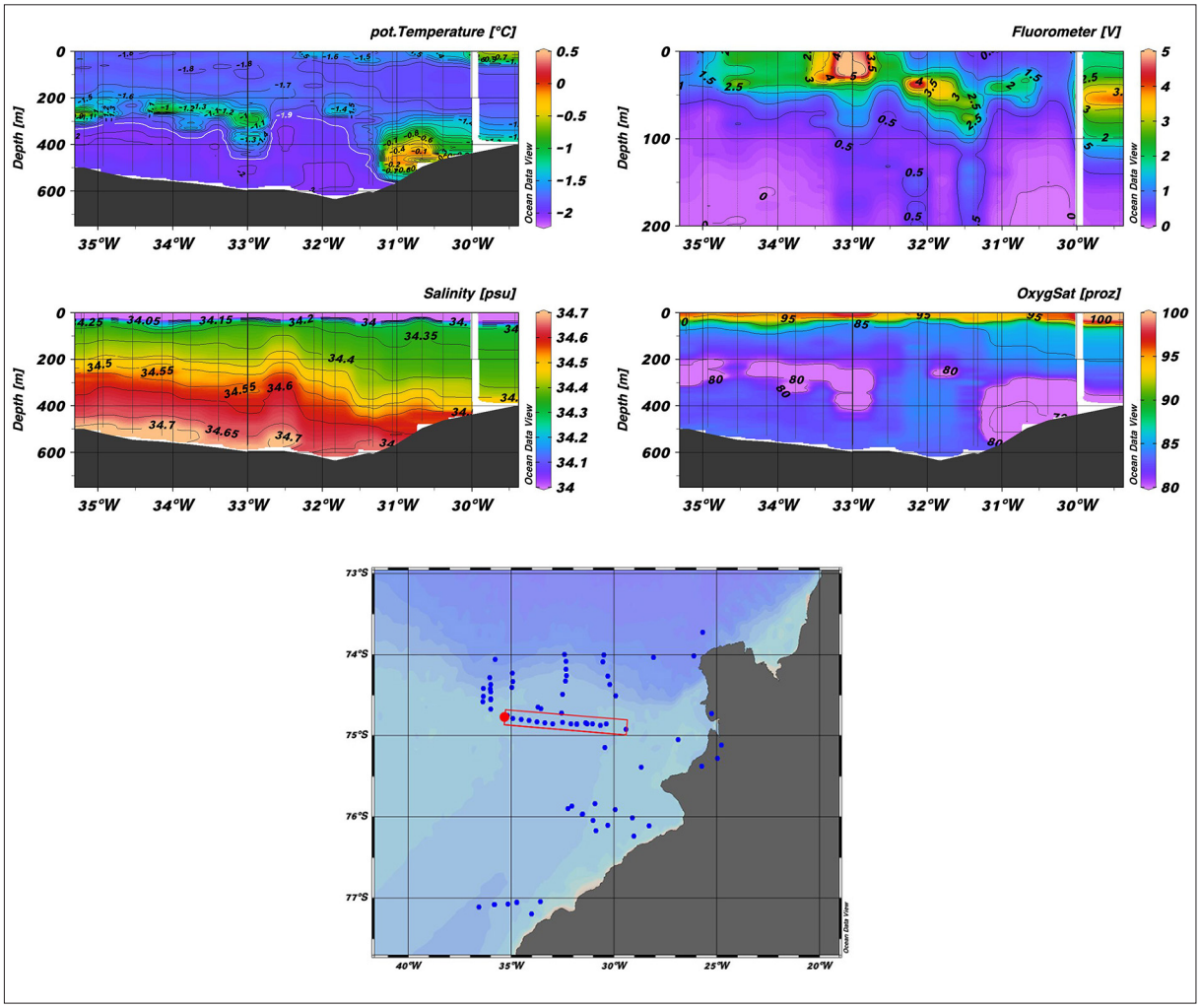

Fig. 3.5: Potential temperature, salinity, fluorescence (upper 200 m), and oxygen saturation along 75°S vs. depth, as indicated on the map

The more western stations in the deeper parts of the trough were characterized by temperatures below –1.9° C. The mWDW presence at this location varies seasonally and interannually as highlighted by the long-term records discussed below.

The cold and dense waters that dominate in Filchner Trough are the main ingredients for the formation of the deep and bottom waters that contribute to the global ocean circulation. However, the exact export pathways of ISW between the trough and the Weddell Sea continental slope are not well known, which is why we performed several cross-slope transects north of Filchner Trough (Fig. 3.1). The hydrographic conditions at the continental slope were characterized by a several hundred meter thick upper layer that is stratified weakly, with near-freezing temperatures and salinities of 34.3–34.4. Below that, WDW dominated the slope north of the 1,000-m isobath with maximum temperature and salinity of 0.7° C and 34.68, respectively (Fig. 3.6).

The shelf break stations and near-bottom waters on the shelf featured mWDW. However, only the westernmost cross-slope transect at 36° W included slope stations where traces of cold dense water were found near the bottom (Fig. 3.6).

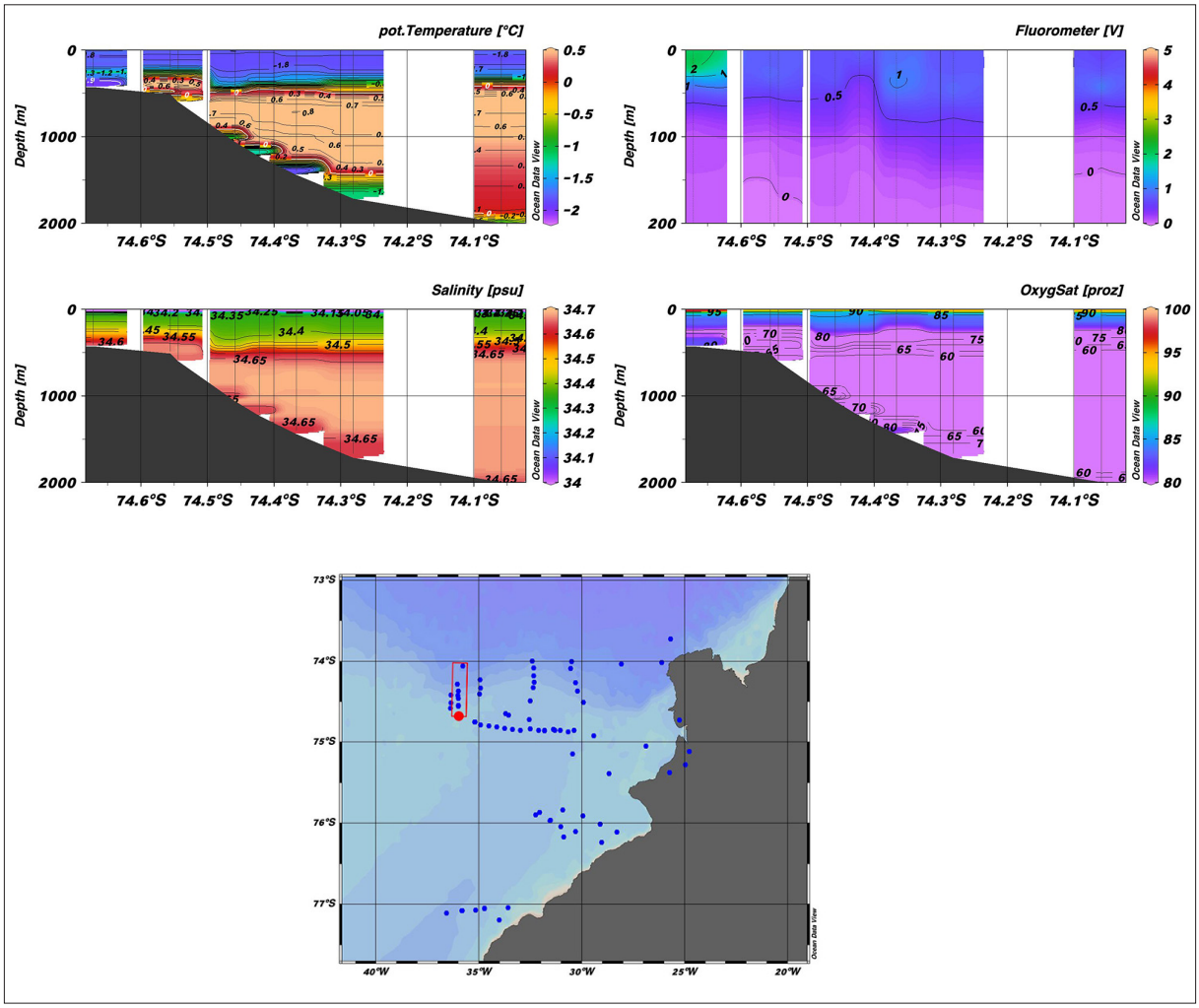

Fig. 3.6: Potential temperature, salinity, fluorescence (upper 200 m), and oxygen saturation along 36°W vs. depth, as indicated on the map

Overall, we could not clearly identify any new bottom water export pathways during PS124. Perhaps these may be found further west of the region surveyed during this expedition or were missed due to periodicity in the flow structure. Dense water export at 36° W was also observed in earlier surveys and was explained by topographic steering along a ridge extending from the upper slope into the abyss. Two oceanographic moorings (SWS-D1 and SWS-W2) were deployed in this region with an emphasis on the near-bottom properties. Current velocities, measured with the ship's ADCP and the CTD-mounted LADCP, showed a strong influence of tides on the shelf, which will require thorough post-processing to extract residual flow patterns there. The strongest flow was observed expectedly at the continental slope west of Filchner Trough. There, the along-slope flow as part of the Slope Current reached up to 60 cm/s (Fig. 3.7). In agreement with the dense bottom water at 36° W, there are near-bottom currents directed northwards (i.e. downslope), which underlines the role of this location as a dense water export pathway.

In contrast to all other stations occupied during PS124, the CTD stations collected during the circumnavigation of A74 showed a well-mixed >500-m deep water column. Inside the gap between Brunt Ice Shelf and A74, the water showed salinities of 34.3 with near-constant temperatures of –1.94° C. This clearly resembles the origin of these waters from underneath Brunt Ice Shelf and raises interesting questions regarding the role of the iceberg on vertical mixing processes. For more details on preliminary results from the A74 passage see Chapter 13.

To complement the oceanographic parameters, we expect important contributions from the noble gas and anthropogenic tracers. These will be used to quantify water mass age and glacial basal melt water fractions, which will be crucial in understanding circulation time scales and improve the understanding of ocean-ice shelf-interaction, as was shown recently by Janout et al. (2021).

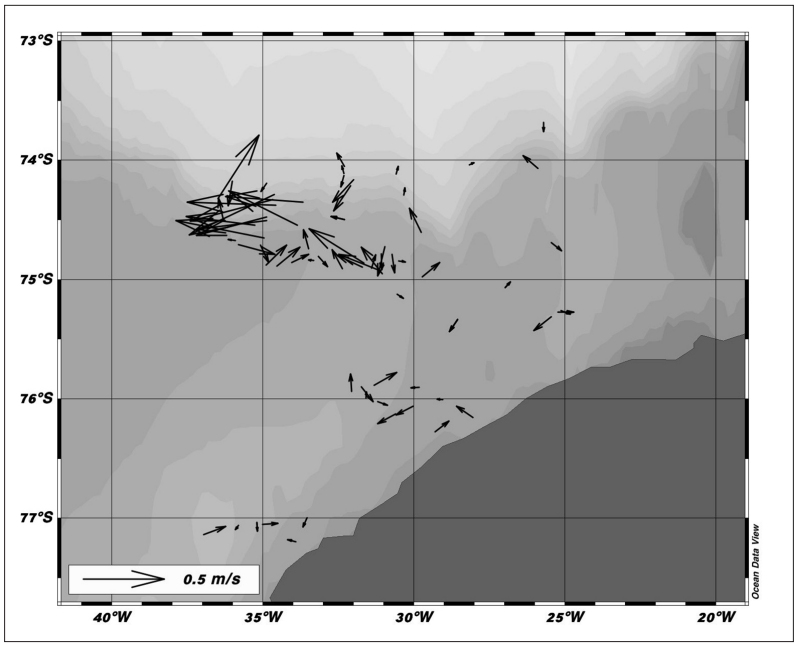

Fig. 3.7: Near-bottom current vectors measured with the LADCP during PS124 Oceanographic moorings

A total number of 16 moorings were recovered from different focus regions on the shelf, providing either 3 or 4 years of new data. The regions include: 1) the continental shelf break; 2) Filchner Sill at 75° S; 3) eastern Filchner Trough at 76° S.

The shelf break moorings

Temperature records from moorings M3 and M6 show high variability on daily and seasonal to interannual timescales. The thermocline depth increases from around 350 m in summer to 700 m in winter, in agreement with previous observations (e.g. Årthun et al. 2012; Semper & Darelius 2017). The seasonal signal is not symmetric; the temperature maximum is reached in late February/early March, followed by a rapid decrease to minimum temperatures in May to July and a slow increase again to the next maximum to complete the cycle. The rapid drop in temperature coincides with an increase in the along-slope current. The highest temperatures are observed in 2018. The mean currents are aligned with the slope, and show a mean, along-slope current of about 0.1 m/s. Both records show a strong tidal signal, which is dominated by counter-clockwise and cross-slope motion. The 35 h-oscillation described in Jensen et al (2013) is apparent in the records, albeit with a slightly shorter period. The diurnal and 35 h-signal

is strongest during the summer months, and they bring about large variability (on the same timescale) in temperature. It has been suggested that the enhanced tides during summer are caused by seasonal resonance of diurnal coastal trapped waves (Semper & Darelius 2017). There is a seasonal signal in velocity, which is most prominent at M6. The mean along-slope velocity here is at its maximum during April to June (about 0.2 m/s) and decreases to a minimum (below 0.05 m/s) from September to October. The seasonal signal in velocity at M3 is similar, but the amplitude is smaller.

The 76° S moorings

The temperature and salinity records from the eastern flank of Filchner Trough at 76° S previously showed strong variability with seasonal mWDW inflows, generally occurring in late austral summer (Ryan et al. 2017). In 2017, the inflow was longer and carried warmer water than during the first part of the record (2013 – 2016), which was explained by the density structure at the continental slope and by upstream ocean properties (Ryan et al. 2020). With the successful recovery of these moorings during PS124, we added three years to the record, which now allow to gain new insights into the complex dynamics of this region. Following the warm anomalies of 2017, waters in 2018 were even warmer featuring maximum temperatures of –0.5° C throughout the record (Fig. 3.8). Interestingly, 2019 and 2020 inflows were colder again at levels comparable to those of the years 2013–2016. Besides the mWDW inflow, these moorings further feature the episodic near-bottom occurrence of ISW (<–2.0° C). However, while temperatures in the first half of the record reached below –2.0° C only episodically, the years 2018–2020 show very cold waters permanently, but temperatures stayed above –2.0° C afterwards. This is particularly apparent in the westernmost mooring (AWI254) (Fig. 3.8). The detailed CTD transects carried out in February 2018 (PS111) already showed an enhanced ISW presence in Filchner Trough. These findings were attributed to enhanced sea ice production in the southwest Weddell Sea, which enhanced the circulation underneath FRIS and led to greater export of ISW out of the FIS cavity (Janout et al. 2021). Hence, at first evaluation the updated mooring records are consistent with the PS111 observations and will provide time scales regarding the impact of enhanced ISW export events.

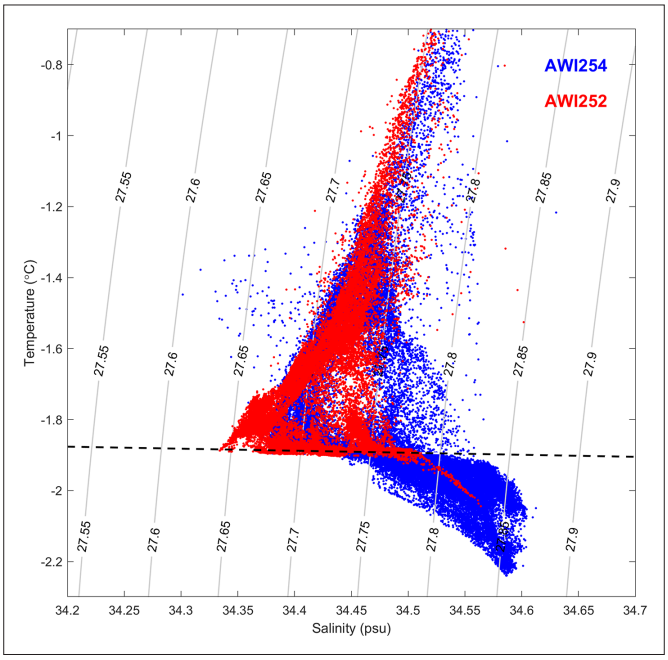

Fig. 3.8: Temperature-salinity-diagram from AWI-moorings 252 (red) and 254 (blue) for the years 2018–2021

The Filchner Sill moorings

As was shown in the 75° S-CTD transect (Fig. 3.5), the Filchner Sill-region is dominated by the inflow of mWDW around 31° W and the outflow of cold waters derived from glacially modified HSSW further west. Preliminary analysis of these mooring records show similar conditions as indicated by the 76° S-moorings. In particular; the ISW-presence after 2018 is a prominent feature indicating that the large ISW volume found during PS111 indeed had a larger impact in Filchner Trough with likely consequences on dense water production and export at the continental slope. The second remarkable feature in the sill-records, besides the strong ISW presence, is the particularly strong mWDW inflow in 2018, which appears to be a strong signal in all moorings across the focus region. However, these subjects will require detailed and collaborative investigations of all datasets collected during PS124.

Autonomous floats

All six APEX floats were registered in near-real time with OceanOPS (https://www.ocean-ops.org/board?t=argo=). For now, they maintain this status as the appropriate decoder is still under development. In parallel, a near-real time data processing chain was established at AWI, which updates information on our operational floats in 6-hour intervals, allowing an early inspection of data recorded so far. Float AWI124-1 (8880) was deployed to the east of Elephant Island on the shallow eastward extension of the Antarctic Peninsula. As of now, it delivered 15 CTD profiles and, as intended, roughly remained in the deployment area (Fig. 3.9).

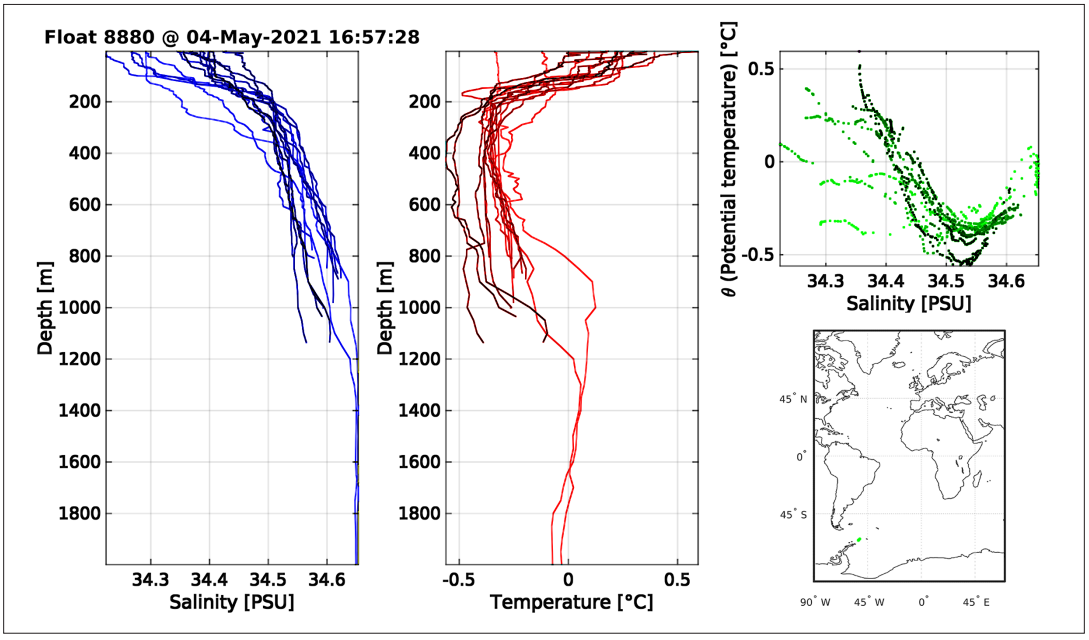

Fig. 3.9: First transmitted profiles of float PS124-1 as obtained by the real-time data processing chain implemented at AWI; darker hues represent older profiles

An extended surface period prior to profile #6 resulted in greater horizontal displacements. Commencing with profile #6 surface periods became minimized in time, resulting in a quasi-stationary float. The longer periods near the surface had been caused by a stagnant pressure reading during the time it takes to extend the piston from its virtual parking depth of 2,000 m to 1,000 m where the float was grounded. The float falsely interpreted its situation as being stuck under an iceberg. This commanded the float not to inflate the air bladder near the surface

hence interfering with satellite communication, which therefore triggered an ice descent/ ascent cycle followed by successful surfacing of the float. While the software bug remains to be fixed, we implemented a temporary fix by setting the “InitialPistonNudge” to 2,000 and the “PistionNudge” to 200. This way, the float extends the piston quickly, avoiding to reach the “HitIce”-timeout during the ascent phase. Floats PS124-2 through PS124-6 did not transmit any records yet expectedly, since the ice sensing algorithm should prevent the floats’ ascents to the sea surface due to the prevailing near-freezing surface temperatures. Considering the often harsh sea-ice conditions in the region, it is expected the floats will not transmit profiles before austral summer 2023 or even 2024.

In contrast to the APEX floats, the ice-tethered system deployed in Atka Bay transmits temperature and salinity data in 30-minute intervals (Fig. 3.10) and thus allows real time monitoring of the hydrographic conditions under the Atka Bay landfast ice. In April 2021, the minimum near-bottom temperatures were –1.95° C and thus below the surface freezing temperature, which indicates the contribution of glacially-modified water. Since the second half of April, water column temperatures are uniform and near the freezing point (Fig. 3.10), coincident with a steady increase of salinity (not shown). Increasing salinities and near-freezing ocean temperatures result from enhanced sea-ice formation in Atka Bay, and associated to that, enhanced brine expulsion into the water column. As the ice-tethered system is expected to transmit data for more than one year, these records may provide new insights regarding potential warm water inflows or Ice Shelf Water outflows to and from Ekström Ice Shelf, respectively.

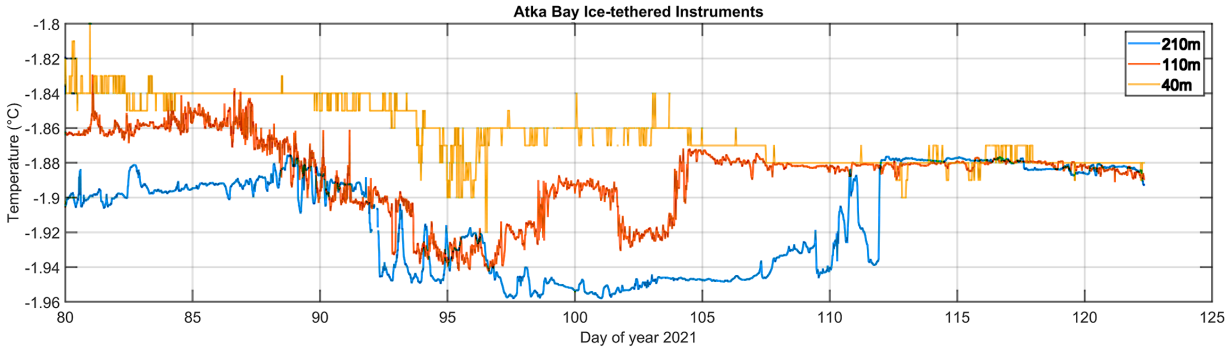

Fig. 3.10: Time series of Atka Bay ocean temperatures (°C) at 40 m (yellow), 110 m (red) and 210 m (blue line) recorded by the ice-tethered Pacific Gyre buoy system

Data management

Environmental data will be archived, published and disseminated according to international standards by the World Data Center PANGAEA Data Publisher for Earth & Environmental Science (www.pangaea.de) within two years after the end of the cruise at the latest. By default the CC-BY license will be applied.

Any other data will be submitted to an appropriate long-term archive that provides unique and stable identifiers for the datasets and allows open online access to the data.

In all publications, based on this cruise, the **Grant No. AWI_PS124_03** will be quoted and the following *Polarstern* article will be cited:

Alfred-Wegener-Institut Helmholtz-Zentrum für Polar- und Meeresforschung. (2017). Polar Research and Supply Vessel POLARSTERN Operated by the Alfred-Wegener-Institute. Journal of large-scale research facilities, 3, A119. https://dx.doi.org/10.17815/jlsrf-3-163.

Soon after the end of the expedition, a final calibration of the hydrographic data will be done using standard procedures. The preparation of the CFC samples as well as the analysis and accurate quality control will be carried out in the labs of the IUP Bremen. Once published, all data sets will be transferred to data archives such as PANGAEA Data Publisher for Earth & Environmental Science (www.pangaea.de) or send to the German Oceanographic Data Center (DOD), where they are available for the international scientific community. PANGAEA guarantees long-term storage of the data in consistent formats and provides open access to data after publication.

References

Årthun M, et al. (2012) Seasonal Inflow of Warm Water onto the Southern Weddell Sea Continental Shelf, Antarctica. Geophysical Research Letters 39(17): L17601.

Darelius E, Sallee J-B (2018) Seasonal outflow of ISW from the Filchner Ice Shelf cavity. Geophys. Res. Lett., 45(8), 3577-3585, https://doi.org/10.1002/2017GL076320.

Foldvik A, Gammelsrod T, Osterhus S, Fahrbach E, Rohardt G, Schröder M, Nicholls KW, Padman L, Woodgate RA (2004) Ice shelf water overflow and bottom water formation in the southern Weddell Sea. J. Geophys. Res. 109(C02015), doi:10.1029/2003JC002008.

Hellmer HH, Kauker F, Timmermann R, Determann J, Rae J (2012) Twenty-first-century warming of a large Antarctic ice-shelf cavity by a redirected coastal current. Nature, 485, 225–228.

Hellmer HH, Kauker F, Timmermann R, Hattermann T (2017) The fate of the southern Weddell Sea continental shelf in a warming climate. J. Clim., 30, 4337–4350, doi:10.1175/JCLI-D-16-0420.1.

Janout M, Hellmer HH, Hattermann T, Huhn O, Sültenfuss J, Osterhus S, Stulic L, Ryan S, Kanzow T (2021) FRIS revisited in 2018: On the circulation and water masses along the Filchner and Ronne Ice Shelves in the southern Weddell Sea, J. Geophys. Res. Oceans, doi:10.1002/essoar.10506824.1.

Jensen MF, Fer I, Darelius E (2013) Low frequency variability on the continental slope of the southern Weddell Sea. J. Geophys. Res., 118, 4256–4272, https://doi.org/10.1002/jgrc.20309.

Ryan S, Hattermann T, Darelius E, Schröder M (2017) Seasonal cycle of hydrography on the eastern shelf of the Filchner Trough, Weddell Sea, Antarctica. J. Geophys. Res, 122, 6437–6453, https://doi.org/10.1002/2017JC012916.

Ryan S, Hellmer HH, Janout M, Darelius E, Vignes L, Schröder M (2020) Exceptionally Warm and Prolonged Flow of Warm Deep Water Toward the Filchner-Ronne Ice Shelf in 2017. Geophys. Res. Lett., 47(13), https://doi.org/10.1029/2020GL088119.

Schaffer J, Timmermann R, Arndt JE, Kristensen SS, Mayer C, Morlighem M, Steinhage D (2016) A global, high-resolution data set of ice sheet topography, cavity geometry, and ocean bathymetry. Earth System Science Data, 8, 543–557, https://doi.org/10.5194/essd-8-543-2016.

Semper S, Darelius E (2017) Seasonal Resonance of Diurnal Coastal Trapped Waves in the Weddell Sea, Antarctica. Ocean Science, 13, 77–93.

Timmermann R, Hellmer HH (2013) Southern Ocean warming and increased ice shelf basal melting in the twenty-first and twenty-second centuries based on coupled ice-ocean finite-element modelling, Ocean Dynamics, 63(9), 1011–1026, https://doi.org/10.1007/s10236-013-0642-0.

Timmermann R, Goeller S (2017) Response to Filchner-Ronne Ice Shelf cavity warming in a coupled ocean-ice sheet model–Part 1: The ocean perspective. Ocean Science, 13, 765–776, https://doi.org/10.5194/os-13-765-2017.

4. SEALS AND OCEANOGRAPHY AT THE FILCHNER-RONNE SHELF ECOSYSTEM (SEAROSE)

Mia Wege[1,2], Elin Darelius[3], Hartmut H. Hellmer[1], Horst Bornemann[1]

[1]DE.AWI
[2]ZA.UP
[3]NO.UIB

Grant No. AWI_PS124_04

Outline

Seals and oceanography at the Filchner-Ronne shelf ecosystem (SEAROSE) is an element integrated within the oceanographic investigations of *Polarstern's* COSMUS expedition (*cf* Chapters 1 and 3). SEAROSE instrumented Weddell seals (*Leptonychotes weddellii*) with Conductivity, Temperature, Depth (CTD) Satellite Relay Data Loggers (SRDL) around the Filchner Trough. This region requires a new inventory of the spreading of Ice Shelf Water (ISW) and related deep and bottom water formation, and the westward continuation of the Antarctic Slope Front. The region is comparatively data deficient and instrumented seals can provide *in-situ* hydrographic data along their tracks to fill this gap – particularly during winter. Ancillary sampling to investigate the seal's health status, diet and potential microplastic ingestion were collected opportunistically. The expedition also extended data collected during PS82 (2013/2014) and PS111 (2018) on the distribution of seals over the ice-covered southern continental shelf. A dedicated small-scale seal census survey provided a ground truthing opportunity to compare the occurrence of seals based on counts derived from visual observations by helicopter with those derived from algorithm-based detection of seals on high-resolution satellite images.

4.1 Instrumentation of Weddell seals

Mia Wege[1,2], Elin Darelius[3], Hartmut H. Hellmer[1], Horst Bornemann[1]

[1]DE.AWI
[2]ZA.UP
[3]NO.UIB

Objectives

We deployed CTD-SRDLs on Weddell seals (*Leptonychotes weddellii*) in the pack ice to get data on the seals' foraging behaviour and concurrent hydrographic data over the continental shelf break and slope, west of the Filchner Trough sill. Satellite tracked Weddell seals spend comparatively more time in the wider area of the Filchner Trough (Nicholls et al. 2008; Årthun et al. 2012; Nachtsheim et al. 2019; Photopoulou et al. 2020). Satellite tracking of marine mammals in the Southern Ocean relies on the ARGOS system, and ARGOS-linked satellite transmitters for marine mammals are designed to provide the animals' at-sea locations and transmit data to the satellites when the animals surface. CTD-combined ARGOS satellite-relayed dive loggers (SRDL) have the capability to record *in-situ* water temperature and conductivity for the entire migration of tracked seals. The data is of suitable quality to characterise the oceanographic settings used by seals (e.g., Nicholls et al. 2008; Boehme et al. 2009; Meredith et al. 2011), and is complementary to the oceanographic investigations described in Chapter 3. Devices

are deployed on the seals' heads after completion of their annual moult and they will shed the tags again the following year during the annual moult resulting in satellite tracks and concurrent behavioural and hydrographic data to be collected over a year. Weddell seals can dive deeper than 1,200 m (Photopoulou et al. 2020) and to the seafloor, and profile the entire water column. Furthermore, their foraging dives also provide indirect information on potential pelagic and demersal or benthic prey.

Work at sea

We used helicopter flights ahead of the *Polarstern* steaming direction within the pack-ice areas to locate Weddell seals for temporary capture and instrumentation (see Tab. 4.2 and Fig. 4.1). Flights were preferably between 10:00 – 15:00 local apparent time, because seals are most likely hauled out on the ice floes during this time.

Ten CTD-SRDLs (Sea Mammal Research Unit, St-Andrews, UK) were deployed on adult male and female Weddell seals after they completed their annual moult (Tab. 4.1; Fig. 4.1).

Seals were anaesthetized following the methods as described in Bornemann and Plötz (1993) and Bornemann et al. (1998). Drugs were initially administered intramuscularly by remote injection using blow-pipe darts. Follow-up doses were usually given intramuscularly by direct manual injection or, in rare cases, intravenously. The dose regime consisted of a ketamine/ xylazine combination. Depending on the course of the immobilisation, dosages were individually adjusted and complemented by the same drug to maintain or deepen the immobilisation if considered necessary. The benzodiazepine diazepam was available to attenuate muscle tremors typically induced by ketamine. Atipamezol was used to reverse the xylazine component in the xylazine/ketamine immobilisation. Doxapram was exclusively reserved to stimulate breathing in the case of extended periods of apnoea, when mechanical obstructions of the upper airways could be excluded.

The CTD-SRDLs were glued to the top of the immobilised animals' heads using a quick setting epoxy resin. A 30 mL blood sample, hair, whiskers, standard length and girth measurements were also collected from the individuals (Tab. 4.1). Blood samples were centrifuged on board (2,000 rpm at 25 min), separated in red blood cells and serum and both deep frozen at -20 °C. Scats and naturally regurgitated vomitus were collected opportunistically. Associated oceanographic and meteorological data using the *Polarstern* on-board automated recording system DSHIP (WERUM, FRG) were also recorded.

Tab. 4.1 and 4.2 and Fig. 4.1 provide overviews on instrumentation procedures and sampling sites.

Tab. 4.1: Data on instrumentation procedures of Weddell seals (*Leptonychotes weddellii*) with satellite tags and sampling during expedition PS124

Event label	Date/Time [UTC]	Latitude	Longitude	Mass (est.)	Length	Girth	Duration	Instrumentation		Sampling		
a = adult, m = male, f = female				[kg]	[mm]	[mm]	[hh:min]	PTT Nr.	Tag body Nr.	Whiskers	Hair	Blood
FIL2021_ wed_a_f_01	2021-02-14 T16:50	-75.667	-34.430	380	2550	1800	1:05	203011	15281	x	x	
FIL2021_ wed_a_f_02	2021-02-17 T15:45	-75.656	-35.894	420	2800	1950	1:00	203012	15282	x	x	
FIL2021_ wed_a_f_03	2021-02-19 T14:00	-74.749	-34.788	380	2510	1780	1:00	203013	15283	x	x	
FIL2021_ wed_a_f_04	2021-02-22 T11:23	-74.425	-36.981	300	2470	1750	1:02	203015	15285	x	x	
FIL2021_ wed_a_f_05	2021-02-22 T15:10	-74.400	-37.045	400	2560	1870	1:05	203019	15286	x	x	
FIL2021_ wed_a_m_06	2021-02-27 T14:48	-75.039	-35.678	380	2360	1980	1:00	203016	15269	x	x	x
FIL2021_ wed_a_m_07	2021-03-04 T17:00	-75.294	-31.154	380	2670	1840	1:00	203018	15287	x	x	x
FIL2021_ wed_a_f_08	2021-03-08 T13:35	-76.644	-37.669	380	2220	1770	1:15	203017	15289	x	x	x
FIL2021_ wed_a_f_09	2021-03-11 T15:24	-74.705	-25.282	480	2900	2100	1:26	203021	15270	x	x	x
FIL2021_ wed_a_m_10	2021-03-11 T16:43	-74.705	-25.282	380	2490	1750	1:27	203020	15271	x	x	x
FIL2021_ wed_a_m_11	2021-02-23 T12:07	-74.055	-35.780	350	n.a.	n.a.	1:30	n.a.	n.a.			
FIL2021_ wed_a_f_12	2021-02-25 T15:10	-74.467	-36.332	380	n.a.	n.a.		n.a.	n.a.			

Tab. 4.2: Data on additional sampling during expedition PS124

Sample no.	Location no.	Date	Latitude	Longitude	Ice type	Scat	Vomitus
1	1	2021-02-14	-75.667	-34.430	ice floe	x	
2	2	2021-02-19	-74.749	-34.788	ice floe	x	
3	3	2021-02-22	-74.425	-36.981	ice floe	x	
4	4	2021-02-22	-74.400	-37.045	ice floe	x	
5	5	2021-02-24	-74.233	-33.550	ice floe	x	
6	6	2021-02-25	-74.510	-35.350	ice floe	x	
7	6	2021-02-25	-74.510	-35.350	ice floe	x	
8	7	2021-02-27	-75.014	-35.667	ice floe	x	
9	8	2021-02-27	-75.039	-35.678	ice floe	x	
10	9	2021-03-04	-75.300	-30.956	ice floe	x	
11	10	2021-03-04	-75.294	-31.154	ice floe	x	
12	11	2021-03-08	-76.644	-37.669	ice floe	x	
13	12	2021-03-11	-74.705	-25.282	fast ice	x	
14	12	2021-03-11	-74.705	-25.282	fast ice	x	
15	13	2021-03-14	-74.700	-26.201	ice floe	x	
16	13	2021-03-14	-74.700	-26.201	ice floe	x	
17	14	2021-03-18	-70.568	-8.582	fast ice	x	
18	14	2021-03-18	-70.568	-8.582	fast ice	x	
19	14	2021-03-18	-70.568	-8.582	fast ice	x	
20	14	2021-03-18	-70.568	-8.582	fast ice	x	
21	15	2021-03-18	-70.629	-8.103	fast ice	x	
22	15	2021-03-18	-70.629	-8.103	fast ice	x	
23	15	2021-03-18	-70.629	-8.103	fast ice	x	
24	15	2021-03-18	-70.629	-8.103	fast ice	x	
25	15	2021-03-18	-70.629	-8.103	fast ice		x

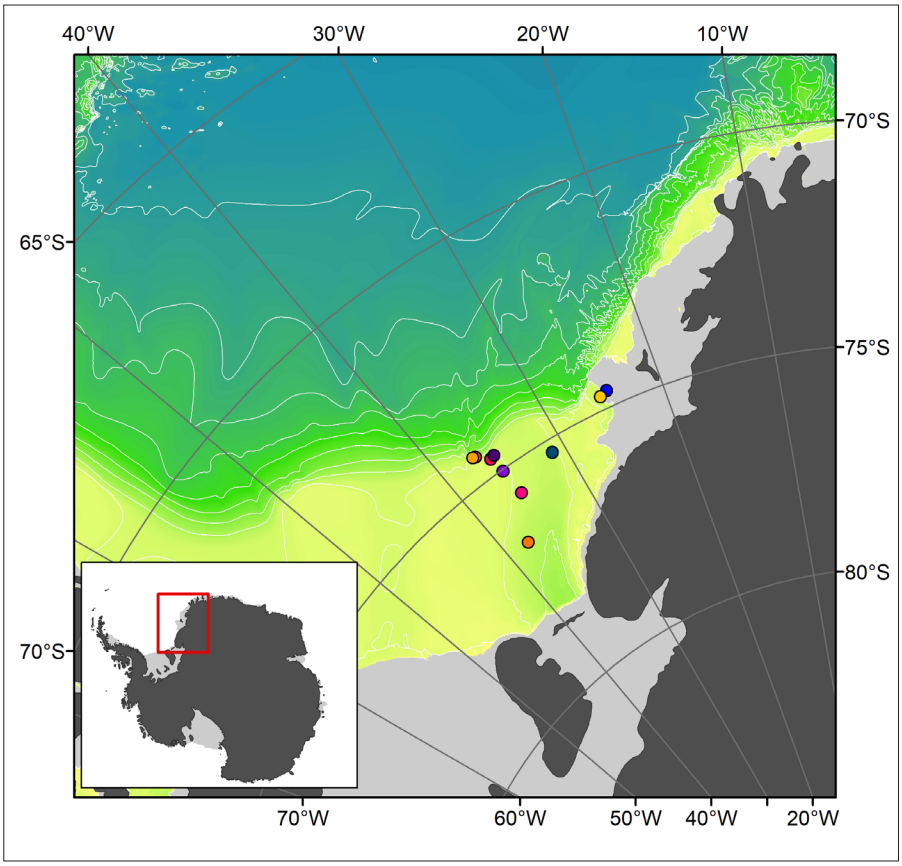

Fig. 4.1: Instrumentation sites of Weddell seals (n = 10) in the Filchner-Ronne Shelf Ecosystem during expedition PS124

Preliminary and expected results

From each of the tagged seals, we expect temperature, salinity, and depth profiles within the Filchner-Ronne Shelf Ecosystem almost in real time. These key physical oceanographic variables collected from the under-sampled coastal shelf seas may assist the refinement of coupled ocean-sea ice-ice shelf models of the Southern Ocean. In addition, the seals' movement and dive data together with its accompanying *in-situ* hydrographic information will allow us to study how changes in the underwater environment alter prey distribution beneath sea ice as indicated by the seals' individual diving and foraging behaviour when comparing data over several seasons and years. Sampling of blood and other material will provide information on the seals' prey spectrum in later laboratory analyses. The comprehensive analyses and synthesis of biological and physical data could determine relationships between hydrographic features, ocean currents, sea floor characteristics, prey dynamics, and the distribution and abundance of marine top predators. To this end we:

- equipped Weddell seals (n = 10) during the course of the expedition with CTD-SRDLs. Two tags could not be deployed after detection of technical malfunctions prior to deployment. Due to technical failures 4 tags stopped transmissions within hours or few days after deployment. In three cases batteries were removed from the epoxy-casted tags and in two cases exchanged against new ones. These two units were re-potted in polyurethane. Both units passed pressure tests and calibration casts to 1,000 m water depth hitch-hiking on the ship's CTD on board *Polarstern* and transferred data in initial satellite contacts. However, only one of the two units could be reprogrammed, while the other one was not considered be deployed since ARGOS transmissions appear to be

incomplete. A further malfunctioning tag could not be restarted and was not considered to replace the battery or deploy (Tab. 4.1, Fig. 4.1),

- collected blood (n = 5) from the animals to research their health status and diet (Tab. 4.1). Within the serum fraction of the blood samples it is possible to analyse for prey specific biomarker proteins that allow for reconciliation with the seals' prey spectrum (e.g. octopine in octopods, specific amines in fishes, homarines and dimethylsulfonio-propionate in molluscs and crustaceans) in later laboratory analyses (*cf*. Hochachka et al. 1977; Ito et al. 1994; Eisert et al. 2005; Eder et al. 2010). The data can recall the recent prey spectrum within a couple of days prior to blood sampling,
- collected hair (n = 10), and whiskers (n = 10) from the seals (Tab. 4.1). The hair and whisker samples will be used to get retrospective information on the prey spectra on intermediate time scales up to a couple of months by means of stable isotope analyses (*cf*. Lewis et al. 2006; Newsome et al. 2010; Hückstädt et al. 2012a; Hückstädt et al. 2012b; Beltran et al. 2016; Goetz et al. 2017; Brault et al. 2019; Lübcker et al. 2020).
- Furthermore, our *in-situ* collection of natural regurgitated vomitus (n = 1) and faecal samples on fast ice (n = 8) and ice floes (n = 16) at geographically different sites (n = 15) for genetic investigation of scats and vomitus (Tab. 4.2) can provide species specific hints on prey items (e.g. isopods as detected during PS96 under the ice of the Drescher Inlet; see Bornemann et al. 2016).
- Finally, our *in-situ* collection of faecal samples (n = 22) at 15 sites (Tab. 4.2) for investigations on microplastics (see Chapter 12, Holm et al.) complemented the sampling protocol.

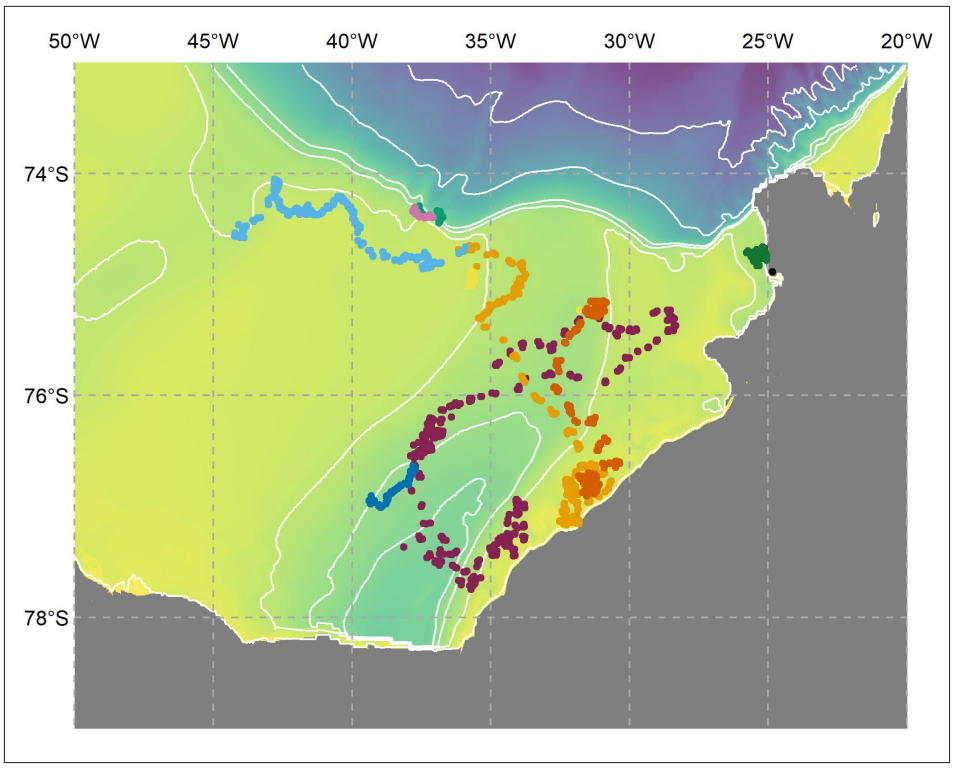

Fig. 4.2: At-sea locations of Weddell seals (n = 10) in the Filchner-Ronne Shelf Ecosystem during the first ~30 days after deployment. Different colours denote different individuals.

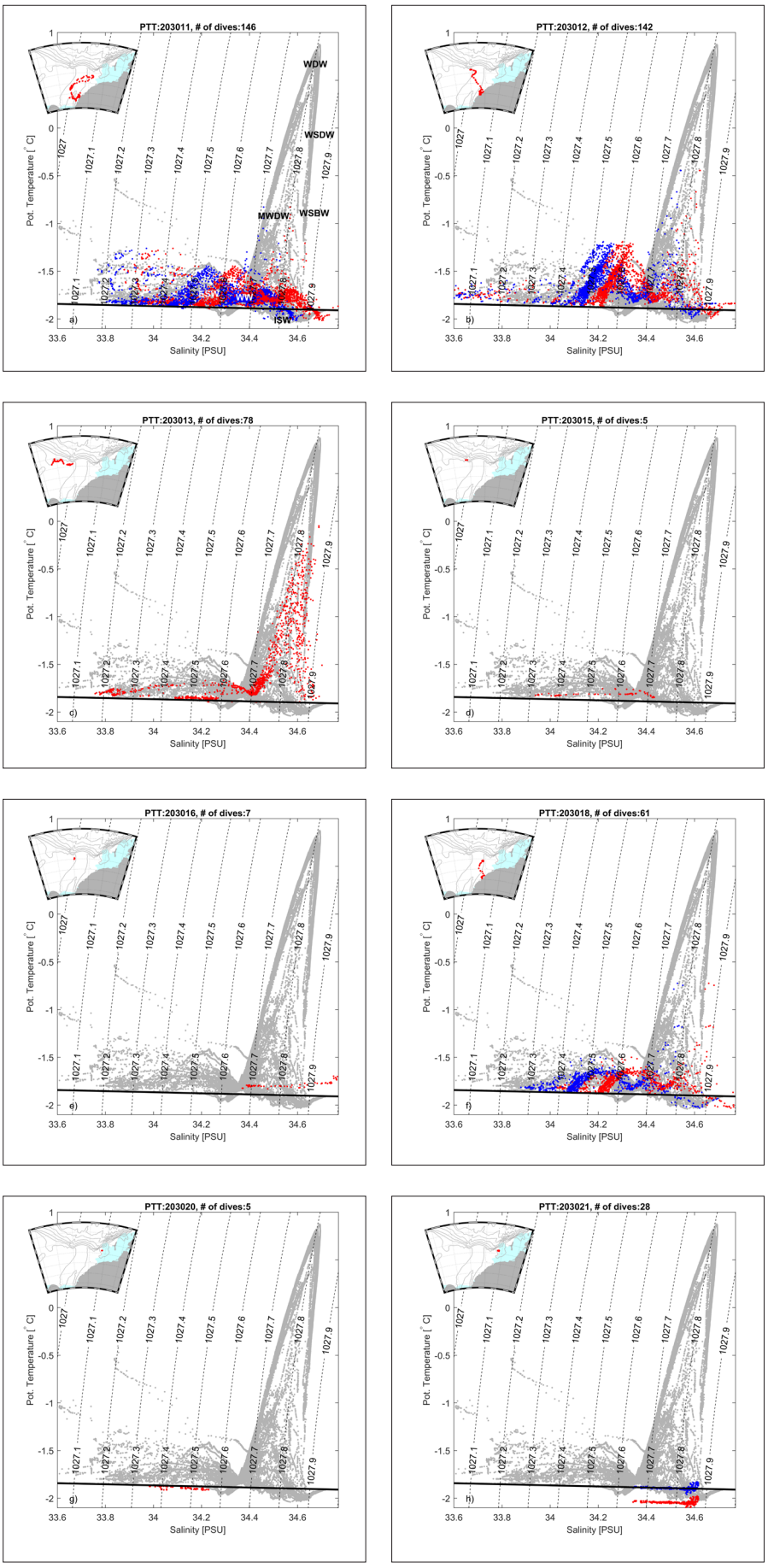

Fig. 4.3a – h: Temperature-Salinity-diagrams showing the data collected by the tagged seals (red) and seal data with the suggested, preliminary correction (blue, Tab.4.2) overlaying the (uncalibrated) data collected by the ship CTD during PS124 (grey). Dashed lines show isopycnals referenced to the surface and the black line shows the surface freezing point. The insets show the location of the dives.

Abbreviations in (a) identified water masses:
ESW – Eastern Shelf Water,
WW – Winter Water,
MWDW –Modified Warm DeepWater,
WDW – Warm Deep Water,
ISW – Ice Shelf Water,
WSDW – Weddell Sea Deep Water,
WSBW – Weddell Sea Bottom Water

Within the first ~30 days after deployment, two female seals, FIL2021_wed_a_f_01 and FIL2021_wed_a_f_02, already travelled > 1,000 km total and are > 200 km away from their deployment locations. Whereas the two animals deployed on in the fast-ice (FIL2021_wed_a_f_09 and FIL2021_wed_a_m_10) each travelled ~250 km in total, but are not more than 20 km away from their deployment locations (Fig. 4.2). Mean diving duration per individual ranged between 3.89 – 8.76 min (standard deviation: ± 3.99 – 8.05 min). The mean maximum diving depth per individual ranged between 106 – 185 m (standard deviation: ± 139 – 189 m). Keep in mind, these are averages across the entire dive record up to date, which includes shallow surface dives. The absolute maximum dive depth per individual ranged between 500 m and 725 m and maximum dive duration ranged between 26 and 29 min.

Fig. 4.3 shows the hydrography observed by the instrumented seals during the first 30 days of deployment. As expected, seals diving within the Filchner Trough observed Ice Shelf Water ($T<T_{freezing,}$ points below the black line in Fig. 4.3) while seals diving close to the continental shelf break observed Modified Warm Deep Water (see Fig. 4.3a for water mass definitions).

Several of the tags display calibration issues, as the water mass properties observed by the seals, do not match those observed by the ship's CTD. A preliminary suggestion for corrections (assuming constant offsets) are given in Tab. 4.3 but these suggestions must evidently be re-evaluated when the final CTD data set is available.

Three of the tags stopped working shortly after deployment (PTT: 203015, 203016, 203020). Only one seal (PTT: 203013) is diving in the primary target area. When we became aware of the calibration issues, we attached the remaining tags (PTT: 203017, 201318, 203021) to the CTD to attempt to re-calibrate. The tags were initially taken from room temperature and attached by cable ties and tape to the CTD-frame, but when the results were communicated to SMRU, they suggested that thermal inertia caused the deviations. The tags were subsequently stored in the 0 °C fridge for >24 h prior to new calibration casts. The tag data (upcast) were linearly interpolated to a grid with 1 dbar resolution and compared with the data from the ship's CTD (down cast). The comparison of up and down cast is evidently a source of error, but the main result – that there is a relatively large offset between the sensors – is not affected. The results of the calibration casts are shown in Fig. 4.4 and summarized in Tab. 4.4.

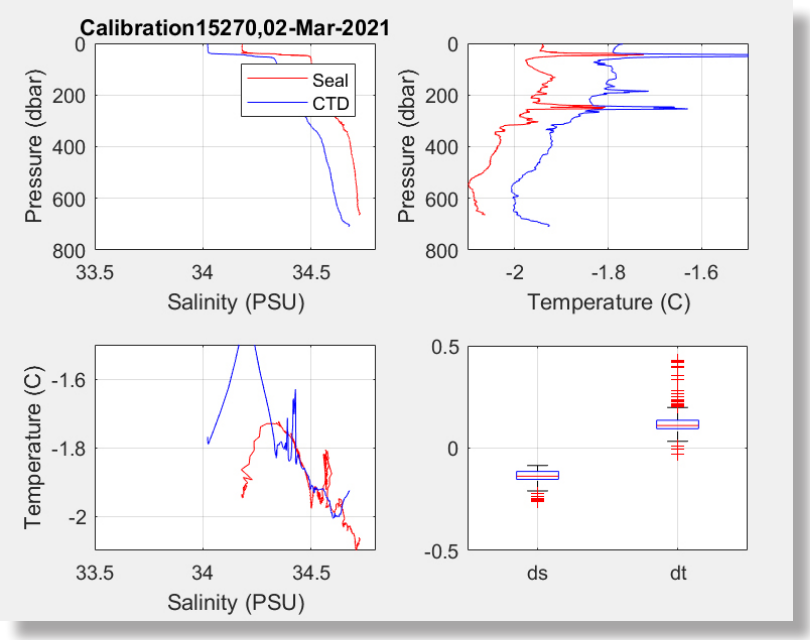

Fig. 4.4: Comparison of CTD data from tag 15270 (PTT 203021) (red) and ship CTD (blue) from calibration casts

The depth of the tag casts did not always match the depth of the CTD casts. The reason for this is evident in Tab. 4.5; when two tags were left on the CTD-frame for several consecutive casts, the data processing of the two tags merged data from two casts into one.

Tab. 4.3: Suggested corrections (preliminary) based on comparison with the cruise CTD data set. No values are given when the current data set does not allow for an estimation of the error.

PTT	Delta T [°C]	Delta S [PSU]
203011	0	-0.11
203012	0	-0.08
203013	0	0
203015	-	-
203016	-	<-0.25
203018	0	-0.13
203020	-	-
203021	0.15	< 0

Tab. 4.4: Details of and results from tag calibration on the ship CTD. The star denotes casts where data from two casts were merged in the processing. Mean values for Delta T / S are given, together with the standard deviation in parentheses.

Tag Nr.	PTT	Date	CTD cast	Cooled sensor	Delta T [°C]	Delta S [PSU]
15270	203021	2021-02-28	68_3	no	0.12 (0.02)	0.52 (0.01)
		2021-03-04	81_1	yes	0.13 (0.02)*	-0.14 (0.02)*
		2021-03-05	83_1	yes	0.13 (0.01)	-0.17 (0.01)
15287	203018	2021-02-28	68_3	no	0.00 (0.01)	0.40 (0.00)
15289	203017	2021-03-04	81_1	yes	-0.06 (0.04)*	0.09 (0.02)*
		2021-03-05	83_1	yes	-0.05 (0.02)	0.07 (0.02)

Tab. 4.5: Extracts from the data collected during the calibration casts for two of the tags. Data were downloaded directly from the tag. The red frames highlight were the processing has merged two casts into one.

Tag Nr.	Date	Time [UTC]	Pressure [dbar]	Temperature [°C]	Salinity [PSU]
15289	2021-03-04 22:02	22:02	264.60	-1.773	34.209
	2021-03-04 22:02	22:02	263.67	-1.773	34.209
	2021-03-04 22:02	22:02	262.73	-1.772	34.209
	2021-03-05 02:42	2:42	261.83	-1.771	34.208
	2021-03-05 02:42	2:42	260.93	-1.771	34.210
	2021-03-05 02:42	2:42	260.00	-1.771	34.210
15270	2021-03-04 22:02	22:02	266.37	-1.962	34.450
	2021-03-04 22:02	22:02	265.40	-1.961	34.450
	2021-03-04 22:02	22:02	264.50	-1.962	34.452
	2021-03-05 02:41	2:41	263.57	-1.964	34.453
	2021-03-05 02:41	2:41	262.63	-1.962	34.451
	2021-03-05 02:41	2:41	261.77	-1.963	34.453

Data management

Satellite linked CTD-SRDL tags (Sea Mammal Research Unit, St Andrews, UK) transmit signals to the polar orbiting ARGOS satellites which relay received signals via the Centre de Localisations Satellites (CLS) in Toulouse, France, where the location data undergo a precision filtering algorithm before they are being harvested for further manufacturer-specific processing and user accessed downloads. FIELAX (Bremerhaven, Germany), will further process and aggregate data on a monthly basis following an established work-flow. All immobilisation, instrumentation and tracking data, and its related meta-information will be made available as open access via the Data Publisher for Earth & Environmental Science PANGAEA (https://www.pangaea.de), and will be attributed to the project label "Marine Mammal Tracking" (https://www.pangaea.de/search?q=project:label:mmt) within two years after the end of the cruise. By default, the CC-BY license will be applied. After publication, data will be shared with the GOOS network Animal Borne Ocean Sensors (AniBOS; http://anibos.com/), the IPY follow-up programme Marine Mammals Exploring the Oceans Pole to Pole (MEOP; http://www.meop.net/), and Movebank (www.movebank.org).

Molecular data will be archived, published and disseminated within one of the repositories of the International Nucleotide Sequence Data Collaboration (INSDC, www.insdc.org) comprising of EMBL-EBI/ENA, GenBank and DDBJ). For archival of data on results of microplastic analyses of the seal scats see Chapter 12 (Holm et al.).

4.2 Helicopter operation and seal survey

Mia Wege[1,2], Elin Darelius[3], Hartmut H. Hellmer[1], Christiaan Oosthuizen[2] (not on board), Marthán N. Bester[2] (not on board), Horst Bornemann[1]

[1]DE.AWI
[2]ZA.UP
[3]NO.UIB

Objectives

We used flights from *Polarstern* into pack-ice covered areas to locate Weddell seals for temporary capture and instrumentation (see Chapter 4.1 for details) and for an aerial seal census survey. Census survey data will act as ground truthing data for seal presence estimates from very high resolution (VHR) satellite imagery.

Historically, methods used for seal census surveys were highly variable (e.g. ship vs. helicopter-based, time of the year surveyed, size of the area covered etc.), which restricts the comparability of data among different surveys. To ensure that new surveys are comparable with earlier surveys, we used the same methods applied in the only seal census data set that is available for the Weddell Sea. This data set was generated by Bester and Odendaal (1999, 2000) from aboard *Polarstern* in 1998 during the multinational circum-Antarctic wide Antarctic Pack Ice Seal (APIS) Programme of SCAR (Southwell et al. 2012; Gurarie et al. 2017), and is comparable with earlier seal surveys that were done in the eastern Weddell Sea by Bester et al. (1995; *cf*. Erickson et al. 1993). Methodologically congruent surveys were conducted at the Filchner Outflow System during *Polarstern* expedition PS82 in 2014 (Bester et al. 2014; Oosthuizen et al. in revision).

Data on marine top predator abundance and distribution are key for the design and management of Marine Protected Areas (MPA), e.g. the Weddell Sea MPA (*cf*. Teschke et al. 2020). Despite being the greatest consumers of krill and fish in the Southern Ocean, our understanding of the status and trends of pack-ice seal populations and their relationship with key habitat characteristics, such as sea ice, still represents a major knowledge gap, and until now, it has

been logistically too challenging and expensive to do regular pack-ice seal surveys at a spatial scale sufficient for assessing their abundance and distribution even on regional scale. As a result, the chance for an analysis or even an estimate of trends against earlier seal counts made in only small longitudinal sectors of the Southern Ocean between 1960s and 1990s are nil. A concerted international effort is needed to accurately count pack-ice seals around the entire continent.

VHR satellite imagery is increasingly used to count and map the distributions of animal populations from space (e.g.) "Censusing of Animal Population from Space" (CAPS) is an international, integrated Southern Ocean Observing System (SOOS) initiative that will facilitate and develop the use of VHR satellite imagery to provide population status data for Antarctic seals with its SCAR related APIS II reassessment. The interpretation of satellite images requires a ground truthing in order to reconcile observer-based counts and image data taken by aircrafts or helicopters and satellites on spatially and temporally synchronous tracks. This reconciliation allows to develop algorithms for the identification of seal specific differences in contours, brightness and contrasts for automated image analysis, and hence allows to determine the detection probability for seals in automated image analyses.

Work at sea

All flights used *Polarstern's* BK117-C1 twin engine helicopters *D-HAOE* and *D-HAPS* (Alfred-Wegener-Institut Helmholtz-Zentrum für Polar- und Meeresforschung 2017). Because COSMUS scientific work was mainly in open water and areas of very low sea ice concentrations, priority was given to deploy the Conductivity, Temperature, Depth (CTD) Satellite Relay Data Loggers (SRDL) on Weddell seals over seal census flights for satellite ground truthing. In total, we flew 30:46 h of which 18:30 were flown in transit and 12:16 h in search to find seals. The transits accumulated to 3,133 km plus another 1,215 km search distance. We landed 80 times, either on ship or land. Tab. 4.6 provides an overview over all helicopter operations.

Tab. 4.6: Summary of helicopter flights flown for ice and seal reconnaissance and surveying during expedition PS124

	Flight time	Search time	Flight dist.	Search dist.	Landing
	[dd:hh:mm]	[hh:mm]	[km]	[km]	[n]
SUM	01:06:46	00:12:16	3133.46	1214.91	80.00
MIN	0:09	0:05	1.49	9.26	1.00
MAX	1:44	1:20	218.55	177.79	6.00
MEDIAN	0:35	0:20	54.88	28.71	1.00
MEAN	0:40	0:26	68.12	43.39	1.74
SD	0:22	0:17	59.05	39.50	1.25

Reconnaissance flights from aboard Polarstern

Deployments of CTD-SRDLs were prioritised over the continental shelf break and slope west of the Filchner Trough sill. This required long outbound flights relative to the ship's position in search for adult Weddell seals dispersed throughout the pack ice. Tab. 4.7 (see end of Chapter) provides an overview of all reconnaissance flights flown to deploy tags and sample animals (*cf.* Chapter 4.1). The flight path for the following day was planned during the helicopter briefing every evening 20:15, and flight orders signed during the weather briefing at 08:15 the following morning before the flight operation. Seals mostly haul out in the afternoon (haulout maximum 12:00 – 13:00 local apparent time [LAT]) and flights preferentially were scheduled for between approximately

11:00 and 16:00 LAT. The core investigation area west of the Filchner Trough is located *ca.* UTC -3 h and the flights were scheduled between 14:00 and 19:00 UTC. Whenever Weddell seals were sighted from the helicopter and after landing approached by foot, Weddell seals were discriminated as pups, juveniles or adults.

Overview of all reconnaissance flights flown to deploy tags in synchrony with the sampling protocol during expedition PS124 are listed in Table 4.7 at the end of this chapter.

Helicopter survey from aboard Polarstern

The satellite ground truthing flights require a combination of preconditions rarely found on an Antarctic research expedition. For the seal census survey flight we require meteorological appropriate flight weather conditions (ceiling ≥500 ft, visibility ≥3,000 m, daylight), flight distance for a predefined ice covered survey area within the helicopter range (≤80 nm ≈ 148 km), while keeping the cumulative distance of the survey grid within the operational flight time of ~1:45 h, and a high seal abundance. For the satellite image we require a cloud free sky and concurrent satellite availability. We communicated our survey area of interest to the satellite image provider Maxar, USA, a day in advance allowing them to prepare the image settings.

Seals were spotted by two observers through sighting bars attached to the windows on each side of the helicopter; the one on the left at the front seat, the one on the right at the back seat of the helicopter. The goal was to see every seal and get its coordinates that would correspond to its location on the satellite image; we therefore created two bins corresponding to 100 m and 200 m distance from the observer. At a flying height of 60 m, the 100 m and 200 m bins are calculated at 59.0° and 73.3° vertical angles, respectively. Physical check marks on the sighing bars delineate a virtual census strip denoted as a bin when being projected on the ice (*cf*. Bester et al. 2014). The obscured area beneath the helicopter was 50 m to the side of the helicopter for both observers. Given that our goal was to identify every seal, the front observer, which was assisted by the pilot, could identify every seal approaching from the front and announce it to the observer in the back. If needed the helicopter made a turn around the animal to identify the animal. This allowed us to eliminate the 50 m obscured bin underneath the helicopter.

To calibrate the sighting bars for each observer, the helicopter flew over flagged marker poles that were laid out on ice along the 50 m, 100 m and 200 m bin distances. This calibration flight (flight no. PS124.4) was made at the beginning of the expedition (2021-02-10; see Tab. 4.7).

Under ideal weather conditions, up to 10 transects of up to 120 min duration each would have been flown at a height of 200 feet (~60 m) and at a velocity of 60 knots (~110 km/h) over sea ice. These settings known from earlier line transect studies can reliably identify seals on species level. However, the aforementioned preconditions coincided only once during the entire cruise (flight no PS124.53 on 2021-03-17). Seal sightings were logged with a handheld GPS (Garmin GPSmap 62s) during the flight, which records date, time and location of each sighting. Seal species were recorded along with the GPS waypoints.

Preliminary and expected results

Reconnaissance flights from aboard Polarstern

The primary purpose of the flights was to spot Weddell seals on sea ice for the deployment of CTD-SRDLs, sampling of whiskers, hair, blood, scats and naturally regurgitated vomitus (see Chapter 4.1). Tab. 4.7 provides an overview over all reconnaissance operations during the helicopter operations. The number of adult Weddell seals spotted on ice flows was very low.

Only 10 singletons were spotted in the pack ice, and groups of Weddell seals were located during the two visits on fast ice (see Tab. 4.8, end of chapter). We, furthermore, observed Weddell seal pups and juveniles in loose aggregations around cracks and ice holes on large drifting ice flows in comparatively high numbers (Tab. 4.8). In total, we counted 78 Weddell seals considered as pup or juvenile. The size of the aggregations varied between 1 and 6 with a Median of 1 and a Mean of 1.7.

Overview of all seal observations during expedition PS124 are listed in Table 4.8 at the end of this chapter.

Helicopter survey from aboard Polarstern

The only census flight survey was on 2021-03-17 (flight no PS124.53, see Tab. 4.6) between 17:20 and 19:04 UTC. We flew 12 transects of 18 nm (33.3 km), spaced by 1.5 nm (2.8 km) covering an area of 27 nm^2 (93 km^2). Fig. 4.5 shows the survey grid. We sighted ten crabeater seals (*Lobodon carcinophaga*), no Weddell seals (*Leptonychotes weddellii*), one Leopard seal (*Hydrurga leptonyx*) and one Ross seal (*Ommotophoca rossii*). Tab. 4.9 provides a summary of the survey flight operation. Mapping and reconciling observer-based detections of seals on ice with those spotted on satellite images provides ground truthing data to train algorithms for automated detections of seals on large-scale image series.

Tab. 4.9: Summary on the locations and number of seals species observed on helicopter survey flight for satellite ground truthing during PS124

Leg	Latitude	Longitude	Latitude	Longitude	Distance	Time	Velocity	Comment	Ice type
	Start	Start	End	End	[km]	Start	[kts]		[#]
0	-70.502	-8.188	-70.223	-8.525	33.39	17:20	60	PS Start	Pack ice 9/10
1	-70.223	-8.525	-70.505	-8.457	31.40	17:31	60		Pack ice 9/10
2	-70.505	-8.457	-70.498	-8.385	2.76	17:45	60		Pack ice 9/10
3	-70.498	-8.385	-70.222	-8.460	30.87	17:50	60		Pack ice 9/10
4	-70.222	-8.460	-70.220	-8.387	2.76	18:05	60		Pack ice 9/10
5	-70.220	-8.387	-70.497	-8.303	30.90	18:07	60		Pack ice 9/10
6	-70.497	-8.303	-70.493	-8.233	2.62	18:18	80		Shelf Ice, pack ice 9/10
7	-70.493	-8.233	-70.218	-8.313	30.70	18:20	80		open water, Pack ice 9/10
8	-70.218	-8.313	-70.217	-8.245	2.58	18:43	80		Pack ice 9/10

Leg	Latitude Start	Longitude Start	Latitude End	Longitude End	Distance [km]	Time Start	Velocity [kts]	Comment	Ice type [#]
9	-70.217	-8.245	-70.490	-8.158	30.54	18:45	80		Pack ice 9/10
10	-70.490	-8.158	-70.502	-8.188	1.71	18:59	80	PS End	Pack ice 9/10

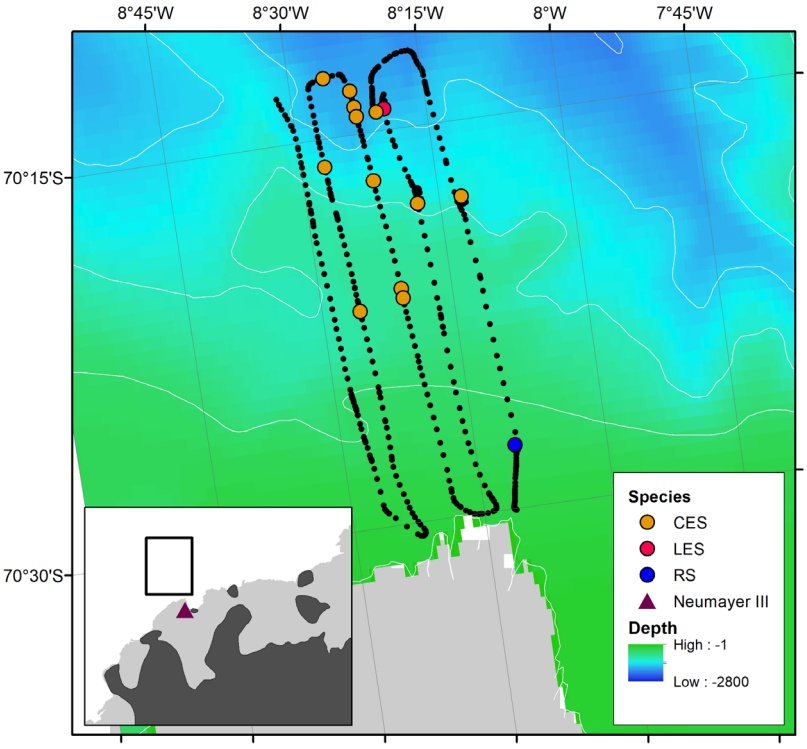

Fig 4.5: Survey grid flown on 2021-03-17 T17:20 –– 2021-03-17 T19:04. The dotted line denotes the flight track. Seals spotted on the ice are denoted as coloured dots, where: CES = Crabeater seal, LES = Leopard seal, RS = Ross seal.The position of Neumayer Station III is also shown.

Data management

All data and related meta-information will be made available in open access via the Data Publisher for Earth & Environmental Science PANGAEA (www.pangaea.de), and will be attributed to a consistent project label denoted as “Marine Mammal Tracking” (MMT, see https://www.pangaea.de/search?q=project:label:mmt).

Acknowledgements

We thank captain Stefan Schwarze and the entire crew of the *Polarstern*, the helicopter pilots and technicians of the *D-HAOE* and *D-HAPS* helicopters Carsten Zillgen, Sebastien Drach, Willem Stenssen and Elena Prieto Turienzo as well as Steffen Schröter, Frank Otte and Christian Rohleder from the Deutscher Wetterdienst for their dedicated and enthusiastic support during the entire expedition PS124 of *Polarstern*.

References

Alfred-Wegener-Institut Helmholtz-Zentrum für Polar- und Meeresforschung (2017) Polar Research and Supply Vessel POLARSTERN Operated by the Alfred-Wegener-Institute. Journal of large-scale research facilities, 3, A119. http://dx.doi.org/10.17815/jlsrf-3-163.

Årthun M, Nicholls KW, Makinson K, Fedak MA, Boehme L (2012) Seasonal inflow of warm water onto the southern Weddell Sea continental shelf, Antarctica. Geophysical Research Letters, 39, L17601.

Beltran RS, Conolly Sadou MC, Condit R, Peterson SH, Reichmuth C, Costa DP (2015) Fine-scale whisker growth measurements can reveal temporal foraging patterns from stable isotope signatures. Marine Ecology Progress Series, 523, 243-253.

Bester MN, Erickson AW, Ferguson JWH (1995) Seasonal change in the distribution and density of seals in the Weddell Sea, Antarctica, during March 1986. Polar Biology, 12, 635-644.

Bester MN, Oosthuizen WC, Steinhage D, Bornemann H (2014) Abundance and distribution of seals, pp 116-125 in Knust R, Schröder M (eds) The Expedition PS82 of the Research Vessel POLARSTERN to the southern Weddell Sea in 2013/2014, Berichte zur Polar- und Meeresforschung = Reports on polar and marine research, Bremerhaven, Alfred Wegener Institute for Polar and Marine Research, 680, 155 p.

Bester MN, Odendaal PN (1999) Abundance and distribution of Antarctic pack ice seals in the Weddell Sea. In: Arntz WE & Gutt J (eds) The Expedition ANTARKTIS XV/3 (EASIZ II) of "*Polarstern*" in 1998. Berichte zur Polarforschung, 301, 102-107.

Bester MN, Odendaal PN (2000) Abundance and distribution of Antarctic pack ice seals in the Weddell Sea. In: Davison W, Howard-Williams C & Broady P (eds) Antarctic Ecosystems: Models for Wider Ecological Understanding, Caxton Press, Christchurch, pp 51-55.

Boehme L, Lovell P, Biuw M, Roquet F, Nicholson J, Thorpe SE, Meredith MP, Fedak M (2009) Technical Note: Animal-borne CTD-Satellite Relay Data Loggers for real-time oceanographic data collection. Ocean Science, 5, 685-695.

Bornemann H, Mohr E, Plötz J, Krause G (1998) The tide as *zeitgeber* for Weddell seals, Polar Biology, 20, 396-403.

Bornemann H, Plötz J (1993) A field method for immobilizing Weddell seals, Wildlife Society Bulletin, 21, 437-441.

Bornemann H, Held C, Nachtsheim D, Owsianowski N, Richter C, Steinmetz R. Seal research at the Drescher Inlet (SEADI), pp 116 - 129 in Schröder M (ed) The Expedition PS96 of the Research Vessel POLARSTERN to the southern Weddell Sea in 2015/2016, Berichte zur Polar- und Meeresforschung = Reports on polar and marine research, Bremerhaven, Alfred Wegener Institute for Polar and Marine Research, 700, 142 p.

Brault EK, Koch PL, Costa DP, McCarthy MD, Hückstädt LA, Goetz KT, McMahon KW, Goebel ME, Karlsson O, Teilmann J, Harkonen T, Harding KC (2019) Trophic position and foraging ecology of Ross, Weddell and crabeater seals revealed by compound-specific isotope analysis. Marine Ecology Progress Series, 611, 1-18.

Eder EB, Lewis MN, Campagna C, Koch PL (2010) Evidence of demersal foraging from stable isotope analysis of juvenile elephant seals from Patagonia. Marine Mammal Science, 26, 430-442.

Eisert R, Oftedal OT, Lever M, Ramdohr S, Breier BH, Barrell GK (2005) Detection of food intake in a marine mammal using marine osmolytes and their analogues as dietary biomarkers. Marine Ecology Progress Series, 300, 815-825.

Erickson AW, Siniff DB, Cline DR, Hofman RJ (1971) Distributional ecology of Antarctic seals, paper presented at Symposium on Antarctic ice and water masses, SCAR, Cambridge, Tokyo, Japan, 19 September 1970, pp 55-76.

Gurarie E, Bengtson JL, Bester MN, Blix AS, Bornemann H, Cameron M, Nordøy ES, Plötz J, Steinhage D, Boveng P (2017) Distribution, density and abundance of Antarctic ice seals in Queen Maud Land and the eastern Weddell Sea. Polar Biology, 40(5), 1149-1165.

Goetz K, Burns JM, Hückstädt LA, Shero MR, Costa DP (2017) Temporal variation in isotopic composition and diet of Weddell seals in the western Ross Sea. Deep-Sea Research II, 140, 36–44.

Hochachka PW, Hartline PH, Fields JHA (1977) Octopine as an end product of anaerobic glycolysis in the chambered nautilus. Science, 195, 72-74.

Hückstädt LA, Burns JM, Koch PL, McDonald BI, Crocker DE, Costa DP (2012a) Diet of a specialist in a changing environment: the crabeater seal along the Western Antarctic Peninsula. Marine Ecology Progress Series, 455, 287-301.

Hückstädt LA, Koch PL, McDonald BI, Goebel ME, Crocker DE, Costa DP (2012b) Stable isotope analyses reveal individual variability in the trophic ecology of a top marine predator, the southern elephant seal. Marine Ecology Progress Series, 455, 287-301.

Ito Y, Suzuki T, Shirai T, Hirano T (1994) Presence of cyclic betaines in fish. Comparative Biochemistry and Physiology B, 109, 115-124.

Lewis R, O'Connell TC, Lewis M, Campagna C, Hoelzel AR (2006) Sex-specific foraging strategies and resource partitioning in the southern elephant seal (*Mirounga leonina*). Proceedings of the Royal Society B-Biological Sciences, 273, 2901-2907.

Lübcker N, Bloemb LM, du Toit T, Swart P, de Bruyn PJN, Swart AC, Millar RP (2020) What's in a whisker? High-throughput analysis of twenty-eight C_{19} and C_{21} steroids in mammalian whiskers by ultra-performance convergence chromatography-tandem mass spectrometry. Journal of Chromatography B 1141 (2020) 122028.

Meredith MP, Nicholls KW, Renfrew IA, Boehme L, Biuw M, Fedak M (2011) Seasonal evolution of the upper-ocean adjacent to the South Orkney Islands, Southern Ocean: Results from a ''lazy biological mooring''. Deep-Sea Research II, 58, 1569-1579.

Newsome SD, Clementz MT, Koch PL (2010) Using stable isotope biogeochemistry to study marine mammal ecology. Marine Mammal Science, 26, 509-572.

Nachtsheim DA, Ryan S, Schröder M, Jensen L, Oosthuizen WC, Bester MN, Hagen W, Bornemann H. Foraging behaviour of Weddell seals (*Leptonychotes weddellii*) in connection to oceanographic conditions in the southern Weddell Sea. Progress in Oceanography, 173, 165-179.

Nicholls KW, Boehme L, Biuw M, Fedak MA (2008) Wintertime ocean conditions over the southern Weddell Sea continental shelf, Antarctica. Geophysical Research Letters, 35, L21605.

Oosthuizen WC, Reisinger RR, Bester MN, Steinhage D, Auel H, Flores H, Knust R, Ryan S, Bornemann H (2020) Spatial modelling of pack-ice seal density in the southern Weddell Sea, Antarctic. Marine Ecology Progress Series, in review.

Photopoulou T, Heerah K, Pohle J, Boehme L (2020) Sex-specific variation in the use of vertical habitat by a resident Antarctic top predator. bioRxiv preprint doi: https://doi.org/10.1101/2020.06.15.152009, version June 26, 2020, 23pp.

Southwell C, Bengtson J, Bester MN, Shytte Blix A, Bornemann H, Boveng P, Cameron M, Forcada J, Laake J, Nordøy E, Plötz J, Rogers T, Steinhage D, Stewart B, Trathan P (2012) A review of data on abundance, trends in abundance, habitat utilisation and diet for Antarctic ice-breeding seals. CCAMLR Science, 19, 49-74.

Teschke K, Pehlke H, Siegel V, Bornemann H, Knust R, Brey T (2020) An integrated data compilation for the development of a marine protected area in the Weddell Sea. Earth System Science Data, 12:1003-1023.

Tab. 4.7: Overview of all reconnaissance flights flown to deploy tags in synchrony with the sampling protocol during expedition PS124

Flight no.	Date	Time Start [UTC]	Time End [UTC]	Latitude Start	Longitude Start	Latitude Target	Longitude Target	Latitude End	Longitude End	Flight time [hh:mm]	Search time [hh:mm]	Flight dist. [km]	Search dist. [km]	Landing [n]	Ice type [#]	Mission [#]
PS124.4	2021-02-10	15:42	17:00	-73.040	-22.788	-73.040	-22.788	-73.167	-22.615	1:18		15		2	ice floe	CAPS survey calibration
PS124.7	2021-02-12	10:21	11:31	-74.913	-29.417	-75.003	-33.017	-74.953	-29.445	1:10	0:30	207	37	1	ice floe	Reconnaissence
PS124.9	2021-02-14	15:38	16:30	-75.143	-30.446	-75.667	-34.430	-75.667	-34.430	0:52	0:24	126	30	1	ice floe	FIL2021_ WED_a_f_01 outbound
PS124.9	2021-02-14	18:30	19:15	-75.667	-34.430	-75.667	-34.430	-75.143	-30.448	0:45		126		1	ice floe	FIL2021_ WED_a_f_01 inbound
PS124.12	2021-02-16	14:31	15:14	-74.867	-30.598	-74.484	-35.265	-74.484	-35.265	0:43	0:12	143	15	1	ice floe	Reconnaissence outbound
PS124.12	2021-02-16	15:42	16:05	-74.484	-35.265	-74.595	-35.376	-74.595	-35.376	0:23	0:20	13	28	1	ice floe	Reconnaissence outbound
PS124.12	2021-02-16	16:50	17:35	-74.595	-35.376	-74.870	-35.598	-74.852	-31.901	0:45		139		2	ice floe	Reconnaissence inbound
PS124.12	2021-02-16	19:12	20:33	-74.855	-31.832	-74.870	-35.598	-74.855	-31.833	1:21		219		2	ice floe	Reconnaissence inbound
PS124.13	2021-02-17	13:06	14:34	-74.849	-32.114	-75.656	-35.894	-75.656	-35.894	1:28	0:45	139	56	2	ice floe	FIL2021_ WED_a_f_02 outbound
PS124.13	2021-02-17	16:35	17:00	-75.656	-35.894	-75.656	-35.894	-74.866	-32.991	0:25		120		1	ice floe	FIL2021_ WED_a_f_02 inbound
PS124.17	2021-02-19	12:12	12:58	-74.915	-29.420	-74.700	-35.772	-74.700	-35.772	0:46	0:30	186	37	3	ice floe	Reconnaissence outbound

Flight no.	Date	Time Start [UTC]	Time End [UTC]	Lati-tude Start	Longi-tude Start	Lati-tude Target	Longi-tude Target	Lati-tude End	Longi-tude End	Flight time [hh:mm]	Search time [hh:mm]	Flight dist. [km]	Search dist. [km]	Land-ing [n]	Ice type [#]	Mission [#]
PS124.17	2021-02-19	13:30	13:52	-74.700	-35.772	-74.646	-35.846	-74.646	-35.846	0:22	0:24	6	30	1	ice floe	FIL2021_ WED_a_f_03 outbound
PS124.17	2021-02-19	15:38	15:51	-74.646	-35.846	-74.749	-34.788	-74.749	-34.788	0:13		33		1	ice floe	FIL2021_ WED_a_f_03 inbound
PS124.19	2021-02-22	10:12	11:41	-74.365	-36.544	-74.425	-36.981	-74.425	-36.981	1:29	0:15	14	46	6	ice floe	FIL2021_ WED_a_f_04 outbound
PS124.19	2021-02-22	13:02	13:40	-74.367	-35.949	-74.425	-36.981	-74.415	-36.371	0:38		50		2	ice floe	FIL2021_ WED_a_f_04 inbound
PS124.19	2021-02-22	14:28	14:50	-74.415	-36.369	-74.400	-37.045	-74.400	-37.045	0:22	0:15	12	46	1	ice floe	FIL2021_ WED_a_f_05 outbound
PS124.19	2021-02-22	16:55	17:04	-74.400	-37.045	-74.400	-37.045	-74.417	-36.373	0:09		20		1	ice floe	FIL2021_ WED_a_f_05 inbound
PS124.23	2021-02-22	11:18	11:58	-74.058	-35.790	-74.121	-35.832	-74.121	-35.832	0:40	0:20	9	22	3	ice floe	FIL2021_ WED_a_m_11* outbound
PS124.23	2021-02-23	14:27	14:50	-74.121	-35.832	-74.121	-35.832	-74.121	-35.832	0:23		9		2	ice floe	FIL2021_ WED_a_m_11* inbound
PS124.28	2021-02-25	13:28	14:12	-74.687	-33.548	-74.445	-36.302	-74.445	-36.302	0:44	0:20	86	28	1	ice floe	Reconnaissence outbound
PS124.28	2021-02-25	14:32	14:53	-74.445	-36.302	-74.441	-36.254	-74.441	-36.254	0:21	0:15	1	19	1	ice floe	FIL2021_ WED_a_f_12* outbound

Flight no.	Date	Time Start [UTC]	Time End [UTC]	Latitude Start	Longitude Start	Latitude Target	Longitude Target	Latitude End	Longitude End	Flight time [hh:mm]	Search time [hh:mm]	Flight dist. [km]	Search dist. [km]	Landing [n]	Ice type [#]	Mission [#]
PS124.28	2021-02-25	16:13	16:44	-74.441	-36.254	-74.467	-36.332	-74.467	-36.332	0:31	0:25	4	28	5	ice floe	FIL2021_ WED_a_f_12* inbound
PS124.28	2021-02-25	17:17	17:43	-74.467	-36.332	-74.722	-33.667	-74.722	-33.667	0:26		84		1	ice floe	Reconnaissence inbound
PS124.30	2021-02-26	13:18	14:31	-74.648	-33.714	-74.877	-34.945	-74.877	-34.945	1:13	1:05	44	130	1	ice floe	Reconnaissence outbound
PS124.30	2021-02-26	14:36	15:08	-74.877	-34.945	-74.943	-34.993	-74.943	-34.993	0:32	0:40	7	93	2	ice floe	Reconnaissence
PS124.30	2021-02-26	15:17	15:29	-74.943	-34.993	-74.943	-34.993	-74.699	-33.548	0:12		50		1	ice floe	Reconnaissence inbound
PS124.31	2021-02-27	12:54	13:43	-74.851	-31.456	-74.854	-31.834	-74.851	-31.456	0:49	0:45	22	93	4	ice floe	Reconnaissence
PS124.31	2021-02-27	13:43	14:41	-74.851	-31.456	-75.039	-35.678	-75.039	-35.678	0:58	0:20	124	22	1	ice floe	FIL2021_ WED_a_m_06 outbound
PS124.31	2021-02-27	16:24	17:20	-75.039	-35.678	-75.015	-35.664	-75.015	-35.664	0:56	0:45	3	83	6	ice floe	Reconnaissence
PS124.31	2021-02-27	18:04	18:42	-75.015	-35.664	-74.734	-31.383	-74.734	-31.383	0:38		128		1	ice floe	FIL2021_ WED_a_m_06 inbound
PS124.34	2021-03-01	13:39	14:05	-76.047	-31.019	-75.608	-34.217	-75.608	-34.217	0:26		100		1	ice floe	Reconnaissence outbound
PS124.34	2021-03-01	14:10	14:28	-75.608	-34.217	-75.597	-34.262	-75.597	-34.262	0:18	0:35	2	11	1	ice floe	Reconnaissence
PS124.34	2021-03-01	15:15	15:38	-75.597	-34.262	-75.597	-34.262	-75.964	-31.538	0:23	0:10	85	56	1	ice floe	Reconnaissence inbound
PS124.37	2021-03-04	15:10	16:02	-76.100	-30.400	-75.293	-30.956	-75.293	-30.956	0:52	0:15	91	19	2	ice floe	Reconnaissence
PS124.37	2021-03-04	16:28	16:46	-75.293	-30.956	-75.294	-31.154	-75.294	-31.154	0:18	0:12	6	15	1	ice floe	FIL2021_ WED_a_m_07 outbound

Flight no.	Date	Time Start [UTC]	Time End [UTC]	Lati-tude Start	Longi-tude Start	Lati-tude Target	Longi-tude Target	Lati-tude End	Longi-tude End	Flight time [hh:mm]	Search time [hh:mm]	Flight dist. [km]	Search dist. [km]	Land-ing [n]	Ice type [#]	Mission [#]
PS124.37	2021-03-04	18:35	19:01	-75.294	-31.154	-75.832	-30.933	-75.865	-30.933	0:26		64		1	ice floe	FIL2021_ WED_a_m_07 inbound
PS124.40	2021-03-07	12:14	13:00	-77.042	-34.155	-77.095	-32.442	-77.029	-33.574	0:46		72		1	ice floe	Reconnaissence
PS124.42	2021-03-08	12:31	13:16	-77.002	-36.473	-76.644	-37.668	-76.644	-37.668	0:45	0:30	50	46	2	ice floe	FIL2021_ WED_a_f_08 outbound
PS124.42	2021-03-08	15:09	15:27	-76.644	-37.668	-76.644	-37.668	-76.833	-36.189	0:18		43		2	ice floe	FIL2021_ WED_a_f_08 inbound
PS124.43	2021-03-11	14:17	15:03	-74.883	-29.283	-74.705	-25.282	-74.705	-25.282	0:46	0:05	118	9	2	fast ice	FIL2021_ WED_a_f_09 and a_m_10 outbound
PS124.43	2021-03-11	19:00	19:27	-74.705	-25.282	-74.705	-25.282	-75.232	-27.813	0:27		93		1	fast ice	FIL2021_ WED_a_f_09 and a_m_10 inbound
PS124.49	2021-03-14	11:05	11:38	-75.233	-24.850	-74.700	-25.117	-74.700	-25.117	0:33	0:19	60	19	1	fast ice	Reconnaissence outbound
PS124.49	2021-03-14	12:30	12:56	-74.700	-25.117	-74.700	-25.117	-75.233	-24.850	0:26		60		1	fast ice	Reconnaissence inbound
PS124.53	2021-03-17	17:20	19:04	-70.502	-8.188	-70.223	-8.525	-70.502	-8.188	1:44	1:20	119	178	1	ice floe	Survey: 5 legs á 18 nm, 1.5 nm spacing
PS124.55	2021-03-18	13:08	13:39	-70.501	-8.187	-70.568	-8.016	-70.568	-8.016	0:31	0:10	10	11	2	fast ice	Reconnaissence outbound
PS124.55	2021-03-18	14:13	14:28	-70.568	-8.016	-70.629	-8.107	-70.501	-8.187	0:15	0:10	22	11	2	fast ice	Reconnaissence inbound
																* incomplete immobilisations without deployments

Tab. 4.8: Overview of all seal observations during expedition PS124

Flight no.	Date	Time Start [UTC]	Time End [UTC]	Latitude Start	Longitude Start	Latitude Target	Longitude Target	Latitude End	Longitude End	Ice type [#]	Observations				
											Weddell seal adult	Weddell seal pup/juv.	Crabeater seal adult	Leopard seal adult	Ross seal adult
PS124.4	2021-02-10	15:42	17:00	-73.040	-22.788	-73.040	-22.788	-73.167	-22.615	floe					
PS124.7	2021-02-12	10:21	11:31	-74.913	-29.417	-75.003	-33.017	-74.953	-29.445	floe			x		
PS124.9	2021-02-14	15:38	16:30	-75.143	-30.446	-75.667	-34.430	-75.667	-34.430	floe	x		x		
PS124.9	2021-02-14	18:30	19:15	-75.667	-34.430	-75.667	-34.430	-75.143	-30.448	floe	x		x		
PS124.12	2021-02-16	14:31	15:14	-74.867	-30.598	-74.484	-35.265	-74.484	-35.265	floe	x	1	x		
PS124.12	2021-02-16	15:42	16:05	-74.484	-35.265	-74.595	-35.376	-74.595	-35.376	floe	x	1	x		
PS124.12	2021-02-16	16:50	17:35	-74.595	-35.376	-74.870	-35.598	-74.852	-31.901	floe			x		
PS124.12	2021-02-16	19:12	20:33	-74.855	-31.832	-74.870	-35.598	-74.855	-31.833	floe			x		
PS124.13	2021-02-17	13:06	14:34	-74.849	-32.114	-75.656	-35.894	-75.656	-35.894	floe	x		x		
PS124.13	2021-02-17	16:35	17:00	-75.656	-35.894	-75.656	-35.894	-74.866	-32.991	floe			x		
PS124.17	2021-02-19	12:12	12:58	-74.915	-29.420	-74.700	-35.772	-74.700	-35.772	floe	x	2	x		
PS124.17	2021-02-19	13:30	13:52	-74.700	-35.772	-74.646	-35.846	-74.646	-35.846	floe	x		x		
PS124.17	2021-02-19	15:38	15:51	-74.646	-35.846	-74.749	-34.788	-74.749	-34.788	floe			x		
PS124.19	2021-02-22	10:12	11:41	-74.365	-36.544	-74.425	-36.981	-74.425	-36.981	floe	x		x		
PS124.19	2021-02-22	13:02	13:40	-74.367	-35.949	-74.425	-36.981	-74.415	-36.371	floe			x		
PS124.19	2021-02-22	14:28	14:50	-74.415	-36.369	-74.400	-37.045	-74.400	-37.045	floe	x		x		
PS124.19	2021-02-22	16:55	17:04	-74.400	-37.045	-74.400	-37.045	-74.417	-36.373	floe			x		
PS124.23	2021-02-22	11:18	11:58	-74.058	-35.790	-74.121	-35.832	-74.121	-35.832	floe	x	1	x		
PS124.23	2021-02-23	14:27	14:50	-74.121	-35.832	-74.121	-35.832	-74.121	-35.832	floe	x		x		
PS124.28	2021-02-25	13:28	14:12	-74.687	-33.548	-74.445	-36.302	-74.445	-36.302	floe	x	6,1,1	x		
PS124.28	2021-02-25	14:32	14:53	-74.445	-36.302	-74.441	-36.254	-74.441	-36.254	floe	x		x		
PS124.28	2021-02-25	16:13	16:44	-74.441	-36.254	-74.467	-36.332	-74.467	-36.332	floe	x	2,1,1	x		
PS124.28	2021-02-25	17:17	17:43	-74.467	-36.332	-74.722	-33.667	-74.722	-33.667	floe	x		x		
PS124.30	2021-02-26	13:18	14:31	-74.648	-33.714	-74.877	-34.945	-74.877	-34.945	floe	x	1,1,1	x		

Flight no.	Date	Time Start	Time End	Lati-tude	Longi-tude	Lati-tude	Longi-tude	Lati-tude	Longi-tude	Ice type	Observations				
		[UTC]	[UTC]	Start	Start	Target	Target	End	End	[#]	Weddell seal adult	Weddell seal pup/juv.	Crabeater seal adult	Leopard seal adult	Ross seal adult
PS124.30	2021-02-26	14:36	15:08	-74.877	-34.945	-74.943	-34.993	-74.943	-34.993	floe	x	1,1,1, 2	x		
PS124.30	2021-02-26	15:17	15:29	-74.943	-34.993	-74.943	-34.993	-74.699	-33.548	floe			x		
PS124.31	2021-02-27	12:54	13:43	-74.851	-31.456	-74.854	-31.834	-74.851	-31.456	floe	x	3,1,5, 3	x		
PS124.31	2021-02-27	13:43	14:41	-74.851	-31.456	-75.039	-35.678	-75.039	-35.678	floe	x	1	x		
PS124.31	2021-02-27	16:24	17:20	-75.039	-35.678	-75.015	-35.664	-75.015	-35.664	floe	x	1,1,2, 2,1,1, 1	x		
PS124.31	2021-02-27	18:04	18:42	-75.015	-35.664	-74.734	-31.383	-74.734	-31.383	floe	x		x		
PS124.34	2021-03-01	13:39	14:05	-76.047	-31.019	-75.608	-34.217	-75.608	-34.217	floe	x	2,2,1, 2,1	x		
PS124.34	2021-03-01	14:10	14:28	-75.608	-34.217	-75.597	-34.262	-75.597	-34.262	floe	x		x		
PS124.34	2021-03-01	15:15	15:38	-75.597	-34.262	-75.597	-34.262	-75.964	-31.538	floe	x		x		
PS124.37	2021-03-04	15:10	16:02	-76.100	-30.400	-75.293	-30.956	-75.293	-30.956	floe	x	2,1,4,1, 2,1,2,1	x		
PS124.37	2021-03-04	16:28	16:46	-75.293	-30.956	-75.294	-31.154	-75.294	-31.154	floe	x	1	x		
PS124.37	2021-03-04	18:35	19:01	-75.294	-31.154	-75.832	-30.933	-75.865	-30.933	floe	x		x		
PS124.40	2021-03-07	12:14	13:00	-77.042	-34.155	-77.095	-32.442	-77.029	-33.574	floe					
PS124.42	2021-03-08	12:31	13:16	-77.002	-36.473	-76.644	-37.668	-76.644	-37.668	floe	x	1,4,2, 1			
PS124.42	2021-03-08	15:09	15:27	-76.644	-37.668	-76.644	-37.668	-76.833	-36.189	floe					
PS124.43	2021-03-11	14:17	15:03	-74.883	-29.283	-74.705	-25.282	-74.705	-25.282	fast ice	x		x		
PS124.43	2021-03-11	19:00	19:27	-74.705	-25.282	-74.705	-25.282	-75.232	-27.813	fast ice	x				
PS124.49	2021-03-14	11:05	11:38	-75.233	-24.850	-74.700	-25.117	-74.700	-25.117	fast ice	x		x		

Flight no.	Date	Time Start [UTC]	Time End [UTC]	Latitude Start	Longitude Start	Latitude Target	Longitude Target	Latitude End	Longitude End	Ice type [#]	Observations				
											Weddell seal adult	Weddell seal pup/juv.	Crabeater seal adult	Leopard seal adult	Ross seal adult
PS124.49	2021-03-14	12:30	12:56	-74.700	-25.117	-74.700	-25.117	-75.233	-24.850	fast ice	x				
PS124.53	2021-03-17	17:20	19:04	-70.502	-8.188	-70.223	-8.525	-70.502	-8.188	floe			x	x	x
PS124.55	2021-03-18	13:08	13:39	-70.501	-8.187	-70.568	-8.016	-70.568	-8.016	fast ice	x				
PS124.55	2021-03-18	14:13	14:28	-70.568	-8.016	-70.629	-8.107	-70.501	-8.187	fast ice	x				

5. BATHYMETRY OF THE SOUTHERN WEDDELL SEA CONTINENTAL SLOPE

Laura Hehemann[1], Ellen Werner[1], Lilian Boehringer[1]

[1]DE.AWI

Grant No. AWI_PS124_06

Objectives

Accurate knowledge of the seafloor topography, hence high-resolution bathymetry data is basic key information necessary to understand many marine processes. It is of particular importance for the interpretation of scientific data in a spatial context. Bathymetry, hence geomorphology, is furthermore a fundamental parameter for understanding the general environment setting of an area. In addition, bathymetry and bathymetry-derived products are essential to understand geological processes such as erosion, sediment transport and deposition, and for characterisation of habitats. Bathymetry can be complemented by video-graphic data and high-resolution sub-bottom data, adding the third dimension to bathymetric maps.

While global bathymetric maps suggest a detailed knowledge of worldwide seafloor topography, most of the world's ocean floor remains unmapped by hydro-acoustic systems. In these areas bathymetry is modelled from satellite altimetry with a corresponding low resolution. Satellite-altimetry derived bathymetry lacks the resolution necessary to resolve small- to meso-scale geomorphological features (e.g. sediment waves, glaciogenic features and small seamounts). Ship-borne multibeam data provide bathymetric information in a resolution sufficient to resolve those features.

Bathymetry data in combination with sub-bottom information can be used to optimise the on-site sampling strategy and support survey planning for towed equipment. For example, areas of outcropping older strata and areas of reduced or enhanced sediment accumulation can be identified.

Perennial sea-ice cover in the southern Weddell Sea renders much of the seafloor unexplored and unmapped. PS124 provided the opportunity to collect high-resolution bathymetry data and shed light on pending scientific research questions. We took the opportunity to map the unexplored area west of the Filcher Trough. Therefore, ship- and OFOBS based micro-bathymetric analyses of seafloor was performed using the ships hydro-acoustic instruments as well as multibeam and sonar systems deployed with the OFOBS.

Work at sea

Bathymetric data were recorded with the hull-mounted multibeam echosounder (MBES) Atlas Hydrosweep DS3, and sub-bottom data were recorded with the hull-mounted sediment echosounder (PARASOUND) Atlas Parasound P70. The MBES is a deep-water system for continuous mapping with the full swath potential. It operates on a frequency of ~15 kHz. On *Polarstern*, the MBES transducer arrays are arranged in a Mills cross configuration of 3 m (transmit unit) by 3 m (receive unit).

The main tasks of the bathymetry group were the collection of bathymetric data, including planning surveys during transit and at the study areas, post processing and data cleaning, and data management for on-site map creation. The raw bathymetric data was calibrated and corrected for sound velocity changes in the water column to remove systematic errors in bottom detection. Sound velocity profiles were taken from WOA13 or CTD casts when available at the site area. The data were further processed for erroneous soundings and artefacts. This high-resolution seabed and sub-bottom data were made available for site selection and cruise planning.

Data acquisition was carried out throughout the entire cruise, as long as the ship was sailing in international waters or the Antarctic EEZ. During station work, both systems were switched off. South of 60 °S, both systems were also switched off, if a marine mammal was sighted 100 m from the ship during the 15 min watch prior to the bathymetric survey start, or if a whale and calf were sighted 100 m from the ship at any point during the survey.

The MBES was operated with Atlas Hydromap Control at a frequency of ~15 kHz and for online data visualization Teledyne PDS was used. The collected bathymetry was stored as raw files in the following formats:

- PHF data in ASD, PDS and S7K format
- PHS data in ASD, PDS and S7K format

Subsequent data processing was performed using Caris HIPS and SIPS. For generating maps the data was exported to Quantum GIS in the GeoTIFF raster format 68. The technical settings of the MBES during PS124 are presented in detail in Table 5.1.

Tab. 5.1: Technical Settings of the MBES during PS124

Applied Settings	Selected Options	Selected Ranges
Mode of Operation	MBES	PHF, SHF
Frequency	PHF	~15 kHz
Pulse Length	No. of Swathes	1
	Length PHF (Inner Swath)	30.61 ms
	Length PHF (Outer Swath)	30.65 ms
Pulse Type	Frequency Modulated (Chirped)	
Transmission	Source Level	231 dB
	Voltage	126 V
Transmission Shading	Full Basis Gaussian	
Mode of Transmission	Single Pulse	Auto according to water depth
Beam Steering	Manual Ref.: V. Axis, Heading	
Beam Pattern	Beam Spacing	Equal Footprint
Swath Width	Manual	
	Port	Shelf: 120 % of Depth Deepsea: 150 % of Depth
	Starboard	Shelf: 120 % of Depth Deepsea: 150 % of Depth
Receiver Band Width	Width PHF (Inner Swath)	127 Hz
	Width PHF (Outer Swath)	127 Hz
Receiver Amplification	TVG Automatic	Gain Shift at 30 %

Applied Settings	Selected Options	Selected Ranges
Reception Shading	PHF Manual	Hamming
System Depth Source	Controlled HYDROSWEEP PHF	Fixed Min./Max. Depth Limit
Data Recording	ASD PHF	hourly files
	ASD PHS	hourly files
	S7K	hourly files

PARASOUND was also operated with Atlas Hydromap Control at two frequencies, 4 kHz secondary low or primary low frequency (SLF or PLF) and 21 kHz primary high frequency (PHF). The data were visualized in Atlas Parastore for both PHF and SLF profiles on screen with a 500 m vertical depth window. For the entire underway time of the cruise, and simultaneously with sounding, PARASOUND data files were stored for:

- PHF data in ASD format and in PS3 format (carrier frequency, lat.lon)
- SLF data in ASD format and PS3 format (carrier frequency, lat.lon)

For best survey results and correct depths, CTD (Conductivity, Temperature, Depth) profiles, collected by the Physical Oceanography group were applied to measure the water sound velocity in different depths. This is essential, as the acoustic signal travels down the water column from the transducer to the seafloor and back to the surface through several different layers of water masses with each a different sound velocity. The sound velocity is influenced by density and compressibility, both depending on pressure, temperature, and salinity. Wrong or outdated sound velocity profiles lead to refraction errors and reduced data quality.

The sound velocity profiles obtained by the CTD were immediately processed and applied within the MBES for correct beamforming during the survey. Throughout PS124 a total of 48 sound velocity profiles (SVP) were applied to the collected MBES data. 28 SVPs were retrieved from CTD casts and 20 synthetic SVPs were generated from the World Ocean Atlas 2013 (e.g. in Drake Passage). Fig. 5.1 shows the SVP-CTD casts for the main research area of the southeastern Weddell Sea.

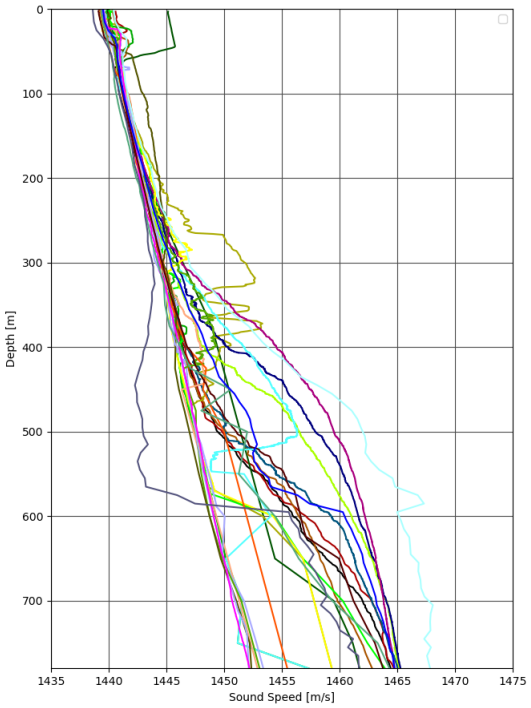

Fig. 5.1: SVP-CTD casts in the main research area exported from Sound Seed Manager

Preliminary (expected) results

MBES and PARASOUND acquisition began at the Falkland Islands 200 nm EEZ on 2021-02-04 15:36:37 until 2021-03-29 16:50:56 with a constant recording of data until the first station. The MBES was switched off during station work, and prior to turning on the MBES, a 15-minute whale watch survey was carried out. During 54 days of cruise, a track length of 6.562 nm (12.152 km) was surveyed,

covering an area of 140.973.4 km² (transit included). The raw data volume of the Hydrosweep DS3 is 922.8 GB for s7k, PDS and ASD files. Fig. 5.2 gives an overview over the collected data and the survey areas summarized in the following chapters. The collected PARASOUND P70 data is 273.7 GB for ASD and PS3 files cover the same recording track as the MBES.

In the main research area of the southeastern Weddell Sea the general data quality was high.

However, quality drops due to sea ice cover had an impact. The terrain was fairly leveled in the main research area with occasional steep slopes around the continental shelf margin. Iceberg A74 calved from the Brunt Ice Shelf during the expedition, which provided an opportunistic endeavor to extend the bathymetry survey into the corridor, as previously performed by the ANTVI/-III *Polarstern* cruise.

During the expedition, seven bathymetry surveys using the deep-sea echosounder Atlas Hydrosweep DS3 were conducted as either pre-site surveys for OFOBS dives or to fill in existing gaps in the AWI bathymetry archive data and IBCAO (International Bathymetric Chart of the Arctic Ocean) / GEBCO (General Bathymetric Chart of the Oceans) coverage, shown in Fig. 5.2. The main research area showed depths between ~200 m and 1,000 m resulting in 50 m resolution. The terrain was mainly flat with evidence of glacial scouring as depicted in Fig. 5.3. Table 5.2 lists the surveys by their surveyed number and provides details of the surveys. No station number was provided for bathymetry surveys during PS124 since, overall, most surveys were opportunistic depending on time available.

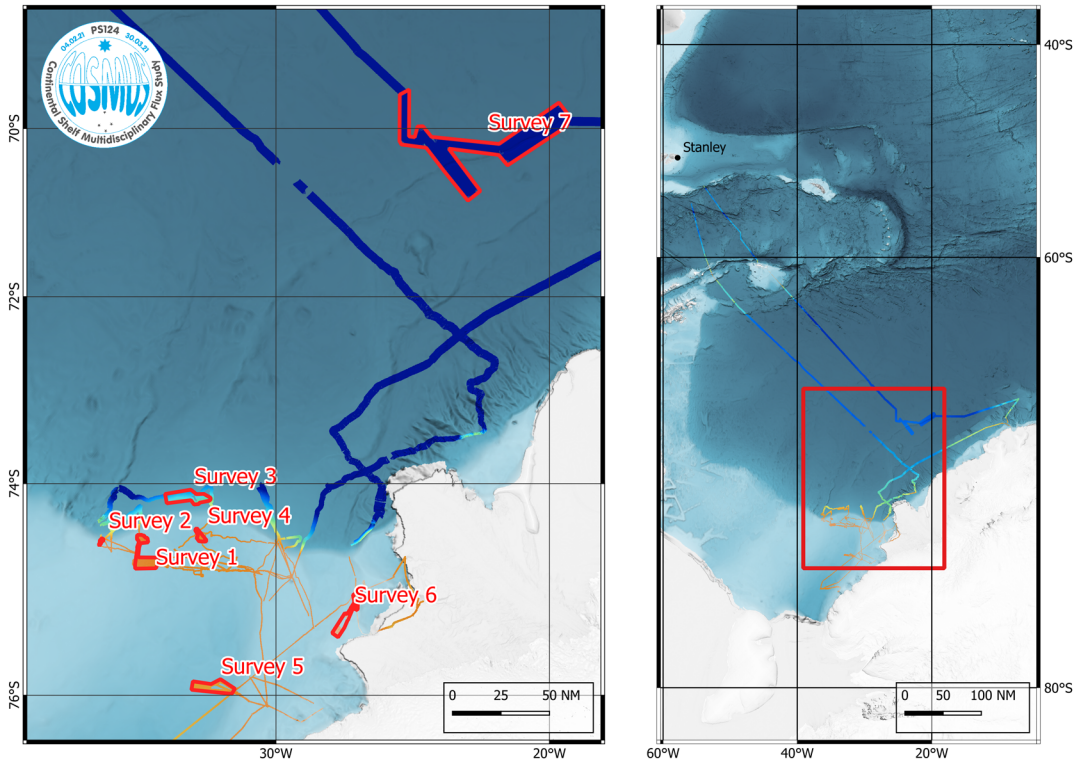

Fig. 5.2: MBES bathymetry data collected during PS124
(Left) Survey areas in the main research area
(Right) Overview of all collected data, including transit to and from the research area
Projection: World Mercator (EPSG:3395), Datum: WGS84

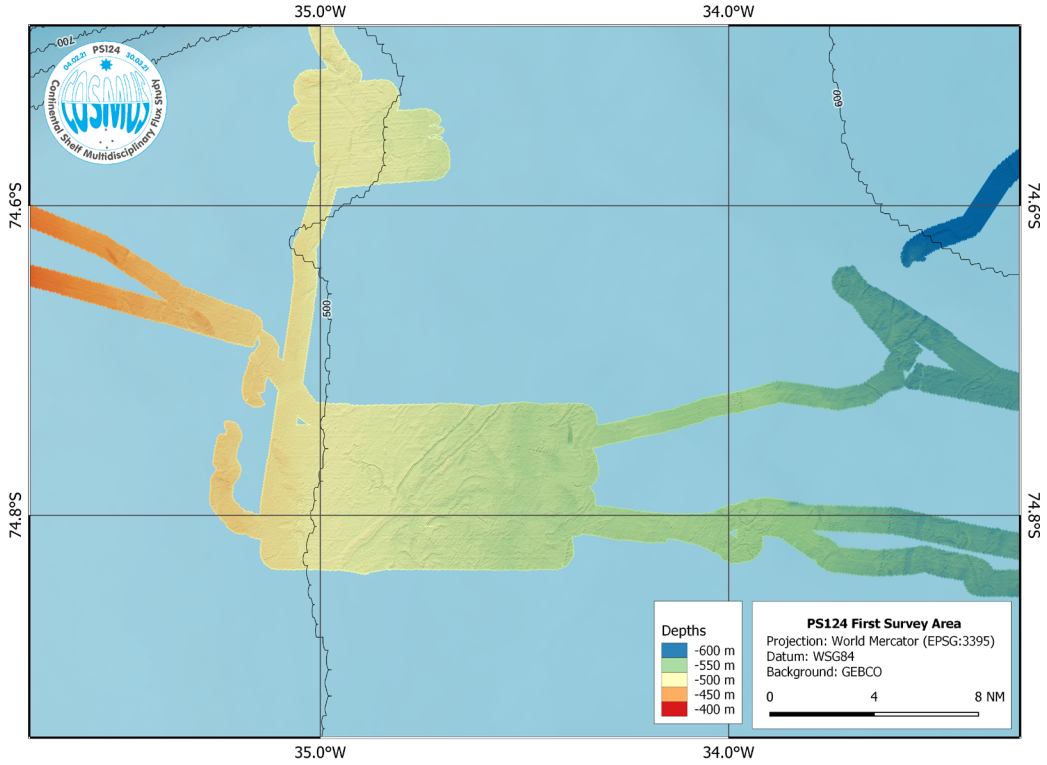

Fig. 5.3: MBES bathymetry data for Survey 1 in the main research area showing evidence of glacial scouring. Projection: World Mercator (EPSG:3395), Datum: WGS84

Table 5.2: Station details of bathymetric surveys in the southeastern Weddell Sea

Name	Start Time [UTC]	End Time [UTC]	Total Time [UTC]	Length [km]	Area [km²]	Mean Speed [kn]
Survey 1	2021-02-19 12:32:47	2021-02-20 09:04:20	18:51:35	288	393	8.23
Survey 2	2021-02-20 22:53:54	2021-02-21 00:24:10	01:30:34	19	17	6.85
Survey 3	2021-02-23 19:49:21	2021-02-24 07:17:50	11:31:47	160	515	7.18
Survey 4	2021-03-09 21:46:21	2021-03-10 05:14:39	07:30:31	94	81	6.86
Survey 5	2021-03-03 02:18:14	2021-03-03 08:18:32	06:01:56	96	377	8.61
Survey 6	2021-03-12 10:10:26	2021-03-13 08:55:56	22:52:09	323	306	7.60
Survey 7	2021-03-21 22:40:53	2021-03-23 23:41:12	49:15:27	737	8341	8.08

Data management

Bathymetric data collected during PS124 will be stored in the World Data Center PANGAEA Data Publisher for Earth & Environmental Science (www.pangaea.de) at the AWI. Furthermore, the data will be provided to mapping projects and included in regional data compilations such as IBCSO (International Bathymetric Chart of the Southern Ocean) and GEBCO (General Bathymetric Chart of the Ocean). Bathymetric data will also be provided to the Nippon Foundation – GEBCO Seabed 2030 Project. All PARASOUND data will be transferred to AWI after the cruise and stored in the data base of the IT department. Once georeferenced, the data will be linked to the data base PANGAEA for external accessibility.

In all publications, based on this cruise, the **Grant No. AWI_PS124_06** will be quoted and the following *Polarstern* article will be cited:

Alfred-Wegener-Institut Helmholtz-Zentrum für Polar- und Meeresforschung. (2017). Polar Research and Supply Vessel POLARSTERN Operated by the Alfred-Wegener-Institute. Journal of large-scale research facilities, 3, A119. http://dx.doi.org/10.17815/jlsrf-3-163.

6. SEA ICE GEOPHYSICS AND BIOCHEMISTRY

Christian Haas[1], Stefanie Arndt[1], Ilka Peeken[1],
Sarah L. Eggers[1], Mara Neudert[1]
Not on board: Juliane Müller[1], Jutta Wollenburg[1],
Georgi Laukert[2], Thomas Schweder[3]

[1]DE.AWI
[2]Geomar
[3]University Greifswald

Grant-No. AWI_PS124_08

Objectives

Antarctic-wide changes of sea-ice extent and, in particular, variations in the Ross, Amundsen, and Bellingshausen Seas have been linked to variations of stratospheric circulation (e.g. Turner et al. 2009; Thompson et al. 2011) or to the freshening of the Southern Ocean by ice shelf melt waters (e.g. Bintanja et al. 2013). However, recent studies on sea-ice drift around Antarctica have shown that, e.g., in the Weddell Sea (WS) wind-driven thermodynamic changes in ice advection are the dominant drivers for the current evolution of sea-ice concentration (Holland & Kwok 2012). The sea-ice extent in the WS has slightly declined during winter, but strongly increased during summer (Turner et al. 2015; Hobbs et al. 2016), although recent summers have seen a sharp drop (e.g. Vernet et al. 2019; Turner et al. 2020). This mean decrease in cyclonicity of the sea-ice cover points toward a deceleration of the Weddell Gyre (Holland & Kwok 2012), suggesting increasing amounts of thick, second-year ice. In addition, deformation caused by sea-ice drift might lead to a significant increase in sea-ice thickness, in particular in coastal regions (e.g. Schwegmann 2011), but provides also surface features for strong snow accumulation. However, a more detailed interpretation and analysis is hampered by the lack of observational data of ice drift and thickness as well as snow characteristics, which are urgently required for model development and satellite data analysis. Sea ice plays a crucial role for the production of dense waters, and the amount of sea ice formed on and exported from the southern WS continental shelf is a robust indicator for the amount of brine expelled in the region to support bottom water formation (Nicholls et al. 2009). The amount of ice formed and exported depends both on thermodynamic processes and ice deformation. While satellite remote sensing can be used to observe thin ice formed in polynyas (Paul et al. 2015), there is presently no reliable method that allows a remote estimate of the export of thicker ice further downstream. In this regard, the use of drifting buoys and electromagnetic ice thickness measurements are particularly important.

In addition to ice growth and deformation, snow on sea ice significantly modifies the sea ice mass balance. However, there is still insufficient information about snow thickness and metamorphism as well as its remote sensing by satellites (Arndt et al. 2016; Arndt & Haas 2019). Therefore, we carried out extensive observations of snow thickness and stratigraphy (Arndt & Paul 2018).

The Weddell Sea hosts a diverse ecosystem, which significantly relies on sea ice associated carbon production (Vernet et al. 2019). Nearly 50 % of the annual Antarctic sea ice primary production (15.8 Tg C) is produced in the Weddell Sea, in particular its eastern margin is one of the most productive regions (Arrigo et al. 1998). In this region, we witness so-called surface biota communities, which result from flooding and internal snowmelt processes. One consequence

of downward heat flux and snow thaw is the percolation of melt water to the snow-ice interface and the formation of gap layers, continuous or highly porous layers in the upper ice filled with seawater or slush and high concentrations of algae and other micro-organisms (e.g. Haas et al. 2001; Kattner et al. 2004). In these habitats, we find a strong accumulation of organic compounds (e.g. Papadimitriou et al. 2009). Nevertheless, due to the patchy distribution of the sea-ice biota both horizontally and vertically, it is still difficult to obtain accurate estimates (Meiners et al. 2012; Meiners 2018). The dissolved and particulate components from the ice can be transferred from the surface to deeper layers and can significantly affect the underlying water column (Laukert et al. 2017). The same is true for gypsum crystals, so far only found in Arctic sea ice (Wollenburg et al. 2018), which could also be a ballasting factor for *Phaeocystis* dominating the gap layers in Antarctic sea ice. In the planned research region of PS124 we expect a widespread occurrence of gap layers, which have rarely been sampled with regard to ice thickness, biodiversity, biomass, dissolved substances, and other biogeochemical processes. In addition, sea ice plays a special role in the temporary accumulation and storage of micro platic MP particles and their transport to other areas far away from the original source (Peeken et al. 2018), and not much is known yet about this in the Weddell Sea.

Finally, the occurrence of Ice Shelf Water (ISW) contributes strongly to sea-ice growth through the formation of platelet ice, provided the ISW emerges from the cavity and rises to the surface. Platelet ice is also a hot spot of biological production (Günther et al. 1999). Derived from Eastern Shelf Water, platelet ice is abundant along the coast of Dronning Maud Land (e.g. Arndt et al. 2020). Thus, surveying fast ice in front of ice shelves will provide an inventory of platelet ice as an indicator of extensive ISW emergence (Haas et al. 2020) and characterize its role in the biological carbon cycle.

Tab. 6.1: Pangaea labels as used for sea-ice measurements during PS124 and the respective parameters associated to the measurements

PANGAEA label	**Description**
Ship based	
ICEOBS	Ice Observations from ship bridge (along track)
Helicopter based	
HEM	Helicopter-based EM ice thickness profiler (EM-Bird)
Field measurements	
SIT	Manual sea-ice thickness drilling
SPIT	Snow pit
SMP	SnowMicroPen
SDMP	Snow depth measured with Magna Probe (SnowHydro)
GEM	Ground electromagnetic sounding (GEM-2, Geophex)
Ice Cores	
CORE-ARC-MP	Archive / Microplastic core
CORE-BIO	Parameters: Nutrients, fractionated Chla (>10 µm, <10 µm), marker pigments, species, DNA (Illumina sequencing), POC/PON & natural ^{13}C and ^{15}N isotopes, biogenic silica
CORE-DNA_1	Parameters: Illumina sequencing (DNA)

PANGAEA label	**Description**
CORE-DNA_2	Parameters: prokaryotic Illumina sequencing, biomarker
CORE-GYPS	Parameters: Gypsum content
CORE-NEO	Parameters: Trace elements and their isotopes
CORE-TEX	Parameters: Texture, Salinity, Oxygen isotopes
CORE-IP25	Parameters: IPSO-25
CORE-IRON	Parameters: Trace metals
Platelet_ICE	
	Parameters: Nutrients, fractionated Chla (>10 µm, <10 µm), marker pigments, species, DNA (Illumina sequencing), POC/PON & natural ^{13}C and ^{15}N isotopes, biogenic silica
Water sampling	
WATER-GAP	Gap water for biological varibales, Parameters: Nutrients, fractionated Chla (>10 µm, <10 µm), marker pigments, species, DNA, POC/PON & natural ^{13}C and ^{15}N isotopes, biogenic silica
WATER-SLUSH	Surface slush water for biological varibales, Parameters: Nutrients, fractionated Chla (>10 µm, <10 µm), marker pigments, species, DNA, POC/PON & natural ^{13}C and ^{15}N isotopes, biogenic silica
WATER-NEO-GAP	Gap water for trace elements and their isotopes
WATER_IRON-GAP	Gap water for trace metals
WATER-UIW	Under-ice water for biological varibales, Parameters: Nutrients, fractionated Chla (>10 µm, <10 µm), marker pigments, species, DNA, POC/PON & natural ^{13}C and ^{15}N isotopes, biogenic silica
WATER-NEO-UIW	Under-ice water for trace elements and their isotopes
WATER-IRON	Water samples for trace metals
Snow sampling	
ISO_SNOW	Parameter: Salinity, Oxygen isotopes
Cryo-Pelagic_ coupling	
STRAP	Parameters: Marker pigments, species, DNA (Illumina sequencing), POC/PON & natural ^{13}C and ^{15}N isotopes, biogenic silica
Buoys (BUOY)	
SB	Snow Buoy
TB	Ice Mass balance Buoy (Thermistor Chain Buoy)
SHARC-BUOY	Southern Hemisphere Antarctic Research Collaborative Buoy
New ice sampling	
OBS	Yellow ice observational surveys (helicopter-based)
IF	ice fishing/sampling of new ice by means of rubber boat or bucket from board

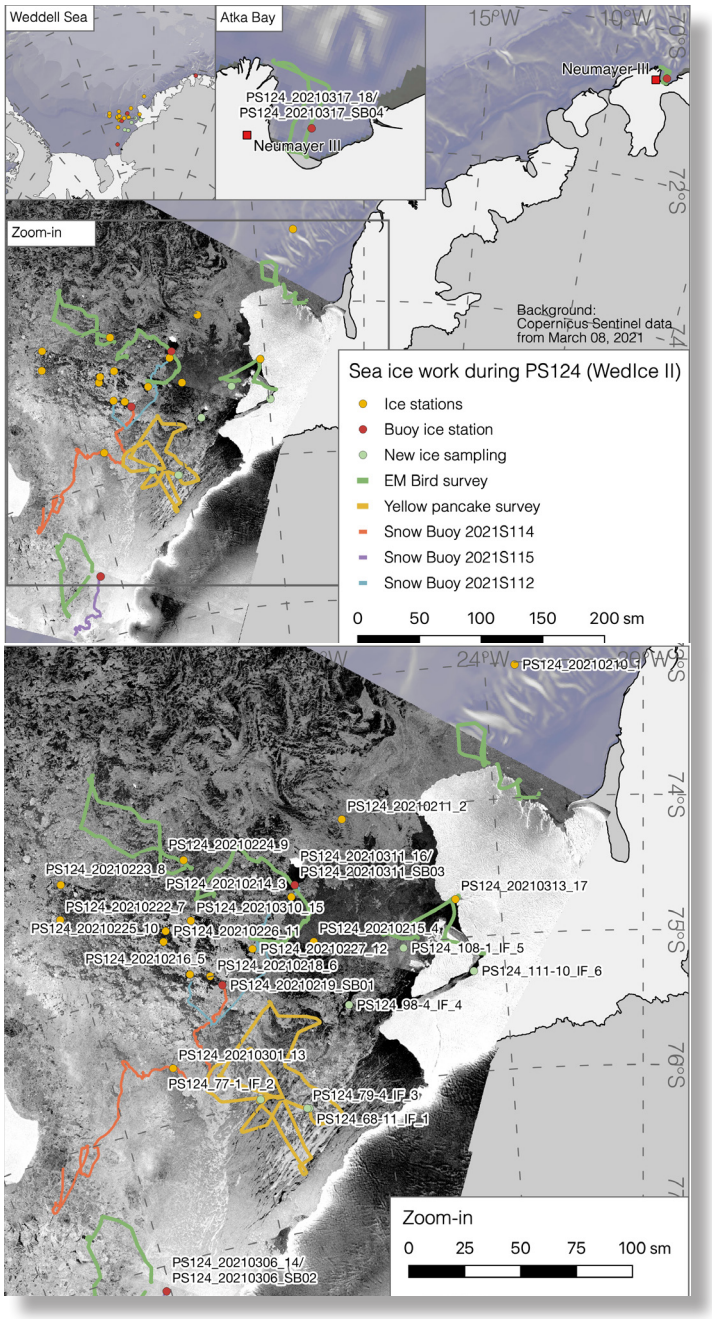

Fig. 6.1: Overview of all sampling activities within the WedIce II project during P124:

Yellow dots denote ice stations, red dots the initial position of the deployed buoys, green dots new ice sampling ice stations, green lines the EM-Bird survey tracks, yellow lines the yellow-ice observational surveys by helicopter, and colored thinner lines the drift trajectories of the deployed buoys (as of March 25, 2021).

All new/yellow-ice sampling activities are detailed in Chapter 13.

Not shown here: Hourly observations of sea ice conditions along the cruise track

Background: Sentinel-1 images recorded on March 08, 2021

All sea-ice stations within the WedIce II project with abbreviations for the used gear are in accordance to the labels listed in Table 6.2 at the end of this chapter. Explicit label names for each gear at the respective station are provided in the following sub-chapters. Ice stations accompanied by the physical oceanography group (OCE) are also marked.

6.1 Airborne ice thickness measurements

Objectives

Sea-ice thickness is one of the most important state variables of sea ice and an important environmental parameter of the study region. The objective of the airborne ice thickness surveys was to characterize the ice thickness variability of the study region and to interpret it in terms of origin and developmental history of the ice. That information is important for the validation of

numerical sea-ice models and for process studies of ice-ocean-atmosphere-interaction in the Weddell Sea. Results will also be used for the validation of satellite ice-thickness retrievals and interpretation of satellite radar images.

Our surveys are a continuation of ice-thickness observations by ULS carried out by AWI between 1992 and 2011 (Behrendt et al. 2015), occasional NASA Operation IceBridge flights (Kwok & Maksym 2014), and extensive *in-situ* observations during the ANT-XIV/3 *Polarstern* cruise in 1997 (Haas et al. 1999, 2001). Results will therefore allow to determine potential decadal ice thickness changes that may have occurred in the last 20+ years.

Work at sea

We used the helicopter-borne frequency-domain electromagnetic induction (HEM) sounding system Rosie (EM-Bird) to measure total sea-ice thickness (ice thickness plus snow depth) along helicopter flight tracks (Haas et al. 2009). The 4 m long instrument, the EM-Bird, is towed on a 20 m long cable underneath the helicopter and measures the sea-ice thickness in a height of 10–15 m above the surface. A laser altimeter and laser scanner are integrated in the EM-Bird system, measuring the distance to the surface in a 30 m wide, 2D swath along the flight. Besides their role for sea-ice thickness calculation, the laser data and accompanying DGPS receivers allow the retrieval of snow freeboard and surface roughness and, accordingly, ridge density and distribution.

In total, we carried out 6 HEM surveys in the vicinity of the cruise track, each approximately 120 nm long. Three surveys included profiling across fast-ice areas (see Chapter 6.6). All HEM surveys are summarized in Table 6.3 and Figs. 6.1 and 6.2.

Tab. 6.3: Overview of all conducted EM-Bird flights. The position indicates the starting point of the respective profile flight. OW: open water, defined as ice thinner than 0.3 m; Mode: Modal thickness, most surveys possessed several modes.

Label	Date	Time [UTC]	Lati-tude	Longi-tude	OW fraction [%]	Mean thick-ness [m]	St.dev. [m]	Mode 1 [m]	Mode 2 [m]	Mode 3 [m]	Mode 4 [m]	Mode 5 [m]
PS124_20210210_HEM1	2021-02-10	18:57	-73.524	-23.288	1.67	1.78	1.11		1.25			
PS124_20210224_HEM2	2021-02-24	16:31	-74.178	-32.342	11.55	1.72	1.33	0.75		1.75	2.15	
PS124_20210227_HEM3	2021-02-27	19:51	-74.750	-31.303	24.63	1.49	1.49	0.55	1.45	1.75		
PS124_20210308_HEM4	2021-03-08	09:44	-77.100	-36.539	16.28	1.38	1.33	0.2	1.25	1.65	2.45	
PS124_20210314_HEM5	2021-03-14	13:55	-75.146	-24.643	37.6	1.36	2.66		1.35			
PS124_20210319_HEM6	2021-03-19	18:37	-70.494	-8.129	0.57	2.12	1.11	0.95	1.55	1.95	2.55	2.85

Preliminary results of pack ice surveys

Figs. 6.1 and 6.2 show the locations of the five ice-thickness surveys in the southeastern Weddell Sea. Due to the low ice concentration in the study region, flights were designed to cover most of the sea ice and prominent ice floes identified on TerraSAR-X images rather than being straight triangular lines. Due to the cruise track and station plan, it was not possible to obtain a full overview of ice thicknesses in the southeastern Weddell Sea, in particular not of the closed ice to the west.

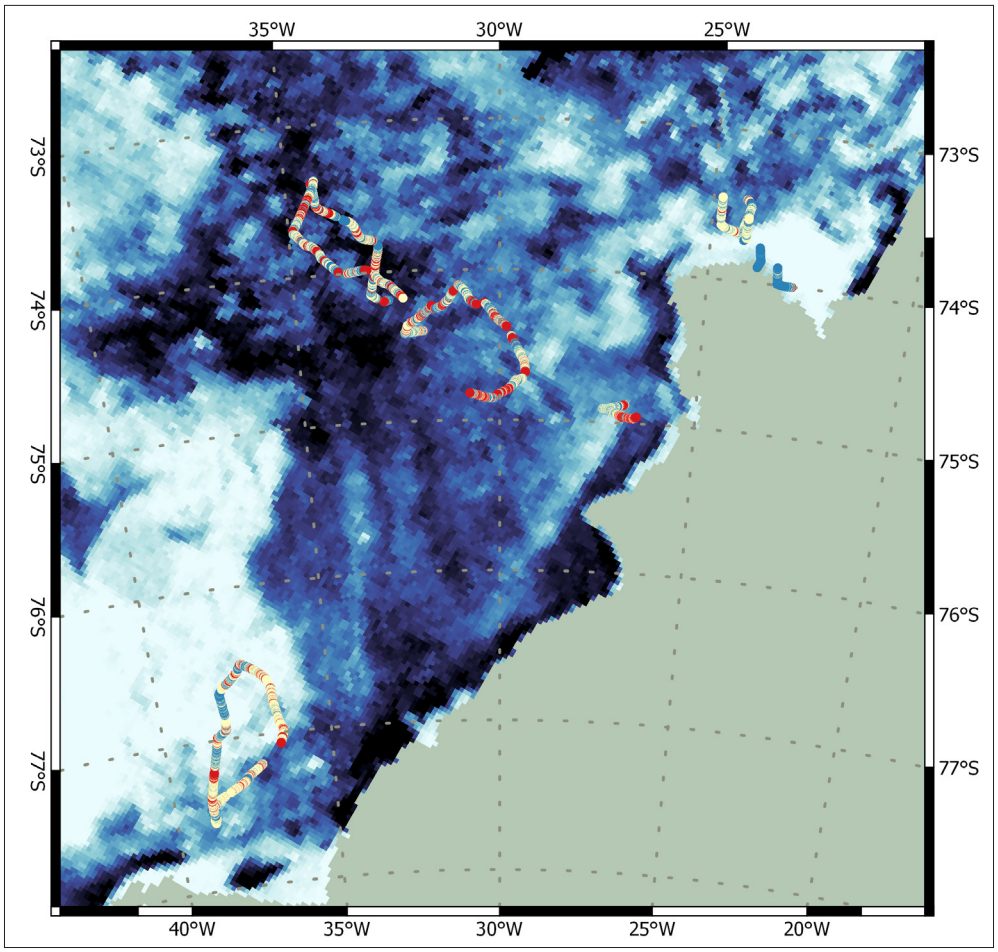

Fig. 6.2: Map of airborne ice-thickness surveys in the southeastern Weddell Sea (Table 6.3) overlaid on sea-ice concentrations on February 27, 2021, derived from AMSR2 passive microwave ice thickness observations (courtesy Lars Kaleschke, AWI; white: 100 % ice cover, dark blue: 0 % ice cover)

Fig. 6.3 shows the pack ice thickness distributions explored on all six flights, sorted from the northeast (pack ice off Atka Bay) to the southwest (southernmost flight north of the Filchner Ice Shelf). The Fig. shows a dominance of thin ice in the south representing newly formed Nilas and open water. The broad secondary peaks of the ice thickness distributions possess several modes (local maxima) representing level ice of different thickness, origin, and age. These are summarized in Table 6.3. Whereas the smaller modal thicknesses correspond with modes found during earlier studies, the study region was also characterized by the presence of quite thick, deformed ice. Overall, there are no indications of ice thinner than found during earlier observations.

Fig. 6.4 shows the thickness distribution of all flights combined. The large amount of open water (OW) can be seen again (22 % of measurements < 0.5 m thick). The mean thickness including open water was 1.65 m ± 2.39 m. Taking open water into account, the ice-only thickness (without open water) was therefore 2.12 m.

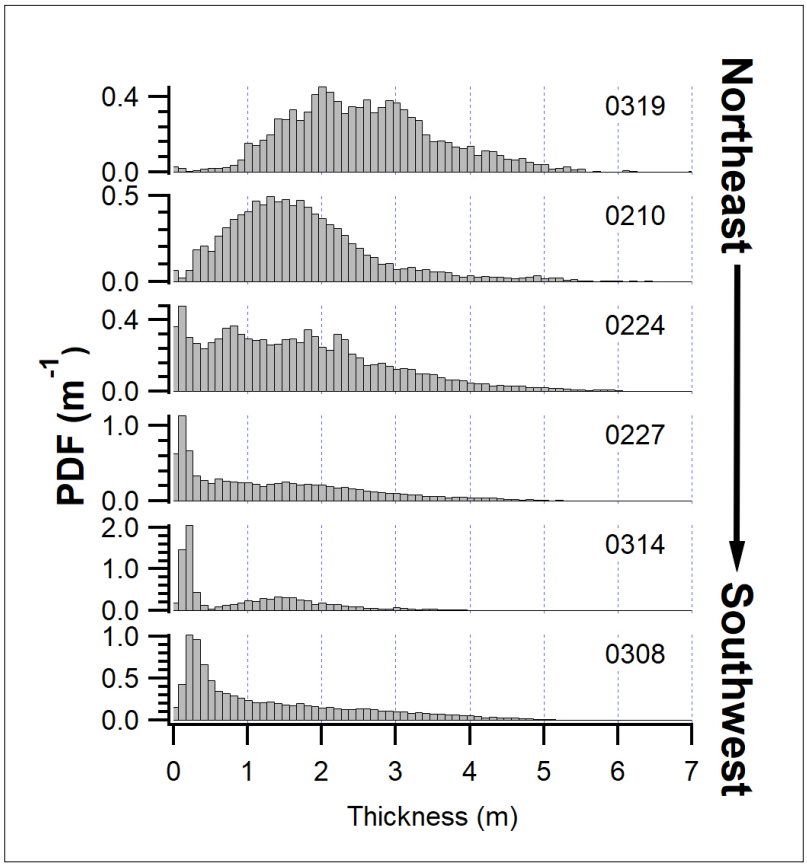

Fig. 6.3: Ice thickness distributions of all flights, from the northeast (top; Atka Bay) to the southwest (bottom; Filchner Trough)

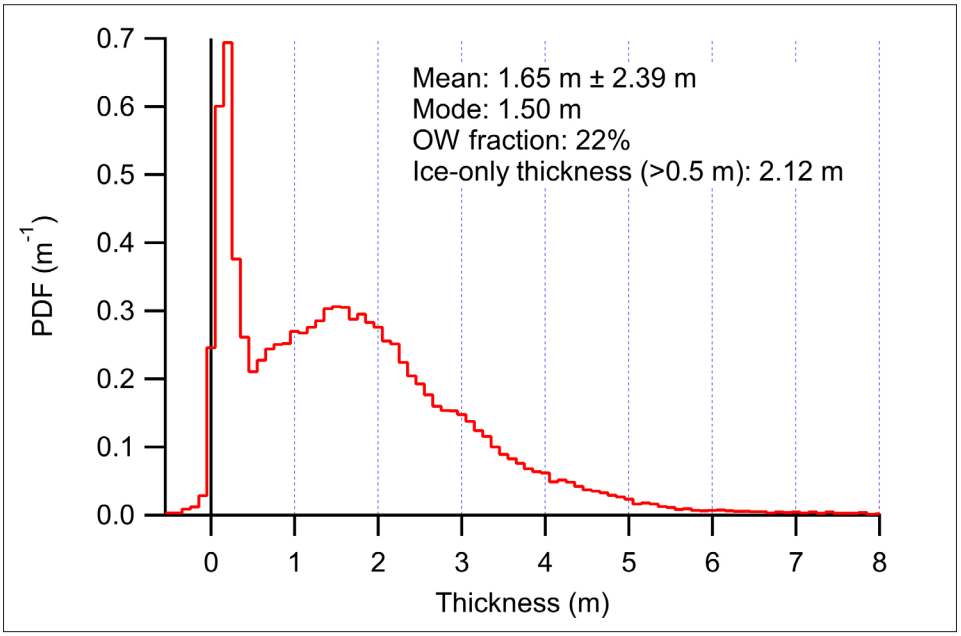

Fig. 6.4: Combined ice thickness distribution of all pack ice flights; ice-only thickness is the mean thickness of all ice thicker than 0.5 m.

Data management

The sea-ice thickness data will be released following final processing after the cruise or, depending on the completion of competing obligations (e.g. PhD projects), upon publication as soon as the data are available and quality-assessed. The data will be archived, published and disseminated according to international standards by the World Data Center PANGAEA Data Publisher for Earth & Environmental Science (www.pangaea.de) within two years after the end of the cruise. By default the CC-BY license will be applied.

6.2 Sea-ice and snow transect measurements

Objectives

The thickness of Antarctic sea ice and its snow cover is one of the most important parameters in terms of total mass and energy balance, but sea-ice thickness datasets are sparse. In addition, there are rarely data sets that combine high-resolution thickness information and large spatial coverage. Therefore, snow depths and sea-ice thicknesses are measured simultaneously on transect lines on selected ice floes.

The final data sets are used to classify other measurements conducted on the floe in the general ice-floe characteristics. Also both sea-ice thickness and snow depth data will be used for validation of satellite remote sensing data products.

Work at sea

Total sea-ice thickness (ice thickness plus snow depth) was measured on the ice during transect measurements with a ground-based multi-frequency electromagnetic induction instrument (GEM-2, Geophex Ltd.). The instrument was mounted on a modified plastic sled and pulled over the snow surface. A GPS-equipped Magna Probe (Snow Hydro, Fairbanks, AK, USA) was operated simultaneously in order to obtain snow depth along the GEM-2 tracks. Snow depth measurements were taken every 1.5 to 2.5 m along the track.

Combined sea-ice and snow thickness measurements were conducted on 15 floes, whereas a single snow-depth transect was performed at station PS124_2021018_6 and single sea-ice thickness transects at the two fast-ice stations PS124_20210313_17 and PS124_20210317_18. All transect measurements are summarized in Table 6.4 at the end of this chapter.

Preliminary (expected) results

Table 6.4 and Fig. 6.5 summarize all conducted snow depth and total sea-ice thickness transect measurements on pack ice during PS124. Taking all data into account, a mean total sea-ice thickness of 186 cm with a mean snow depth of 24 cm was observed. The 14 combined snow and sea-ice thickness transects show similar distributions where thinner and level sea ice is accompanied by a thinner snow layer, and vice versa. Thus, mean snow depth of all sampled stations ranged from 16 ± 12 cm (PS124_20210214_3) to 52 ± 23 cm (PS124_20210310_15). At the same stations, averaged minimum and maximum sea-ice thicknesses of 93 ± 55 cm and 370 ± 50 cm, respectively, were measured.

However, it must be considered that the transects across the floe might cover different proportions of level and ridged sea-ice areas. Thus, PS124_20210224_9 indicates a rather wide and equally distributed value range in both snow depth and sea-ice thickness (Fig. 6.5). This indicates a balanced transect line in level and ridged ice regimes. In contrast, PS124_20210306_14 shows a rather narrow thickness range of 42 cm around a mean value of 185 cm revealing that the respective transect was mainly conducted on level ice. In a next step, it is therefore crucial to distinguish between level and ridged ice regimes in order to increase the quality of the given statistics and associated results.

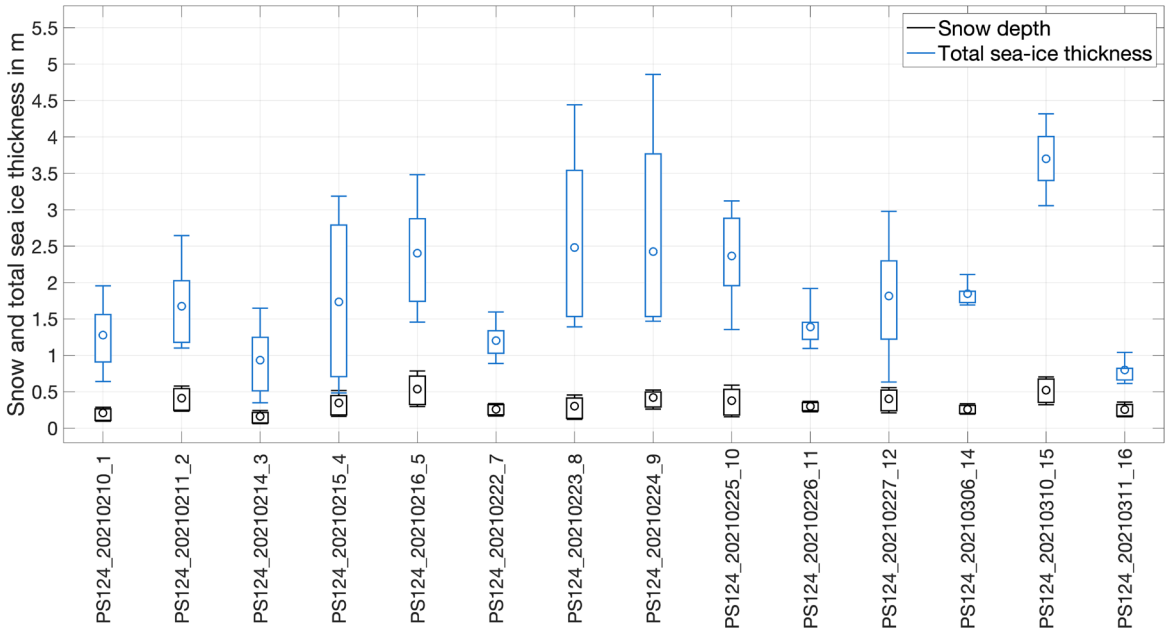

Fig. 6.5: Summary of all combined snow depth (MagnaProbe, black) and total sea-ice thickness (GEM, blue) measurements conducted during PS124: Boxes are the first and third quartiles. Whiskers display the 10- and 90-percentiles. Circles indicate mean values.

Data management

The sea-ice thickness data will be released following final processing after the cruise or, depending on the completion of competing obligations (e.g. PhD projects), upon publication as soon as the data are available and quality-assessed. The data will be archived, published and disseminated according to international standards by the World Data Center PANGAEA Data Publisher for Earth & Environmental Science (www.pangaea.de) within two years after the end of the cruise at the latest. By default the CC-BY license will be applied.

6.3 Physical and biological properties of sea ice

Objectives

Summer thaw-freeze cycles in the snow and upper ice layers result in strong, destructive snow metamorphism, and eventually in the formation of superimposed ice and gap layers. These gap layers receive comparably much light and are thus known to be highly productive regions within the ice. While metamorphic snow was studied in snow pits and with lateral profiling methods (Chapter 6.4), different ice types indicative of specific ice developmental histories including the transformation from snow to ice, and the porosity and state of ice deterioration can only be observed from ice cores. In addition, ice cores are the easiest way to measure bio-geochemical iwce properties and to determine the sea-ice biomass and other biogeochemical variables, which can be put into context of the physical ice observations. Ice cores are sectioned according to these physical properties and compared with gap and under ice water allowing to distinguish the exchange processes of species and biogeochemical parameters within the ice and the underlying ocean.

Work at sea

A regular ice station for biogeochemical sampling involved the collection of sea ice cores, the sampling of gap water or surface slush water, and seawater directly under the ice (Table 6.5). Up to 10 ice cores were collected at each ice station. The TEX cores were sampled to obtain a larger data set of the development of superimposed ice and further properties of the sea ice. Whenever possible, TEX cores were combined with cores for other biogeochemical variables as BIO, DNA, Gypsum, IPSO-25 (Table 6.5). Only at one ice station Nilas ice was also sampled (Table 6.5), however an extensive young-ice sampling was carried out from the ship (for details see Chapter 13, Table 13.1). At the two fast ice stations, additional platelet ice was sampled (Table 6.5). Within 2 days after sampling, cores for Gypsum were processed in the ships laboratories. Ice core sections were melted immediately in hand warm water and the water was filtered over a 20 µm mesh stored in 4 °C ethanol for further analysis in the home laboratory. In addition, surface algae lumps from 10 MUC stations were stored in ethanol to study the presence of gypsum. Cores for trace elements (NEO) and their isotopes and archive/microplastic (ARC-MP) were stored in core bags after retrieval and kept frozen at –20 °C. For the isotopes, additional snow under ice and gap water samples were collected (Table 6.5). Bottom sections were further sampled at several stations for prokaryotic associated biomarker (DNA_2) and the biomarker IPSO-25 (IP25). Cores for biological variables (BIO) were usually sectioned into a top, above and below gap, 1 to 5 middle and a 10–14 cm bottom section (Fig. 6.6). Ice samples were transferred to the cool container (4 °C) for sea-ice melting. Volume and salinity of all melted ice core sections were determined and water samples were taken for nutrients and cell counts. The remaining water was divided for filtering the following parameters: size-fractionated chlorophyll a (>10; <10 µm), marker pigments, particulate biogenic silicate, particulate organic carbon and nitrogen (POC, PON), and the isotopic composition of POC and PON (δ^{13}CPOC and δ^{15}NPON; Table 6.1.). Usually, an additional core was taken for Illumina sequencing analysis. From this core the high biomass accumulation sections and bottom sections were collected and the core sections also transported to the cool container (4 °C), where filtered sea water was added to each sample to reduce the osmotic shock of the organism. After melting, samples for DNA (Illumina sequencing) were filtered on >10 µm, 3–10 µm, and 0.2–3 µm filters. If time did not permit to sample an additional core or if other high biomass accumulations were obtained during the sampling of the BIO ice core, additional samples for DNA were taken from these sections. All parameters collected for the BIO core were also filtered from the sampled under ice water (UIW), the slush water, and the gap layer water (GAP). In addition, for the large-scale characterization of the surface algae communities, surface samples were collected by using an automatic filtration device for marine microorganisms (AUTOFIM) connected to the ship's pumping system. This device was programmed to filter up to 2 L of water roughly every six hours. The collected samples were stored at –80 °C until processing.

In cooperation with the Southern Ocean Carbon Cycling team (Chapter 7), at two ice stations, (Table 6.2, Fig. 6.7) short-term sediment traps were deployed for one day in 5 and 25 m depth to determine the export of sea ice derived material. After recovery of the samples, they were split and filtered for various parameters (see Table 6.1).

To understand the physical properties of sea-ice cores, a total of 19 TEX cores from pack ice (and two from fast ice, see Chapter 6.6) were analyzed on board for ice texture and salinity (Table 6.5). In the cold laboratory (–20 °C), vertical thick sections were produced and their texture was deµµµtermined visually in polarized light. Ice cores were subsequently cut into up to 15 cm long sections according to their texture, and melted for measurements of vertical profiles of bulk ice salinity. Melted ice samples were further stored for later measurements of δ^{18}O back in Germany.

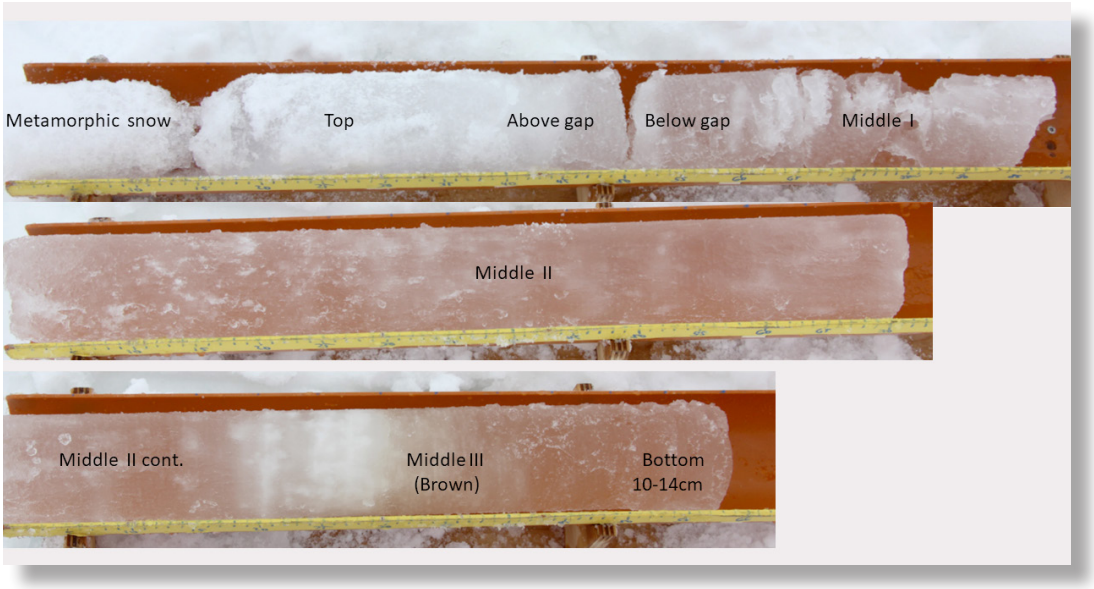

Fig. 6.6: Example for a sea-ice core from the surface (upper panel) to the bottom part (lowest panel): Indicated are the usual subsections taken for BIO core sampling.

Fig. 6.7: Short-term sediment trap deployment on the ice floe

Tab. 6.5: Overview of all samples collected during the ice station

Station	Date	Time [UTC] start	Lati-tude start	Longi-tude start	Ice cores (CORES-)										Water sampling (WATER-)							Snow sampling	New_ ICE	Platelet_ ICE
					ARC-MP	BIO	DNA_1	DNA_2	IP-25	GYPS	NEO	TEX	Iron	Total number of cores	GAP	NEO-GAP	IRON-GAP	SLUSH	UIW	NEO-UIW	IRON-UIW	NEO		
PS124_20210210_1	2021-02-10	10:43	-73.02	-23.23	1	1	1	3	1	1	1	1		10					1	1		1		
PS124_20210211_2	2021-02-11	18:10	-74.03	-28.09		1	1					1		3				1	1					
PS124_20210214_3	2021-02-14	10:06	-74.54	-29.78	1	1	1		1	1	1	1		7				1	1	1		1		
PS124_20210215_4	2021-02-15	13:25	-74.89	-29.37		2	1	3	1	1		2		10	1				1					
PS124_20210216_5	2021-02-16	10:07	-74.95	-33.00	1	1	1				1	1		5	1	1			1	1		1		
PS124_20210218_6	2021-02-18	9:29	-75.00	-32.45		1	1	3				1		6				1	1					
PS124_20210222_7	2021-02-22	9:19	-74.32	-36.12	1	1	1		1	1	1	1		7	1	1		1	1	1				
PS124_20210223_8	2021-02-23	10:50	-74.07	-35.84		3	1	3		1		1		9	1				1					
PS124_20210224_9	2021-02-24	9:28	-74.12	-32.47		4	1				1	1		7	1	1		1	1	1		1		
PS124_20210225_10	2021-02-25	9:19	-74.67	-33.51	1	1	1	3		1	1	1		9	1	1			1	1		1	2	
PS124_20210226_11	2021-02-26	9:29	-74.60	-33.39		1	1			1	2	1		6	1				1	1		1		
PS124_20210227_12	2021-02-27	9:13	-74.86	-31.11		1	1	3	1	1		1		8	1				1					
PS124_20210301_13	2021-03-01	10:05	-75.60	-34.12		1	1							2				1	1					
PS124_20210306_14	2021-03-06	9:11	-77.18	-36.15		1	1					1		3	1				1					
PS124_20210310_15	2021-03-10	14:57	-74.57	-32.64		2						2	2	6	1		1	1	1		1			
PS124_20210311_16	2021-03-11	9:50	-74.46	-29.63		1	1					1		3	1				1					
PS124_20210313_17	2021-03-13	9:49	-74.71	-25.26		1						1		2					1					2
PS124_20210317_18	2021-03-17	15:17	-70.62	-7.84		1						1		2					1					2
				Sum:	5	25	15	18	5	8	8	19	2	105	11	4	1	8	18	7	1	6	2	4

Preliminary (expected) results

The aim of this study is to understand the variability and biodiversity of the sea ice-associated biomass and the biogeochemical parameters with respect to the physical sea-ice properties and its exchange with the underlying water. This will allow assessing the role of sea-ice biota for the cryo-pelagic, cryo-benthic coupling under different environmental scenarios in the southeastern Weddell Sea from the south to the north. Contrary to the western Weddell Sea, ice cores in this region were characterized by an extremely high biomass content, both in the gap and in the bottom layers and sometimes throughout the entire sea-ice core, suggesting a high permeability within the ice floe.

First microscopic investigations revealed a more similar appearance of the under-ice water plankton compared to the sea-ice cores. In most cases, a *Corethron* spp. and *Phaeocystis* spp. dominated under ice water community was found. At the western flank of the Filchner Trough and towards the south of the study area, also *Fragilariopsis* spp. and *Chaetoceros* spp. species appeared to be more abundant. The only real difference in appearance of the under-ice community was at the southwestern most station, which was dominated by large *Chaetoceros* spp. species and a high abundance of various *Chaetoceros* spores.

This station was also characterized by an unusual algae composition throughout the ice core, which was almost exclusively dominated by centric diatoms as *Thalassiosira* spp. Similar species have been found in association with platelet ice (Smetacek et al. 1992) and were also present in the landfast ice core collected at the Brunt Ice Shelf during this study (Chapter 6.6). It is, therefore, likely that this large ice floe developed in close proximity to landfast ice.

The bottom sections of most sea-ice cores were usually dominated by *Navicula* spp., *Nitzschia* spp., and *Fragilariopsis* spp. species. In addition, other pelagic species like *Corethron* spp., *Chaetoceros* spp, and *Thalassiosira* spp. were also trapped in the sea ice. In contrast to this, the ice gap layer rather showed the reflection of the associated under ice water, usually dominated *Phaeocystis* spp. Often the gap layer water was also dominated by small copepods and juvenile krill larvae highlighting the importance of sea ice for the development stages of keystone species in the Antarctic. Overall, the variability of pelagic and sea-ice algae species, including spore formation in the ice cores, suggests that the sea ice might also serve as a lateral transporter for seeding phytoplankton in the next spring. These point measurements will be upscaled with the floe-wide observations (Chapter 6.2) and set into context with the large-scale EM-Bird observations (Chapter 6.1) in order to elucidate the role of sea ice for biological and biogeochemical cycles in the southeastern Weddell Sea.

The physical sea-ice characteristics were already analyzed on board *Polarstern*. In total, 19 cores of the pack ice have been sampled for texture and salinity (Fig. 6.8), while for four cores only the surface section was sampled and analyzed. The lengths of fully sampled cores range between 55 and 197 cm, including snow.

Most of the ice cores sampled possessed a negative freeboard, causing flooding of the snow/ice interface. Therefore, we found rather high salinity values in the flooded lower snowpack as well as in the top-most part of the actual ice (Fig. 6.9). In order to quantify the amount of snow ice with certainty, i.e., sea ice formed by refreezing of flooded snow, additional oxygen isotope analysis will be performed in the lab back home.

Ice texture analysis classified the top part of the ice cores widely as orbicular granular or a mixture of granular and columnar ice. Large-grained, polygonal granular texture associated with superimposed ice at the top was only identified at ice station PS124_20210311_16, leaving large uncertainties of the visual analysis. This will be re-evaluated by oxygen isotope analysis in the lab back home later.

Analyzing the bottom part of the ice cores, 7 of them revealed mainly columnar ice texture, while the other 8 bottom sections were dominated by orbicular granular or a mixture of granular and columnar ice texture classes. Granular and mixed ice texture classes give evidence for initial ice formation under rather turbulent ocean conditions. In contrast, columnar ice is mainly formed under calm ocean surface conditions. Consequently, we assume that the ice cores with granular bottom sections are formed in the wind-driven coastal polynya in the eastern Weddell Sea and ice cores with columnar bottom sections either in the northeastern or southeastern Weddell Sea. A detailed backtracking analysis of all sampled ice stations based on satellite remote sensing data will reveal more detailed evidence of the source regions of the ice cores.

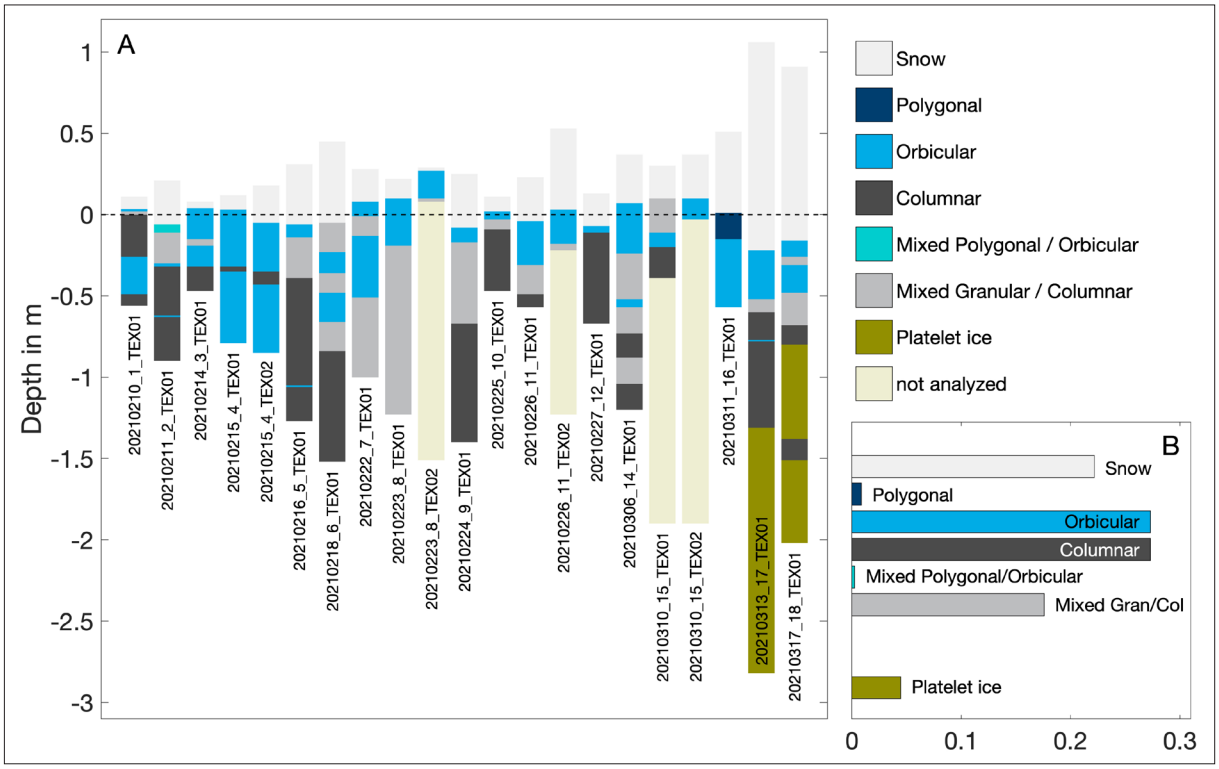

Fig. 6.8: A. Overview of all ice cores sampled colored according to the respective crystal texture: Beige-colored parts were not analyzed for texture. Ice core freeboard and draft are plotted relative to the water level (z = 0 cm, dotted black line). B. Relative frequency distribution of ice texture classes of the whole ice core, including snow

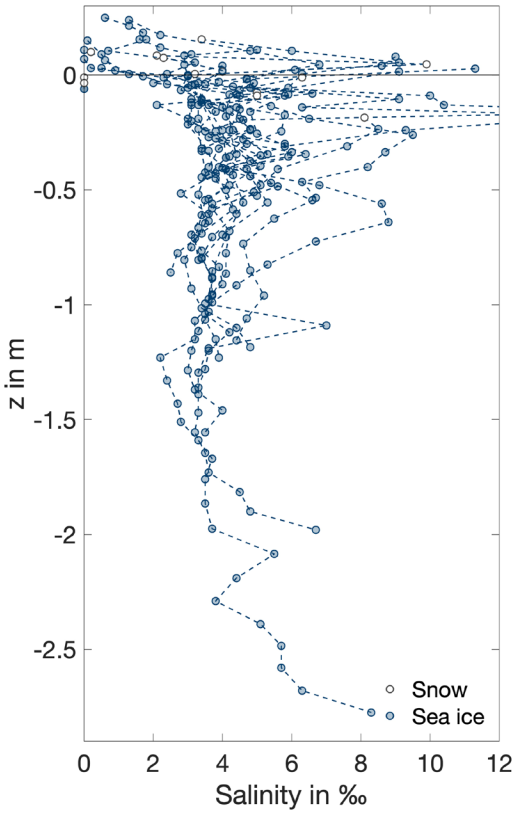

Fig. 6.9: Composition of all measured salinity profiles from the texture cores; blue dots are related to actual ice samples, while white dots denote snow samples taken in connection with the ice cores.

Data management

All Ice-core data will be released following its analysis in the home laboratories after the cruise or depending on the completion of competing obligations (e.g. PhD projects), upon publication as soon as the data are available and quality assessed. The data will be archived, published and disseminated according to international standards by the World Data Center PANGAEA Data Publisher for Earth & Environmental Science (www.pangaea.de) within two years after the end of the cruise. By default the CC-BY license will be applied. DNA data will be deposited in NCBI's Sequence Read Archive.

6.4 Physical properties of snow

Objectives

Physical snow properties are highly variable even on small horizontal scales. The spatial and temporal variations in the snow pack characteristics (e.g., temperature, density, stratigraphy) and their dimension have a crucial impact on the energy and mass budget of Antarctic sea ice. Therefore, the snow pack on different ice floes was characterized in detail.

Snow stratigraphy will be used as ground truth for the interpretation of retrieved snowmelt signatures from passive and active microwave data.

Work at sea

Physical snow properties were analyzed on all 16 pack-ice floes sampled. Here, the work can be subdivided into two parts: Snow pits to describe essential physical snow parameters and their stratigraphy, and SnowMicroPen measurements deriving a high-resolution density profile of the prevalent snowpack.

Snow pits

Snow pit measurements were taken on the undisturbed shaded working wall of the snow pit. First, the temperature was measured every 1 to 5 cm from top (snow-air interface) to bottom (snow-ice interface) with a hand-held thermometer (Testo). Next, the different layers of the snow pack and their stratigraphic parameters were described. For each layer the snow grain size and type (e.g., rounded crystals, facetted crystals, depth hoar) were determined with a magnifying glass and a 1–3 mm grid card. In addition, every layer was characterized by its hardness with the following categories: fist (F), 4 fingers (4F), 1 finger (1F), pencil (P), and knife (K). Afterwards, the density of each snow layer was measured volumetrically by removing a defined snow block with a density cutter from each layer (density cutter weight: 155 g, volume: 100 ml) and weighing it with a spring scale.

Overall, 22 snow pits were analyzed on 16 different pack-ice floes with the pit-specific measurements summarized in Table 6.6 at the end of this chapter, which gives an overview of all sampled snow pits. Possible measurements are: temperature (TEMP), density (DENS), stratigraphy (STR), and samples for salinity (SAL) and oxygen isotopes (ISO).

SnowMicroPen

The SnowMicroPen (SMP) is a high-resolution snow penetrometer. It objectively measures the bonding force between snow grains, with high vertical resolution and high speed. During the measurement, the SMP is pressed down to the snow surface while the rod is driven into the snow pack. A piezoelectric force sensor measures penetration resistance as function of depth. The measured data are displayed on the controller and stored in binary format on a SD card.

During PS124 the SMP was used to perform transect measurements on straight lines with one measurement every other meter on distances of up to 64 m, as well as three measurements in close vicinity of most of the snow pits. In total, 442 SMP profiles were taken (Table 6.7).

Tab. 6.7: Overview of all SMP measurements. Start/end time and position indicate the start/end point of the respective profile line.

Station	Label	Date	Time [UTC] start	Latitude start	Longitude start	Time [UTC] end	Latitude end	Longitude end	Profile length [m]
PS124_20210210_1	-1	2021-02-10	11:37	-73.019	-23.234	13:04	-73.014	-23.237	60
PS124_20210210_1	-1	2021-02-10	11:30	-73.019	-23.234	11:34	-73.019	-23.234	SPIT
PS124_20210210_1	-1	2021-02-10	12:47	-73.015	-23.237	12:51	-73.015	-23.236	SPIT
PS124_20210211_2	-1	2021-02-11	18:35	-74.031	-28.097	19:52	-74.036	-28.111	64
PS124_20210211_2	-1	2021-02-11	19:41	-74.035	-28.110	19:45	-74.035	-28.116	SPIT
PS124_20210214_3	-1	2021-02-14	11:08	-74.545	-29.781	11:34	-74.549	-29.779	30
PS124_20210214_3	-1	2021-02-14	11:38	-74.549	-29.777	11:41	-74.549	-29.777	SPIT
PS124_20210215_4	-1	2021-02-15	14:06	-74.889	-29.361	15:07	-74.882	-29.358	60
PS124_20210215_4	-1	2021-02-15	15:11	-74.882	-29.357	15:14	-74.882	-29.357	SPIT
PS124_20210216_5	-1	2021-02-16	11:12	-74.957	-32.992	12:24	-74.963	-32.973	60
PS124_20210216_5	-1	2021-02-16	12:35	-74.964	-32.968	12:39	-74.964	-32.967	SPIT
PS124_20210218_6	-1	2021-02-18	10:43	-75.004	-32.439	11:51	-75.009	-32.430	60
PS124_20210218_6	-1	2021-02-18	11:53	-75.010	-32.428	11:56	-75.010	-32.428	SPIT

Station	Label	Date	Time [UTC] start	Latitude start	Longitude start	Time [UTC] end	Latitude end	Longitude end	Profile length [m]
PS124_20210222_7	-1	2021-02-22	09:49	-74.322	-36.122	10:45	-74.320	-36.139	60
PS124_20210222_7	-1	2021-02-22	10:48	-74.319	-36.142	10:52	-74.319	-36.143	SPIT
PS124_20210223_8	-1	2021-02-23	11:26	-74.074	-35.840	12:17	-74.074	-35.835	60
PS124_20210223_8	-1	2021-02-23	12:35	-74.072	-35.834	12:39	-74.072	-35.834	SPIT
PS124_20210223_8	-1	2021-02-23	12:40	-74.072	-35.833	12:42	-74.072	-35.833	SPIT
PS124_20210224_9	-1	2021-02-24	10:08	-74.116	-32.478	10:54	-74.113	-32.486	52
PS124_20210224_9	-1	2021-02-24	11:02	-74.113	-32.488	11:05	-74.113	-32.488	SPIT
PS124_20210225_10	-1	2021-02-25	10:07	-74.673	-33.523	10:29	-74.672	-33.526	32
PS124_20210225_10	-1	2021-02-25	10:07	-74.673	-33.523	10:07	-74.673	-33.523	SPIT
PS124_20210225_10	-1	2021-02-25	10:13	-74.672	-33.523	10:14	-76.672	-33.524	SPIT
PS124_20210226_11	-1	2021-02-26	10:20	-74.599	-33.405	11:14	-74.597	-33.431	60
PS124_20210226_11	-1	2021-02-26	11:19	-74.596	-33.432	11:21	-74.596	-33.433	SPIT
PS124_20210226_11	-1	2021-02-26	11:24	-74.596	-33.436	11:28	-74.596	-33.436	SPIT
PS124_20210227_12	-1	2021-02-27	09:49	-74.870	-31.108	10:31	-74.874	-31.095	60
PS124_20210227_12	-1	2021-02-27	10:34	-74.875	-31.096	10:36	-74.875	-31.096	SPIT
PS124_20210306_14	-1	2021-03-06	09:53	-77.185	-36.152	10:14	-77.185	-36.157	30
PS124_20210306_14	-1	2021-03-06	10:18	-77.185	-36.157	10:21	-77.185	-36.158	SPIT
PS124_20210311_16	-1	2021-03-11	10:42	-74.458	-29.632	11:36	-74.461	-29.624	60
PS124_20210311_16	-1	2021-03-11	11:40	-74.461	-29.625	11:42	-74.461	-29.625	SPIT
PS124_20210317_18	-1	2021-03-17	16:24	-70.623	-7.843	16:28	-70.623	-7.843	SPIT

Preliminary (expected) results

Fig. 6.10 shows a typical snow pit data set from station PS124_20210222_7. The snow pit was sampled in a representative area of the floe with a snow depth of 31 cm. The snow pack contained 8 different layers (from top to bottom): a fresh snow layer (1), followed by a thin wind slab layer (2), and a 17-cm thick uniform layer of small-grained angular crystals of medium hardness (1 finger) (3). Below, a loose layer of poorly layered depth hoar crystals was identified (4), followed by a hard and compacted layer of the same crystal type (5). The bottom 10 cm of the snow pit were flooded or soaked from below, causing a general “softening” of the snowpack. However, an ice layer was identified at 10 cm (6), followed by a hard layer of melt-freeze grains (7). At the bottom, the water and salt softened the snow completely towards a slushy layer (8).

Throughout the sampled snowpack the grain sizes slightly increased, which correlated with the weak temperature gradient from –4.0 °C (top) to –1.7 °C (bottom). This grain type distribution throughout the snowpack is typical for all sampled snow pits during PS124. Thus, there is no clear dominant grain type class, but both layers of wind slab and fragmented crystals were rather common (Fig. 6.11) caused by winds within the last year.

Snow density obtained every two meters with the SnowMicroPen along a transect line at station PS124_20210222_7 is shown in Fig. 6.12. The layout of the transect was chosen to

be representative for the ice floe, including small snow dunes. The above-described melt-forms and ice layers in the bottom part of the snowpack sometimes prevented the SMP to penetrate throughout the entire snow column. The resistance of those layers exceeded 40 N and therefore the measurement was aborted. However, the given transects indicate a clearly layered soft snowpack in the top 5 to 10 cm with a typical density between 250 and 300 kg m^{-3}, followed by a slightly more compacted layer with density between 300 and 400 kg m^{-3}. In the bottom section, as soon as melt-forms and ice lenses dominate the snowpack, the profile gets rather heterogeneous and highly variable due to different bonding forces and grain transitions in the rather icy layer. Also, due to the softening of the snowpack by sea water flooding, retrieved density values became more uncertain at lower depths.

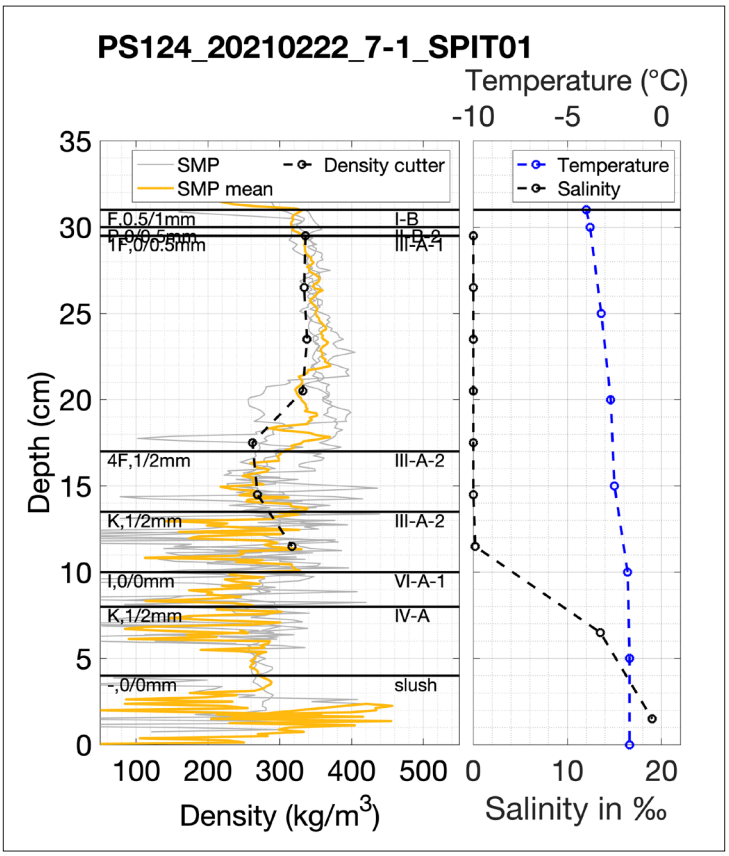

Fig. 6.10: Example of snow pit analysis from station PS124_20210222_7:
On the left: Density measurements with the density cutter are marked in black, derived density from SMP measurements in gray (all) and its average in yellow. Horizontal lines indicate the different layer interfaces. Below the lines grain type classifications for the respective layer are given.
On the right: Vertical profiles of snow temperature (blue) and salinity (black)

Data management

Data from all snow pit and SMP measurements will be archived, published and disseminated according to international standards by the World Data Center PANGAEA Data Publisher for Earth & Environmental Science (www.pangaea.de) within two years after the end of the cruise. By default the CC-BY license will be applied.

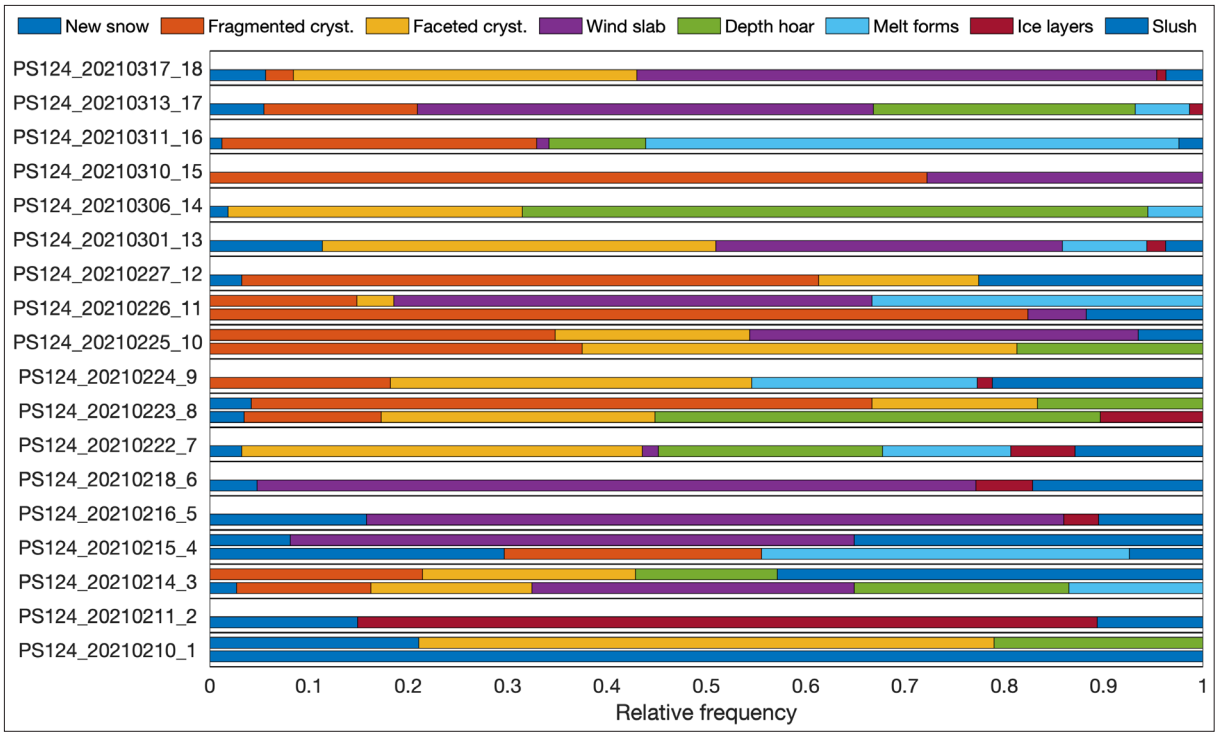

Fig 6.11: Overview of relative occurrence of grain types within all sampled snow pits

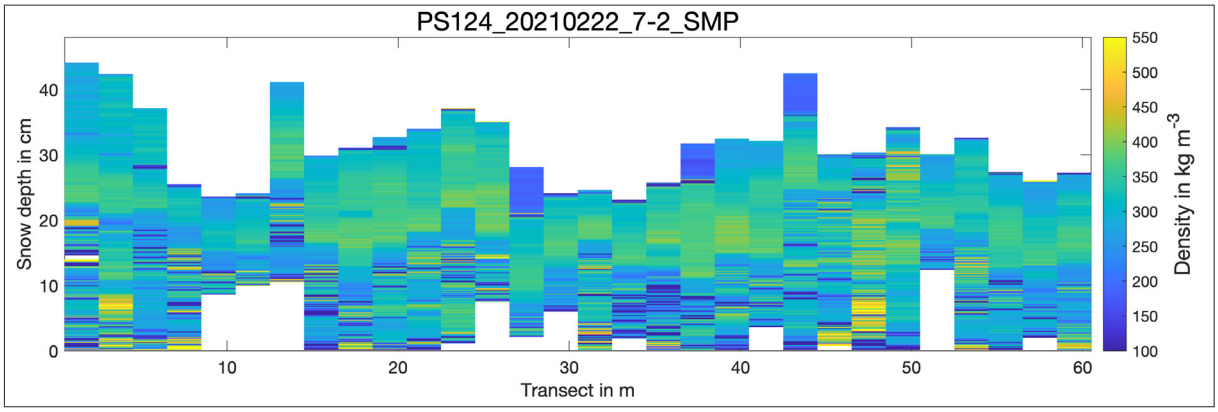

Fig. 6.12: Example of snow density transect obtained with the SMP at station PS124_20210222_7: Missing data at lower depths indicate an overload of the instrument due to too high densities.

6.5 Deployments of autonomous ice tethered platforms (buoys)

Objectives

In-situ snow and ice measurements only provide snap-shot observations of ice properties. In order to also obtain information about the seasonal and interannual variability and evolution of the observed ice floes, we deployed autonomous ice tethered platforms (buoys), which measure ice and snow characteristics beyond the cruise period. We deployed two kinds of buoys: Ice Mass Balance buoys (IMBs) observing the sea-ice temperature and growth, and Snow (depth) Buoys measuring snow accumulation over the course of the year. In addition, some buoys are equipped with sensors measuring air and/or body temperature and sea level pressure.

Furthermore, the Departments of Electrical Engineering and Oceanography at University of Cape Town and the South African Weather Service (SAWS) developed an ice-tethered buoy system (SHARC Buoy), equipped with Global Positioning System (GPS) sensors, inertial measurement units (IMU) for wave observations (wave height, wave period and power spectrum), and environmental sensors (temperature, humidity, pressure). These instruments provide valuable *in-situ* environmental data, which will be used to better understand the sea-ice life cycle in this region.

Combining all long-term data from these autonomous sensors, we will be able to better observe sea-ice processes and feedback mechanisms in the ice-covered Weddell Sea.

Beyond the immediate value for our sea-ice mass balance research, the Snow Buoys report their position together with measurements of surface temperature and partially atmospheric sea-level pressure directly to the Global Telecommunication System (GTS) used by weather prediction and atmospheric reanalysis systems. This activity is a contribution to the International Programme for Antarctic Buoys (IPAB) coordinated by AWI.

Work at sea

Fig. 6.1 and Table 6.8 give an overview of 4 Snow Buoys deployed, 1 Ice Mass Balance Buoy, and the SHARC Buoy. Three of the Snow Buoys were deployed on large ice floes in the pack ice of the southeastern Weddell Sea, the last one accompanied by the SHARC Buoy. The fourth Snow Buoy was deployed together with the IMB on the fast ice in Atka Bay.

Tab. 6.8: List of all buoys deployed with their initial deployment position and time. Buoy names are identical to their name in www.meereisportal.de, where all data and buoy information are available in real time.

Station	Label	Date	Time [UTC]	Name	IMEI	Lati-tude	Longi-tude
PS124_20210219_SB01	PS124_20210219_SB01	2021-02-19	10:35	2021S114	300534061254970	-75.086	-32.167
PS124_20210306_14	PS124_20210306_SB02	2021-03-06	10:51	2021S115	300534061350010	-77.185	-36.150
PS124_20210311_16	PS124_20210311_SB03	2021-03-11	12:46	2021S112	300534061251920	-74.463	-29.447
PS124_20210311_16	PS124_20210311_SHARC01	2021-03-11	12:46	-	-	-74.463	-29.447
PS124_20210317_18	PS124_20210317_TB01	2021-03-17	17:45	2021T86	300234068454520	-70.623	-7.675
PS124_20210317_18	PS124_20210317_SB04	2021-03-17	18:15	2021S113	300534061251930	-70.623	-7.675

Preliminary (expected) results

The Snow Buoys measure the snow accumulation at four spots by sonar sensors, whereas the main measuring device of the IMB is a thermistor string going through the ice into the water. By measuring the temperature and thermal conductivity every 2 cm, it is possible to identify the boundaries between ice and water, ice and snow, and snow and air. Combining both data sets, information on snow depth changes, sea ice growth, and eventually observations of flooding can be expected from the data.

Fig. 6.13 gives an example for snow accumulation of Snow Depth Buoy 2021S114 for the period from February 19 to March 25, 2021. During this period, a total snow accumulation of

approx. 10 cm was recorded. Overall, the time series is characterized by small-scale changes of snow depth, shown by highly variable snow readings from the single sensors. Even though temperatures remained around 0 °C for some time, no significant surface melt was evident. Since mid-March, temperatures slowly decreased, accompanied by two temperature drops associated with high pressure influence.

Sea-ice growth data from the IMBs will only be processed after the cruise. Finally, all data will be combined with findings of former buoy deployments to enhance our understanding of temporal and spatial variability in snow accumulation, sea-ice growth, and eventually flooding of Antarctic sea ice.

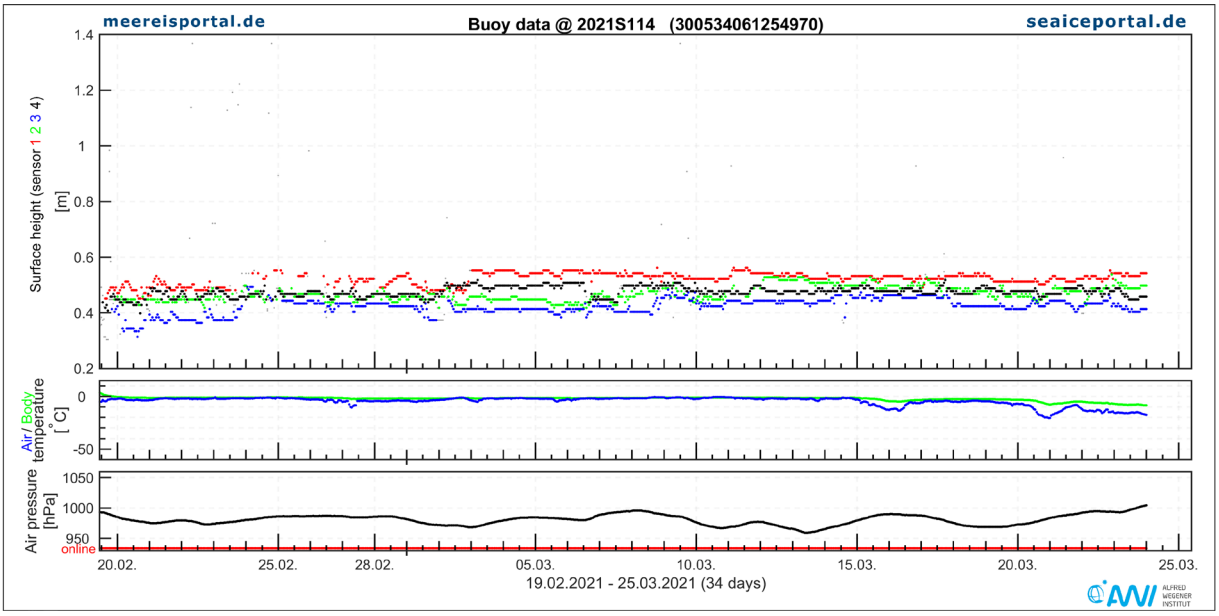

Fig. 6.13: Example of time series of snow accumulation along with respective meteorological conditions for Snow Buoy 2021S114, deployed on February 19, 2021

Data management

All buoy positions and raw data are available in near real time through the sea-ice data portal www.meereisportal.de. At the end of their lifetime (end of transmission of data), all data will be finally processed, archived, published and disseminated according to international standards by the World Data Center PANGAEA Data Publisher for Earth & Environmental Science (www.pangaea.de) within two years after the end of the cruise. By default the CC-BY license will be applied. All Snow Buoys report their position and atmospheric pressure directly to the Global Telecommunication System (GTS). Furthermore, all data are exchanged with international partners via the International Programme for Antarctic Buoys.

6.6 Fast ice

Objectives

Landfast ice in the vicinity of ice shelves is often underlain by a sub-ice platelet layer (SIPL), which forms in the presence of near-surface, supercooled Ice Shelf Water (ISW). For example, it is well known that there is an abundance of platelet ice under fast ice along the shores of the southwestern Weddell Sea, i.e., in the PS111 study region (e.g. Arndt et al. 2020). Mapping the occurrence and thickness of the SIPL under landfast ice, now possible by means of airborne

electromagnetic (EM) sounding (Haas et al. 2020), can therefore provide important information on the characteristics of ISW. It was therefore an objective of our work to map as much landfast ice as possible whenever we operated near the coast. These surveys complement a project using AWI's Polar 5 and 6 aircraft: the Circum-Antarctic Platelet Ice Survey (CAPIS). They have surveyed major parts of the Dronning Maud Land coast in December 2018 (Haas and Irvin, 2019) and will continue to do so in late 2022 (AWI aircraft proposal under review).

The SIPL under landfast ice is also known to be one of the most productive sea-ice habitats around Antarctica. In addition to the airborne surveys, we therefore carried out ice coring and other *in-situ* measurements during ice stations on fast ice.

Work at sea

We have carried out three airborne EM surveys over fast ice inlets in the Stancomb-Wills Ice Stream and Brunt Ice Shelf (on February 10 and March 14, respectively), and over Atka Bay (on March 19; see Fig. 6.1 and Table 6.3).

On March 13 and 17, we carried out snow studies, ice coring, and ground-based thickness surveying on the inlet in the Brunt Ice Shelf and in Atka Bay, respectively (Stations PS124_20210313_17 and PS124_20210317_18, respectively; Fig. 6.1, Table 6.2).

Preliminary results

Fig. 6.14 shows the flight tracks of the fast-ice surveys overlaid on TerraSAR-X radar images. The images show some distinct ice type variability, which is visible in the ice thickness profiles, representing different ice agees and roughnesses. There was little platelet ice on the eastern side of the Stancomb-Wills Ice Stream, maybe because in summer it is exposed to the relatively warm surface waters of the Coastal Current. In contrast, the measurements showed some platelet ice under the fast ice in the Brunt Ice Shelf, in good agreement with our *in-situ* measurements, which confirmed a 0.86 m thick layer of sub-ice platelet ice under 2.79 m of consolidated ice and 1.05 m of snow (total thickness 4.7 m; Fig. 6.10, station 17).

Sections of high biomass inclusions characterized the ice core taken from the Brunt landfast ice, which had zero freeboard but a moist snow/ice-interface. In the upper one meter of the ice core, ice associated algae like *Navicula* spp. and *Nitzschia* spp. were mainly found. Below, *Chaetoceros spores*, *Fragilariopsis* spp., and *Thalassiosira* spp. type species dominated the community. The occurrence of fecal pellets and zooplankton larval stages as well as foraminifera throughout the core underscore the importance of landfast ice ecosystems for the Antarctic carbon cycle.

The survey over Atka Bay on March 19 showed the most platelet ice along the eastern profile, increasing in thickness from north to south (Fig. 6.14 and 6.15). This is in agreement with the *in-situ* measurements of 1.10 m of snow on 1.83 m of ice (Fig. 6.7, station 18), underlain by a 2.47 m thick SIPL. The ice had negative freeboard of more than –10 cm, but it was relatively dry and only once the core hole filled with water. Results of the eastern profile were in stark contrast to the western profile, which covered some of the older, rougher ice to the west. It did not show clear indications of the presence of a SIPL. The difference between the western and eastern profiles may indicate a different late-summer ocean circulation in Atka Bay, with warmer waters to the west where platelet ice is normally also observed during winter.

Data management

The AEM and *in-situ* data will be managed in the same way as the data presented in Chapters 6.1 and 6.2. All data will be archived, published and disseminated according to international standards by the World Data Center PANGAEA Data Publisher for Earth & Environmental

Science (www.pangaea.de) within two years after the end of the cruise. By default the CC-BY license will be applied.

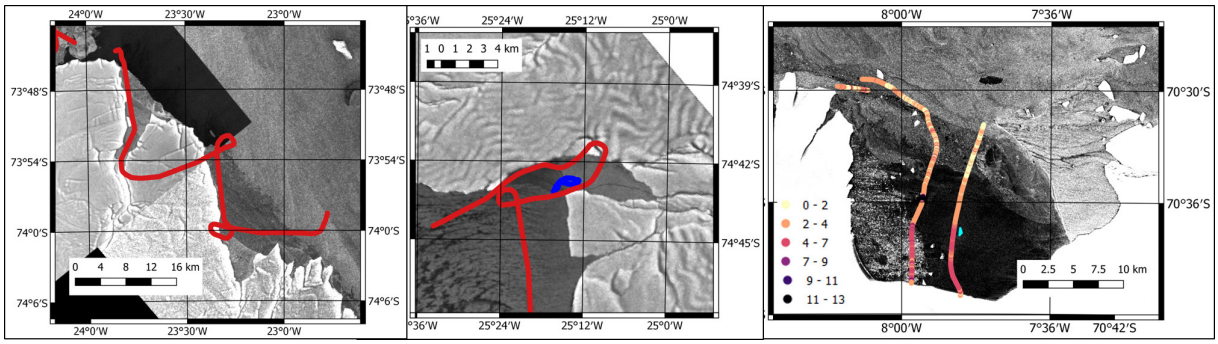

Fig. 6.14: TerraSAR-X images of the fast ice inlets surveyed, with flight tracks overlaid: Left: Stancomb-Wills Ice Shelf; middle: Brunt Ice Shelf; right: Atka Bay Blue tracks indicate location of ground-based EM profiles at ice stations. Colors in right map show ice thickness in meters.

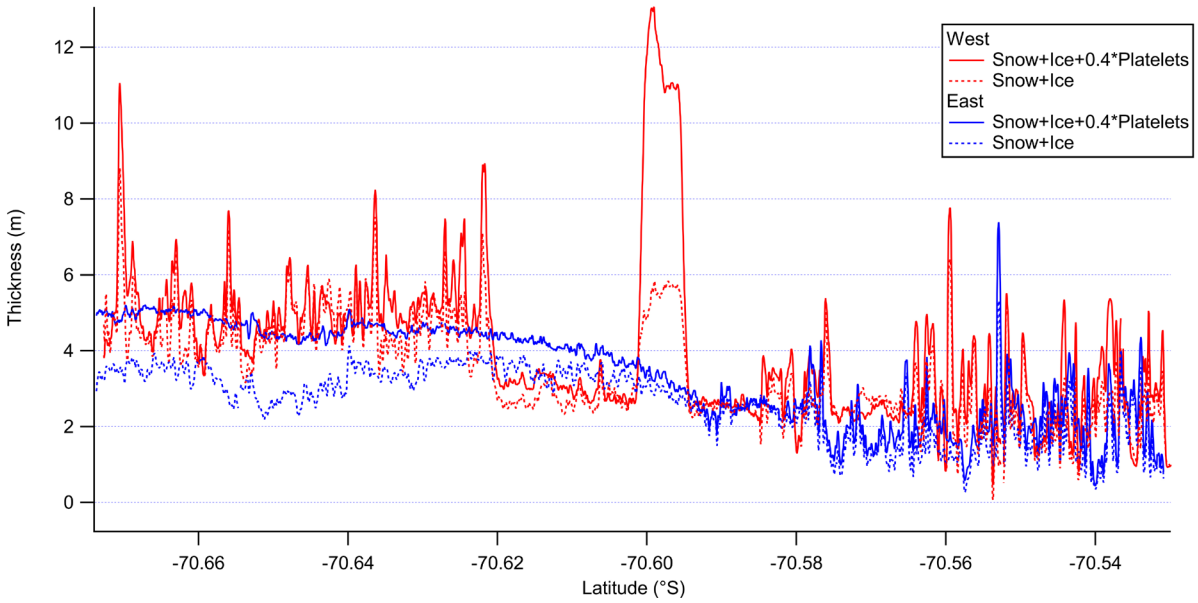

Fig. 6.15: Ice thickness versus latitude of the western (red) and eastern (blue) flight tracks (see Fig. 6.14 right); solid lines show total thickness of snow, ice, and platelets (scaled), stippled lines show thickness of snow plus ice.

6.7 Along track observations of sea-ice conditions

Objectives

Over the last three decades, ship-based visual observations of the state of the sea ice and its snow cover have been performed over all seasons and represent the best-available observational data set of Antarctic sea ice. The recordings follow the Scientific Committee on

Antarctic Research (SCAR) Antarctic Sea Ice Processes and Climate (ASPeCt) protocol and include information on sea-ice concentration, sea-ice thickness and snow depth as well as sea-ice type, surface topography, and floe size. The data is combined with information about meteorological conditions as air temperature, wind speed, and cloud coverage. The protocol is a useful method to obtain a broad range of characterization and documentation of different sea-ice states and specific features during the cruise.

Work at sea

Every full daytime hour during steaming, sea-ice observations were carried out by trained scientists. The observations follow the ASPeCt protocol (Worby 1999), with a software following the ASPeCt standard and being provided on a notebook on the ship's bridge. For every observation, pictures were taken in three different directions (portside, ahead, starboard).

Date, time, and position of the observation were obtained from the DSHIP system, along with standard meteorological data (current sea temperature, air temperature, true wind speed, true wind direction, visibility). The characterization of the ice conditions was estimated by taking the average between observations to port side, ahead, and to starboard side. Ice thicknesses of tilted floes were estimated by observing a ruler stick attached to the ship's starboard side.

Preliminary (expected) results

During PS124, first drifting ice patches were passed on February 09, 2021 at 04:30 UTC. However, hourly sea-ice observations were started as soon as those patches occurred more frequently, on February 09, 2021 16:00 at 71°10.266'S/27°36.834'W. The last sea ice observation was done on March 15, 2021 at 23:00 UTC at 73°22.256'S/27°29.1394'W. We left the pack ice in the southeastern Weddell Sea during the following night. Over the period of 35 days, 258 individual observations were recorded. Sea-ice observations were skipped when the ship was stopped for station work (e.g., CTD, biology/geology station). Due to limited sight, ice observations were also skipped during civil twilight/nighttime.

After stopping the official ice observation programme, we crossed again sea-ice covered areas when approaching *Neumayer Station III*. However, those areas were not considered for further ice observations.

Fig. 6.16 summarizes all conducted sea-ice observations during PS124. The mean sea-ice concentration was calculated as 52.5 ± 33.4 % with a mean sea-ice thickness of 0.53 ± 0.42 m and 0.23 ± 0.17 m snow on top. However, it needs to be recognized that we steamed through wide areas of newly formed thin ice, causing the low mean ice thickness values. Therefore, averaging pack-ice floes of first- and second-year ice only, the mean sea-ice thickness amounts to 0.96 ± 0.44 m with 0.30 ± 0.20 m snow on top.

Data management

The visual sea-ice observations were already post-processed on board and will be archived, published and disseminated together with the taken pictures according to international standards by the World Data Center PANGAEA Data Publisher for Earth & Environmental Science (www.pangaea.de) within two months after the cruise. By default the CC-BY license will be applied.

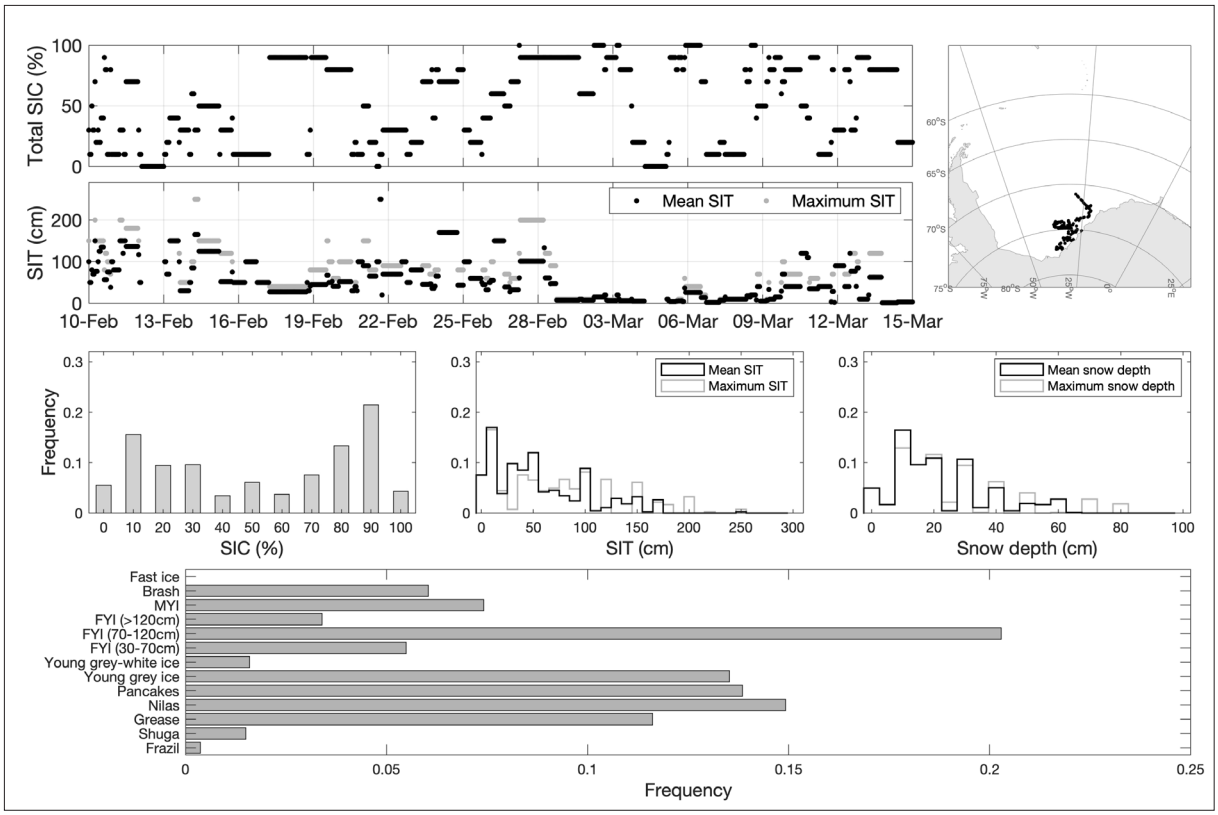

Fig. 6.16: Overview of all conducted sea-ice observations from the ship's bridge: Total sea-ice concentration (SIC) displays the overall sea-ice concentration around the ship. Sea-ice thickness (SIT) and snow depth data are subdivided into calculated mean (black) and maximum values (gray) per ice observation. Bottom panel displays the overall sea-ice type distribution from all ice observations. Upper right panel displays all locations of ice observations.

References

Arndt S, Hoppmann M, Schmithüsen H, Fraser AD, Nicolaus M (2020) Seasonal and interannual variability of landfast sea ice in Atka Bay, Weddell Sea, Antarctica. The Cryosphere, 14, 2775–2793, https://doi.org/10.5194/tc-14-2775-2020.

Arndt S, Haas C (2019) Spatiotemporal variability and decadal trends of snowmelt processes on Antarctic sea ice observed by satellite scatterometers. The Cryosphere, 13, 1943–1958, https://doi.org/10.5194/tc-13-1943-2019.

Arndt S, Paul S (2018) Variability of winter snow properties on different spatial scales in the Weddell Sea. Journal of Geophysical Research - Oceans, 123, 8862–8876, https://doi.org/10.1029/2018JC014447.

Arndt S, Nicolaus M, Dierking W, Willmes S (2016) Timing and regional patterns of snowmelt on Antarctic sea ice from passive microwave satellite observations. Journal of Geophysical Research-Oceans, 121(8), 5916–5930, https://doi.org/10.1002/2015JC011504.

Arrigo K, Worthen DL, Dixon PL, Lizotte MP (1998) Primary productivity of near surface communities within Antarctic pack ice. Antarctic Sea Ice: Biological Processes, Interactions and Variability, 73, 23-43.

Behrendt A, Dierking W, Witte H (2015), Thermodynamic sea ice growth in the central Weddell Sea, observed in upward-looking sonar data, J. Geophys. Res. Oceans, 120, 2270–2286, https://doi.org/10.1002/2014JC010408.

Bintanja R, van Oldenborgh G, Drijfhout S, Wouters B, Katsman C (2013) Important role for ocean warming and increased ice-shelf melt in Antarctic sea-ice expansion: Nat. Geosci., 6(5), 376–379, https://doi.org/10.1038/ngeo1767.

Günther S, Gleitz M, Dieckmann GS (1999) Biogeochemistry of Antarctic sea ice: a case study on platelet ice layers at Drescher Inlet, Weddell Sea. Mar Ecol-Prog Ser 177, 1–13.

Haas C, Liu Q, Martin T (1999). Retrieval of Antarctic sea-ice pressure ridge frequencies from ERS SAR imagery by means of *in-situ* laser profiling and usage of a neural network, International Journal of Remote Sensing, 20/15/16, 3111–3123.

Haas C, Thomas DN, Bareiss J (2001) Surface properties and processes of perennial Antarctic sea ice in summer. Journal of Glaciology, 47(159), 613–625.

Haas C, Lobach J, Hendricks S, Rabenstein L, Pfaffling A (2009). Helicopter-borne measurements of sea ice thickness, using a small and lightweight, digital EM system, Journal of Applied Geophysics, 67(3), 234-241. https://doi.org/10.1016/j.jappgeo.2008.05.005.

Haas C, Irvin A (2019), CAPIS – Circum-Antarctic Platelet Ice Survey. In: Fromm, T., C. Oberdieck, T. Heitland, and P. Köhler (Eds.), Expeditions to Antarctica: ANT-Land 2018/19 Neumayer Station III, Kohnen Station, Flight Operations and Field Campaigns, Reports on Polar and Marine Research, 733, 126–130. ISSN 1866-3192. http://hdl.handle.net/10013/epic.d6385ca6-e1d3-4cca-a0d8-c62778473d63 and https://doi.org/10.2312/BzPM_0733_2019

Haas C, Langhorne PJ, Rack W, Leonard GH, Brett GM, Price D, Beckers JF, Gough AJ (2020) Airborne mapping of the sub-ice platelet layer under fast ice in McMurdo Sound, Antarctica. The Cryosphere Discussion, tc-2020–268.

Hobbs WR, Massom R, Stammerjohn S, Reid P, Williams G, Meier W (2016) A review of recent changes in Southern Ocean sea ice, their drivers and forcings. Global and Planetary Change, 143, 228–250, https://doi.org/10.1016/j.gloplacha.2016.06.008.

Holland PR, Kwok R (2012) Wind-driven trends in Antarctic sea-ice drift. Nat. Geosci., 5, 872, https://doi.org/10.1038/ngeo1627.

Kattner G, Thomas DN, Haas C, Kennedy H, Dieckmann GS (2004) Surface ice and gap layers in Antarctic sea ice: highly productive habitats. Marine ecology-progress series, 277, 1–12.

Kwok R, Maksym T (2014), Snow depth of the Weddell and Bellingshausen sea ice covers from IceBridge surveys in 2010 and 2011: An examination, J. Geophys. Res. Oceans, 119, 4141–4167, https://doi.org/10.1002/2014JC009943.

Laukert G, Frank M, Hathorne EC, Krumpen T, Rabe B, Bauch D, Werner K, Peeken I, Kassens H (2017) Pathways of Siberian freshwater and sea ice in the Arctic Ocean traced with radiogenic neodymium isotopes and rare earth elements. Polarforschung, 87,3–13.

Meiners KM, Vancoppenolle M, Carnat G, Castellani G, Delille B, Delille D, Dieckmann GS, Flores H, Fripiat F, Grotti M, Lange BA, Lannuzel D, Martin A, Mcminn A, Nomura D, Peeken I, Rivaro P, Ryan KG, Stefels J, Swadling KM, Thomas DN, Tison JL, Van Der Merwe P, Van Leeuwe MA, Weldrick C, Yang EJ (2018) Chlorophyll-a in Antarctic Landfast Sea Ice: A First Synthesis of Historical Ice Core Data. J Geophys Res-Oceans, 123, 8444–8459.

Meiners KM, Vancoppenolle M, Thanassekos S, Dieckmann GS, Thomas DN, Tison JL, Arrigo KR, Garrison DL, Mcminn A, Lannuzel D, Van Der Merwe P, Swadling KM, Smith WO, Melnikov I, Raymond B (2012) Chlorophyll *a* in Antarctic sea ice from historical ice core data. Geophys. Res. Lett., 39.

Nicholls KW, Østerhus S, Makinson K, Gammelsrød T, Fahrbach E (2009) Ice-ocean processes over the continental shelf of the southern Weddell Sea, Antarctica: A review. Rev. Geophys., 47, RG3003, https://doi.org/10.1029/2007RG000250.

Papadimitriou S, Thomas DN, Kennedy H, Kuosa H, Dieckmann GS (2009) Inorganic carbon removal and isotopic enrichment in Antarctic sea ice gap layers during early austral summer. Marine Ecology Progress Series, 386, 15–27.

Paul S, Willmes S, Heinemann G (2015) Long-term coastal-polynya dynamics in the southern Weddell Sea from MODIS thermal-infrared imagery. The Cryosphere, 9(6), 2027–2041, https://doi.org/10.5194/tc-9-2027-2015.

Peeken I, Primpke S, Beyer B, Gütermann J, Katlein C, Krumpen T, Bergmann M, Hehemann L, Gerdts G (2018) Arctic sea ice is an important temporal sink and means of transport for microplastic. Nature Communications, 9, 1505.

Schwegmann S, Haas C, Fowler C, Gerdes R (2011) A comparison of satellite-derived sea-ice motion with drifting-buoy data in the Weddell Sea, Antarctica. Ann. Glaciol., 52 (57), 103–110.

Smetacek V, Scharek R, Gordon LI, Eicken H, Fahrbach E, Rohardt G, Moore S (1992) Early spring phytoplankton blooms in ice platelet layers of the southern Weddell Sea, Antarctica. Deep-Sea Research 39: 153–168.

Thompson DWJ, Solomon S, Kushner PJ, England MH, Grise KM, Karoly DJ (2011) Signatures of the Antarctic ozone hole in Southern Hemisphere surface climate change. Nature Geosci. 4, 741–749, https://doi.org/10.1038/ngeo1296.

Turner J, Comiso JC, Marshall GJ, Lachlan-Cope TA, Bracegirdle TJ, Maksym T, Meredith MP, Wang Z, Orr A (2009) Non-annular atmospheric circulation change induced by stratospheric ozone depletion and its role in the recent increase of Antarctic sea ice extent. Geophys. Res. Lett., 36, L08502, https://doi.org/10.1029/2009GL037524.

Turner J, Hosking JS, Bracegirdle TJ, Marshall GJ, Phillips T (2015) Recent changes in Antarctic Sea Ice. Phil. Trans. R. Soc. A, 373, 20140163, https://doi.org/10.1098/rsta.2014.0163.

Turner J, Guarino M.V, Arnatt J, Jena B, Marshall GJ, Phillips T, et al. (2020) Recent decrease of summer sea ice in the Weddell Sea, Antarctica. Geophys. Res. Lett., 47, e2020GL087127, https://doi.org/10.1029/2020GL087127.

Observational Techniques and Results, Antarctic CRC Reports, 23. Vernet M, Geibert W, Hoppema M, Brown PJ, Haas C, Hellmer HH, et al. (2019) The Weddell Gyre, Southern Ocean: Present knowledge and future challenges. Reviews of Geophysics, 57, https://doi.org/10.1029/2018RG000604

Wollenburg JE, Katlein C, Nehrke G, Nothig EM, Matthiessen J, Wolf-Gladrow DA, Nikolopoulos A, Gazquez-Sanchez F, Rossmann L, Assmy P, Babin M, Bruyant F, Beaulieu M, Dybwad C, Peeken I (2018) Ballasting by cryogenic gypsum enhances carbon export in a Phaeocystis under-ice bloom. Sci Rep-Uk 8.

Worby A, Allison I (1999) A ship-based technique for observing Antarctic sea ice: Part I.

Tab. 6.2: List of all sea-ice stations within the WedIce II project during PS124. Abbreviations for the used gear are in accordance to the labels given in Table 6.1.

Station	Date	Time [UTC] start	Lati-tude start	Longi-tude start	Time [UTC] end	Lati-tude end	Longi-tude end	Gear									
								SIT	SPIT	SMP	SDMP	GEM	CORE	WATER	BUOY	STRAP	OCE
PS124_20210210_1	2021-02-10	10:43	-73.018	-23.235	14:22	-73.010	-23.232	X	X	X	X	X	X	X			
PS124_20210211_2	2021-02-11	18:10	-74.031	-28.095	20:18	-74.937	-28.121	X	X	X	X	X	X	X			
PS124_20210214_3	2021-02-14	10:06	-74.539	-29.781	13:53	-74.556	-29.760	X	X	X	X	X	X	X			
PS124_20210215_4	2021-02-15	13:25	-74.892	-29.368	16:46	-74.876	-29.363	X	X	X	X	X	X	X			
PS124_20210216_5	2021-02-16	10:07	-74.953	-33.000	13:14	-74.966	-32.959	X	X	X	X	X	X	X			
PS124_20210218_6	2021-02-18	09:29	-74.998	-32.447	13:58	-75.021	-32.407	X	X	X	X		X	X		X	
PS124_20210222_7	2021-02-22	09:19	-74.323	-36.116	11:43	-74.315	-36.156	X	X	X	X	X	X	X			
PS124_20210223_8	2021-02-23	10:50	-74.075	-35.841	14:19	-74.070	-35.832	X	X	X	X	X	X	X			
PS124_20210224_9	2021-02-24	09:28	-74.119	-32.472	12:15	-74.112	-32.507	X	X	X	X	X	X	X			
PS124_20210225_10	2021-02-25	09:19	-74.673	-33.512	12:22	-74.669	-33.541	X	X	X	X	X	X	X		X	
PS124_20210226_11	2021-02-26	09:29	-74.600	-33.387	12:23	-74.591	-33.460	X	X	X	X	X	X	X			
PS124_20210227_12	2021-02-27	09:13	-74.865	-31.113	11:43	-74.877	-31.081	X	X	X	X	X	X	X			
PS124_20210301_13	2021-03-01	10:05	-75.599	-34.116	11:41	-75.603	-34.159		X				X	X			
PS124_20210306_14	2021-03-06	09:11	-77.184	-36.147	11:11	-77.186	-36.167	X	X	X	X	X	X	X	X		
PS124_20210310_15	2021-03-10	14:57	-74.567	-32.639	17:04	-74.598	-32.648	X	X		X	X	X	X			
PS124_20210311_16	2021-03-11	09:50	-74.456	-29.633	12:56	-74.463	-29.613	X	X	X	X	X	X	X	X		
PS124_20210313_17	2021-03-13	09:49	-74.713	-25.260	16:20	-74.713	-25.260	X	X			X	X	X			
PS124_20210317_18	2021-03-17	15:17	-70.623	-7.843	20:00	-70.623	-7.843	X	X	X		X	X	X	X		X

Tab. 6.4: List of all snow and (total) sea-ice thickness (sea-ice thickness + snow depth) transect measurements during PS124. A single snow-depth transect was performed at station PS124_2021018_6 and single sea-ice thickness transects at the two fast ice stations PS124_20210313_17 and PS124_20210317_18. Modal values were given only for dominant modes in the respective data set. Abbreviations (according to Table 6.1): SDMP – Snow depth measured with Magna Probe (snow depth transect), GEM – Ground electromagnetic sounding (sea-ice thickness transect).

Station	Label SDMP	Label GEM	Date	Time [UTC] start	Latitude start	Longitude start	Time [UTC] end	Latitude end	Longitude end	Profil length [m]	Snow depth [mean, cm]	Snow depth [mode, cm]	Total ice thickness [mean, cm]	Total ice thickness [mode, cm]
PS124_20210210_1	-1	-1	2021-02-10	12:43	-73.015	-23.237	13:21	-73.012	-23.235	1004	21 ± 13	10	128 ± 50	130
PS124_20210211_2	-1	-1	2021-02-11	19:37	-74.035	-28.109	20:02	-74.036	-28.116	629	41 ± 21	38	168 ± 59	110
PS124_20210214_3	-1	-1	2021-02-14	11:42	-74.549	-29.778	12:20	-74.554	-29.768	1010	16 ± 13	5	93 ± 55	60
PS124_20210215_4	-1	-1	2021-02-15	14:56	-74.884	-29.357	15:40	-74.879	-29.358	968	35 ± 23	25	173 ± 112	60
PS124_20210216_5	-1	-1	2021-02-16	11:59	-74.961	-32.980	12:58	-74.965	-32.961	1073	54 ± 27	50	240 ± 79	240
PS124_20210218_6	-1	-	2021-02-18	12:11	-75.011	-32.426	12:57	-75.016	-32.417	1166	53 ± 24	55		-
PS124_20210222_7	-1	-1	2021-02-22	10:49	-74.319	-36.142	11:24	-74.316	-36.153	1088	26 ± 10	25	120 ± 28	100
PS124_20210223_8	-1	-1	2021-02-23	12:36	-74.072	-35.834	13:02	-74.071	-35.832	686	30 ± 24	15	248 ± 120	150
PS124_20210224_9	-1	-1	2021-02-24	11:15	-74.112	-32.491	12:05	-74.112	-32.504	847	42 ± 22	35	242 ± 134	150
PS124_20210225_10	-1	-1	2021-02-25	11:13	-74.671	-33.535	11:49	-74.670	-33.540	936	38 ± 24	15	236 ± 74	270
PS124_20210226_11	-1	-1	2021-02-26	11:39	-74.595	-33.439	12:10	-74.592	-33.453	897	30 ± 9	25	139 ± 31	120
PS124_20210227_12	-1	-1	2021-02-27	10:38	-74.875	-31.095	11:10	-74.877	-31.086	843	40 ± 20	35	182 ± 85	170
PS124_20210306_14	-1	-1	2021-03-06	10:36	-77.185	-36.161	11:07	-77.186	-36.169	582	26 ± 9	25	185 ± 17	170
PS124_20210310_15	-1	-1	2021-03-10	16:14	-74.586	-32.642	16:51	-74.595	-32.647	1096	52 ± 23	60	370 ± 50	390
PS124_20210311_16	-1	-1	2021-03-11	11:47	-74.461	-29.625	12:29	-74.462	-29.618	1182	26 ± 11	23	80 ± 27	60
PS124_20210313_17	-	-1	2021-03-13	12:15	-74.713	-25.260	14:15	-74.713	-25.260	4958	-	-	457 ± 127	365
PS124_20210317_18	-	-1	2021-03-17	16:15	-70.623	-7.843	17:05	-70.623	-7.843	1577	-	-	377 ± 9	375

Tab. 6.6: Overview of all sampled snow pits

Label	Date	Time [UTC]	Latitude	Longitude	OW fraction [%]	Mean thick-ness [m]	St. dev. [m]	Mode 1 [m]	Mode 2 [m]	Mode 3 [m]	Mode 4 [m]	Mode 5 [m]
PS124_20210210_HEM1	2021-02-10	18:57	-73.524	-23.288	1.67	1.78	1.11		1.25			
PS124_20210224_HEM2	2021-02-24	16:31	-74.178	-32.342	11.55	1.72	1.33	0.75		1.75	2.15	
PS124_20210227_HEM3	2021-02-27	19:51	-74.750	-31.303	24.63	1.49	1.49	0.55	1.45	1.75		
PS124_20210308_HEM4	2021-03-08	9:44	-77.100	-36.539	16.28	1.38	1.33	0.2	1.25	1.65	2.45	
PS124_20210314_HEM5	2021-03-14	13:55	-75.146	-24.643	37.6	1.36	2.66		1.35			
PS124_20210319_HEM6	2021-03-19	18:37	-70.494	-8.129	0.57	2.12	1.11	0.95	1.55	1.95	2.55	2.85

7. SOUTHERN OCEAN CARBON CYCLING

Clara Flintrop[1], Andreas Rogge[1,2], [1]DE.AWI
Barbara Glemser[3], (not on board): [2]DE.CAU
Morten Iversen[1], Scarlett Trimborn[1] [3]DE.MPIMM

Grant No. AWI_PS124_13

Objectives

Climate changes in the Southern Ocean have large implications for the global marine carbon cycle. These changes include shifts in phytoplankton productivity and community structure as well as oceanographic phenomena such as currents and cross-shelf transport.

One important process for marine carbon sequestration is the biological carbon pump. The strength of the biological carbon pump depends on the present functional types of phytoplankton, which act as vectors for vertical carbon export. Studies have reported a possible shift in phytoplankton community structure from diatoms to small flagellates such as *Phaeocystis* sp. in the Southern Ocean due to climate change effects (e.g., Trimborn et al. 2016), with unknown consequences for nutrient and carbon cycling.

Currents also play an important role for carbon sequestration due to their ability to inject particles into deeper layers. In the Southern Ocean, High Salinity Shelf Water (HSSW, e.g. Jacobs et al. 1985) is of special interest, because it flows along the sea floor where it potentially re-suspends organic material and transports it across the continental slope towards the deep sea. A similar process was recently observed in the Arctic Ocean where propagating dense Barents Sea bottom water caused a widespread particle plume at ~1,000 m depth in the Eurasian Basin (Rogge et al. in prep.).

To assess the potential for future biological CO_2 sequestration in the Southern Ocean, we deployed instruments to measure present-day carbon fluxes in the Weddell Sea and to determine the factors driving carbon flux in the study area. On board, we tested taxon-specific aggregation capacities of differing phytoplankton assemblages to evaluate how a predicted shift from large diatoms to small diatoms and *Phaeocystis* sp. will influence the efficiency of the biological carbon pump.

Work at sea

Drifting sediment traps

Drifting sediment traps were deployed at 6 stations (Fig. 7.1, Table 7.1). A drifting sediment trap consists of three trap stations at depths of 100, 200, and 300 m, each equipped with four collection cylinders attached via a gyroscopic mounting. We aimed for a 24 h deployment time for each drifting sediment trap to capture the day-night cycle of carbon flux in the study area. The final deployment times of the 6 sediment traps varied from 18 – 52 h.

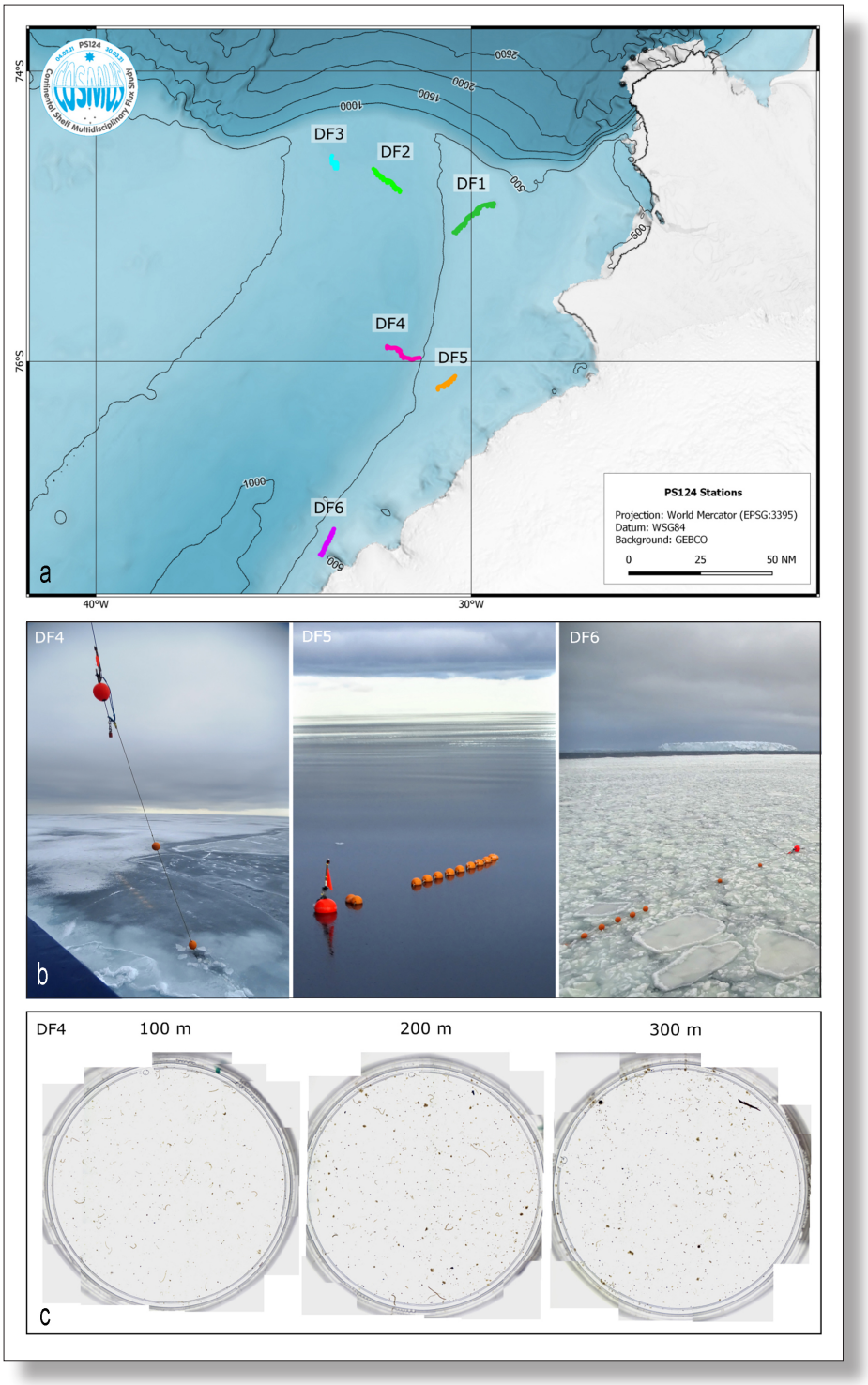

Fig. 7.1: a) Map of free-drifting sediment trap tracks (top);
b)sea-ice conditions during three recoveries (middle);
c) gel cups with structurally preserved particles (bottom)

At every trap depth, one of the four collection cylinders was equipped with a viscous cryogel to structurally preserve fragile marine snow aggregates and fecal pellets, and to determine their abundance and size-distribution. Aggregates collected in the gel cups were imaged on board to analyze aggregate types and particle size-distribution at the respective depths. Gels were frozen and stored at –20 °C for high-resolution imaging at home.

Material from one trap tube per depth was fixed with 2 % mercury chloride and stored at 4 °C for later determination of mass fluxes of carbon, nitrogen, biogenic opal, calcium carbonate, and lithogenic (non-biogenic) material. The material from the remaining trap tubes was frozen at –20 °C for analyses of monosaccharides and 16S/18S rDNA in the home laboratory.

Tab. 7.1: Deployments of free-drifting sediment traps

Action	Station name	Date	Time [UTC]	Latitude	Longitude
DF1 deployment	PS124_8-4	12-02-21	11:45	74°57.190'S	029°26.724'W
DF1 recovery	PS124_16-1	14-02-21	15:40	75°08.570'S	030°26.790'W
DF2 deployment	PS124_26-1	16-02-21	17:29	74°51.113'S	031°54.038'W
DF2 recovery	PS124_31-2	18-02-21	8:59	74°42.072'S	032°37.448'W
DF3 deployment	PS124_54-8	25-02-21	12:01	74°40.961'S	033°34.123'W
DF3 recovery	PS124_54-13	26-02-21	13:59	74°38.713'S	033°42.871'W
DF4 deployment	PS124_71-1	01-03-21	15:59	75°58.599'S	031°22.128'W
DF4 recovery	PS124_74-1	02-03-21	14:08	75°53.980'S	032°15.100'W
DF5 deployment	PS124_79-1	04-03-21	9:15	76°05.541'S	030°25.299'W
DF5 recovery	PS124_85-1	05-03-21	11:44	76°10.040'S	030°53.354'W
DF6 deployment	PS124_90-1	06-03-21	14:33	77°02.405'S	033°39.240'W
DF6 recovery	PS124_91-1	07-03-21	8:55	77°11.562'S	034°01.114'W

Marine Snow Catchers

The size, composition and sinking velocity of marine aggregates influence the efficiency of the biological carbon pump, because they determine the amount (and rate) of microbial degradation and zooplankton grazing. We sampled marine aggregates *in-situ* using Marine Snow Catchers (MSCs; OSIL) to assess the composition, size, settling velocity, microbial respiration rate, and particulate organic carbon and nitrogen content of individual aggregates.

Marine Snow Catchers were deployed at 18 stations during PS124 to sample marine aggregates at selected depths (Table 7.2). Samples were typically collected from 10 – 20 m below the peak of the chlorophyll maximum (as seen from the CTD chlorophyll sensors). After recovery, aggregates collected in the 95 l volume were left to settle to the base of the MSC on deck for 5 – 20 h. Individual particles were gently collected using a wide-mouth bore pipette and transferred to a flow chamber system equipped with an O_2 microsensor for onboard measurements of aggregate size, sinking velocity, and microbial respiration (see Ploug and Jørgensen (1999) for further details).

Tab. 7.2: Deployments of the Marine Snow Catcher

Station name	Date	Time [UTC]	Latitude	Longitude	Sampling depth [m]
PS124_5-7	09-02-21	5:51	70°25.190'S	030°01.359'W	20
PS124_5-7	09-02-21	6:17	70°25.078'S	030°01.233'W	75
PS124_8-6	12-02-21	13:33	74°55.220'S	029°25.382'W	55
PS124_8-6	12-02-21	13:54	74°55.232'S	029°25.409'W	55
PS124_16-4	14-02-21	17:36	75°08.562'S	030°26.740'W	100

Station name	Date	Time [UTC]	Latitude	Longitude	Sampling depth [m]
PS124_16-4	14-02-21	17:57	75°08.559'S	030°26.775'W	100
PS124_21-3	16-02-21	00:21	74°52.058'S	030°39.863'W	100
PS124_26-3	16-02-21	19:26	74°51.325'S	031°49.823'W	90
PS124_30-3	17-02-21	19:22	74°51.110'S	032°59.417'W	90
PS124_33-3	19-02-21	2:20	74°45.006'S	035°08.160'W	30
PS124_37-2	20-02-21	19:48	74°34.870'S	036°23.774'W	50
PS124_45-4	22-02-21	9:29	74°21.017'S	036°02.480'W	75
PS124_54-5	25-02-21	9:20	74°40.002'S	033°35.222'W	25
PS124_54-6	25-02-21	9:42	74°40.060'S	033°35.630'W	60
PS124_72-3	01-03-21	18:51	75°57.700'S	031°32.558'W	75
PS124_76-3	02-03-21	22:41	75°51.978'S	032°08.066'W	50
PS124_78-3	03-03-21	20:23	76°02.343'S	031°02.962'W	50
PS124_90-6	06-03-21	18:32	77°02.344'S	033°34.777'W	60
PS124_90-7	06-03-21	19:02	77°02.398'S	033°34.565'W	60
PS124_94-2	07-03-21	18:29	77°02.728'S	034°44.196'W	50
PS124_100-3	10-03-21	7:46	74°29.752'S	032°32.931'W	50
PS124_107-6	12-03-21	6:02	75°02.156'S	026°56.527'W	70

Particle imaging

To assess particle dynamics in the water column, we performed 86 depth profiles with an Underwater Vision Profiler 5hd camera system (UVP 5hd). The UVP 5hd is a high-frequency (20 Hz) particle quantification and imaging system that was mounted on the CTD rosette. It automatically recognizes and counts particles >100 µm (equivalent spherical diameter, ESD) and stores images of particles >1 mm (ESD). This allowed high-resolution particle profiles (acquisition every 5 cm with 1m s^{-1} winch speed) for every CTD cast in parallel to water mass property measurements.

To relate particle dynamics to mass fluxes, the *In-Situ* Camera system (ISC) was deployed four times, attached to the free-drifting sediment traps at 150-m water depth (DF2, DF3, DF4, DF5; Table 7.1). The ISC consists of an industrial camera with removed infrared filter (Basler) and backend electronics for timing, image acquisition and storage of data, and a fixed focal length lens (16 mm Edmund Optics). A DSPL battery (24 V, 38 Ah) was used to power the system. Images were captured over the whole duration of the trap deployment at a frequency of 0.2 Hz. The ISC was mounted on a platform together with a Seabird SBE19 CTD equipped with an oxygen sensor, a turbidity sensor, and a fluorescence sensor, which sampled at a frequency of one measurement every 60 seconds.

In addition, the long-term acquisition camera system UVP6 (frequency 0.2 Hz) was deployed three times attached to the free-drifting sediment traps at 250-m water depth (DF2, DF4, DF5; Table 7.1), and three times attached to the eddy lander (Table 7.3). Towards the end of the cruise, the UVP6 was successfully deployed with the BGC-1 mooring (see Chapters 3 and 10), which was additionally equipped with two long-term sediment traps. The UVP6 and the long-term sediment traps will image and capture settling particles for approximately one year.

Tab. 7.3: Eddy lander deployments including UVP6

Action	Station name	Date	Time [UTC]	Latitude	Longitude
UVP6 on eddy lander 1	Deployment: PS124_054-10	25-02-21	14:10	74°41.954'S	033°33.031'W
	Recovery: PS124_054-14	26-02-21	16:17	74°41.813'S	033°33.885'W
UVP6 on eddy lander 2	Deployment: PS124_090-02	06-03-21	15:12	77°01.525'S	033°33.096'W
	Recovery: PS124_090-14	07-03-21	13:42	77°01.782'S	033°34.517'W
UVP6 on eddy lander 3	Deployment: PS124_107-09	12-03-21	08:21	75°01.857'S	026°50.537'W
	Recovery: PS124_107-09	13-03-21	10:43	75°01.983'S	026°52.116'W

On-board aggregation experiments

To investigate the aggregation potential of different in-situ phytoplankton communities and the properties of aggregates formed from differing phytoplankton assemblages, we incubated samples from 12 different stations in roller tanks. Phytoplankton was sampled from the chlorophyll maximum layer at four large BioGeo stations (Table 7.4) using the CTD rosette. In addition to the open water stations, seven ice-associated samples were taken for the experiments (Table 7.5). These samples originated from under-ice water sampled at three ice stations, and from melted pancake ice sampled at two locations.

All samples were screened through a 500 µm mesh to remove large grazers before they were incubated in roller tanks. Depending on the amount of water available, between two to nine roller tanks (diameter = 20 cm; length = 8.7 cm; volume= 2,733 cm^3) were filled. Before the start of the incubation, samples for POC/PON content, dissolved organic matter, biogenic silica, inorganic carbon, cell numbers, monosaccharides, as well as transparent exopolymeric particles (TEP) and Coomassie-stainable particles (CSP) were taken. The tanks were placed on roller tables where they rotated at a constant speed. The aggregation process was tracked by filming the tanks at several time points. From the video recordings, the size and settling velocity of the aggregates could be obtained (Ploug et al. 2010).

Depending on the cell concentrations and the type of phytoplankton present in the sample, incubation times ranged between four and nineteen days. When aggregates had formed, the incubation was stopped and aggregates were carefully picked for further analyses. Whenever possible, selected aggregates were transferred to a flow chamber for additional size and settling velocity measurements as well as microbial respiration measurements. All other aggregates were preserved for, e.g., microscopy, cell counts, and POC/PON measurements. From the background water of the tanks, samples were also taken for POC/PON, DOM, biogenic silica, cell numbers, monosaccharides, TEP, and CSP.

Tab. 7.4: Open-water stations sampled for on-board aggregation experiments

Station name	Date	Time [UTC]	Latitude	Longitude	Sampling depth [m]	Phyto-plankton community
PS124_5-4	08-02-21	20:53	70°25.127'S	030°00.152'W	25	NA
PS124_8-9	12-02-21	18:06	74°55.238'S	029°25.458'W	58	Mixed
PS124_26-6	16-02-21	21:20	74°51.278'S	031°49.883'W	50	*Phaeocystis* sp.
PS124_37-2	22-02-21	19:48	74°34.870'S	036°23.774'W	50	Large Diatoms
PS124_68-2	28-02-21	22:27	76°06.160'S	030°18.291'W	36	Mixed
PS124_93-1	07-03-21	15:48	77°03.069'S	034°44.484'W	33	Small diatoms

Tab. 7.5: Ice stations sampled for on-board aggregation experiments

Station name	Date	Time [UTC]	Latitude	Longitude	Sample type	Phytoplankton community
PS124_20210211_2	11-02-21	18:10	74°01.832’S	028°05.695’W	Under-ice water	NA
PS124_20210218_6	18-02-21	9:29	74°59.886’S	032°26.831’W	Under-ice water	Large diatoms
PS124_20210225_10	25-03-21	9:19	74°40.394’S	033°30.704’W	Under-ice water	Mixed
PS124_20210227_12	27-03-21	9:13	74°51.360‘S	031°06.360‘W	Slush ice	Mixed
PS124_68-11_IF_1	01-03-21	11:10	76°06.293’S	030°21.031’W	Pancake ice	Large diatoms/ mixed
PS124_77-1_IF_2	03-03-21	09:20	75°58.323’S	031°45.924’W	Pancake ice	Mixed

Preliminary results

The drifting sediment traps were always deployed in patches of open water but were recovered in variable conditions, ranging from completely ice-free, over pancake-ice, to 100 % ice-covered (Fig. 7.1b). Particles commonly caught in the gel traps included krill fecal pellets, phytoplankton aggregates, copepod fecal pellets, and sediment particles. Less commonly, single copepod and pteropod shells were also found. There was no visible particle attenuation as observed from the gel traps, however, POC flux attenuation might be evident after the biogeochemical analyses are done in the home laboratory (Fig. 7.1c).

Overall, the 86 UVP5 deployments resulted in ~350.000 images and the 6 deployments of the UVP6 in ~8,000 images of marine snow, as well as zooplankton (Fig. 7.2). Interestingly, images of platelet ice in the water column were acquired at stations between the iceberg A74 and the Brunt Ice Shelf (Fig. 7.2c). Preliminary analyses of the particle size-distribution generally showed a strong decrease of the particle abundance with increasing depth in the upper ~50 m of the water column, pointing towards high grazing activity (exemplified by transect ~76 °S, Fig. 7.3). In addition, increased particle abundances directly above the seafloor (up to 20 m above, at some stations up to 100 m above the seafloor) point towards resuspension of particles, most probably driven by tidal influences. Increased particle abundances, especially of larger size classes >250 µm were detected along the sill of Filchner Trough (Fig. 7.3). The abundances correlated with a density interface between High Salinity Shelf Water (HSSW) and modified Warm Deep Water (mWDW), pointing to the retention of particles at the pycnocline.

Drivers and implications of this phenomenon on carbon export will be elucidated in further analyses, including image, CTD, and ADCP data, as well as drifting sediment trap samples.

The phytoplankton communities sampled for the aggregation experiments could be sorted into four broad categories:

1. communities dominated by large diatoms (e.g., *Corethron* sp., long chains of *Chaetoceros* sp.),
2. communities dominated by small diatoms (e.g., single *Fragilariopsis* sp., single small *Chaetoceros* sp.),
3. communities dominated by *Phaeocystis* sp., and
4. communities composed of a mixture of *Phaeocystis* sp. and diatoms (Table 7.4 and Table 7.5).

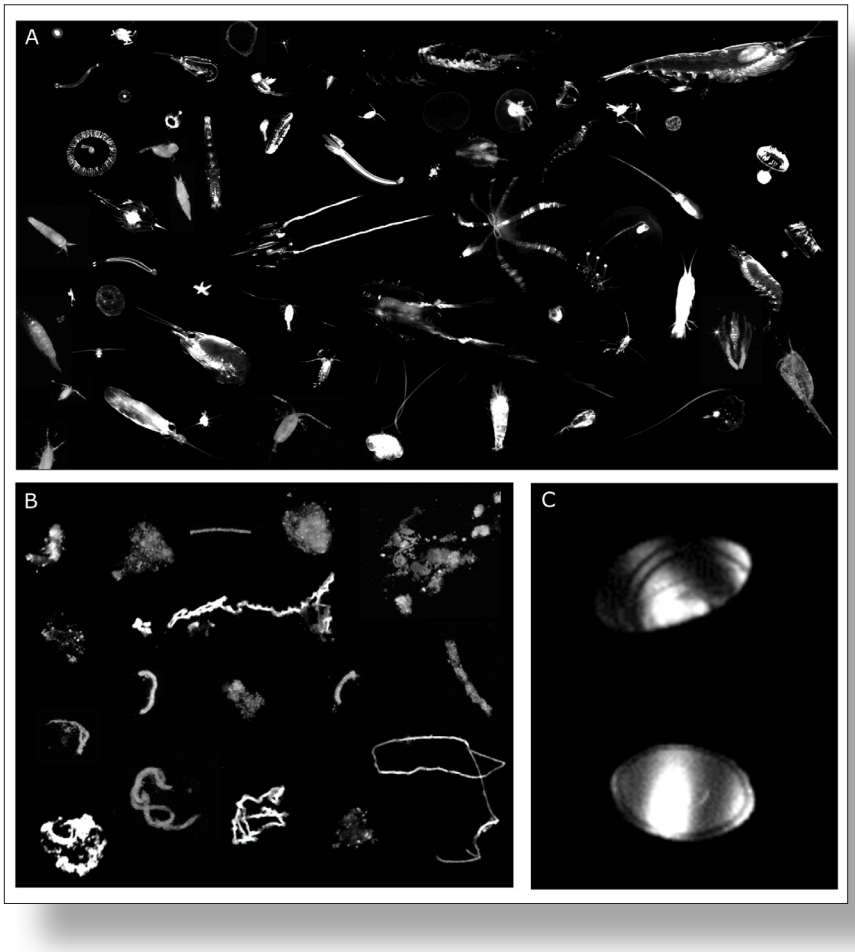

Fig. 7.2: Selection of particles photographed with the UVP5 and UVP6 (not to scale); a) zooplankton, b) marine snow and fecal pellets, c) platelet ice in the water column between A74 and the Brunt Ice Shelf

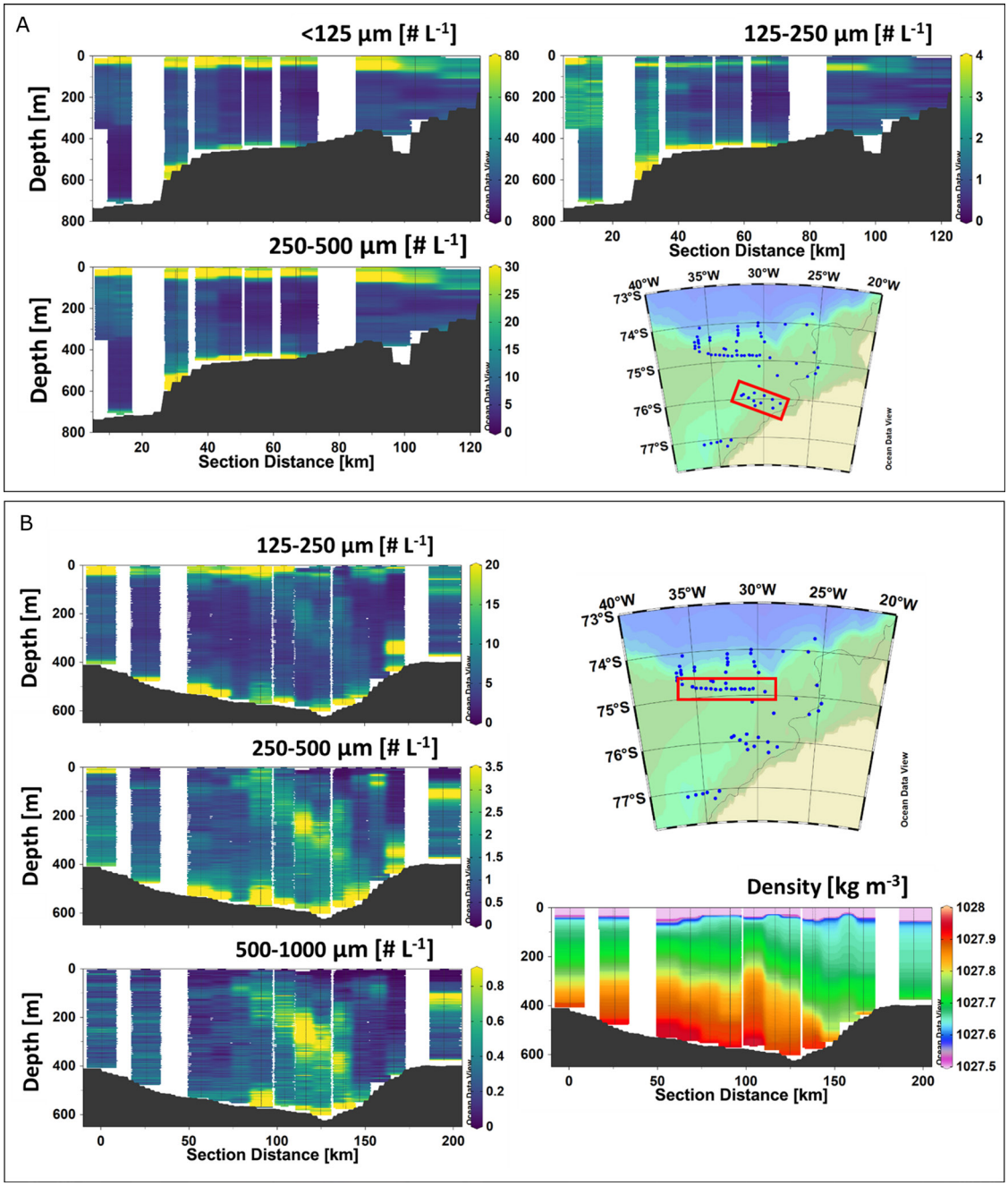

Fig. 7.3: A) UVP5 transect at approx. 76°S exemplifies the general particle distribution. Formed particles in the upper water column are being grazed intensely, leading to rapid flux attenuation; increased particle abundances near the sea floor point towards re-suspension processes, most likely caused by tidal effects. B) Observed particle concentration in the central water column along the Filchner Trough sill; particles of larger size classes (>250 µm) accumulate at the density interface between modified Warm Deep Water (green) and Ice Shelf Water (orange).

Aggregates formed from the different source communities differed in their size-specific settling velocities as well as in the composition and appearance of the aggregates formed (Fig. 7.4). Generally, ice-associated communities formed larger aggregates with higher size-specific settling velocities compared to open-water communities. Furthermore, aggregates formed from

mixed communities had higher size-specific settling velocities compared to diatom-dominated communities. These observations will be further analysed and linked to controlled laboratory process studies, which investigate the effects of a shift towards *Phaeocystis*-dominated plankton communities on the efficiency of the biological carbon pump.

In summary, the *in-situ* and onboard studies will provide a detailed full water column perspective on the export of organic matter as a function of varying phytoplankton assemblages, and a possible inflow of particles by lateral transport. These studies are essential to understand the impact of community shifts and deep particle injection on the biological pump and, thus, its role in providing nutrients to pelagic and benthic ecosystems as well as carbon export and carbon sequestration in Antarctic sediments and deep waters.

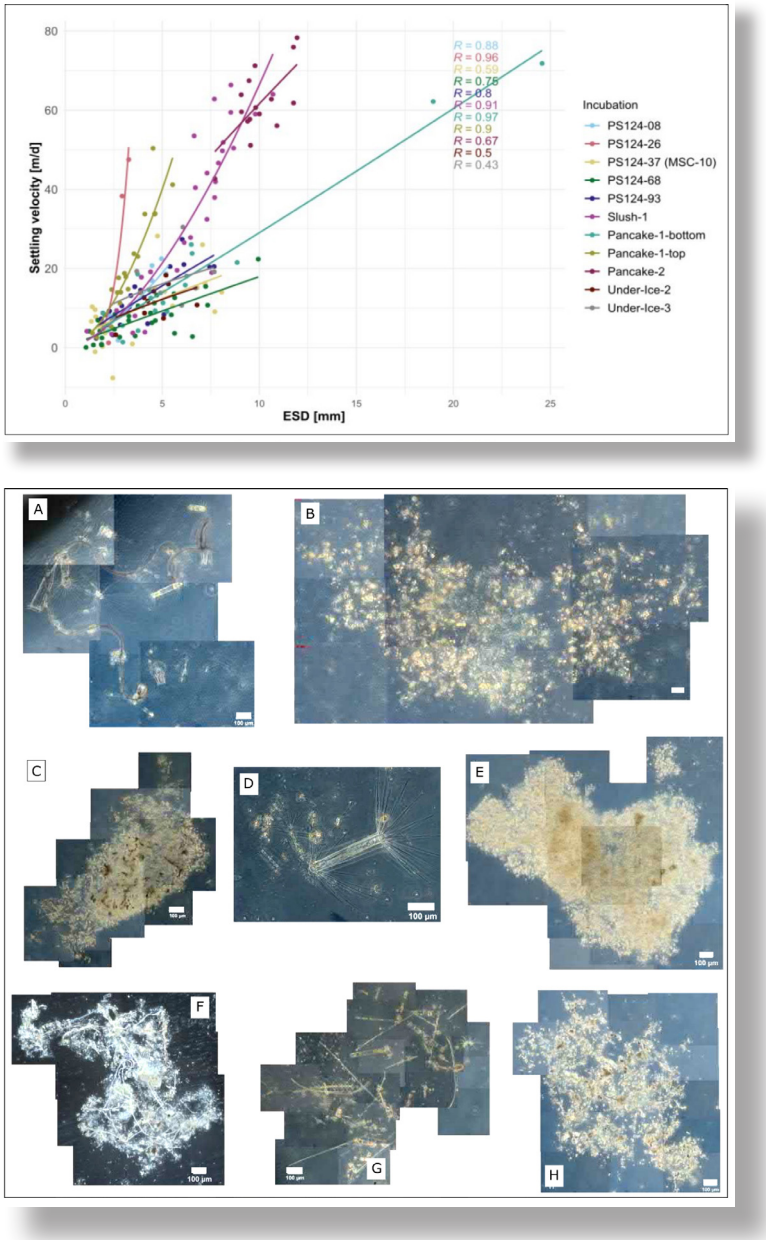

Fig. 7.4: Size versus settling velocity of aggregates formed in roller tanks (top) Microscopic images of aggregates formed from the following incubations (bottom): A) PS124–68, B) Pancake-1-bottom, C) Pancake-2, D) Under-Ice-3, E) Slush-1, F) PS124-26, G) PS124-93, H) Pancake-1-top; scale bar = 100 µm

Data management

Environmental data will be archived, published, and disseminated according to international standards by the World Data Center PANGAEA Data Publisher for Earth & Environmental Science (www.pangaea.de) within two years after the end of the cruise at the latest. By default the CC-BY license will be applied.

Molecular data (DNA and RNA data) will be archived, published, and disseminated within one of the repositories of the International Nucleotide Sequence Data Collaboration (INSDC, www.insdc.org) comprising of EMBL-EBI/ENA, GenBank and DDBJ).

Any other data will be submitted to an appropriate long-term archive that provides unique and stable identifiers for the datasets and allows open online access to the data.

In all publications, based on this cruise, the **Grant No. AWI_PS124_13** will be quoted and the following *Polarstern* article will be cited:

Alfred-Wegener-Institut Helmholtz-Zentrum für Polar- und Meeresforschung. (2017). Polar Research and Supply Vessel POLARSTERN Operated by the Alfred-Wegener-Institute. Journal of large-scale research facilities, 3, A119. http://dx.doi.org/10.17815/jlsrf-3-163.

References

Jacobs SS, Fairbanks RG, Horibe Y (1985) Origin and evolution of water masses near the Antarctic continental margin: Evidence from H218O/H216O ratios in seawater. Antarctic Research Series, 43, 59–83.

Ploug H, Terbrüggen A, Kaufmann A, Wolf-Gladrow D, Passow U (2010) A novel method to measure particle sinking velocity in vitro, and its comparison to three other in vitro methods. Limnology and Oceanography, 8, 386–393.

Ploug H, Jørgensen BB (1999) A net-jet flow system for mass transfer and microsensor studies of sinking aggregates. Marine Ecology Progress Series, 176, 279–290.

Rogge A, Zakharova N, Trudnowska E, Hörstmann C, Schulz K, Janout M, Waite AM, Povazhnyy VV (in prep.) Sequestration of particulate carbon in the deep Eurasian Basin is associated with the transport of modified Atlantic waters.

Trimborn S, Thoms S, Brenneis T, Heiden J, Beszteri S, Bischof K (2016) Two Southern Ocean diatoms are more sensitive to ocean acidification and changes in irradiance than the prymnesiophyte *Phaeocystis antarctica*. Physiologia Plantarum, 160(2), 155–170.

8. BIOGEOCHEMICAL CYCLING IN THE SOUTHERN WEDDELL SEA

Florian Koch[1], Christian Völkner[1], [1]DE.AWI
Jenna Balaguer[1], Henning Hellmer[1],
Scarlett Trimborn[1] (not on board)

Grant No. AWI_PS124_01

Objectives

In 30–50 % of the World Ocean plankton biomass is low even though nutrients and light are plentiful (de Baar et al. 2005). Rather than macronutrients such as nitrate or phosphate, in these high nutrient low chlorophyll (HNLC) regions it is the scarcity of certain trace metals (TM) such as iron (Fe) and/or vitamins, which govern primary production and/or plankton species composition (Martin & Fitzwater 1988; de Baar et al. 2005; Bertrand et al. 2007; Koch et al. 2011). The Southern Ocean (SO) is the world's largest HNLC region, and responsible for roughly 40 % of all oceanic uptake of anthropogenic carbon and an area where iron limitation to phytoplankton has been reported (de Baar et al. 2005; Trimborn et al. 2015). In addition, the SO is an important region contributing disproportionally to upwelling of deep water and formation of intermediate and bottom waters linking the Pacific, Indian and Atlantic Oceans, thus being of global importance in climate regulation, biodiversity and biogeochemical cycles (Buesseler 1998; Lumpkin & Speer 2007).

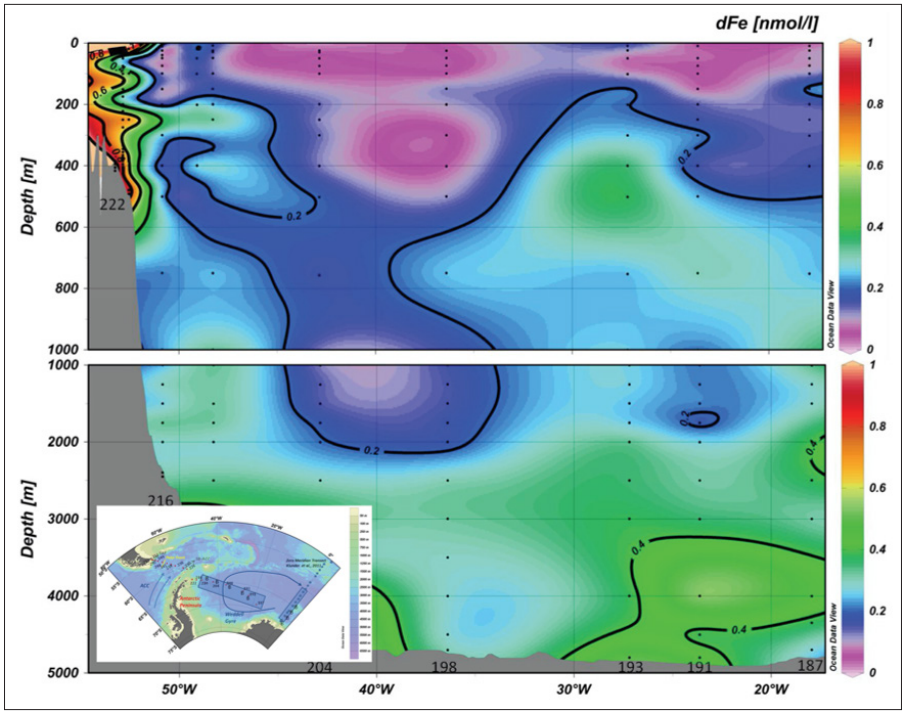

Fig. 8.1: Distribution of dissolved iron across the northern Weddell Sea; adapted from Klunder et al. (2014)

The southern Weddell Sea continental shelf is an area of intense sea-ice and bottom water formation, which coincides with a high, patchily distributed primary production, most likely sequestering CO_2 at significant rates. According to recent IPCC-scenario simulations, the south-eastern Weddell Sea is extremely sensitive to climate change, causing transformations of water mass characteristics, ocean circulation, and biological production. To date, dissolved TM concentrations have only been published for the northern most Weddell Sea (Klunder et al. 2011, 2014) and revealed very low (<0.2 nM, Fig. 8.1) and potentially biomass limiting iron and manganese concentrations at the surface, while concentrations of vitamin B_{12} has never been measured. Cycling of TMs, including grazing mediated recycling rates are also unknown. Phytoplankton productivity and community structure in the Weddell Sea bear important implications for the global marine carbon cycle. Indeed, the strength of the biological carbon pump depends on the functional types of phytoplankton present, since each group will contribute differentially to vertical carbon export. While the flagellate *Phaeocystis antarctica* is considered to be insignificant for vertical transport of biogenic matter, diatoms can significantly affect carbon export. Over the last decade, studies have reported a shift in phytoplankton community structure from diatoms to small flagellates, such as *Phaeocystis* sp., due to elevated temperatures and ice-melting with unknown consequences for nutrient and carbon cycling (Heiden et al. 2019). The impacts of different iron sources and trace nutrients such as manganese and vitamin B_{12} and physical changes such as altered light availability on the plankton community composition in the Weddell Sea, however, have never been investigated.

Our overall goals were:

- to characterize the biochemistry of the water masses, focusing on the key players in the plankton community responsible for primary and secondary production,
- to assess primary and bacterial production rates in the euphotic zone,
- to measure concentrations and cycling (uptake, recycling) of trace metals and vitamins,
- to conduct nutrient amendment and grazing manipulation experiments in order to identify key bottom up and top down processes driving the biological pump and thus carbon export.

Work at sea

In order to characterize the water chemistry and the plankton community, water was collected at 20 stations. In addition, at two contrasting stations targeted bottle manipulation experiments looking at the effects of TMs/vitamins and varying light regimes were conducted. Depth integrated primary- and bacterial production and uptake of iron and vitamin B_{12} was also assessed at 17 stations. More specifically:

Pelagic biogeochemistry

At 20 stations (Table 8.1) and >6 depths, water was collected with AWI's new, state-of-the-art, trace metal clean sampling infrastructure including a Teflon CTD equipped with GoFlo bottles (12 L/bottle capacity). To characterize the community composition (virus, bacteria, phytoplankton), samples for light microscopy, size fractionated pigments (HPLC), particulate organic carbon and nitrogen (POC/PON), biogenic silica (BSi) as well as flowcytometry were taken at the top (15 m, chlorophyll max, bottom of chlorophyll max) three depths. To shed light on the trace metal requirements of the plankton community, samples for particular trace metals were collected and stored frozen for subsequent analysis by ICP-MS. Water from >6 depths was also filtered and frozen or acidified for later dissolved trace metal and dissolved nutrient analysis at the AWI. For vitamins, 2 L of water from each depth was filtered (0.2 µm), acidified with HCl (pH ~6.4) and slowly preconcentrated onto C18 resin for later analysis on a HPLC-MS/MS.

Tab. 8.1: Stations sampled on PS124. HA-like, PP and BP refer to humic acid like compounds, primary production and bacterial production, respectively, while TMxLI and DilX denote trace metal/light manipulation experiments and dilution series grazing experiments, respectively. With the exception for PS124/005, all stations were sampled with the trace metal clean CTD equipped with Teflon coated GoFlo bottles.

Station	Depths sampled	Dissolved trace metals	HA-Like	TM-Quota	PP and BP	Fe and B_{12} uptake rates	Plankton community composition	TMxLi	DilX
PS124-5*	1	x	x	x	x	x	x	x	x
PS124-8-8	6	x	x	x	x	x	x		x
PS124-11-2	6	x							
PS124-16-3	5	x	x	x	x	x	x		
PS124-21-2	5	x							
PS124-26-5	6	x	x	x	x	x	x		x
PS124-30-2	6	x	x	x	x	x	x		
PS124-33-2	5	x	x	x	x	x	x		
PS124-45-3	5	x							
PS124-54-4	5	x	x	x	x	x	x		
PS124-68-4*	5	x	x	x	x	x	x	x	x
PS124-72-2	5	x	x	x	x	x	x		
PS124-76-2	6	x							
PS124-78-2	5	x	x	x	x	x	x		
PS124-88-2	7	x	x	x	x	x	x		x
PS124-90-2	5	x	x	x	x	x	x		x
PS124-94-1	5	x	x	x	x	x	x		
PS124-107-2	6	x	x	x	x	x	x		
PS124-110-2**	6	x	x		x	x	x		
PS124-111-3**	6	x	x		x	x	x		
PS124-112-2**	6	x	x		x	x	x		

** stations at which the Teflon pump was used to fill bottles for the experiments and*
*** stations around iceberg A74 at which only surface samples (15 m) were taken.*
For all other stations: parameters other than dissolved trace metals and HA-like were obtained from the top three depths (see main text).

Pelagic production and iron/vitamin cycling

At 17 stations (Table 8.1) and three depths (15 m, chlorophyll max, bottom of chlorophyll max), ^{14}C-bicarbonate and ^{3}H-leucine were used to measure size fractionated (Total, 0.2–2 µm, >2 µm) primary- and total bacterial production rates, respectively (JGOFS 1996; Kirchman 2001). Removal rates of dissolved trace metals/vitamins by the plankton were measured using triplicate 125 mL polycarbonate (PC) bottles, spiked with either 50 nCi ^{57}Co-B_{12} or ^{55}FeCl and incubated in an on-deck flow through incubator (Koch et al. 2011). Bottles were incubated in polycarbonate tubes covered with neutral density screening corresponding to light levels for

the appropriate depths. Two 2.5 L PC bottles of whole water were allowed to incubate along the spiked bottles, and dissolved vitamin- and trace metal concentrations were determined after 24–48 hours as described above.

Micro-zooplankton grazing impacts on TM/vitamin dynamics

The impacts of microzooplankton grazing on trace metal and vitamin cycling rates were measured at six stations (PS124/005, PS124/008, PS124/026, PS124/068, PS124/088 and PS124/090). Using a dilution series the recycling/remineralization rates of trace metals, due to grazing by microzooplankton, were determined. For this method, seawater was collected and triplicate 2 L PC bottles were diluted to 15, 30, 50, 75 and 100 % of the whole seawater using 0.2 µm FSW from the same location. The bottles were then incubated at ambient light and temperature. After 62 hours the experiment was terminated by sampling each bottle for pigments, POC/PON and flow cytometry, as described above, in order to measure the growth rates of the various plankton groups. Concentration changes of trace metals, vitamins and macronutrients will be assed for each dilution allowing calculation of remineralization rates.

Assessing the impacts of trace metals/vitamins on plankton community composition

At two stations *(PS124/005, PS124/068)*, seawater was pumped on board with the help of a Teflon membrane pump. For this, a LDPE hose was lowered to 25 m depth and seawater (~1,500 L) was pumped directly into a trace metal clean container. Two sets of 4 L polycarbonate bottles were filled and amended, in triplicate, with Fe (0.5 nM), Mn (1 nM), B_{12} (100 pM), and a combination of FeMn, FeB_{12}. One set of bottles was grown at 'low light' (30 µE) and one at 'medium light' (10 µE) in a climate controlled room (-1° to +1° C) with a 20:4 h light/dark cycle, mimicking *in-situ* conditions. At the end of the experiments, samples for the characterization of the plankton community and water chemistry were sampled as described above. In addition, a small aliquot from each bottle was used to determine primary and bacterial production rates.

Preliminary (expected) results

In combination with data from the geochemistry group (see Chapter 9), this will be the first data set to characterize the biogeochemistry and to investigate the possible role of micronutrients (trace metals/vitamins) in the plankton ecology of the southern Weddell Sea. Due to the methodologically challenges connected with trace metals clean sampling, the distribution of iron and other biologically relevant micronutrients in this region are poorly resolved.

Pelagic biogeochemistry

The majority of the samples collected will have to be analysed back at AWI. We did, however, generate some data on board. This includes total surface chlorophyll *a* concentrations (from GFF) as well as Fv/Fm measurements, an indicator of the photosynthetic efficiency of the plankton community. Surface chlorophyll *a* concentrations were very low, ranging from 0.01–2.24 µg L^{-1} with a cruise mean of 0.63 ± 0.57 µg L⁻1 (mean ± stdev, n=17; Fig. 8.2). This compared to a mean chlorophyll *a* concentration in the chlorophyll maximum of 0.90 ± 0.31 µg L^{-1} with a narrower range of 0.46–1.37 µg L^{-1}. Fv/Fm values were also very low, with the majority (>80 %) falling below 0.30 (Fig. 8.2). In laboratory work, phytoplankton cultures usually display Fv/Fm values <0.30 when limited by trace nutrients (Koch et al. 2019). Coupled to the high macronutrients observed along our cruise track (nitrate, phosphate, silicate; Chapter 10), these low biomass and Fv/Fm values suggest that growth of the phytoplankton in the eastern Weddell Sea polynya sampled during PS124 was likely limited by trace nutrients. Once analyzed, dissolved trace metal and vitamin concentrations collected during the cruise should shed further light on the potential of this region for being yet another significant HNLC region in the Southern Ocean. In addition to pelagic samples, in corporation with the groups

geochemistry (Chapter 9) and benthic fluxes (Chapter 11), bottom water was collected from the Multicorer (MUC) at PS124/062-2, PS124/078-6, PS124/088, PS124/090-11, PS124/094-4, PS124/098-2, PS124/107-4, PS124/110-4 and PS124/111-5, 0.2 µm filtered and frozen for later dissolved vitamin analysis.

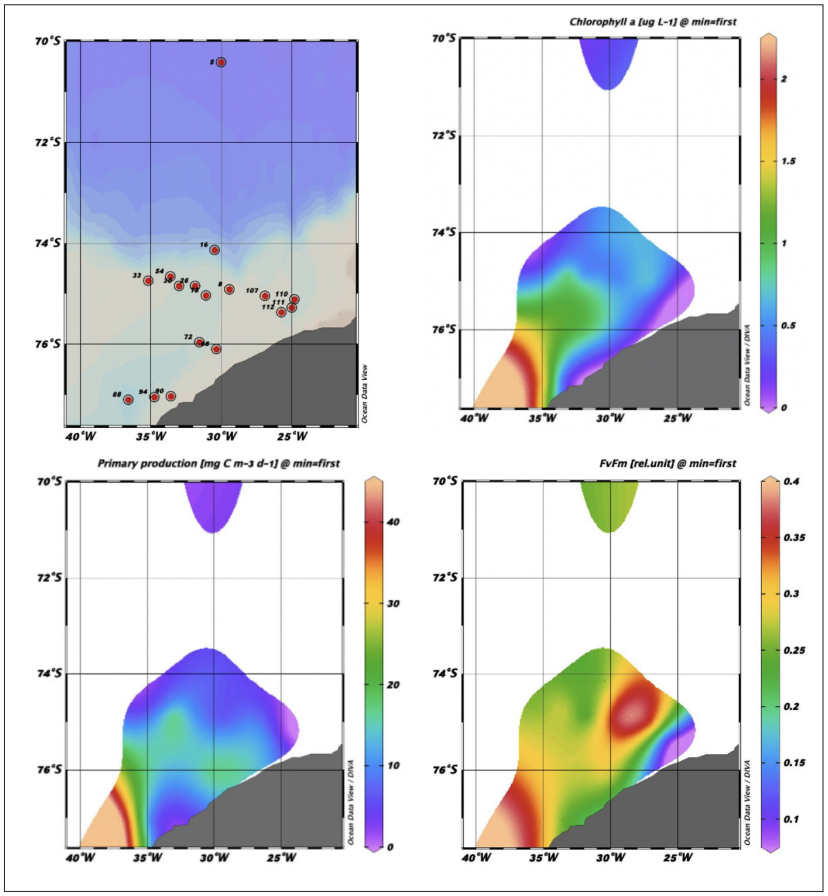

Fig 8.2: Surface chlorophyll a concentrations, primary production rates, and values of photosynthetic efficiency of the phytoplankton community (Fv/Fm) during PS124: Chlorophyll a concentrations are reported as µg L^{-1}, primary production rates measured with ^{14}C-bicarbonate as µgC L^{-1} d^{-1}. Fv/Fm is unitless.

Pelagic production and iron/vitamin cycling

One of the main objectives of PS124 was to characterize the pelagic production of the upper water column. To this end, primary and bacterial production rates were assessed at 17 stations and three depths. Primary production largely mirrored trends observed in the chlorophyll a (Fig. 8.2). Surface primary production ranged from 1.17– 41.81 µgC L^{-1} d^{-1} with a cruise mean of 10.52 ± 9.44 µgC L^{-1} d^{-1}. The highest rates were observed at the southernmost (77°S) transect station PS124/088 while the lowest rates were measured at PS124/110, the northern station behind the calved A74 iceberg (Fig. 1.2, Fig. 8.2). Primary production rates in the chlorophyll a maximum were similar to the observed ones in the surface (8.88 ± 4.51 µgC L^{-1} d^{-1}) but ranged only from 4.02–18.31 µgC L^{-1} d^{-1}. The deepest depth sampled for primary production was always the bottom of the chlorophyll a maximum. Thus, as expected, primary production rates at this depth were lower than at the surface and chlorophyll *a* maximum (3.44 ± 2.64 µgC L^{-1} d^{-1}) ranging from 0.50–8.48 µgC L^{-1} d^{-1}. Due to an instrument error at the end of the expedition, the corresponding bacterial production rates could not be analyzed on board. Upon *Polarstern's* return to Bremerhaven the samples will be analysed in the laboratory of the AWI. Uptake rates of iron and vitamin B_{12} were also measured at the 17 stations and at three depths. Since

calculation of these rates involved knowledge of ambient concentrations of iron and B_{12} and these will still need to be analysed back at AWI, no data can be shown here. Just like on PS112, however, the majority of B_{12} uptake occurred in the smaller size fraction (0.2–2 µm) while uptake of iron was either shared equally by both, or dominated by the larger size class (>2 µm). Once the rates are calculated, they will be combined with concentration data from the t=48 incubations to calculate daily iron and vitamin cycling rates.

Micro-zooplankton grazing impacts on TM/vitamin dynamics

In order to assess the impact of microzooplankton grazing on the biogeochemistry, dilution experiments were conducted. Chlorophyll a from the experiments was analyzed on board and first results indicate a dynamic picture of microzooplankton grazing on the phytoplankton community. Stations PS124/008 and PS124/068 had primary production rates of 6.03 ± 1.18 µgC L^{-1} d^{-1} and 17.01 ± 0.63 µgC L^{-1} d^{-1}, respectively. At the former station, the intrinsic growth rates of phytoplankton (growth without grazing losses) were 0.27 d^{-1} and outpaced slightly by losses due to grazing (–0.37 d^{-1}; Fig. 8.3). In contrast, at PS124/068 the intrinsic growth rate was 1.5 x greater than losses due to grazing (0.23 d^{-1} vs. –0.16 d^{-1}; Fig. 8.3).

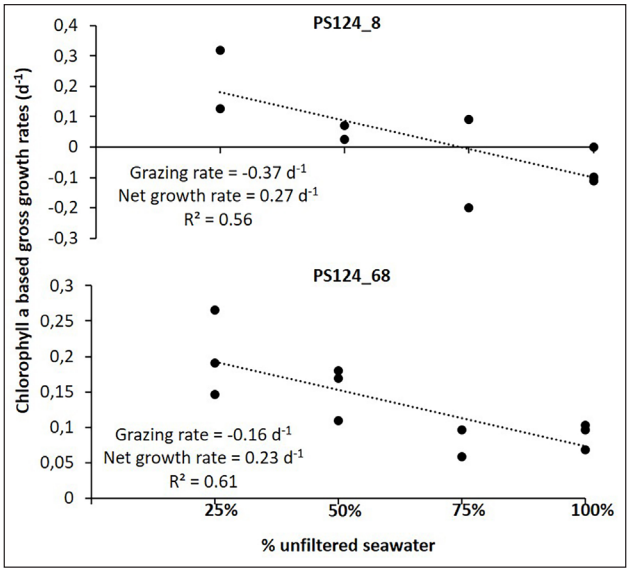

Fig 8.3: Results from two grazing experiments conducted on PS124: Whole seawater was diluted with 0.2 µm filtered seawater and the growth of plankton measured using total chlorophyll a. Growth rates are given as d^{-1}. Station locations for PS124/008 and PS124/068 are given in Fig. 8.2. The slope of the linear line of best fit is the grazing rate while the y-intercept represents the intrinsic growth rate of the phytoplankton in the absence of grazing.

Assessing the impacts of trace metals/vitamins on plankton community composition

These results are the first to investigate the role of trace metals on the plankton ecology of the Weddell Sea. First results showed a strong chlorophyll a response to Fe additions at both locations (Fig. 8.4 A). Indeed, Fe is the main driver of chlorophyll synthesis in the cell and used as a proxy of total phytoplankton biomass. Therefore, an increase in chlorophyll a due to the addition of Fe suggests a potential relieve of Fe limitation. The combined effects of trace metals on the phytoplankton biomass are more difficult to dismantle. However, we expect changes in phytoplankton species composition as requirements for trace metals differ among the different members of the plankton community. Indeed, in the +FeMn addition the biomass increase seems to be driven mainly by an increase of large diatoms (Fig. 8.4 B). However, a detailed analysis of changes in community composition (pigments, flow cytometry, microscopy) from

samples collected at the end of the experiment will have to be analysed back at the laboratory. In addition, in the field the photosynthetic efficiency of the cells (Fv/Fm) is often used as a quick proxy to detect Fe-limitation. However, our last study (Balaguer et al., submitted) suggests that this proxy can also be correlated to low concentrations of other trace metals such as Mn. Interestingly, the results of TMxLi1 show that a combination of Fe and Mn are needed to fully relieve the community trace metal limitation and enhance the photosynthetic efficiency, since our results reveal an increase of Fv/Fm only when both trace metals are added together.

Tab. 8.2: The dark-adapted maximum photosystem II quantum yields (F_v/F_m) determined at the start (initial) and the end of TMxLi1 for 30 µE and 100 µE: +Mn, +B_{12} and +Fe stand for 1.0 nM manganese, 100 pM B_{12} and 0.5 nM iron additions – the +FeB_{12} and +FeMn are combinations of the above mentioned treatments. Bold numbers indicate values which differ significantly ($p<0.01$, ANOVA) from the control.

	Light =30 uE	**Light =100 uE**
Initial	0.26 ± 0.02	0.26 ± 0.02
Control	0.26 ± 0.06	0.27 ± 0.03
+Fe	0.36 ± 0.02	0.28 ± 0.01
+Mn	0.31 ± 0.01	0.30 ± 0.01
+FeMn	0.38 ± 0.01	0.32 ± 0.02
+B12		0.26 ± 0.02
+FeB12		0.32 ± 0.01

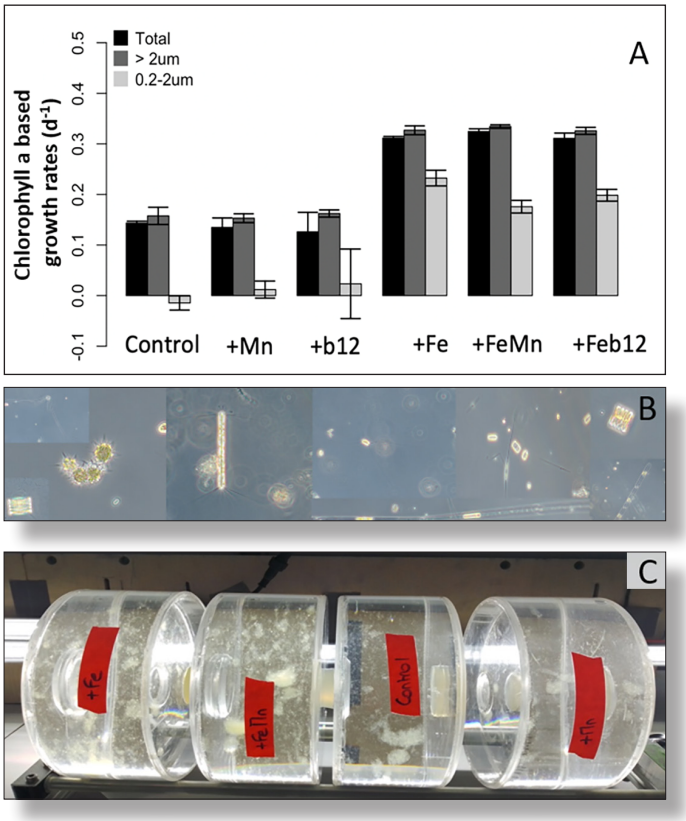

Fig 8.4 A-C: Preliminary results from TMxLi1 conducted with water collected at PS124/068:
*(A) Chlorophyll a based growth rates calculated for each treatment; +Mn,+B_{12} and +Fe denote additions of 1 nM manganese, 100 pM B_{12} and 0.5 nM iron, respectively, while the +FeMn and +FeB_{12} treatments are combination treatments of the former. Values are mean ± standard deviation (n=3) with * denoting significant ($p<0.05$) differences compared to the control.*
(B) Light microscopy revealed large diatoms dominating the +FeMn treatment.
(C) Subsamples of the control, +Mn, +Fe and +FeMn treatments were placed in roller tanks and the resulting aggregates will be characterized in corporation with the Southern Ocean Carbon Cycling group.

In corporation with the Southern Ocean Carbon Cycling group (Chapter 7), small aliquots of each treatment were placed in roller tanks and incubated for 72 more hours. The resulting aggregates (Fig. 8.4 C) were collected and will be characterized back at AWI.

In conclusion, rate measurements of primary and secondary production, coupled to uptake and recycling rates of TMs and vitamins, should shed light on cycling and dynamics between essential trace nutrients and the pelagic plankton community. In addition, targeted experiments, in which natural plankton communities were exposed to various co-limiting nutrients (manganese, B_{12}) and light regimes (high/low) may highlight possible shifts in the plankton community due to the climatic changes expected in the coming decades.

Data management

Environmental data will be archived, published and disseminated according to international standards by the World Data Center PANGAEA Data Publisher for Earth & Environmental Science (www.pangaea.de) within two years after the end of the cruise at the latest. By default the CC-BY license will be applied.

Molecular data (DNA and RNA data) will be archived, published and disseminated within one of the repositories of the International Nucleotide Sequence Data Collaboration (INSDC, www.insdc.org) comprising of EMBL-EBI/ENA, GenBank and DDBJ).

Any other data will be submitted to an appropriate long-term archive that provides unique and stable identifiers for the datasets and allows open online access to the data.

In all publications, based on this cruise, the **Grant No. AWI_ PS124_01** will be quoted and the following *Polarstern* article will be cited:

Alfred-Wegener-Institut Helmholtz-Zentrum für Polar- und Meeresforschung. (2017). Polar Research and Supply Vessel POLARSTERN Operated by the Alfred-Wegener-Institute. Journal of large-scale research facilities, 3, A119. http://dx.doi.org/10.17815/jlsrf-3-163.

References

Balaguer J, Koch F, Hassler C, Trimborn S (submitted) Limitation of phytoplankton communities in the Drake Passage by iron and manganese.

Bertrand EM, et al. (2007) Vitamin B_{12} and iron colimitation of phytoplankton growth in the Ross Sea. Limnol. Oceanogr., 52 (3), 1079–1093.

Buesseler KO (1998) The decoupling of production and particulate export in the surface ocean. Glob. Biogeochem. Cycle, 12(2), 297–310.

de Baar HJW, et al. (2005) Synthesis of iron fertilization experiments: From the iron age in the age of enlightenment. J. Geophys. Res.-Oceans, 110 (C9), 1–24.

Heiden JP, Völkner C, Jones EM, van de Poll WH, Buma AGJ, Meredith MP, de Baar HJW, Bischof K, Wolf-Gladrow D, Trimborn S (2019) Impact of ocean acidification and high solar radiation on productivity and species composition of a late summer phytoplankton community. Limnol. Oceanogr., doi.org/10.1002/lno.11147.

JGOFS (1996) Protocols for the Joint Global Ocean Flux Study Core Measurements. Knap A, Michaels A,

Close A, Ducklow H and Dickson A (eds) JGOFS Report Nr. 19, vi+170 pp.

Kirchman D (2001) Measuring bacterial biomass production and growth rates from Leucine incorporation in natural aquatic environments. In: Paul JH (ed) Methods in Microbiology Volume 30: Marine Microbiology. Academic Press, 227–237.

Koch F, et al. (2011) The effect of vitamin B_{12} on phytoplankton growth and community structure in the Gulf of Alaska. Limnol. Oceanogr., 56 (3), 1023–1034.

Koch F, Trimborn S (2019) Limitation by Fe, Zn, Co and B_{12} results in similar physiological responses in two Antarctic phytoplankton species. Frontiers in Marine Science, 6 (514), 1–17.

Klunder MB, Laan P, Middag R, de Baar H J W, van Ooijen, JC (2011) Dissolved Fe in the Southern Ocean (Atlantic sector). Deep-Sea Res. II, 58, 2678–2694.

Klunder MB, Laan P, DeBaar HJW, Middag R, Neven I, van Ooijen JC (2014) Dissolved Fe across the Weddell Sea and Drake Passage: impact of DFe on nutrient uptake. Biogeosciences, 11, 651–669.

Lumpkin R, Speer K (2007) Global ocean meridional overturning. J. Phys. Oceanogr., 37(10), 2550–2562.

Martin JH, Fitzwater SE (1988) Iron deficiency limits phytoplankton growth in the Northeast Pacific Subarctic. Nature, 331 (6154), 341–343.

Trimborn S, et al. (2015) Physiological characteristics of open ocean and coastal phytoplankton communities of Western Antarctic Peninsula and Drake Passage waters. Deep-Sea Res. Part I-Oceanogr. Res. Pap., 98, 115–124.

Twining BS, Baines SB (2013) The Trace Metal Composition of Marine Phytoplankton. Annual Review of Marine Science, Vol 5. Carlson CA and Giovannoni SJ. Palo Alto, Annual Reviews, 5, 191–215.

9. GEOCHEMISTRY

Susann Henkel[1], Ingrid Stimac[1], Claudia Ehlert[2], Torben Stichel[1] (not on board), Walter Geibert[1] (not on board), Hendrik Grotheer[1] (not on board)

[1]DE.AWI
[2]DE.UNI-Oldenburg

Grant No. AWI_PS124_07

Objectives

Iron supplies regulate primary productivity in large parts of the Southern Ocean (Boyd & Ellwood 2010). Potential sources of iron include meltwater deriving from ice shelves and icebergs (Arrigo et al. 2015), sea-ice (Sedwick & DiTullio 1997) as well as coastal and shelf sediments (e.g. Monien et al. 2014; Henkel et al. 2018). Climate change is expected to result in an increase of iron supplies, thus counter-acting the warming trend by stimulating the biological C pump (e.g. Raiswell et al. 2008). Unfortunately, trace metal data for the Southern Ocean are sparse. One of the main areas for presumably important iron supplies, the southern Weddell Sea shelf, is basically an uncharted area in terms of geochemistry. Only two previous cruises to the Antarctic continental shelf focused on gaining data concerning iron and assessing respective fluxes (Klunder et al. 2011; 2014). Several perceivable pathways of iron for the Weddell Gyre could thus not be tested so far, namely sedimentary shelf inputs, basal melting of glaciers, sea-ice, icebergs or subglacial discharge. Geochemical tracers such as Fe and Ra isotopes will be used to evaluate the relative importance of different nutrient sources in the working area. The potential of an integrated approach including physical oceanography, biology, geochemical tracer studies, and biogeochemistry has been demonstrated for the eastern Weddell Gyre (Geibert et al. 2010) and is applied here to new areas.

Silicon isotopes ($\delta^{30}Si$) are applied as tracers to investigate nutrient utilization by diatoms in the surface waters (De La Rocha et al. 2000), but can also provide information about dissolution of particles in the water column as well as water mass mixing of intermediate and deep waters (De Souza et al. 2012; Liguori et al. 2020). Fe is a major limiting factor for diatom growth in the Southern Ocean, and fertilization by Fe affects nutrient (Si:N) uptake ratios by diatoms (Brzezinski et al. 2003). Furthermore, Pichevin et al. (2014) have shown that bSi burial might strongly be affected by Fe availability, a process with great implications for paleoceanographic studies. $\delta^{30}Si$ was introduced recently as tracer for early diagenetic processes in sediments like dissolution of diatoms as well as the formation of authigenic silicate phases (Ehlert et al. 2016), a process with potential effects on global trace metal cycling (e.g., Michalopoulos & Aller 2004). During PS124, water column samples for $\delta^{30}Si$ analyses were collected in order to investigate varying nutrient (silicate) utilization in surface waters as a function of e.g. ice coverage, phytoplankton assemblage composition, as well as micronutrient (Fe) availability; a crucial information, which will help us also to improve interpretations of palaeoceanographic records from the Southern Ocean. Sediments and pore waters, on the other hand, were sampled in order to gain information on bSi accumulation and early diagenetic turnover e.g. as a function of organic matter and biogenic silicate sedimentation rates and lithogenic:biogenic silicate material composition, providing information on the long-term storage capacity of biogenic silica and benthic fluxes of Si and associated other elements.

In the Weddell Sea, a key-area of deep and bottom water formation, the end-member composition of water masses is of vital importance for the application of paleo-oceanographic tracers such as neodymium isotopes (expressed in εNd) which are used to investigate past ocean circulation patterns (Frank 2002). Previous studies suggest a modification of εNd in Antarctic Bottom Water (AABW) during its formation by exchange processes with the continental shelf (Carter et al. 2012; Stichel et al. 2012a; 2012b) constituing a need to assess the modification of source waters when they enter the Filchner or Central Trough located in different geological settings. The source regions of the ice streams feeding the Filchner-Ronne Ice Shelf also are of distinct geologies (Dalziel 1992). Characterizing the impact of the ice sheet on the Nd isotopic composition of AABW is crucial for paleo-oceanographic reconstructions.

Our overall objective is to quantify the Antarctic continental shelf's contribution to global nutrient/iron budgets including:

- a chemical characterization of water masses in the southern Weddell Sea,
- the determination of fluxes of macro- and micronutrients from shelf and slope sediments to the water column and the assessment of their potential to fertilize the high nutrient low chlorophyll (HNLC) Weddell Sea,
- the assessment of post depositional degradation of organic matter and the long-term C storage capacity of Weddell Sea sediments.

Work at sea

The main tasks onboard *Polarstern* were to collect and conserve water, sediment, and ice samples for onshore analyses which enable us to (1) characterize water masses based on nutrient, radionuclide and radiogenic isotope concentrations, (2) assess potential nutrient sources such as sediments, sea ice and icebergs, and (3) characterize depositional regimes and sedimentary redox zones based on sediment and pore water geochemistry and the calculation of accumulation rates to assess the post depositional degradation of organic matter. Specific parameters, sampling devices, sample volumes and treatments are listed in Table 9.1.

Water sampling for Si utilization and provenance studies as well as a few samples for age dating of dissolved organic carbon ($DO^{14}C$) were collected with a CTD-rosette equipped with standard Niskin bottles. Sampling depths were chosen based on oceanographic features recorded during the downcast and equaled those for oceanographic (noble gas) and biological/ biogeochemical sampling (see Chapters 3,10).

At selected stations, water samples for trace metals (joint sampling with Pelagic Production group, see Chapter 8) and Fe isotopes ($\delta^{56}Fe$) were taken by use of a CTD-rosette equipped with teflon-coated GoFlo bottles. GoFlo bottles were transported to a clean container, where water was filtered through pre-cleaned 0.2 µm Acopak filter capsules. Samples were acidified with double distilled HCl and stored for on-shore analysis. Sampling procedures were largely compliant with the GEOTRACES guidelines (www.geotraces.org).

Where multicorer (MUC) deployments were successful, cores were sampled for pore water and solid phase analyses. Where available, two cores were reserved for pore water extraction. One was dedicated to solid phase sampling for bulk element composition, biogenic Si, TOC, TN, and potential Fe and P extractions and the other (usually after having been incubated for a few days, see Chapter 11) was dedicated to ^{210}Pb analyses. At four stations the MUC deployment failed but we have been able to sample short push-cores from the MultiGrab for solid phase analyses. Bottom water was collected from MUC cores, filtered through 0.1 µm and treated the same way as pore water samples.

Tab. 9.1: Types of samples taken during PS124 for geochemical analyses

	Parameter	Device	Sample volume/mass	Treatment
Water	REEs	CTD-rosette with Niskins	0.125 L	Filtration through 0.2 µm Acropak capsules, acidification
	εNd		10–20 L	Filtration through 0.2 µm Acropak capsules, acidification
	^{226}Ra			
	DO^{14}C		1 L	Frozen at –20 °C
	Si and δ^{30}Si		0.125–0.5 L	Filtration through 0.2 µm Acropak capsules
	^{226}Ra/^{228}Ra	Seawater line	several 100 L	Filtration through filter cartridge[2], adsorption onto MnO_2
	^{226}Ra		1 L	Filtration through filter cartridge[2]
	δ^{56}Fe	CTD-rosette with GoFlos	8–10 L	Filtration through 0.2 µm Acropak capsules, acidification
Sediment	^{210}Pb	MUC (MG)	~20 cm³	Frozen at –20 °C
	Biogenic Si		5 cm³	Frozen at –20 °C
	Water content/porosity		10 cm³	Frozen at –20 °C in gastight, Ar-flooded bags
	TOC, TC, TN			
	Bulk element composition			
	P and/or Fe extractions			
Pore water[1]	Alkalinity	MUC	0.5–1 mL	Titration with HCl
	DIC		2 mL	$HgCl_2$ addition, storage at 4 °C
	Fe^{2+}		0.2–1 mL	Photospectrometric analysis (ferrozine)
	Cations		0.5–1 mL	Acidification, storage at 4 °C
	Sulfate/chloride		100 µL	Frozen at –20 °C
	Nutrients (NO_3^-, NO_2^-, NH_4^+, PO_4^{3-}, $SiOH_4$)		0.5–8 mL	
	δ^{30}Si		0.5–20 mL	Acidification, storage at 4 °C
	δ^{56}Fe		0.5–20 mL	
	Ra isotopes[3]		<40 mL	
Ice	Dissolved Fe (DFe) and total dissolvable Fe (TDFe)	Ice drilling/ saw	0.125 mL/ 0.5–5 kg	Filtered & unfiltered, acidification to pH 1.8; partly kept untreated and stored at –20 °C
	δ^{30}Si		~100 mL	Filtered (10 µm and 0.2 µm), filters stored at –20 °C, dissolved fraction stored at 4 °C

[1] Extraction by use of rhizons, pore size 0.1 µm (Seeberg-Elverfeldt et al. 2005)
[2] 0.1 µm pore size
[3] One station only

Pore water was extracted with rhizons (Seeberg-Elverfeldt et al. 2005) in 1 to 2 cm intervals a couple of hours after core retrieval. In the meantime, cores were stored at 0 °C, sampling was done at 4 °C. The first 0.5 mL of extracted pore water was discarded as it has mixed with ultrapure water in which rhizons were soaked before use. When enough pore water was available, dissolved Fe(II) was analyzed spectrophotometrically using the ferrozine method by Stookey (1970). When time allowed, pore water samples were titrated with 10 mM HCl to determine the alkalinity. At station PS124_97-1, we extracted pore water from four cores to get sufficient pore fluid volume for radionuclide analyses. All stations sampled for the geochemical analyses mentioned above are listed in Table 9.2 at the end of this Chapter.

At three locations, PS124_68-11, PS124_77-1, and PS124_100-7, sea-ice including yellow pancakes and nilas as well as water from below the sea ice were collected for trace metal and Si isotope (station PS124_77-1 only) analysis (see Chapters 8, 13). Furthermore, in total 30 samples for Ra analysis were taken at stations as well as during transit between working areas. Analysis of ^{226}Ra concentrations requires a volume of ~1 L seawater and we directly collected those from the seawater line in the lab. Samples were filtered, acidified with 1 mL HCl and stored at 4 °C. ^{228}Ra is much less abundant and therefore has to be determined through the $^{226}Ra/^{228}Ra$ ratio after pre-concentration of Ra via adsorption onto MnO_2-coated fibre. A cartridge filled with MnO_2-coated fibre was connected to the seawater line and filtered seawater was continuously run through the system for about 6 to 12 hours at flow rates of 0.5 – 1 L/min. The MnO_2-fibre was packed and stored at 4 °C.

Preliminary and expected results

Alkalinity and dissolved Fe^{2+} in pore water were the only parameters directly analysed on board. Fig. 9.1 exemplarily shows the respective pore water profiles for station PS124_78-6 (473 m depth).

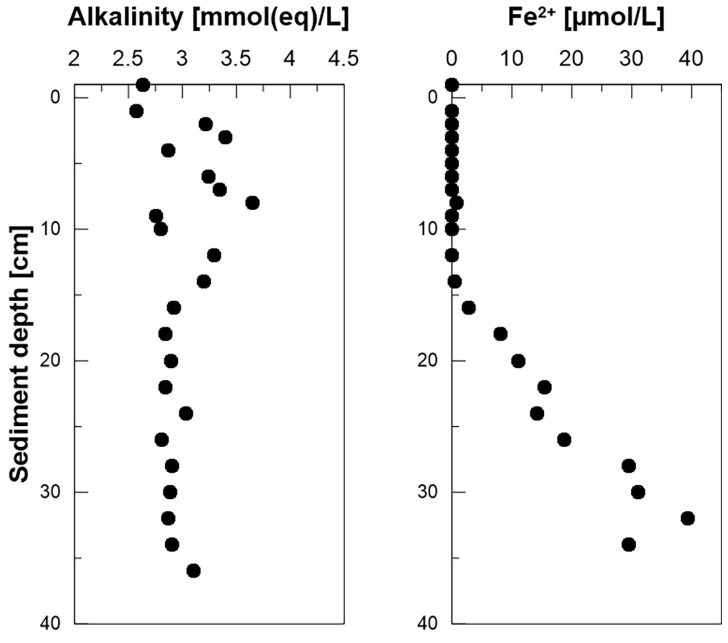

Fig. 9.1: Alkalinity and dissolved Fe^{2+} profiles for station PS124_78-6

Alkalinity was usually ~2.5 mmol(eq)/L in bottom water and showed a slight increase to ~3.5 mmol(eq)/L with sediment depth. Only at station PS124_110-4, behind iceberg A74 (see Chapter 13), bottom water alkalinity reached 4.3 mmol(eq)/L and exceeded pore water alkalinity. The presence of dissolved Fe^{2+} in pore water is indicative for dissimilatory iron reduction (DIR), which indicates the use of iron oxides as an electron acceptor during the degradation of organic carbon. Redox zones can overlap, but generally DIR occurs, when O_2, NO_3 and MnO_2 have already been consumed. In the sediments investigated during PS124, ferruginous conditions prevail, if at all, only below ~5 cm sediment depth and Fe^{2+} concentrations do not exceed 60 µM. We could not smell sulfide in any of cores sampled during PS124. It appears as if Fe^{2+} profiles are strongly dependent on grain sizes (see below). Coarse intervals yielded high volumes of pore water with low Fe^{2+} concentrations. At some stations, e.g. PS124_88-5 and PS124_111-5, we did not detect any Fe^{2+} using the ferrozine method (detection limit ~1 µM). Onshore analyses and comparison of data with other groups (e.g. snow catcher data) will show whether this can be linked to low organic carbon accumulation and/or high sedimentation rates and reworking.

At most locations, intervals of muddy sediment intercalated with coarse sand or even gravel. Some cores recovered clay, which was so sticky that pore water extraction and sediment sampling has been a challenge. At Site PS124_33, MUC core F, which was to be sampled for solid phase, collected a stone as large as the diameter of the core liner (Fig. 9.2).

Fig. 9.2: The "lucky catch" – a stone of 10 cm diameter in PS124_33-5 MUC F

The samples taken during this expedition will improve the data availability for trace metal concentrations in the Weddell Sea and our understanding of nutrient and, in particular, Fe and Si fluxes in this remote area. We expect that the data will enable us to draw conclusions about the relative importance of different nutrient sources (e.g. benthic release from shelf sediments vs. melting of sea-ice and shelf-ice). The detailed investigation of radiogenic isotopes (Nd) and REE will be of great value for paleoceanographic studies.

Data management

Environmental data will be archived, published, and disseminated according to international standards by the World Data Center PANGAEA Data Publisher for Earth & Environmental Science (www.pangaea.de) within two years after the end of the cruise at the latest. By default the CC-BY license will be applied.

Any other data will be submitted to an appropriate long-term archive that provides unique and stable identifiers for the datasets and allows open online access to the data.

In all publications, based on this cruise, the **Grant No. AWI_PS124_07** will be quoted and the following *Polarstern* article will be cited:

Alfred-Wegener-Institut Helmholtz-Zentrum für Polar- und Meeresforschung. (2017). Polar Research and Supply Vessel POLARSTERN Operated by the Alfred-Wegener-Institute. Journal of large-scale research facilities, 3, A119. http://dx.doi.org/10.17815/jlsrf-3-163.

References

Arrigo KR, van Dijken GL, Strong AL (2015) Environmental controls of marine productivity hot spots around Antarctica. J. Geophys. Res., 120(8), 5545-5565, doi:10.1002/2015JC010888.

Boyd PW, Ellwood MJ (2010) The biogeochemical cycle of iron in the ocean. Nat. Geosci., 3, 675, doi:10.1038/ngeo964.

Brzezinski MA, Dickson ML, Nelson DM, Sambrotto RN (2003) Ratios of Si, C and N uptake by microplankton in the Southern Ocean. Deep Sea Res. II, 50(3–4), 619–633, doi:10.1016/S0967-0645(02)00587-8.

Carter P, Vance D, Hillenbrand CD, Smith JA, Shoosmith DR (2012) The neodymium isotopic composition of waters masses in the eastern Pacific sector of the Southern Ocean. Geochim. Cosmochim. Acta, 79, 41–59, doi:10.1016/j.gca.2011.11.034.

Dalziel IWD (1992) Antarctica - a tale of 2 supercontinents. Ann. Rev. Earth Planet. Sci., 20, 501–526.

De La Rocha CL, Brzezinski MA, DeNiro MJ (2000) A first look at the distribution of the stable isotopes of silicon in natural waters. Geochim. Cosmochim. Acta, 64(14), 2467–2477.

De Souza GF, Reynolds BC, Rickli J, Frank M, Saito MA, Gerringa LJA, Bourdon B (2012) Southern Ocean control of silicon stable isotope distribution in the deep Atlantic Ocean. Global Biogeochem. Cycles, 26(GB2035), doi:10.1029/2011GB004141.

Ehlert C, Doering K, Wallmann K, Scholz F, Sommer S, Grasse P, et al. (2016) Stable silicon isotope signatures of marine pore waters – biogenic opal dissolution versus authigenic clay mineral formation. Geochim. Cosmochim. Acta, 191, 102–117, doi:10.1016/j.gca.2016.07.022.

Frank M (2002) Radiogenic isotopes: Tracers of past ocean circulation and erosional input. Rev. Geophys., 40, doi:10.1029/2000RG000094.

Geibert W, Assmy P, Bakker DCE, Hanfland C, Hoppema M, Pichevin LE, Schröder M, Schwarz JN, Stimac I, Usbeck R, Webb A (2010) High productivity in an ice melting hotspot at the eastern boundary of the Weddell Gyre. Global Biogeoch. Cycles, 24, 15, doi:Gb3007/10.1029/2009gb003657.

Henkel S, Kasten S, Hartmann JF, Silva-Busso A, Staubwasser M (2018) Iron cycling and stable Fe isotope fractionation in Antarctic shelf sediments, King George Island. Geochim. Cosmochim. Acta, 237, 320-338, doi:10.1016/j.gca.2018.06.042.

Klunder MB, Laan P, De Baar HJW, Middag R, Neven I., Van Ooijen J (2014) Dissolved Fe across the Weddell Sea and Drake Passage: impact of DFe on nutrient uptake. Biogeosciences, 11(3), 651-669.

Klunder MB, Laan P, Middag R, De Baar HJW, van Ooijen JC (2011) Dissolved iron in the Southern Ocean (Atlantic sector). Deep Sea Res. II, 58(25–26), 2678-2694, doi:10.1016/j.dsr2.2010.10.042.

Liguori BTP, Ehlert C, Pahnke K (2020) The Influence of Water Mass Mixing and Particle Dissolution on the Silicon Cycle in the Central Arctic Ocean. Frontiers Mar. Sci., 7(202).

Michalopoulos P, Aller RC (2004) Early diagenesis of biogenic silica in the Amazon delta: Alteration, authigenic clay formation, and storage. Geochim. Cosmochim. Acta, 68(5), 1061–1085, doi: 10.1016/j.gca.2003.07.018.

Monien P, Lettmann KA, Monien D, Asendorf S, Wölfl A-C, Lim CH, Thal J, Schnetger B, Brumsack H-J (2014) Redox conditions and trace metal cycling in coastal sediments from the maritime Antarctic. Geochim. Cosmochim. Acta, 141, 26-44, doi:10.1016/j.gca.2014.06.003.

Pichevin LE, Ganeshram RS, Geibert W, Thunell RC, Hinton, RW (2014) Silica burial enhanced by iron limitation in oceanic upwelling margins. Nature Geosci., 8–13, doi:10.1038/NGEO2181.

Raiswell R, Benning LG, Tranter M, Tulaczyk S (2008) Bioavailable iron in the Southern Ocean: the significance of the iceberg conveyor belt. Geochem. Transactions, 9:7, doi:10.1186/1467-4866-9-7.

Sedwick PN, DiTullio GR (1997) Regulation of algal blooms in Antarctic Shelf Waters by the release of iron from melting sea ice. Geophys. Res. Lett., 24(20), 2515-2518, doi:10.1029/97GL02596.

Seeberg-Elverfeldt J, Schlüter M, Feseker T, Kölling M (2005) Rhizon sampling of pore waters near the sediment-water interface of aquatic systems. Limnol. Oceanogr. Methods 3, 361–371.

Stichel T, Frank M, Rickli J, Haley BA (2012a) The hafnium and neodymium isotope composition of seawater in the Atlantic sector of the Southern Ocean. Earth Planet. Sci. Lett., 317–318, 282–294, doi:10.1016/j.epsl.2011.11.025.

Stichel T, Frank M, Rickli J, Hathorne EC, Haley BA, Jeandel C, Pradoux C (2012b) Sources and input mechanisms of hafnium and neodymium in surface waters of the Atlantic sector of the Southern Ocean. Geochim. Cosmochim. Acta, 94, 22–37, doi:10.1016/j.gca.2012.07.005.

Stookey LL (1970) Ferrozine-A new spectrophotometric reagent for iron. Anal. Chem., 42-7, 779-781.

Tab. 9.2: Stations sampled for geochemical analyses

Station-Cast	Date (Device at depth)	Latitude (Device at depth)	Longitude (Device at depth)	Water depth [m]	REE	εNd, Ra	$\delta^{30}Si$	$DO^{14}C$	$\delta^{56}Fe$	Pore water	Solid phase
PS124_005-02	08.02.2021	70° 25.052‘ S	030° 00.099‘ W	4487.2	x	x	x	x			
PS124_005-04	08.02.2021	70° 25.076‘ S	029° 59.916‘ W	4488.9		x					
PS124_006-02	11.02.2021	73° 43.415‘ S	025° 41.908‘ W	3204.2	x	x	x	x			
PS124_007-04	11.02.2021	74° 01.817‘ S	028° 04.803‘ W	2520.1	x	x	x				
PS124_008-05	12.02.2021	74° 55.221‘ S	029° 25.325‘ W	401.9	x	x	x	x			
PS124_008-08	12.02.2021	74° 55.228‘ S	029° 25.471‘ W	401.0					x		
PS124_009-01	13.02.2021	74° 00.288‘ S	030° 30.242‘ W	2189.8	x	x	x	x			
PS124_011-01	13.02.2021	74° 15.879‘ S	030° 18.229‘ W	1544.1	x	x	x				
PS124_011-02	13.02.2021	74° 15.881‘ S	030° 18.267‘ W	1545.2					x		
PS124_011-03	13.02.2021	74° 15.875‘ S	030° 18.171‘ W	1547.0						x	x
PS124_016-02	14.02.2021	75° 08.540‘ S	030° 26.772‘ W	451.6	x	x	x				
PS124_016-06	14.02.2021	75° 08.572‘ S	030° 26.822‘ W	454.3						x	x
PS124_021-01	15.02.2021	74° 52.109‘ S	030° 40.239‘ W	496.5	x	x	x				
PS124_021-02	15.02.2021	74° 52.089‘ S	030° 40.039‘ W	497.0					x		
PS124_026-02	16.02.2021	74° 51.331‘ S	031° 49.828‘ W	635.6	x	x	x	x			
PS124_026-05	16.02.2021	74° 51.294‘ S	031° 49.951‘ W	637.9					x		
PS124_026-08	17.02.2021	74° 50.880‘ S	031° 51.050‘ W	636.1							x
PS124_026-09	17.02.2021	74° 50.878‘ S	031° 51.069‘ W	636.2						x	
PS124_026-10	17.02.2021	74° 50.884‘ S	031° 51.061‘ W	636.5							x
PS124_030-01	17.02.2021	74° 51.129‘ S	032° 59.457‘ W	593.6	x	x	x				
PS124_030-02	17.02.2021	74° 51.112‘ S	032° 59.431‘ W	593.3					x		
PS124_030-05	17.02.2021	74° 51.144‘ S	032° 59.501‘ W	594.9						x	x
PS124_030-06	17.02.2021	74° 51.122‘ S	032° 59.561‘ W	595.3							x

Station-Cast	Date (Device at depth)	Latitude (Device at depth)	Longitude (Device at depth)	Water depth [m]	REE	εNd, Ra	$\delta^{30}Si$	$DO^{14}C$	$\delta^{56}Fe$	Pore water	Solid phase
PS124_033-01	19.02.2021	74° 44.979‘ S	035° 11.119‘ W	500.2	x	x	x				
PS124_033-02	19.02.2021	74° 45.007‘ S	035° 09.062‘ W	502.9					x		
PS124_033-05	19.02.2021	74° 43.496‘ S	035° 10.815‘ W	497.0						x	x
PS124_036-01	20.02.2021	74° 13.755‘ S	034° 57.085‘ W	1601.7	x	x	x				
PS124_037-01	20.02.2021	74° 34.799‘ S	036° 24.164‘ W	424.7	x	x	x				
PS124_037-04	20.02.2021	74° 35.855‘ S	036° 25.995‘ W	411.5							x
PS124_040-01	21.02.2021	74° 40.295‘ S	036° 00.992‘ W	429.7	x	x	x				
PS124_043-01	22.02.2021	74° 27.507‘ S	036° 00.496‘ W	1063.8	x						
PS124_045-02	22.02.2021	74° 21.968‘ S	036° 01.191‘ W	1445.2	x	x	x				
PS124_045-03	22.02.2021	74° 21.756‘ S	036° 02.737‘ W	1459.4					x		
PS124_045-06	22.02.2021	74° 20.434‘ S	036° 03.692‘ W	1542.0							x
PS124_046-01	22.02.2021	74° 24.874‘ S	036° 22.290‘ W	1244.5	x	x	x				
PS124_047-01	22.02.2021	74° 16.868‘ S	036° 04.030‘ W	1717.8	x	x	x				
PS124_048-01	23.02.2021	74° 03.496‘ S	035° 47.748‘ W	2026.8	x	x	x				
PS124_052-02	24.02.2021	74° 15.612‘ S	032° 20.289‘ W	928.5							x
PS124_054-03	25.02.2021	74° 39.940‘ S	033° 33.975‘ W	593.0	x	x	x				
PS124_054-04	25.02.2021	74° 39.952‘ S	033° 34.768‘ W	591.3					x		
PS124_054-12	25.02.2021	74° 42.433‘ S	033° 34.656‘ W	588.4						x	x
PS124_062-02	26.02.2021	74° 42.408‘ S	033° 34.562‘ W	589.1							x
PS124_068-03	28.02.2021	76° 06.177‘ S	030° 18.783‘ W	470.7	x	x	x	x			
PS124_068-04	01.03.2021	76° 06.121‘ S	030° 19.136‘ W	468.9					x		
PS124_068-08	01.03.2021	76° 05.381‘ S	030° 20.173‘ W	476.2						x	x
PS124_072-01	01.03.2021	75° 57.755‘ S	031° 31.958‘ W	616.1	x	x	x				
PS124_072-02	01.03.2021	75° 57.965‘ S	031° 33.874‘ W	621.4					x		
PS124_072-07	01.03.2021	75° 56.791‘ S	031° 40.460‘ W	688.8							x

Station-Cast	Date (Device at depth)	Latitude (Device at depth)	Longitude (Device at depth)	Water depth [m]	REE	εNd, Ra	$\delta^{30}Si$	$DO^{14}C$	$\delta^{56}Fe$	Pore water	Solid phase
PS124_076-01	02.03.2021	75° 51.981‘ S	032° 04.059‘ W	734.7	x	x	x				
PS124_076-05	03.03.2021	75° 52.321‘ S	032° 04.463‘ W	736.8						x	
PS124_076-06	03.03.2021	75° 52.225‘ S	032° 04.186‘ W	735.2							x
PS124_078-01	03.03.2021	76° 02.545‘ S	031° 01.561‘ W	472.8	x	x	x				
PS124_078-05	03.03.2021	76° 02.826‘ S	031° 01.687‘ W	474.7							
PS124_078-06	03.03.2021	76° 02.808‘ S	031° 01.263‘ W	473.1						x	x
PS124_080-01	04.03.2021	75° 50.014‘ S	030° 56.226‘ W	474.6			x				
PS124_081-01	04.03.2021	75° 54.528‘ S	029° 56.710‘ W	498.4	x		x				
PS124_082-01	05.03.2021	76° 00.449‘ S	029° 07.531‘ W	403.3			x				
PS124_083-01	05.03.2021	76° 06.605‘ S	028° 18.302‘ W	359.9			x				
PS124_084-01	05.03.2021	76° 14.035‘ S	029° 03.255‘ W	324.0			x				
PS124_088-01	05.03.2021	77° 06.455‘ S	036° 35.026‘ W	1107.6	x	x	x	x			
PS124_088-02	05.03.2021	77° 06.473‘ S	036° 34.505‘ W	1109.2					x		
PS124_088-05	06.03.2021	77° 06.502‘ S	036° 33.610‘ W	1100.4						x	x
PS124_090-04	06.03.2021	77° 02.550‘ S	033° 36.203‘ W	378.8	x	x	x				
PS124_090-05	06.03.2021	77° 02.336‘ S	033° 34.713‘ W	378.1					x		
PS124_090-11	06.03.2021	77° 02.645‘ S	033° 32.051‘ W	349.1						x	x
PS124_093-02	07.03.2021	77° 03.005‘ S	034° 44.395‘ W	778.7	x	x	x				
PS124_094-01	07.03.2021	77° 02.636‘ S	034° 43.608‘ W	794.2					x		
PS124_094-04	07.03.2021	77° 02.966‘ S	034° 44.250‘ W	779.5						x	x
PS124_097-01	08.03.2021	77° 05.986‘ S	036° 32.065‘ W	1097.6			x			x	
PS124_098-01	09.03.2021	75° 23.205‘ S	028° 40.643‘ W	453.7		x	x				
PS124_098-02	09.03.2021	75° 23.662‘ S	028° 41.423‘ W	443.4						x	x
PS124_100-05	10.03.2021	74° 32.918‘ S	032° 39.600‘ W	661.9						x	x
PS124_107-01	11.03.2021	75° 02.821‘ S	026° 52.866‘ W	289.5		x	x				

Station-Cast	Date (Device at depth)	Latitude (Device at depth)	Longitude (Device at depth)	Water depth [m]	REE	εNd, Ra	$\delta^{30}Si$	$DO^{14}C$	$\delta^{56}Fe$	Pore water	Solid phase
PS124_107-02	11.03.2021	75° 02.742‘ S	026° 53.314‘ W	288.8					x		
PS124_107-04	12.03.2021	75° 02.902‘ S	026° 54.517‘ W	295.9						x	x
PS124_110-01	13.03.2021	75° 06.852‘ S	024° 47.684‘ W	576.2		x	x	x			
PS124_110-02	13.03.2021	75° 06.740‘ S	024° 47.922‘ W	575.3					x		
PS124_110-04	13.03.2021	75° 06.775‘ S	024° 47.746‘ W	578.4						x	x
PS124_111-02	13.03.2021	75° 16.630‘ S	024° 58.064‘ W	635.5		x	x				
PS124_111-03	13.03.2021	75° 16.631‘ S	024° 57.926‘ W	635.9					x		
PS124_111-05	14.03.2021	75° 16.629‘ S	024° 57.977‘ W	636.1						x	x
PS124_112-01	14.03.2021	75° 22.290‘ S	025° 43.854‘ W	782.5		x	x				
PS124_112-02	14.03.2021	75° 22.295‘ S	025° 43.941‘ W	781.9					x		
PS124_112-04	14.03.2021	75° 22.373‘ S	025° 43.397‘ W	793.4							x
PS124_115-01	15.03.2021	74° 01.022‘ S	026° 07.987‘ W	2863.3		x	x				

10. THE C-PUMP AND ITS IMPRINT ON BENTHIC FAUNA

Moritz Holtappels[1], Claudio Richter[1] (not on board), [1]DE.AWI
Georg Brenneis[2], Santiago E.A. Pineda-Metz[1], [2]DE.UNI-Greifswald
Allison Schaap[3], Alexandra Dürwald[2], [3]UK.NOC
Theresa Hargesheimer[1], Henning Schröder[1]

Grant No. AWI_PS124_05 and AWI_PS124_11 (Pycnogonida, Georg Brenneis)

Outline and objectives

The southern Weddell Sea (WS) features one of the largest shelves of the Antarctic continent. It is characterized by the large Filchner-Ronne Ice Shelf (FRIS) and is a hot spot for sea ice production and bottom water formation, amounting to ~5 Sv of bottom water exported from the shelf to deep sea (Huhn et al. 2008). In summer, the polynyas along the shelves enlarge to form vast contiguous open water areas (~100,000 km²) exhibiting high rates of primary production of up to 1,600 mg C/m²/d (von Bröckel 1985; von Bodungen et al. 1988; Gleitz et al. 1994). This region of elevated biological production coincides directly with sites of bottom water formation, so that the biological CO_2 fixation in surface waters, the downward flux of particulate organic carbon and the export of bottom shelf waters are hypothesized to combine to an effective bio-physical carbon pump which may significantly contribute to the sequestration of CO_2.

At the same time, the downward flux of carbon is assumed to sustain a rich, well adapted benthic fauna (Arntz et al. 1994). The seafloor provides an integrated signal of the downward carbon flux and reflects the efficiency of the biological carbon pump. Benthic oxygen uptake provides an integrated measurement of benthic mineralization and is crucial for balancing the benthic carbon cycle. So far, benthic fauna studies in this region did not include oxygen flux measurements leaving the receiving carbon flux, as well as the return flux of essential nutrients to the water column, largely unknown. In addition, the response of benthic fauna biomass to organic carbon supply needs a better understanding to evaluate the expected change in primary production and its effect on blue carbon storage. The WS continental shelf harbors unique benthic communities dominated by suspension feeders, which are often structured by sponges (Federwisch et al. 2020). Despite a good documentation of benthic community types and composition, little is known about community dynamics. Repeated observations in the western WS suggest that growth of benthic fauna can be significantly higher than previously assumed, most likely due to the changed carbon supply (Fillinger et al. 2013). So far, repeated observations to detect benthic community change and megafauna growth are scarce at these latitudes, and oxygen flux measurements are entirely lacking.

In polar regions, research on carbon cycling – from primary production and benthic turnover to lateral transport and down slope export – is dependent on automated measuring devices to provide reliable *in-situ* data and coherent time series, especially seasonal data. In recent years, the development of autonomous measuring systems has advanced to determine *in-situ* oxygen fluxes and mass transport across the bentho-pelagic interface. This includes stationary landers, which allow quantifying the integrated benthic oxygen uptake of large areas (10 – 100 m²), i.e., on ecosystem level (Holtappels et al. 2013). Further, the analysis of seawater properties has been automated and miniaturized so that “Lab-on-Chip” (LoC)

sensors are able to record temporal changes of nutrient concentrations in seawater at high precision now (Beaton et al. 2012). LoC sensors complement a growing suite of environmental sensors (e.g. for pCO_2, particle dynamics) to monitor the production and fate of organic carbon. The automation of environmental measurements and its use in marine research is of utmost importance especially for polar regions where most of the data have been collected in summer and little is known throughout the rest of the year.

In summary, the objectives of the conducted research were to

- establish a DIC/POC/DOC/nutrient inventory of major water masses on the southern shelf to estimate C-export by deep water formation;
- characterize the euphotic waters in terms of nutrients, chlorophyll *a*, bacterial metaproteomgenomics and polysaccharide utilization mechanism (all in cooperation with the other groups, see Chapters 7, 8, 9);
- use LoC-sensors for automated measurements of pH, TA and nutrients in surface waters but also for *in-situ* incubations of benthic chamber landers (see Chapter 11);
- assemble and deploy a joint “biogeochemical” mooring (BGC-1) as part of a multi-disciplinary initiative across various AWI-sections;
- use a Benthic Lander to determine benthic mineralization and turnover by measuring the diffusive and total benthic oxygen uptake as well as particle fluxes at sites with contrasting primary production;
- determine the abundance, biomass, and diversity of benthic fauna on the shelf and at the shelf break in relation to organic carbon availability, seafloor substrate, and bottom current regime;
- identify temporal trends in benthic fauna composition by repeating sampling at stations occupied in earlier expeditions;
- determine biodiversity of sea spiders and sample sea spiders for subsequent neuroanatomical and developmental investigations.

Work at sea

The interdisciplinary research programme of COSMUS was reflected in the diverse work programmes of the research group studying “The C-Pump and its Imprint on Benthic Fauna”. The activities mentioned below were implemented in close connection with the work described in Chapters 3, 5, 7, 8, 9 and 11. We summarize the work by the topics following:

1. Carbon inventory of major water masses (T. Hargesheimer, A. Dürwald, M. Holtappels)

Water samples were taken with a CTD-Rosette equipped with standard Niskin bottles. The stations and water depths were selected in close cooperation with the oceanographic and (bio)geochemical disciplines (Chapters 3, 7, 8, 9) to allow a multi-parameter investigation of water column properties. Criteria for the chosen depths were: (1) a high resolution of the upper water column in order to sample the layer with the highest productivity and carbon turnover, (2) a high resolution of the benthic boundary layer (up to 100 m above seafloor) in order to sample particulate resuspension and the densest water mass, (3) targeting distinct intermediate water masses defined by characteristic temperature-salinity profiles. Upon retrieval, the Niskin bottles were sampled for:

1. Dissolved inorganic carbon (DIC) and total alkalinity (TA): 250 ml stored poisoned in glass vials at 4 °C
2. Dissolved organic matter (DOM): 2,000 ml filtered and stored acidified in polycarbonate bottles at 4 °C
3. Nutrients, such as nitrate and nitrite (NO_x), phosphate (PO_4^{3-}), silicate (Si), total nitrogen (TN) and total phosphate (TP): 2 x 15 ml filtered and stored in plastic vials frozen at –20 °C
4. Particulate organic matter (POM): 2,000 ml filtered on GFF filter and stored frozen at –20 °C
5. Chlorophyll *a*: 1,000 ml filtered on GFF filter and stored frozen at –20 °C

In total, 49 stations were sampled (Fig. 10.1) and up to 274 samples were taken covering the major water masses on the shelf and continental slope (Fig. 10.4, Table 10.1).

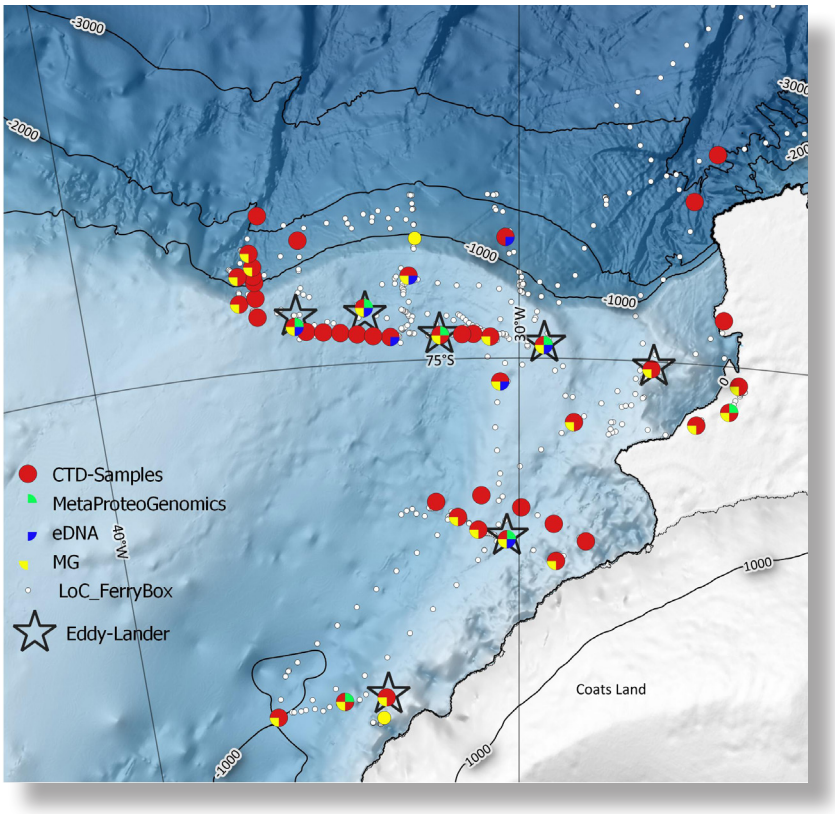

Fig.10.1: Map of the south-eastern Weddell Sea shelf showing stations of CTD-Rosette samples for carbon and nutrient (red), MetaProteoGenomics (green), environmental DNA (blue), MG deployments (yellow) and Lander deployments (star). Underway sampling of nutrients by the LoC-FerryBox is indicated by small white dots.

Tab. 10.1: List of CTD-Rosette stations for the sampling of nutrients and carbon compounds

Station	Date	Time	Latitude [°S]	Longitude [°W]	Water depth [m]	DIC/TA samples	Nutrient samples	DOC samples	POM/ Chl *a* samples
PS124_5-2	2021-02-08	12:21	-70.418	-30.002	4436	8	8	8	8
PS124_6-2	2021-02-11	02:02	-73.719	-25.714	3143	8	8	8	8
PS124_8-5	2021-02-12	12:18	-74.921	-29.421	380	6	6	6	6
PS124_11-1	2021-02-13	16:37	-74.265	-30.303	1502	8	8	8	8
PS124_16-2	2021-02-14	15:46	-75.143	-30.447	435	6	6	6	6
PS124_21-1	2021-02-15	20:55	-74.869	-30.672	477	6	6		6
PS124_26-2	2021-02-16	17:58	-74.855	-31.831	607	8	8	8	8
PS124_30-1	2021-02-17	17:15	-74.852	-32.991	569	6	6	6	6
PS124_33-1	2021-02-19	00:26	-74.749	-35.199	482	6	6	6	6
PS124_36-1	2021-02-20	13:15	-74.229	-34.952	1601	8	8	8	8
PS124_37-1	2021-02-20	18:44	-74.580	-36.403	381	6	6	6	6
PS124_40-1	2021-02-21	17:22	-74.673	-36.014	414	6	6		6
PS124_41-1	2021-02-21	19:52	-74.556	-36.019	493	6	6		6
PS124_43-1	2021-02-21	23:14	-74.459	-36.008	1030	6	6		6
PS124_44-1	2021-02-22	01:03	-74.422	-36.026	1197	6	6		6
PS124_45-2	2021-02-22	05:56	-74.367	-36.017	1406	7	7	7	7
PS124_46-1	2021-02-22	14:42	-74.415	-36.371	1209	6	6		6
PS124_47-1	2021-02-22	22:38	-74.281	-36.067	1663	7	7		7
PS124_48-1	2021-02-23	10:16	-74.060	-35.800	1965	7	7		7
PS124_54-3	2021-02-25	07:21	-74.666	-33.564	556	8	8	8	8
PS124_55-1	2021-02-25	20:18	-74.786	-34.929	495	2			
PS124_56-1	2021-02-25	22:09	-74.798	-34.539	527	2			
PS124_57-1	2021-02-25	23:51	-74.811	-34.147	537	2			
PS124_58-1	2021-02-26	01:35	-74.825	-33.759	546	2			
PS124_59-1	2021-02-26	03:10	-74.842	-33.388	555	2			
PS124_64-1	2021-02-27	07:32	-74.851	-31.062	551	4	4	4	4
PS124_65-2	2021-02-27	11:48	-74.852	-31.329	584	4	4	4	4
PS124_66-1	2021-02-27	14:06	-74.854	-31.830	603	4	4	4	4
PS124_68-3	2021-02-28	23:10	-76.103	-30.310	447	6	6	6	6
PS124_72-1	2021-03-01	16:54	-75.962	-31.527	594	6	6		6
PS124_76-1	2021-03-02	20:03	-75.869	-32.062	715	8	8		8
PS124_78-1	2021-03-03	18:37	-76.043	-31.018	451	6	6		6
PS124_80-1	2021-03-04	18:20	-75.835	-30.951	458	4	4		4
PS124_81-1	2021-03-04	21:12	-75.908	-29.941	473	4	4		4
PS124_82-1	2021-03-05	00:03	-76.007	-29.115	388	4	4		4
PS124_83-1	2021-03-05	02:24	-76.110	-28.305	339	4	4		4
PS124_84-1	2021-03-05	04:30	-76.234	-29.054	308	4	4		4
PS124_88-1	2021-03-05	21:57	-77.108	-36.586	1064	8	8	3	8
PS124_90-4	2021-03-06	16:40	-77.041	-33.601	359	6	6		6
PS124_93-1	2021-03-07	15:42	-77.051	-34.741	775	7	6	2	6
PS124_98-1	2021-03-09	05:51	-75.385	-28.674	436	6	6		6

Station	Date	Time	Latitude [°S]	Longitude [°W]	Water depth [m]	DIC/TA samples	Nutrient samples	DOC samples	POM/ Chl *a* samples
PS124_100-1	2021-03-10	05:57	-74.484	-32.499	633	6	6		6
PS124_107-1	2021-03-11	21:59	-75.047	-26.884	278	6	6		6
PS124_109-1	2021-03-13	15:13	-74.726	-25.273	626	4	4		4
PS124_110-1	2021-03-13	19:29	-75.114	-24.796	553	6	6		6
PS124_111-2	2021-03-14	01:33	-75.277	-24.967	608	6	6		6
PS124_112-1	2021-03-14	19:26	-75.370	-25.724	782	6	6		6
PS124_115-1	2021-03-15	11:22	-74.018	-26.132	2862	6	6		6
PS124_117-1	2021-03-24	06:24	-69.000	-26.998	4718	4	4		

2. Automated Lab-on-Chip measurements of nutrients, pH and TA in the upper mixed water layer (A.Schaap)

Lab-on-Chip (LoC) devices perform automated *in-situ* chemical measurements. The sensors all operate using a common hardware platform (Beaton 2012). At the heart of each system is a microfluidic chip: a plastic disc with a network of channels machined into the plastic. Pumps, valves, electronics, and fluidic connectors are attached to the plastic disc. Seawater is pumped into the channels, where it mixes with chemical reagents. The products of the reaction form or change colour of the mixed solution and the colour is read out in optical cells, also built into the microfluidic chip. All reagents and calibration materials are stored in flexible bags outside of the sensor housing, as are waste products of the reactions. On this cruise, LoC sensors for pH, total alkalinity (TA), nitrate, phosphate, and silicate were included. Due to the small scale of the microchannels, the consumption of reagents and power is low, with a typical ~2 W power consumption during operation.

The nitrate, phosphate, and silicate sensors perform standard spectrophotometric analysis, using assays that are common for seawater measurements. The nitrate sensor uses the Griess assay: nitrate is reduced to nitrite in a cadmium reduction column, then forms a coloured azo dye with N-(1-naphthyl)-ethylenediamine dihydrochloride (Beaton 2012). The phosphate sensor uses the phosphomolybdate blue assay (Clinton-Bailey 2017; Grand 2017) and the silicate sensor uses the silicomolybdate blue assay (Clinton-Bailey 2019). All three nutrient sensors carry and routinely measure analytical blanks and standards to provide regular recalibration during use.

The pH sensor performs a spectrophotometric measurement with the pH indicator metacresol purple (Yin 2021). The TA sensor implements the single-point open-cell titration method and also carries 2–3 reference materials for *in-situ* calibrations.

Various Lab-on-Chip (LoC) sensors were run on the ship's underway seawater system throughout most of the cruise, from the 'Test' Station (2021-02-08) through arrival at the South Orkney Islands on the return trip (2021-03-27). Originally this was set up simply to test the sensors. However, it was decided to continue running this throughout the expedition as the data would support the scientific objectives around measuring primary production and carbon fluxes.

Sensors that were not used on other platforms and which were not undergoing maintenance were put on the underway system, typically running an analysis every hour. To implement this system, tubing from the ship's underway tap was run to a T-junction. One side of the junction was fed to a syringe with continuous flow-through, from which the LoC sensors sampled. This yielded between 500 and 1,000 measurements of each parameter during the entire cruise (Fig. 10.1).

In addition to the underway system, three LoC sensors were deployed on the large biogeochemical mooring (BGC-1, see below). These data, along with those of the other euphotic-zone equipment on the mooring, will contribute to studies of the seasonal productivity and carbon export of the region. The deployed LoC sensors and their setup is described in Table 10.2. Each sensor was powered by its own pack of 24 D-cell batteries and the water intake of each is filtered through a 0.45 µm pore size PES syringe filter.

Tab. 10.2: List of deployed LoC sensors and their setup for the BGC-1 mooring

Sensor Chemistry	Serial number	Calibration materials	Measurement frequency
pH	40	n/a	twice daily: noon and midnight UTC
TA	9	3 reference materials with TA ~ 2200, 2400, 2600 µmol/kg	once daily: noon UTC
Silicate	10	blank, 50 µM standard, 100 µM standard	once daily: noon UTC

3. Biogeochemical mooring (H. Schröder, A.Schaap, T. Hargesheimer, M. Holtappels)

A mooring with a suite of biogeochemical and oceanographic sensors was deployed at the end of the cruise, at station PS124-117-2 (Fig. 10.2). The equipment (Table 10.3) was contributed by several groups and the deployment was conducted in close cooperation with the oceanographic and biogeochemical groups (see Chapters 3, 7). Several sensor packages for the measurement of nutrients, carbon chemistry, oxygen, fluorescence, currents, CTD were positioned in the mixed layer at around 50m water depth to monitor the seasonality and short-term dynamics of the primary production. Below the pycnocline at ca. 250 m depth carbon export is visualized with an Underwater Vision Profiler and further below at 500 m and 1,500 m depth sediment traps collect the sinking material. The intended position for the deployment of the BGC-1 mooring was at Maud Rise, on the prime meridian at 66°S. However, at that time strong winds prevailed in this region, so that a new location was picked in the Weddell Gyre at 69°S and 27°W. The recovery of that mooring is planned for the *Polarstern* cruise next year (PS129).

Tab. 10.3: List of deployed sensors and samplers on the BGC-1 mooring

Sensor/ Sampler	est. Water Depth [m]	Measurement interval
LoC (pH)	42	12 hours
LoC (TA)	42	24 hours
LoC (Silicate)	42	24 hours
Remote Access sampler (24x 0.5 L)	44	7-10 days
ISUS nitrate sensor	44	2 hours
SAMI pCO2 sensor	44	2 hours
CTD-O2 sensor	44	2 hours
Ecotriplet Fluorescence sensor	44	1 hour
ADCP Current Profiler RDI 300 kHz	46	30 minutes
SBE-56 Temperature sensor	90	2 minutes

Sensor/ Sampler	est. Water Depth [m]	Measurement interval
SBE-37 CTD sensor	130	30 minutes
SBE-56 Temperature sensor	170	2 minutes
SBE-37 CT sensor	220	30 minutes
ET-861 Transponder	220	-
Underwater Vision Profiler 6	230	5 seconds
SUNA Nitrate sensor	230	1 hour
SBE-56 Temperature sensor	230	2 minutes
Sediment trap (20 cups)	590	15-30 days
Devologic SonoVault Sound Recorder	1000	-
Sediment trap (20 cups)	1600	15-30 days
Releaser	4680	-

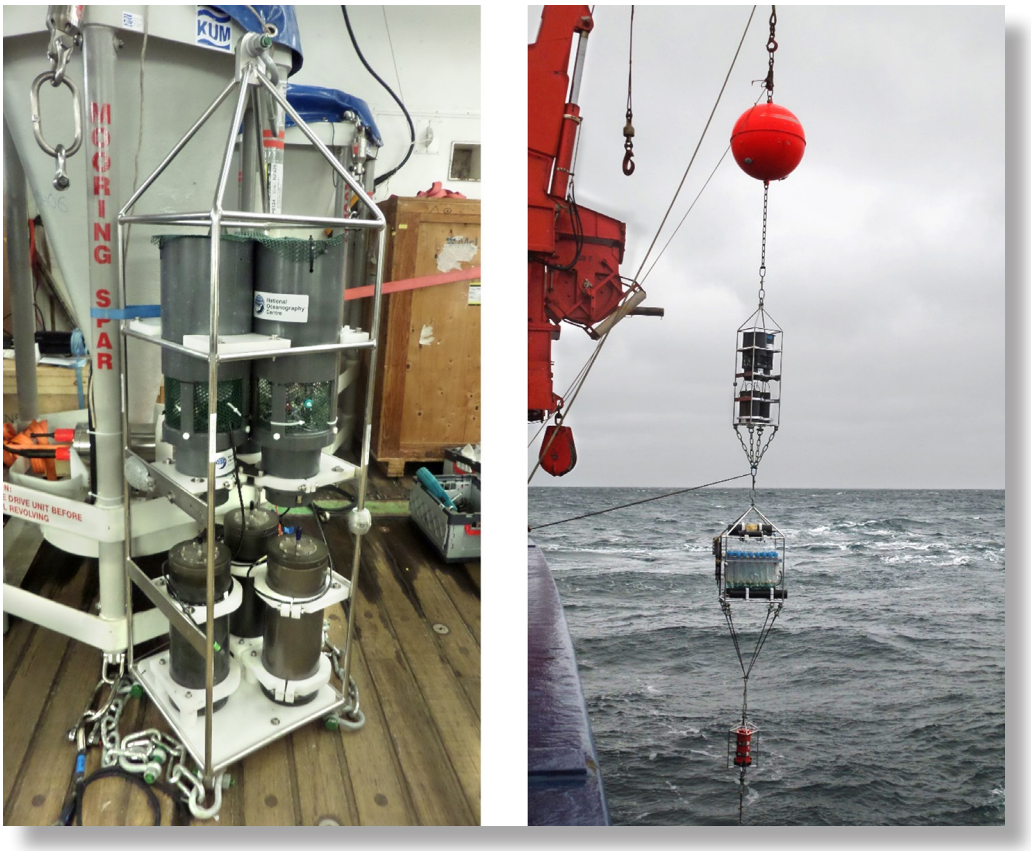

Fig. 10.2: (Left) The frame holding three LoC sensors (upper section) and battery canisters (lower section) in front of the 2 sediment traps. (Right) The deployment of the 2 upper-most frames on the mooring. (Photos: Allison Schaap)

4. Metaproteogenomics in euphotic water masses (A. Dürwald)

Bacteria are highly abundant in the phytoplankton-rich waters of the mixed layer. The carbon-rich phytoplankton (main component: polysaccharides) is the nutrient source for the growth of bacteria, that are found either attached to the phytoplankton cells or free-living in the adjacent water masses. In order to relate the microbial community with its metabolic activity, a metagenomic and metaproteomic approach was applied. The work was conducted in close cooperation with the Biogeochemistry group (Chapter 8).

At 8 stations, 80 liters of water were collected from the *chlorophyll a* maximum with the CTD-Rosette and sequentially filtered through 10 µm, 3 µm and 0.2 µm filters. Filters were stored at -80 °C. Macro- and microalgae retained on the 10 µm and 3 µm filters will be analyzed for polysaccharide composition, whereas bacteria retained by the 0.2 µm filter will be analyzed using metagenomics and metaproteomics.

In addition, at 4 stations bacterial cultivations were performed to identify and isolate new pectin degrading bacteria. 1 L water was sequentially filtered through 1.2 µm and 0.2 µm filters. The bacteria were removed from the 0.2 µm filter and resuspended in cultivation media with pectin derivates as only carbon source (triplicates). Growth was determined by density of the culture. Cultures were frozen, with and without glycerol, at –80 °C.

For comparison of bacterial metabolic activity between water column and sediments, sediment samples were taken with the Multi-Corer (MUC) in close cooperation with the groups Benthic Habitats and Geochemistry (Chapters 9 and 11). At 5 stations, the upper 1 cm from the sediment was taken and stored at –80 °C. Further, in cooperation with the Sea Ice group (see Chapter 6), ice cores were sampled for metaproteogenomics.

All samples will be processed at University of Greifswald.

Tab. 10.4: List of stations for metaproteogenomic sampling and bacterial cultivation

Station	Date	Time	Lat [°S]	Lon [°W]	Depth [m]	Sample	Sample Device	Sample Target
PS124_5-4	2021-02-08	19:37	-70.418	-29.999	65	Water	CTD	Meta-P/G & Cult
PS124_8-9	2021-02-12	17:31	-74.920	-29.424	59	Water	CTD	Meta-P/G & Cult
PS124_26-6	2021-02-16	21:25	-74.855	-31.833	50	Water	CTD	Meta-P/G
PS124_26-9	2021-02-17	05:45	-74.848	-31.851	600	Sediment	MUC	Meta-P/G
PS124_32-1	2021-02-18	23:31	-74.747	-35.222	30	Water	CTD	Meta-P/G
PS124_33-5	2021-02-19	06:33	-74.725	-35.180	470	Sediment	MUC	Meta-P/G
PS124_54-2	2021-02-25	06:09	-74.665	-33.560	25	Water	CTD	Meta-P/G
PS124_54-12	2021-02-25	16:21	-74.707	-33.578	550	Sediment	MUC	Meta-P/G
PS124_68-2	2021-02-28	22:16	-76.103	-30.305	36	Water	CTD	Meta-P/G & Cult
PS124_68-8	2021-03-01	06:31	-76.090	-30.336	450	Sediment	MUC	Meta-P/G
PS124_93-1	2021-03-07	15:40	-77.051	-34.741	33	Water	CTD	Meta-P/G & Cult
PS124_94-4	2021-03-07	19:57	-77.049	-34.738	740	Sediment	MUC	Meta-P/G
PS124_111-1	2021-03-14	00:49	-75.277	-24.966	60	Water	CTD	Meta-P/G

5. Sampling of environmental DNA from seawater and sediments (T. Hargesheimer)

Samples for environmental DNA (eDNA) were collected in order to detect cephalopod biodiversity and potential cephalopod foodfalls in the Antarctic Ocean. Remaining eDNA extracts will be used to assess gelatinous zooplankton biodiversity. At 8 stations, seawater was collected at 2–3 water depths with a CTD-Rosette and filtered with single-use sterile syringes through 0.22 µm sterivex filters (Merck). The filters were stored at –80 °C. In addition, sediment retrieved by the Multi-Corer was sampled at the same stations by collecting the first 1 cm of sediment in sterile falcon tubes. This work was conducted in close cooperation with groups Physical Oceanography, Geochemistry, and Benthic Fluxes and Habitats (Chapters 3, 9 and 11). The samples will be analyzed by Veronique Merten and Dr. Henk-Jan Hoving (both GEOMAR), who also initiated this work.

Tab. 10.5: List of stations sampled for eDNA

Station	Date	Lat [°S]	Lon [°W]	Sampling Device	Sampling Depths [m]
PS124_8-5	2021-02-12	-74.921	-29.421	CTD	15, 150, 375
PS124_11-1	2021-02-13	-74.265	-30.303	CTD	15, 600, 1402
PS124_11-3	2021-02-13	-74.265	-30.305	MUC	1545
PS124_16-2	2021-02-14	-75.143	-30.447	CTD	15, 250, 442
PS124_16-6	2021-02-14	-75.143	-30.448	MUC	454
PS124_30-1	2021-02-17	-74.852	-32.991	CTD	310, 584
PS124_30-5	2021-02-17	-74.852	-32.991	MUC	595
PS124_33-1	2021-02-19	-74.748	-35.203	CTD	60, 480
PS124_33-5	2021-02-19	-74.725	-35.183	MUC	497
PS124_54-3	2021-02-25	-74.665	-33.562	CTD	330, 585
PS124_54-10	2021-02-25	-74.707	-33.579	MUC	588
PS124_68-3	2021-02-28	-76.103	-30.306	CTD	200, 460
PS124_68-8	2021-03-01	-76.090	-30.336	MUC	476
PS124_110-1	2021-03-13	-75.114	-24.796	CTD	360, 546
PS124_110-4	2021-03-13	-75.114	-24.799	MUC	572

6. Benthic fluxes of oxygen and particles (M. Holtappels, H. Schröder, T. Hargesheimer)

An autonomous Benthic Lander was used to determine benthic oxygen consumption and particle fluxes in the benthic boundary layer (BBL). The so-called Eddy-Lander (Fig. 10.3) was equipped with an Eddy Covariance System (ECS) for non-invasive turbulent flux measurements of oxygen (Holtappels et al. 2013, 2015). The ECS consists of an Acoustic Doppler Velocimeter (ADV) and up to 3 fast measuring oxygen Optodes, which allow to construct a turbulent oxygen flux. In parallel, sedimentary oxygen profiles were measured using a vertical lance with 4 needle Optodes attached (Ahmerkamp et al. 2017). The lance was mounted on a slide which allowed a horizontal positioning. At 4 consecutive positions the 4 Optode-Microsensors were inserted by up to 20 cm into the sediment in order to measure a transect of 16 oxygen profiles, each 5 cm apart. The oxygen profiles were used to construct the diffusive oxygen uptake (DOU) while the Eddy device integrated a large benthic footprint and thus measured the total oxygen uptake (TOU) of the benthic fauna.

Fig. 10.3. Retrieval of the Eddy-Lander (Photo: Moritz Holtappels)

The backscatter of the ADV was used to construct a particle flux. In parallel, a McLane Phyto Plankton Sampler (PPS) was mounted on the lander to sample and filter water in the BBL at an interval of 1–2 hour in order to analyze the POM concentration and variability in the BBL. At each deployment, up to 20 filters were sampled and stored at –20 °C for further processing. The POM data will be used to calibrate the backscatter from the ADV in terms of POC. In close cooperation with the group Carbon Cycling (Chapter 7), the Underwater Vision Profiler (UVP 6) was mounted to the lander during 3 deployments to measure the temporal variability of the larger particle fraction (>100 µm) in the BBL.

The Eddy-Lander was deployed in concert with the Benthic Lander of the group Benthic Fluxes and Habitats (Chapter 11) enabling 3 complementary approaches for benthic oxygen uptake measurements (microsensor profiling, chamber incubations, turbulent eddy measurements). The Eddy-Lander was further equipped with an upward looking ADCP (150 kHz) and a CTD-O2 (SeaBird). The Eddy-Lander was deployed as a moored system with 3–4 additional CTDs throughout the water column and an upward looking ADCP (300 kHz) at approximately 50 m water depth. During PS124, the Eddy-Lander was deployed at 7 stations with a bottom time ranging from 22 to 95 hours (Table 10.6).

Tab. 10.6: Deployments of the Eddy-Lander for benthic flux measurements

Station Deployment	Station Recovery	Lat [°S]	Lon [°W]	Water Depth [m]	Date Deployment	Date Recovery	Bottom time [hours]
PS124_8-2	PS124_8-12	-74.907	-29.411	407	2021-02-12	2021-02-15	73
PS124_26-11	PS124_26-14	-74.848	-31.851	637	2021-02-17	2021-02-18	32
PS124_33-7	PS124_33-9	-74.688	-35.144	484	2021-02-19	2021-02-21	47
PS124_54-10	PS124_54-14	-74.699	-33.549	588	2021-02-25	2021-02-26	25
PS124_68-10	PS124_68-13	-76.082	-30.308	470	2021-03-01	2021-03-05	95
PS124_90-2	PS124_90-14	-77.024	-33.546	375	2021-03-06	2021-03-07	22
PS124_107-8	PS124_107-9	-75.030	-26.828	293	2021-03-12	2021-03-13	25

7. Benthic fauna community structure (S.E.A. Pineda-Metz, G. Brenneis)
Epifauna (S.E.A. Pineda-Metz) was assessed in close cooperation with the group Benthic Fluxes and Habitats (Chapter 11) using non-invasive image analyses of the video material collected with the OFOBS (see Chapter 11). OFOBS transects lasted 2.5 to 13 h and were usually done at a speed of 0.5 knots (see Chapter 11) with seabed images being taken every 20 seconds. For the aims of our studies, we only consider images in which the seafloor and benthic epifauna can be clearly seen and easily identified. Following this protocol, the number of seabed images per OFOBS transect varied in between 196 and 2,165, with a total of 13,816 seabed images.

Infauna (S.E.A. Pineda-Metz, G. Brenneis) was collected with a Multibox Corer (MG); (Gerdes 1990; Gerdes et al. 1992) which allows parallel sampling of up to 9 box-cores. It was highly appreciated that E. Werner from the bathymetry group (Chapter 5) joined the MG-team throughout the entire cruise. For most stations that were planned in advance of the cruise, up to 8 cores were used for infauna sampling (Table 10.7). At additional, opportunistic stations, a maximum of 5 cores were used due to limitations in fixation agents and containers. At several stations, one core was set aside to be checked for the presence of microplastics (see Chapter 12). In stations where Multi-Corer deployment (MUC, see Chapter 9) was unsuccessful, an additional core from the MG was provided to the Geochemistry group (Chapter 9) for analysis of sediment biogeochemistry. Only 21 from 27 MG deployments during PS124 were successful, giving a total of 140 cores. Infauna samples were sieved over 1,000 and 500 µm mesh. Two cores were conserved in 96 % ethanol and stored at –20 °C for qualitative systematic and molecular genetic analyses and voucher specimens. The other core samples were preserved in borax-buffered 5 % formalin in sea water to assess densities, biomass, composition, and distribution patterns of infauna.

Pycnogonida (G. Brenneis): During processing of MG samples, live sea spider specimens were picked from the sieves prior to bulk preservation. In addition to the MG cores, also MUC cores were screened for pycnogonids previous to their processing (see Chapter 9). Live specimens were identified to genus level and included in the community structure data set. Subsequently, animals intended for immunohistochemical study of the central nervous system were fixed for 1 or 8 h in 4 % paraformaldehyde in filtered seawater, rinsed in phosphate-buffered saline and transferred into cryoprotectant buffer (sodium phosphate buffer w/sucrose, ethylene glycol and polyvinylpyrrolidone) for storage at –20 °C. Specimens intended for histological study and micro-computed tomography were placed in Bouin's solution. Preceding fixation, single legs were removed with surgical micro-scissors and placed in 100 % ethanol for DNA barcoding to confirm morphological species identification.

Tab. 10.7: Locations and annotations for Multibox Corer deployments

Station	Date	Lat. [°S]	Lon. [°W]	Depth [m]	Cores	Pycnogonid counts, genus (family)	Comment
PS124_8-10	2021-02-12	-74.921	-29.424	405	8	1, *Austropallene* (Callipallenidae)	
PS124_16-7	2021-02-14	-75.143	-30.445	455	8	1, *Nymphon* (Nymphonidae) 1, Austropallene (Callipallenidae	*Austropallene* from MUC core
PS124_21-6	2021-02-16	-74.868	-30.664	496	5	1, *Nymphon*, (Nymphonidae)	Fish eggs preserved in Ethanol at -20°C

Station	Date	Lat. [°S]	Lon. [°W]	Depth [m]	Cores	Pycnogonid counts, genus (family)	Comment
PS124_26-8	2021-02-17	-74.848	-31.851	636	8	1, *Anoplodactylus* (Phoxichilidiidae)	Provided 2 cores to MUC group
PS124_33-6	2021-02-19	-74.724	-35.164	498	8	0	
PS124_37-4	2021-02-20	-74.595	-36.414	412	8	0	Provided 1 core to MUC group
PS124_45-6	2021-02-22	-74.340	-36.067	1542	8	4, *Pallenopsis* (Pallenopsidae)	Provided 1 core to MUC group
PS124_46-2	2021-02-22	-74.415	-36.366	1239	0	0	Sandy bottom
PS124_47-3	2021-02-23	-74.255	-36.096	1785	0	0	Sandy bottom
PS124_52-2	2021-02-24	-74.260	-32.334	929	8	1, undetermined ammotheid (Ammotheidae)	Provided 1 core to MUC group
PS124_54-11	2021-02-25	-74.707	-33.571	588	8	1, *Pallenopsis* (Pallenopsidae) 1, *Nymphon* (Nymphonidae)	
PS124_68-7	2021-03-01	-76.066	-30.278	468	8	1, *Nymphon* (Nymphonidae)	
PS124_72-7	2021-03-01	-75.947	-31.664	689	8	0	
PS124_78-7	2021-03-03	-76.046	-31.023	474	5	0	
PS124_84-2	2021-03-05	-76.234	-29.055	327	5	0	Qualitative Sponge mat
PS124_88-4	2021-03-06	-77.108	-36.568	1102	8	0	
PS124_90-9	2021-03-06	-77.038	-33.432	272	0	0	
PS124_90-10	2021-03-06	-77.038	-33.432	271	0		
PS124_90-12	2021-03-06	-77.039	-33.504	342	3	1, *Pycnogonum gaini* (Pycnogonidae)	Solid ground (rocks) Sponge & bryozoan mat; pycnogonid from MUC core
PS124_92-1	2021-03-07	-77.166	-33.705	269	5	0	Qualitative Bryozoan mat
PS124_94-3	2021-03-07	-77.050	-34.741	779	5	0	
PS124_98-5	2021-03-09	-75.397	-28.657	444	0	0	
PS124_100-6	2021-03-10	-74.556	-32.675	664	5	0	
PS124_107-3	2021-03-11	-75.046	-26.900	297	0	0	MG did not fire
PS124_110-3	2021-03-13	-75.113	-24.798	542	4	0	Solid ground (rocks)
PS124_111-6	2021-03-14	-75.277	-24.966	639	8	0	
PS124_112-3	2021-03-14	-75.372	7	791	7	0	

Preliminary (expected) results

Carbon and nutrient sampling

The compiled T-S plot of more than 90 CTD deployments show the characteristics of the major water masses in the southern Weddell Sea (Fig. 10.4). Water samples, taken at 49 stations covering all relevant depths and water masses, will be processed on shore to establish a carbon and nutrient inventory for the investigated region. The results will be combined and interpreted in relation with trace metal abundance, primary production and POC export (Chapters 7, 8, 9), but also put in context with flux measurements in the benthic boundary layer and the turnover and abundance of benthic fauna (below and Chapter 11). With this we expect to elucidate the major routes of carbon cycling and their connection to the major water mass circulation in the region.

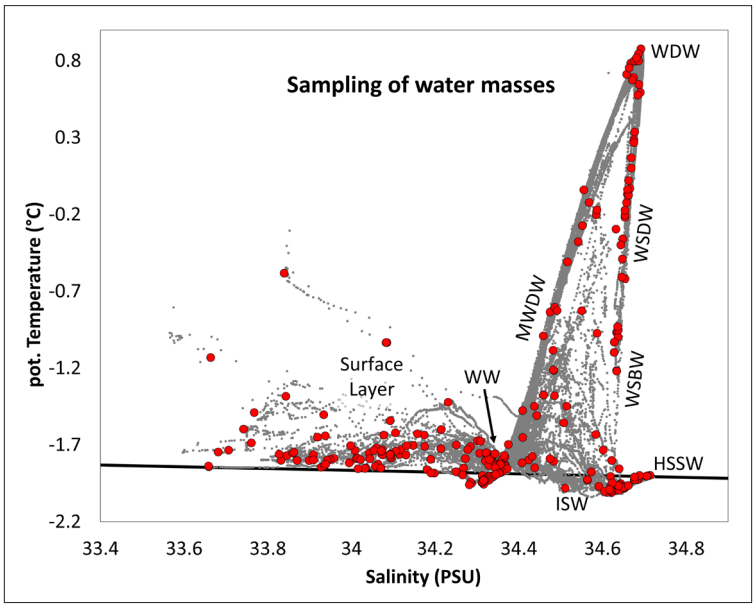

Fig.10.4: T-S plot compiled from all CTD casts (grey dots) and from Niskin-bottle sampling (red dots); the solid line indicates the surface freezing temperature. T-S characteristics of water masses are indicated: WW (Winter Water), MWDW (Modified Warm Deep Water), WDW (Warm Deep Water), WSDW (Weddell Sea Deep Water), WSBW (Weddell Sea Bottom Water), ISW (Ice Shelf Water), HSSW (High Salinity Shelf Water).

Throughout the cruise, the surface water showed high concentrations of the macronutrients being measured with the LoC devices run on the ship's underway seawater system. This supports the general characterization that the region's primary production is limited by iron or other micronutrients/trace elements. Data from the LoC measurements will be compared with the measurements taken by the FerryBox system on board, which includes measurements of complementary parameters such as oxygen and chlorophyll.

Within the south-eastern Weddell sea, preliminary results show typical measurements of 60–70 µM silicate, 20–30 µM nitrate + nitrite, 1–2 µM phosphate, 2250–2350 µmol/kg TA, and 8.1–8.25 pH units. The FerryBox sensors showed oxygen of 310–340 µmol/l and 0-5 µg/L chlorophyll *a*, although these measurements are not fully calibrated and in their present state more reliable as indicators of trend and gradients than as absolute numbers.

The surface water temperature and salinity are measured by a SBE probe on the ship's keel. Throughout the underway measurements, these parameters ranged from –1.93 °C to –0.42 °C (mean: –1.56 °C) for temperature and from 32.98 to 34.51 PSU (mean: 33.88 PSU) for salinity.

The Eddy-Lander

Visuals from the Eddy-Lander deployments revealed sediments with sparse traces of macro fauna in the western stations (Fig. 10.5 A-D), but elevated fauna abundance at the eastern stations (Fig. 10.5 E-G).

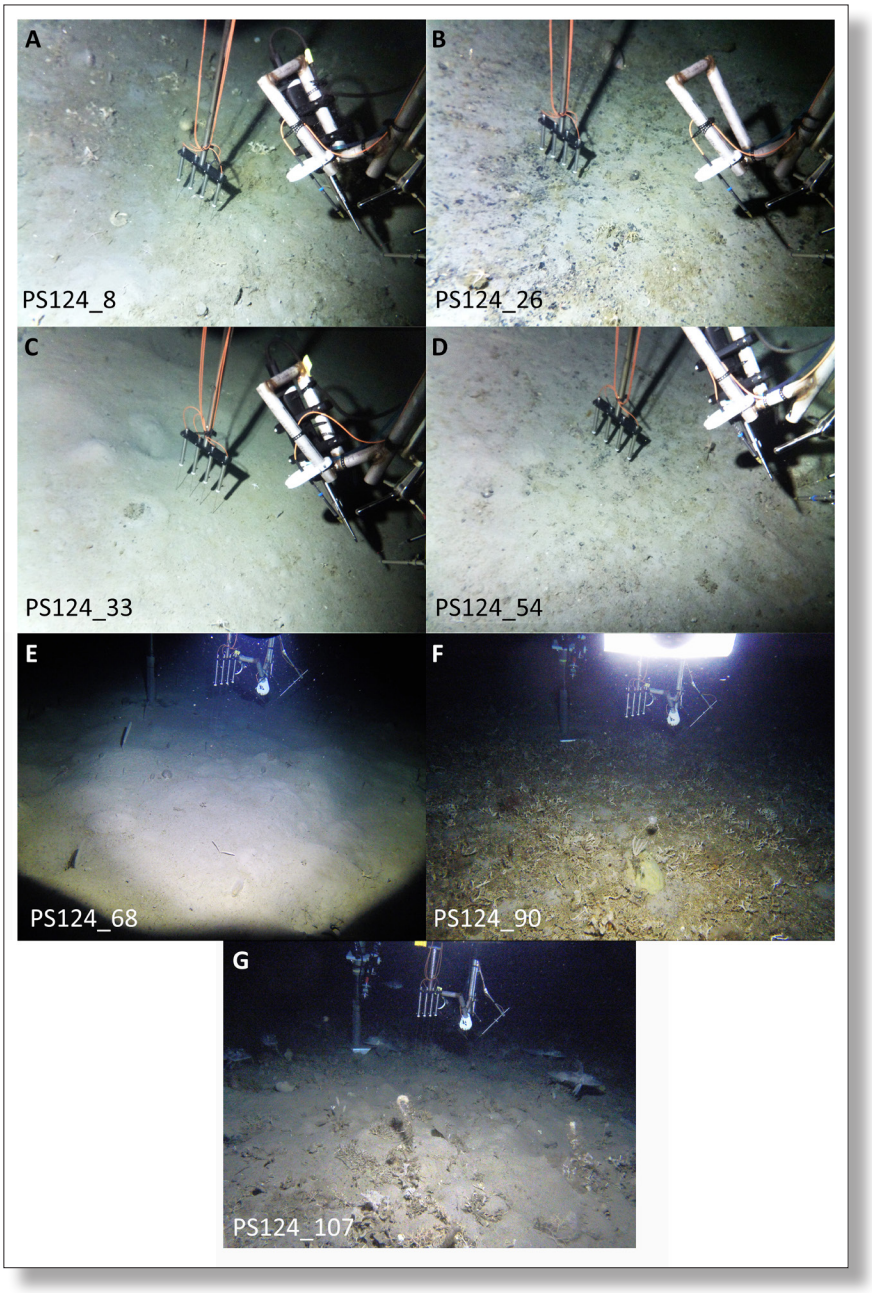

Fig.10.5: Images of the seafloor underneath the Eddy-Lander during (A, B, C, D) and before (E, F, G) the profiling of the 4 Micro-Optodes

Preliminary results can be reported for the oxygen measurements of the Eddy-Lander as the raw data were readily extracted. The oxygen profiles exhibit oxygen penetration depths of 15 cm in the shallow eastern stations and of 5–15 cm in the western stations (Fig. 10.6). Occasionally, some of the micro-optodes broke due to high abundance of rock fragments, but the redundancy of the profiling system (4 optodes in parallel, inserted 4 times) provided

successful measurements at all stations. The Eddy-covariance system recorded significant turbulent oxygen fluxes in the range 3–5 mmol m^{-2} d^{-1} at the eastern stations (Fig. 10.7), whereas the flux at western stations was close to the detection limit of ~0.5 mmol m^{-2} d^{-1}. There, oxygen profiles provide more reliable estimates of the oxygen uptake.

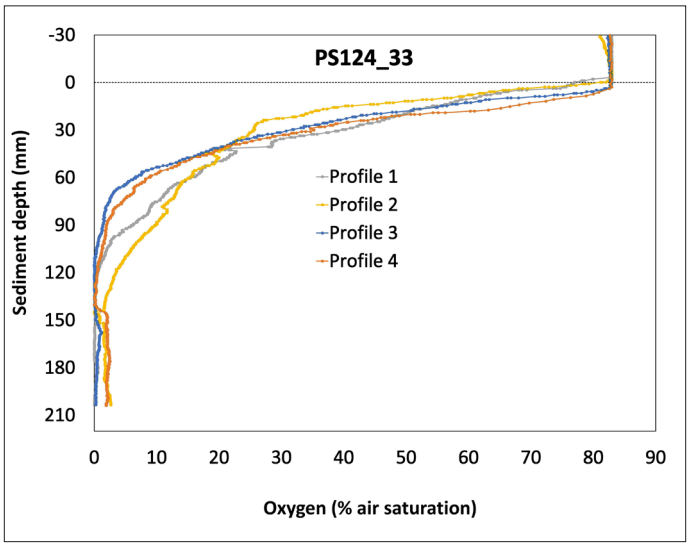

Fig.10.6: Oxygen profiles (preliminary data) at station PS124_33, consecutively measured by one of the 4 micro-optodes along the 80 cm long transect

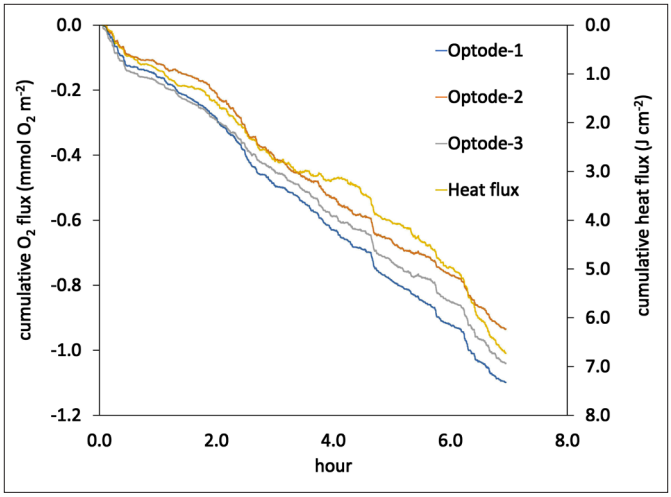

Fig.10.7: Eddy covariance measurements of cumulative oxygen and heat flux (preliminary data) at station PS124_90; the oxygen flux, measured in parallel by 3 fast-responding micro-optodes ranged from to –3.2 to –3.8 mmol m^{-2} d^{-1} (negative flux points towards the seafloor). The heat flux was measured with a fast thermistor and amounts to 2.7 W m^{-2}.

Epifauna from OFOBS visuals

Based on first visual checks of seabed, benthic epifauna of the Filchner region appears rather heterogeneous and, in some areas, shows pronounced patchy distribution patterns. At a first glance we could distinguish the five community types described by Pineda-Metz et al. (2019) for the region, as well as a sixth community, the FNC, which represents the one-station group previously described (group “C” in Pineda-Metz et al. 2019), which we here refer to as Fish

Nest associated Community (FNC). In addition to these communities we could differentiate a new community type represented by one station (Station PS_124-47), which we refer to as a Sand associated community (Sand; Fig. 10.8). This community was characterized by lower abundance than elsewhere in the region, and dominated by ophiuroids, equinoids and serolid amphipods. When comparing our analysis with results from previous cruises (Pineda-Metz et al. 2019), the distribution of the local benthic communities remained relatively unchanged (Fig. 10.8). In some stations, the community classification could change after detailed analysis of the large-scale seabed imagery surveys performed via OFOBS transects, because of high patchiness and mix of communities. Examples are the transects done at stations 30-7 and 54-1 which were characterized by a mix between ESC and CSC, as well as that of station 107-5 where a mix between ESC and I/ISWC was encountered.

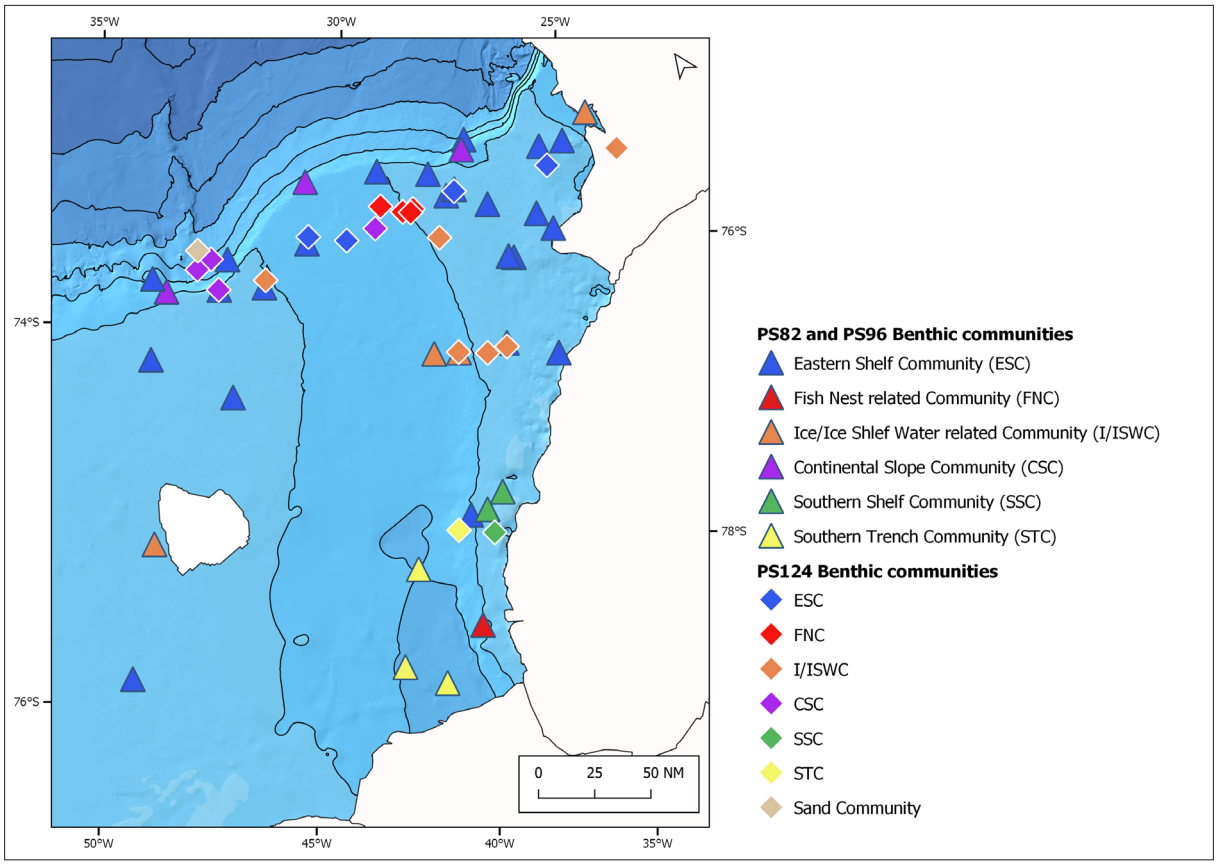

Fig.10.8: Station map of PS82, PS96 (both in triangles) and PS124 (diamonds) where imagery transects were taken. The colours represent the different benthic faunal communities defined by Pineda-Metz et al. (2019)

Samples from Multi-Box-Corer

Based on observations while sieving, abundances for PS124 could be roughly estimated. These estimations are shown in Fig. 10.9 in comparison with data collected during PS82 and PS96 (Pineda-Metz & Gerdes 2019). The general pattern remained relatively stable, i.e. higher abundances on shallower stations (< 400 m depth) and in proximity of the continental or ice shelf edges, where dense aggregations of ESC and SSC are found. Our observations from PS82, PS96 and PS124 point to a gradual decrease of abundance, overall biomass and diversity in southward and westward directions, which is consistent with preliminary results of the oxygen uptake measurements (see above). This supports the hypothesis that benthic

characteristics in the Filchner region are regulated by sea-ice cover, depth and water mass, as suggested by Pineda-Metz et al. (2019). To validate this hypothesis, in-depth analysis of the benthos data of PS124 is still needed in combination with the results of other groups (Chapter 6, 7, 8, 9 and 11).

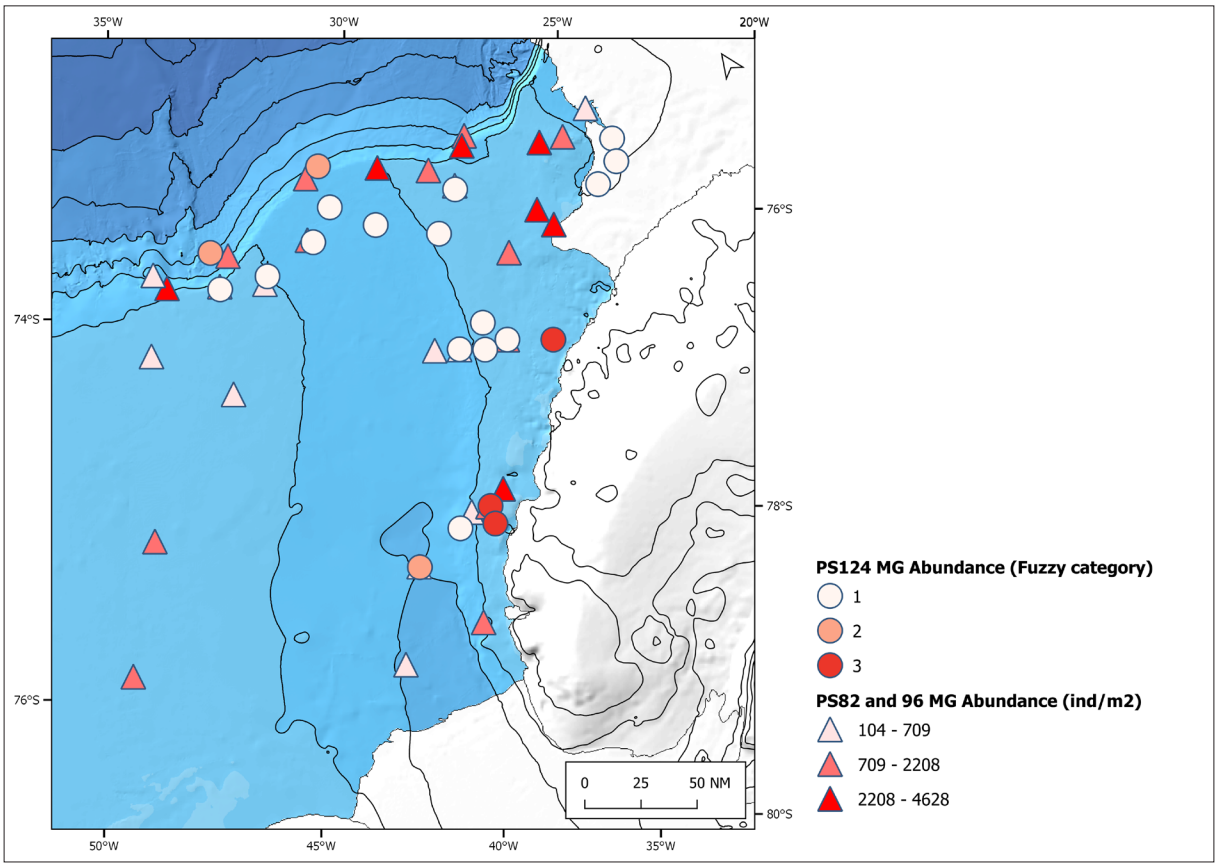

Fig.10.9: Station map of PS82, PS96 (both in triangles) and PS124 (circles) where the multi-boxcorer was deployed. The colours represent low (pale red) to high (red) abundances of benthic fauna.

Temporal dynamics in the Filchner region

Based on a first screening of the MG samples, benthic invertebrate abundance showed little difference to abundance values determined during PS82 and PS96 (Pineda-Metz & Gerdes 2019). Furthermore, the distribution of benthic communities observed in seabed images from the OFOBS matched previous descriptions for the region (Pineda-Metz et al. 2019). The preliminary data, combining in- and epifaunal surveys during PS124, do not indicate a similar change as reported for the area at Kapp Norvegia/Austasen in the eastern Weddell Sea (Pineda-Metz et al. 2020).

Pycnogonida in the Filchner region

A total of 12 sea spider specimens belonging to five different families and five genera (e.g. Fig. 10.10; Table 10.7) were collected with the MG. Additionally, two more specimens were recovered from MUC cores, one of them representing a sixth family and genus. The individuals obtained were mostly found related to ESC and CSC which are characterized by a medium to high abundance of suspension feeders (Fig. 10.11), especially hydrozoans and gorgonians (Pineda-Metz et al. 2019). Several of the pycnogonids collected were attached to a

colonial organism known to be potential prey, e.g., hydrozoans or bryozoans (Dietz et al. 2018). However, the number of collected specimens is surprisingly low, even when considering the expected lower biodiversity at stations in greater depths in the Filchner Trough or along the continental slope. At least part of this is likely attributable to the applied sampling gear and scheme (see next section).

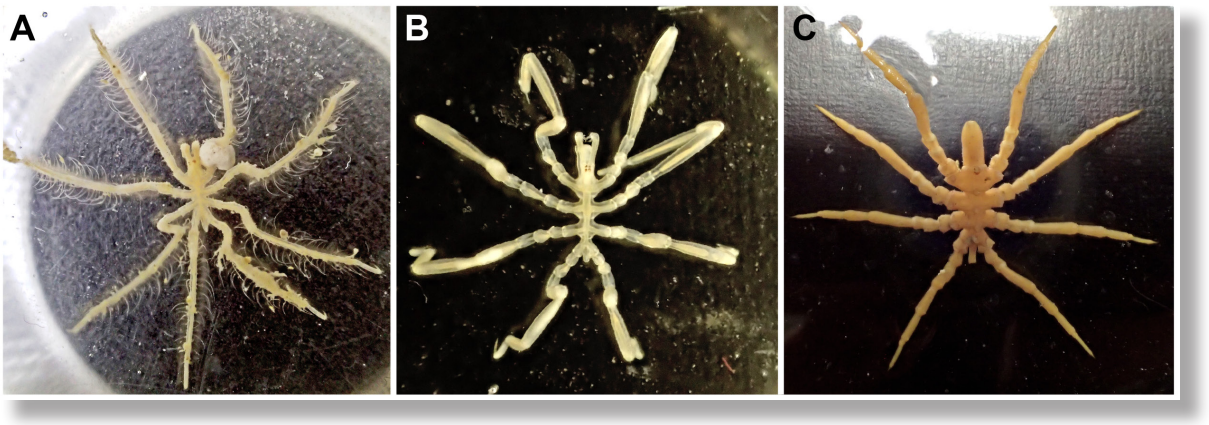

Fig.10.10: Selected pycnogonid specimens obtained during PS124; live specimens in dorsal view: A: Pallenopsis sp. (Pallenopsidae), station PS124-054, 588 m depth, 25 Feb. 2021; B: Anoplodactylus sp. (Phoxichilidiidae). station PS124-026, 636 m depth, 17 Feb. 2021; C: Pycnogonum gaini (Pycnogonidae), station PS124-090, 342 m depth, 06 Mar. 2021.

Sampling complications

PS124 marked one of the few Antarctic expeditions onboard *Polarstern* (Alfred-Wegener-Institut, 2017), if not the only one, in which the MG was deployed without a video system for guidance. Due to its weight and robust construction, the MG is a device which can obtain samples from most sediments, even when they are covered by dense biological mats comprised of, e.g. glass sponges or largely calcified bryozoan colonies. However, the lack of a camera system resulted in a lower sampling efficiency. This resulted in deployments bringing no samples, due to the fact that the gear landed in a patch of sand or on top of medium to large stones, both of which could have been avoided by live observation of the seafloor with a camera prior to the actual sampling. This resulted in a reduced sampling success rate (21 out of 27, i.e. ~77 %) in comparison to the latest reference for the region, i.e. PS82 and PS96 (~96 % and ~91 %, respectively).

The lack of live camera monitoring is also one factor to take into consideration for the representativeness of the surprisingly low local diversity and number of pycnogonids found in the PS124 MG samples. Many pycnogonids – especially groups with leg spans of just a few millimeters – are known to be predominantly associated with their prey to which they cling while feeding. Several of the sampling stations featured a patchy distribution of sessile invertebrates, as evidenced by subsequent OFOBS transects in the respective areas (see Chapter 11). In some cases, the visually unguided MG deployments seem to have led to sampling right between those patches of higher diversity. As a consequence, the MG data obtained likely result in an underestimation of the actual local diversity. For instance, preliminary screening of the OFOBS transect images taken near station PS124-37 clearly prove the presence of different pycnogonid groups of various sizes, but neither MG, nor MUC recovered a single specimen (Table 10.7). To address this issue not only for pycnogonids but also for other macrobenthos, future cruises should prioritize live camera observation, ideally

coupled to repeated MG sampling at the same station to increase coverage at sampling sites with patchy benthos distribution. Furthermore, employment of additional sampling gear, such as an Agassiz trawl or an epibenthic sledge promise to provide a more complete overview of the overall benthic macrofauna in the area.

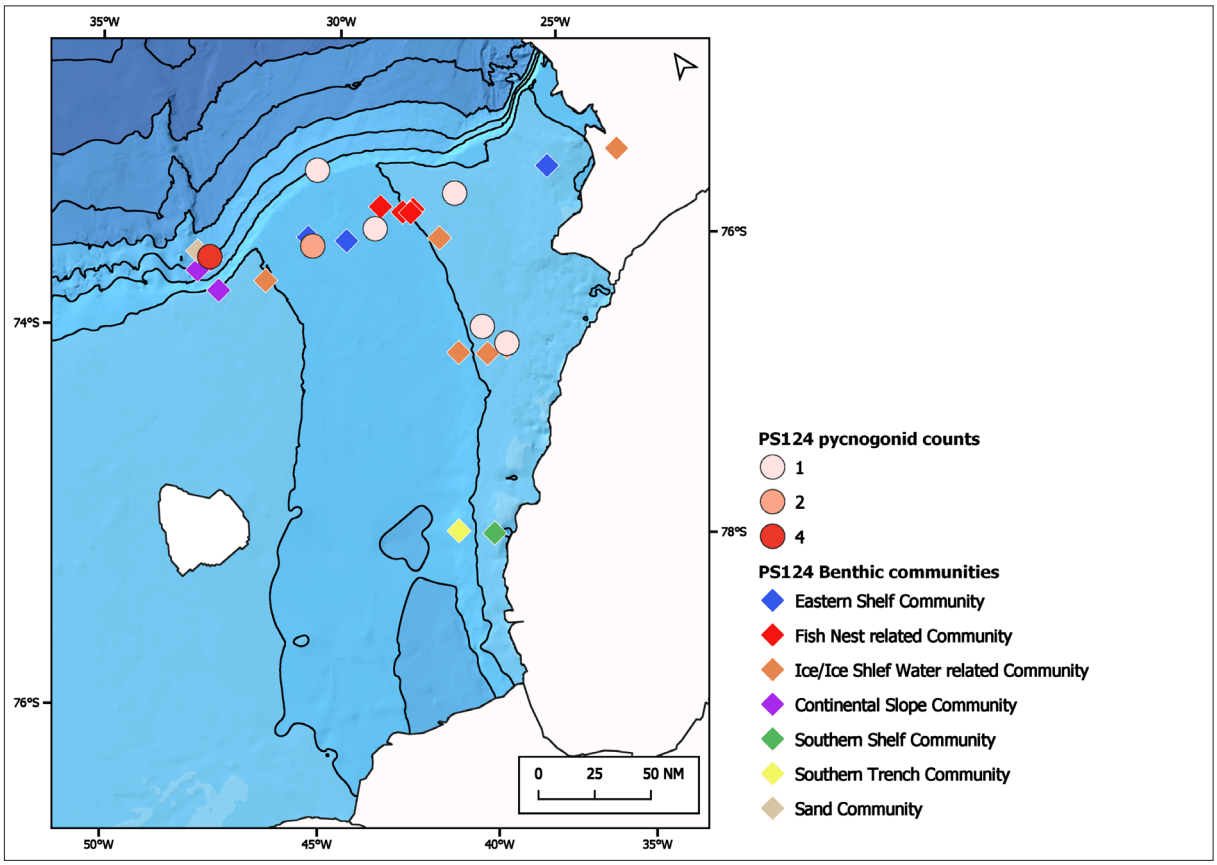

Fig.10.11: Station map including OFOBS transects with corresponding benthic community type (diamonds) and MG stations (circles) where pycnogonids were found; the colours represent the number of pycnogonids found.

Data management

Sample processing will be carried out at AWI, Geomar and at the University of Greifswald. Data acquisition from several types of investigation will require different time spans. The time periods from post processing to data provision will vary from one year maximum for sensor data to several years for metaproteogenomic and environmental DNA datasets. The latter samples will be analysed using sequencing-based methods. All (meta)genome sequence data will be made public by submission to the European Bioinformatics Institute's (EBI) (and) European Nucleotide Archive (ENA) database. These submissions will adhere to the current emerging standards as suggested by the Genomic Standards Consortium and thus include metadata such as information on the sampling location and its physicochemical conditions. Metatranscriptome data will be stored at GEO (https://www.ncbi.nlm.nih.gov/geo/). Proteome data will be made available to the public by using the online resource PRIDE (http://www.ebi.ac.uk/pride). The eDNA data will be deposited at PANGAEA and at GenBank (NCBI – National Center for Biotechnology Information). Until then all preliminary data will be available to the cruise participants as well as external users after request to the senior scientist. The final processed data generated by this project will be made available publicly

according to international standards by the World Data Center PANGAEA Data Publisher for Earth & Environmental Science (www.pangaea.de). The unrestricted availability on PANGAEA will depend on the required time and effort for acquisition of individual datasets and its status of scientific publication.

In all publications, based on this cruise, the AWI Grant No. AWI_PS124_05 and AWI Grant No. AWI_PS124_11 (Pycnogonids, Georg Brenneis) will be quoted and the following *Polarstern* article will be cited:

Alfred-Wegener-Institut Helmholtz-Zentrum für Polar- und Meeresforschung. (2017). Polar Research and Supply Vessel POLARSTERN Operated by the Alfred-Wegener-Institute. Journal of large-scale research facilities, 3, A119. http://dx.doi.org/10.17815/jlsrf-3-163.

References

Alfred-Wegener-Institut Helmholtz-Zentrum für Polar- und Meeresforschung (2017) Polar Research and Supply Vessel POLARSTERN Operated by the Alfred-Wegener-Institute. Journal of large-scale research facilities, 3, A119. http://dx.doi.org/10.17815/jlsrf-3-163.

Ahmerkamp S, Winter C, Krämer K, Beer D d, Janssen F, Friedrich J, Kuypers M, Holtappels M (2017) Regulation of benthic oxygen fluxes in permeable sediments of the coastal ocean. Limnology and Oceanography, 62(5), 1935 – 1954.

Arntz WE, Brey T, Gallardo VA (1994) Antarctic zoobenthos. Oceanography and Marine Biology: an Annual Review, 32, 241 –304.

Beaton AD, Cardwell CL, Thomas RS, Sieben VJ, Legiret FE, Waugh EM, Statham PJ, Mowlem MC, Morgan H (2021) Lab-on-chip measurement of nitrate and nitrite for in situ analysis of natural waters. Environmental science & technology, 46(17), 9548 – 56.

Clinton-Bailey GS, Grand MM, Beaton AD, Nightingale AM, Owsianka DR, Slavik GJ, Connelly DP, Cardwell CL, Mowlem MC (2017) A Lab-on-Chip Analyzer for in Situ Measurement of Soluble Reactive Phosphate: Improved Phosphate Blue Assay and Application to Fluvial Monitoring. Environmental Science and Technology, 51(17), 9989–9995.

Clinton-Bailey GS, Beaton AD, Patey M, Davey E, Fowell S, Martin A, White SN, Birchill AJ, Mowlem MC (2019) 'Lab-on-Chip' Sensor for in Situ Determination of Silicate in Natural Waters, in Goldschmidt Abstracts 2019, 634.

Dietz L, Dömel JS, Leese F, Lehmann T, Melzer RR (2018) Feeding ecology in sea spiders (Arthropoda: Pycnogonida): what do we know? Frontiers in Zoology 15: 7.

Federwisch L, Janussen D, Richter C (2020) Macroscopic characteristics facilitate identification of common Antarctic glass sponges (Porifera, Hexactinellida, Rossellidae). Polar Biology, 43(2), 91 – 110.

Fillinger L, Janussen D, Lundälv T, Richter C (2013) Rapid Glass Sponge Expansion after Climate-Induced Antarctic Ice Shelf Collapse. Current Biology, 23(14), 1330 – 1334.

Gerdes D (1990) Antarctic trials of the multi-box corer, a new device for benthos sampling. Polar Records 26, 35 – 38.

Gerdes D, Klages M, Arntz WE, Herman RL, Galéron J, Hain S (1992) Quantitative investigations on macrobenthos communities of the southeastern Weddell Sea shelf based on multibox corer samples. Polar Biology 12: 291 – 301.

Gleitz M, Bathmann UV, Lochte K (1994) Build-up and decline of summer phytoplankton biomass in the eastern Weddell Sea, Antarctica. Polar Biology, 14(6), 413–422.

Grand MM, Clinton-Bailey GS, Beaton AD, Schaap AM, Johengen TH, Tamburri MN, Connelly DP, Mowlem MC, Achterberg EP (2017) A Lab-On-Chip Phosphate Analyzer for Long-Term In Situ Monitoring at Fixed Observatories: Optimization and Performance Evaluation in Estuarine and Oligotrophic Coastal Waters. Frontiers in Marine Science, 4.

Holtappels M, Glud R N, Donis D, Liu B, Hume A, Wenzhoefer F & Kuypers M M M (2013) Effects of transient bottom water currents and oxygen concentrations on benthic exchange rates as assessed by eddy correlation measurements. Journal of Geophysical Research-Oceans, 118(3), 1157–1169. doi:10.1002/jgrc.20112.

Holtappels M, Noss C, Hancke K, Cathalot C, McGinnis D F, Lorke A & Glud R (2015) Aquatic Eddy Correlation: Quantifying the Artificial Flux Caused by Stirring-Sensitive O2 Sensors. Plos One, 10(1), e0116564.

Huhn O, Hellmer HH, Rhein M, Roether W, Rodehacke C, Schodlok M, Schröder M (2008) Evidence of deep and bottom water formation in the western Weddell Sea. Deep-Sea Research II, 55/8-9, 1098–1116, doi:10.1016/j.dsr2.2007.12.015.

Pineda-Metz SEA, Gerdes D (2019) Abundance and biomass of macrozoobenthos in surface sediments sampled during POLARSTERN cruises PS82 and PS96. Alfred Wegener Institute, Helmholtz Centre for Polar and Marine Research, Bremerhaven, PANGAEA, https://doi.org/10.1594/PANGAEA.908128.

Pineda-Metz SEA, Isla E, Gerdes D (2019) Benthic communities of the Filchner Region (Weddell Sea, Antarctica). Marine Ecology Progress Series, 628, 37–54.

Pineda-Metz SEA, Gerdes D, Richter C (2020) Benthic fauna declined on a whitening Antarctic continental shelf. Nature Communications 11(1), 1–7.

von Bodungen B, Nöthig E.-M, Sui Q (1988) New production of phytoplankton and sedimentation during summer 1985 in the south eastern Weddell Sea, Comparative Biochemistry and Physiology Part B: Comparative Biochemistry, 90(3), 475–487, doi.org/10.1016/0305-0491(88)90286-6.

von Bröckel K (1985) Primary production data from the south-eastern Weddell Sea. Polar Biology, 4(2), 75–80, doi:10.1007/BF00442903.

Yin T, Papadimitriou S, Rérolle V, Arundell M, Cardwell CL, Walk J, Palmer M, Fowell S, Schaap A, Mowlem M, Loucaides S (2021) A Novel Lab-on-Chip Spectrophotometric PH Sensor for Autonomous in Situ Seawater Measurements to 6,000 m Depth on Stationary and Moving Observing Platforms, in review.

11. BENTHIC FLUXES AND HABITATS

Frank Wenzhöfer[1], Autun Purser[1], [1]DE.AWI
Axel Nordhausen[2] [2]DE.MPIMM

Grant No. AWI_PS124_02

Objectives

Benthic communities are strictly dependent on carbon supply through the water column, which is determined by temporal and spatial variations in the vertical export flux from the euphotic zone but also lateral supply from shelf areas. Most organic carbon is recycled in the pelagic, but a significant fraction of the organic material ultimately reaches the seafloor, where it is either re-mineralized or retained in the sediment record. One of the central questions is to what extent sea-ice cover controls primary production and subsequent export of carbon to the seafloor on a seasonal and interannual scale. Benthic oxygen fluxes provide the best and integrated measurement of the metabolic activity of surface sediments. They quantify benthic carbon mineralization rates and thus can be used to evaluate the efficiency of the biological pump.

Seafloor habitats and associated benthic fauna was investigated with the Ocean Floor Observation and Bathymetry System (OFOBS). OFOBS is a towed device capable of deployment in moderately ice-covered regions and capable of concurrently collecting acoustic as well as video and still image data from the seafloor (Purser et al. 2018). This data will serve two purposes: (1) habitat mapping, and (2) macroecological studies of megabenthic biodiversity patterns. Habitat mapping OFOBS data streams will be integrated to produce high-resolution 3D spatial models (topographic maps) of the seafloor. These models will allow subsequent high-resolution analysis of terrain variables such as slope, aspect and rugosity, and their relationship to the distribution of benthic fauna on a finer scale than has previously been possible in the Weddell Sea. Moreover, OFOBS-derived information supported the work of the other biology/ecology cruise participants (see Chapter 10) and onshore collaborators. OFOBS images for macroecological studies were analyzed for the composition, diversity, and distribution of megabenthic assemblages. Megabenthic fauna are of very high ecological significance for the Antarctic shelf ecosystem. They strongly affect the small-scale topography of seafloor habitats and do, thus, exert prime influence on the structure of the entire benthic community.

Work at sea

Benthic fluxes

Seafloor carbon mineralization was studied *in-situ* using a benthic lander system (Fig. 11.1; Hoffmann et al. 2018). The benthic O_2 uptake is a commonly used measure for the total benthic mineralization rate. The autonomous benthic lander system was used to study benthic oxygen uptake across the sediment-water interface. The free-falling system was equipped with three benthic chambers and a 2-axis re-locatable microprofiler for electrodes and optodes (Fig. 11.1).

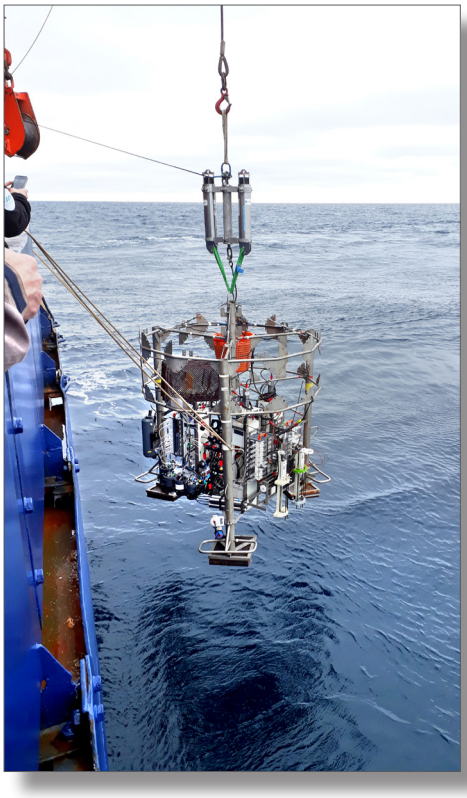

Benthic chambers

After arrival at the seafloor, the benthic chambers enclose a 0.04 m^2 large sediment patch together with an approx. 0.15-m high layer of overlying water. During the respective deployments the overlying water was kept mixed by gentle stirring and changes in oxygen concentrations were monitored by means of optical oxygen sensors attached to the chamber lid. Total fluxes of oxygen (TOU) across the sediment-water interface are calculated from the change in concentration per time times height of the overlying water column. Additionally, up to 4 lab-on-chip sensors for continuous *in-situ* measurements in the enclosed water body were added on some deployments. pH and alkalinity sensors were added on 5 deployments, and silicate and nitrate sensors were added on three deployments. Details of the lab-on-chip sensors are provided in Chapter 10 of this report.

Fig. 11.1: In-situ benthic flux lander being deployed (Photo: Allison Schaap)

Microprofiler

The fine-scale distribution of dissolved oxygen across the sediment-water interface and within pore waters was determined by means of two different profiling systems: (1) Clark-type oxygen micro-electrodes were incrementally (100 µm steps) inserted into the sediment to investigate the upper horizon (ca. 10 cm). The individual sensors were custom-made from glass with typical tip-diameters in the range of 25 – 50 µm. Up to seven oxygen electrodes were attached to a 150-mm in diameter titanium housing that contained electronics for signal amplification and processing. (2) To account for the deep oxygen penetration, the recently developed fibre-optical microprofiler was deployed in parallel. It uses two sets of four fibre-optical sensors (230 micrometer tip diameter, Pyroscience, DE) that are embedded in hypodermic needles mounted to solid shafts made from carbon-reinforced plastic. This allows to record longer profiles that are suited better for low-respiration environments and deep oxygen penetration sites. The sensors allowed to take 25 – 30 cm long profiles with a step resolution of 150 µm.

In addition to the linear drive, responsible for vertical profiling of both systems, a second, horizontally-oriented drive enabled for lateral relocation of the electronic housing and sensors between profiler runs to make sure that replicate profiles were measured at distinct sediment spots. Diffusive oxygen uptake is calculated from the change in oxygen concentration across the diffusive boundary layer (DBL) or the uppermost sediment layer times the diffusion coefficient d (T, S) or based on the derivative of the entire profile.

Habitat mapping

OFOBS is a cabled/towed system (Fig. 11.2), deployed ~1.5 m above the seafloor at low ship speeds (typically 0.5 knots, up to 1.5 knots (for more detailed information see Purser et al. (2018)). While in operation, the exact location of the georeferenced system is determined and verified continuously by *Polarstern*'s POSIDONIA system, and refined by the new integrated Inertial Navigation System (INS) and Dynamic Velocity Logger (DVL).

Fig. 11.2: OFOBS being deployed from the Polarstern A-frame during PS124 (Photo: Georg Brenneis)

In addition to collecting image data comparable with those obtained from the region and surrounding areas by preceding survey cruises, OFOBS also collected in parallel high-resolution topographical information from the seafloor by using a side scan sonar system and a forward-facing acoustic camera. The side scan system allows a ~100 m swath of seafloor to be investigated acoustically at the same time as the collection of still and video camera images. During recent cruises, the feasibility for this combined system to generate useful data on geological structure distribution, high-resolution topographical products, and faunal distribution maps has been demonstrated.

Tab. 11.1: OFOBS deployments

	Cruise label	Date / Time	Action	Latitude	Longitude	Depth [m]
1	PS124_5-6	09.02.21 04:02	Test	70°25.087'S	030°00.867'W	4487
2	PS124_8-1	12.02.21 03:52	profile start	74°54.401'S	029°24.611'W	406
	PS124_8-1	12.02.21 06:11	profile end	74°55.358'S	029°25.456'W	408
3	PS124_16-8	14.02.21 23:25	profile start	75°08.927'S	030°25.653'W	452
	PS124_16-8	15.02.21 03:36	profile end	75°08.572'S	030°16.442'W	438
4	PS124_21-7	16.02.21 03:48	profile start	74°52.115'S	030°39.731'W	494
	PS124_21-7	16.02.21 06:32	profile end	74°52.162'S	030°35.891'W	486
5	PS124_26-7	17.02.21 00:22	profile start	74°50.881'S	031°51.034'W	638
	PS124_26-7	17.02.21 03:32	profile end	74°50.930'S	031°56.031'W	634

	Cruise label	Date / Time	Action	Latitude	Longitude	Depth [m]
6	PS124_30-7	18.02.21 00:24	profile start	74°48.657'S	032°42.403'W	600
	PS124_30-7	18.02.21 05:18	profile end	74°46.991'S	032°34.278'W	593
7	PS124_33-4	19.02.21 03:13	profile start	74°43.237'S	035°11.913'W	497
	PS124_33-4	19.02.21 05:16	profile end	74°43.166'S	035°07.791'W	501
8	PS124_37-6	21.02.21 01:09	profile start	74°34.572'S	036°24.472'W	424
	PS124_37-6	21.02.21 05:01	profile end	74°36.609'S	036°25.492'W	408
9	PS124_45-1	22.02.21 03:48	profile start	74°21.739'S	036°05.019'W	1467
	PS124_45-1	22.02.21 04:55	profile end	74°21.813'S	036°02.754'W	1457
10	PS124_46-3	22.02.21 19:10	profile start	74°21.864'S	036°32.827'W	1200
	PS124_46-3	22.02.21 20:47	profile end	74°22.543'S	036°30.397'W	1188
11	PS124_47-2	23.02.21 01:51	profile start	74°15.255'S	036°14.067'W	1726
	PS124_47-2	23.02.21 05:29	profile end	74°15.285'S	036°06.166'W	1785
12	PS124_54-1	25.02.21 02:43	profile start	74°38.099'S	033°32.621'W	608
	PS124_54-1	25.02.21 05:09	information	74°39.481'S	033°33.167'W	593
13	PS124_63-1	27.02.21 00:51	profile start	74°50.909'S	030°56.969'W	533.7
	PS124_63-1	27.02.21 06:00	profile end	74°53.412'S	030°30.966'W	476.5
14	PS124_67-1	27.02.21 18:00	profile start	74°43.837'S	031°24.087'W	587.6
	PS124_67-1	28.02.21 06:16	profile end	74°51.513'S	030°26.118'W	468
15	PS124_68-5	01.03.21 01:36	profile start	76°05.405'S	030°20.071'W	476.3
	PS124_68-5	01.03.21 03:15	profile end	76°06.065'S	030°17.602'W	469.8
16	PS124_72-8	02.03.21 00:35	profile start	75°56.519'S	031°40.739'W	688.7
	PS124_72-8	02.03.21 06:16	profile end	75°55.917'S	031°26.418'W	597.5
17	PS124_78-8	04.03.21 00:56	profile start	76°03.472'S	030°56.521'W	466
	PS124_78-8	04.03.21 06:18	profile end	76°04.122'S	030°40.934'W	460.9
18	PS124_90-13	07.03.21 01:39	profile start	77°12.154'S	033°48.548'W	548.5
	PS124_90-13	07.03.21 06:57	profile end	77°10.446'S	033°37.326'W	270.7
19	PS124_94-5	07.03.21 22:34	profile start	77°02.489'S	034°44.773'W	776
	PS124_94-5	08.03.21 01:51	profile end	77°02.090'S	034°35.713'W	781
20	PS124_101-1	10.03.21 23:16	profile start	74°53.368'S	030°45.606'W	509.2
	PS124_101-1	11.03.21 00:08	profile end	74°52.398'S	030°42.735'W	504.4
	PS124_101-1	11.03.21 01:47	profile start	74°52.948'S	030°46.063'W	508.4
	PS124_101-1	11.03.21 03:37	profile end	74°51.349'S	030°41.046'W	497.4
21	PS124_107-5	12.03.21 02:12	profile start	75°03.582'S	026°44.742'W	291.3
	PS124_107-5	12.03.21 03:54	profile end	75°03.397'S	026°39.718'W	349.4
22	PS124_111-8	14.03.21 10:37	profile start	75°10.004'S	024°44.543'W	604.4
	PS124_111-8	14.03.21 14:28	profile end	75°08.653'S	024°37.263'W	665.9

During PS124, OFOBS was deployed a total of 21 times (Table 11.1). The great majority of deployments were made at night, under challenging deck work conditions. The continued good humor and working spirit of the ship crew was appreciated by the OFOBS team throughout the entire cruise, and was beneficial in collecting the extensive data set.

Image data were collected with a frequency of one timed image per 20 seconds, with seafloor video, forward and side scan data collected throughout all deployments continuously. In cooperation with the Physical Oceanography group, a MicroCAT sensor was mounted onto OFOBS for the majority of dives (Table 11.1), to monitor the different water masses in contact with the seafloor and infer the relation to seafloor community or habitat change.

Preliminary (expected) results

The overall aim of the lander deployments was to cover the spatial variation in settling organic matter on the seafloor with contrasting and changing food supplies and to resolve the impact on the benthic community respiration activity. From the *in-situ* measurements we expect new insights in the benthic oxygen consumption rates in this area. The collection of images and acoustic topographical high-resolution data of the seafloor is envisaged which will improve our understanding of habitat distributions in the southern Weddell Sea. By using the same camera system as previously deployed on Weddell Sea expeditions such as PS118, time series studies of seafloor community change can be determined, in collaboration with onboard colleagues (see Chapter 10). The use of new underwater technologies will thereby enhance the capabilities to improve our knowledge on the effects of climate change on the Antarctic ecosystem.

The benthic flux lander was deployed seven times (Table 11.2). Further information is given in Table 11.2 at the end of this chapter.

Because of the rough and rocky seafloor most sensors broke already during the first measurements. Thus, compared to the number of sensors and measurement cycles only few electrode profiles were obtained. All in all, deployments during PS124 resulted in 25 oxygen profiles suitable for quantification of the diffusive oxygen uptake (DOU) and three chamber incubations for total oxygen uptake rates (TOU). Data will be used to characterize the benthic carbon remineralization capacities of the southeastern Weddell Sea. In this respect, the calving of iceberg A74 will allow thus to quantify the benthic oxygen consumption of a seafloor covered by shelf ice for more than 30 years. The initial lab-on-chip deployments failed due to problems with integration onto the lander or due to mechanical/electrical problems with the sensors, primarily caused by the low temperatures. After these issues were resolved, pH data were obtained on three deployments, alkalinity on two, and silicate on one. The pH and alkalinity measurements can be used to derive concentrations of DIC and, therefore, fluxes of dissolved inorganic carbon.

In addition to the *in-situ* investigations, sediment samples were taken with the MUC. Sediment cores were used for *ex-situ* oxygen profiling and incubation as well as for sub-sampling to analyze biogenic compounds indicating the input of organic matter to the seafloor (Table 11.3).

Tab. 11.3 MUC cores used for *ex-situ* flux studies (profiles, DOU (diffusive oxygen uptake and incubations, TOU (total oxygen uptake) and analyzes of the microbial community and chlorophyl a content

No	Cruise Lable	Latitude	Longitude	Depth [m]	DOU	TOU	Microbio	Chl *a*
1	PS124_11-3	74°15.875'S	030°18.171'W	1547	X	X	X	X
2	PS124_16-6	75°08.572'S	030°26.822'W	454	X	X	X	X
3	PS124_26-10	74°50.884'S	031°51.061'W	637	X	X	X	X

No	Cruise Lable	Latitude	Longitude	Depth [m]	DOU	TOU	Microbio	Chl *a*
4	PS124_30-6	74°51.122'S	032°59.561'W	595	X	X	X	X
5	PS124_33-5	74°43.496'S	035°10.815'W	497	X	X	X	X
6	PS124_62-2	74°42.408'S	033°34.562'W	589	X	X		
7	PS124_68-6	76°05.367'S	030°20.229'W	474	X	X	X	X
8	PS124_76-5	75°52.321'S	032°04.463'W	737	X		X	X
9	PS124_76-6	75°52.225'S	032°04.186'W	735	X		X	X
10	PS124_78-5	76°02.826'S	031°01.687'W	475	X		X	X
11	PS124_78-6	76°02.808'S	031°01.263'W	473		X	X	X
12	PS124_88-5	77°06.502'S	036°33.610'W	1100	X	X	X	X
13	PS124_94-4	77°02.966'S	034°44.250'W	780	X	X	X	X
14	PS124_97-1	77°05.986'S	036°32.065'W	1098	X		X	X
15	PS124_98-2	75°23.662'S	028°41.423'W	443	X	X	X	X
16	PS124_100-5	74°32.918'S	032°39.600'W	662	X	X	X	X
17	PS124_107-4	75°02.902'S	026°54.517'W	296	X	X	X	X
18	PS124_110-4	75°06.775'S	024°47.746'W	578	X	X	X	X
19	PS124_111-5	75°16.629'S	024°57.977'W	636	X	X	X	X
20	PS124_112-4	75°22.373'S	025°43.397'W	793	X		X	X

Additional sub-samples were taken to analyze the abundance and community patterns of bacteria. Sediment-bound chloroplastic pigments (chlorophyll a and its degradation products, i.e. phaeopigments) represent a suitable indicator for the input of phytodetritus to the seafloor, representing the major food source for benthic organisms. All sub-samples were stored for later analyses at the home lab. Pigments will be analyzed with high sensitivity by fluorometric methods. To investigate the benthic bacterial community structure, we collected sediment samples for the extraction of DNA and RNA (storage at –20° C and –80° C) at all MUC stations; the results will be interpreted in conjunction with environmental parameters.

Fig. 11.3: OFOBS image of the seafloor recently freed from the ice shelf cover by A72 breakoff; numerous small black stones litter the seafloor, colonised by sponges and other fauna, such as bryzoa and tubed polychaetes. Image diameter is 1 m.

OFOBS collected a total of 15886 seafloor habitat and fauna images, and more than 100 hours of seafloor video and side scan data. A great diversity of seafloor habitats were imaged during the cruise; perhaps most spectacularly, areas with abundant sponge gardens (Fig. 11.4), the seafloor recently exposed by the calving of iceberg A74 (Fig. 11.3), and areas of abundant ice fish brooding. To further investigate the unexpected high abundance of fish nests, a long-term camera mooring ("Wetcam") was assembled on board as a multidisciplinary effort between the groups 'Benthic flux and habitat', 'Benthic Fauna', and 'Physical Oceanography'. Two camera systems will monitor the fish nests, together with CTD recordings, for the next 2 years (PS124_67-2: 74°51.663'S 030°48.539'W, 524 m).

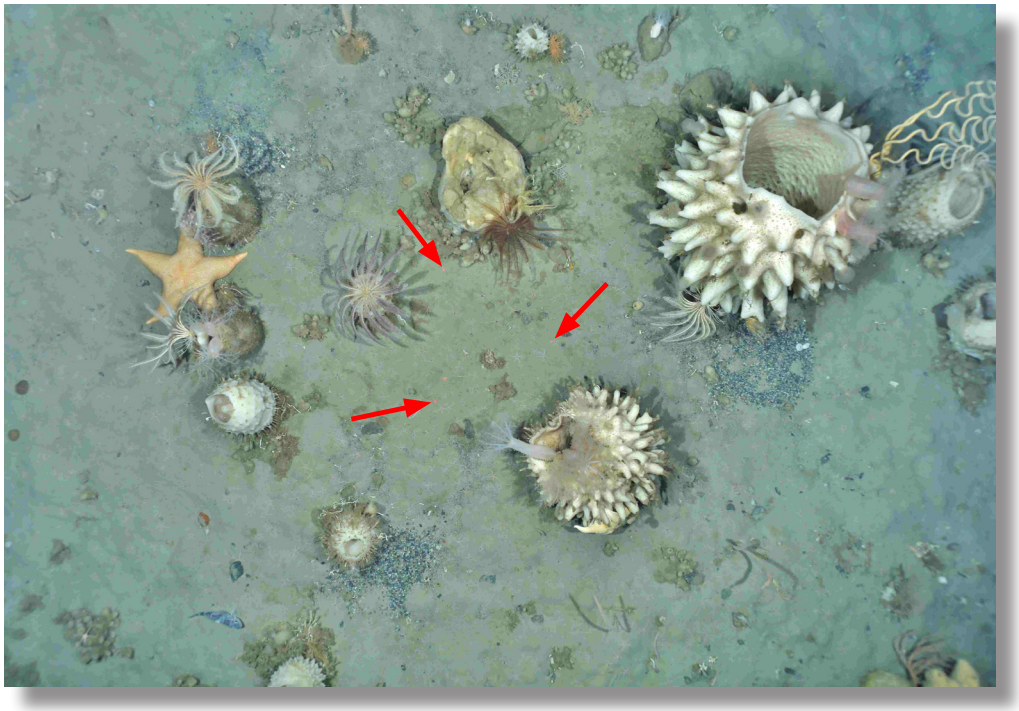

Fig. 11.4: OFOBS image taken at Station PS124_107_06; the seafloor during this transect was observed to support a range of sponge species and associate megafauna. The three red laser points indicate a spacing of 50 cm.

The collected OFOBS image and video data from the PS124 expedition will be used in a new collaborative study with Dr Emily G.H. Mitchell, Cambridge University, UK. Dr Mitchell will work on developing a Bayesian network approach for the temporal analysis of benthic fauna and habitat change over time; a particularly prescient use of the collected data given the A74 break off survey and the apparent temporal aspect of fish nest utilization on the Filchner Trough eastern slope.

Data management

Sample processing will be carried out at AWI and at the Max Planck Institute for Marine Microbiology (MPIMM) in Bremen. Data acquisition from the several types of investigation will require different time spans. The time periods from post processing to data provision will vary from one year maximum for sensor data to several years for microbial related datasets.

Microbial samples will be analyzed using sequencing-based methods. Obtained data and software code will be deposited at public databases (EMBL, GEO, Pangaea, GitHub) and hence be publicly available to the scientific community. Video, still image and positioning data as well as all derived scientific products from OFOS deployments (fauna distribution plots, 3D seafloor reconstructions) will be made available to the public via the open access AWI GIS projects within a year of cruise completion. Additionally, all OFOBS image and acoustic data will be uploaded to PANGAEA in April 2021, and made accessible to the general public following publication of an 'Earth System Science Data' paper, ideally within 2021.

Until then all preliminary data will be available to the cruise participants and external users after request to the senior scientist. The finally processed data generated by this project will be made publicly available according to international standards by the World Data Center PANGAEA Data Publisher for Earth & Environmental Science (www.pangaea.de). The unrestricted availability from PANGAEA will depend on the required time and effort for acquisition of individual datasets and its status of scientific publication.

In all publications, based on this cruise, the **Grant No. AWI_PS124_02** will be quoted and the following *Polarstern* article will be cited:

Alfred-Wegener-Institut Helmholtz-Zentrum für Polar- und Meeresforschung. (2017). Polar Research and Supply Vessel POLARSTERN Operated by the Alfred-Wegener-Institute. Journal of large-scale research facilities, 3, A119. http://dx.doi.org/10.17815/jlsrf-3-163.

References

Purser A, Marcon Y, Dreutter S, Hoge U, Sablotny B, Hehemann L, Lemburg J, Dorschel B, Biebow H, Boetius A (2018) OFOBS – Ocean Floor Observation and Bathymetry System: A new towed camera/sonar system for deep sea exploration and survey. IEEE Journal of Oceanic Engineering, doi: 10.1109/JOE.2018.2794095.

Hoffmann R, Braeckman U, Hasemann C, Wenzhöfer F (2018) Deep-sea benthic communities and oxygen fluxes in the Arctic Fram Strait controlled by sea-ice cover and water depth. Biogeosciences 15, 4849–4869.

Tab. 11.2: Benthic flux lander deployments

No	Cruise lable	Date	Action	Latitude	Longitude	Depth	Profiles		Cham-bers	LoC			
				S	W	[m]	short	long		pH	Alk	Si	NOx
1	PS124_8-3	2021-02-12	deployed	74°54.763‘	29°24.986‘	403	X	X	X	X	X	X	X
	PS124_8-13	2021-02-15	on deck	74°54.652‘	29°24.743‘	403							
2	PS124_26-12	2021-02-17	deployed	74°50.724‘	31°52.732‘	633	X	X	X				
	PS124_26-13	2021-02-18	on deck	74°50.683‘	31°52.934‘	632							
3	PS124_33-8	2021-02-19	deployed	74°40.963‘	35°10.910‘	499	X	X	X	X	X		
	PS124_33-10	2021-02-20	on deck	74°40.933‘	35°10.850‘	498							
4	PS124_54-9	2021-02-25	deployed	74°41.229‘	33°32.898‘	588	X		X	X	X	X	X
	PS124_54-15	2021-02-26	on deck	74°41.204‘	33°33.278‘	590							
5	PS124_68-9	2021-03-01	deployed	76°05.452‘	30°20.273‘	479	X		X	X	X	X	X
	PS124_68-12	2021-03-04	on deck	76°05.478‘	30°20.325‘	479							
6	PS124_88-6	2021-03-06	deployed	77°05.827‘	36°31.607‘	1095	X		X	X	X		
	PS124_88-7	2021-03-08	on deck	77°05.858‘	36°31.387‘	1101							
7	PS124_111-7	2021-03-14	deployed	75°15.179‘	24°54.952‘	587	X						
	PS124_111-9	2021-03-14	on deck	75°15.268‘	24°55.089‘	590							

12. OCCURRENCE OF MICROPLASTICS IN THE SOUTHERN OCEAN

Patricia Burkhardt-Holm[1];
Clara Leistenschneider[1,2],
Gunnar Gerdts[2] (not on board)

[1]CH.UNIBAS
[2]DE.AWI

Grant No. AWI_PS124_10

Objectives

Our aim is to study the occurrence, concentration, distribution, composition and, eventually, the possible sources and sinks of microplastics (MP) in the Antarctic marine ecosystem. We aim to achieve the following results by:

1. Sampling and analyzing surface - and sub-surface waters of the Southern Ocean.
2. Characterizing the MP in the Southern Ocean with respect to particle size, morphology, polymer types and color to ascertain origins and possible (former) uses.
3. Assessing the characteristics, concentration and distribution of MP in the relatively pristine Weddell Sea (WS) to compare it (in future cruises and in collaboration with other partners) to the more anthropogenically-impacted Scotia Sea (SS) and Western Antarctic Peninsula (WAP).
4. Analyzing MP in scats of Weddell Seals to assess the amount of MP in an exemplary marine mammal predator and to gain insight on the importance of MP in the Antarctic food web.
5. Sampling and analyzing potential sinking MP throughout the water column (at 100 m, 200 m, 300 m depth) by means of drift trap samples.
6. Investigating the occurrence of MP in sediments, a potential sink for MP pollution.

Work at sea

Surface water was sampled for MP (10 µm – 500 µm) with an immersion pump (HOMA, CH432; n = 17). To sample surface water out of the reach of vessel-induced contamination we made use of the rubber boat to deploy a small Manta Trawl (Hydro-Bios, Microplastic net, 43827; mesh size: 300 µm) for 20 minutes at a distance of 600 m and 500 m to *Polarstern*, respectively (n = 2). Sub-surface water was sampled by filtering pumped seawater from beneath the vessel at approximately 11.2 m depth (n = 18).

In addition to water samples, seal scats were collected for MP analyses by the SEAROSE and the Sea Ice team (see Chapters 4 and 6, respectively, n= 23). Sediment samples collected with the Multi Grab were provided to us by the Benthic Fauna group and drifting sediment trap gels were taken in cooperation with the Particle Flux group (see Chapter 7 and Chapter 10, respectively).

Samples which were taken for MP >300 µm (Manta trawl and Drifting Trap) were screened visually for MP on board using a stereo microscope (Olympus SZ61) equipped with a camera (Olympus SC50). Particles were imaged and the longest diameter of each particle was measured (CellSense. Version 2.1). Suspicious particles will be analyzed using Attenuated Total Reflection (ATR) Fourier Transform Infrared Spectrometry (FT-IR) to confirm that particles are synthetic polymers and to evaluate the polymer composition. Samples that will be analyzed for small MP (10 µm – 500 µm) were stored frozen at -20 °C and will be analyzed at the laboratories of AWI Heligoland in cooperation with Gunnar Gerdts (AWI) applying Focal Plane Array (FPA) based FT-IR subsequently to a purification treatment.

Surface water sampled by in-situ immersion pump

17 surface water samples were collected by means of the immersion pump on PS124 (Fig. 12.1, Table 12.1).

Fig. 12.1: Immersion pump in action to sample surface water

Tab. 12.1: Samples taken with the *in-situ* immersion pump

Sample ID	Station ID	Date and Time	Position	Filtered Vol. [L]
IP01	PS124_5-8	09.02.21 07:14	70° 25.066' S 030° 01.214' W	821.2
IP02	PS124_7-3	11.02.21 18:51	74° 01.535' S 028° 04.000' W	273.9
IP03	PS124_8-7	12.02.21 14:37	74° 55.231' S 029° 25.393' W	874.0
IP04	PS124_16-5	14.02.21 18:44	75° 08.543' S 030° 26.653' W	891.7
IP05	PS124_21-4	15.02.21 23:32	74° 52.069' S 030° 39.909' W	882.2
IP06	PS124_26-4	16.02.21 20:05	74° 51.339' S 031° 49.895' W	885.2
IP07	PS124_30-4	17.02.21 20:11	74° 51.112' S 032° 59.498' W	870.9
IP08	PS124_37-3	20.02.21 20:26	74° 34.796' S 036° 23.988' W	854.4
IP09	PS124_45-5	22.02.21 10:14	74° 20.802' S 036° 02.543' W	893.3
IP10	PS124_54-7	25.02.21 10:33	74° 40.112' S 033° 35.769' W	853.3
IP11	PS124_72-4	01.03.21 19:41	75° 57.673' S 031° 32.994' W	862.2
IP12	PS124_76-4	02.03.21 23:29	75° 51.823' S 032° 09.251' W	884.4

Sample ID	Station ID	Date and Time	Position	Filtered Vol. [L]
IP13	PS124_78-4	03.03.21 21:06	76° 02.404' S 031° 03.864' W	905.7
IP14	PS124_88-3	06.03.21 01:06	77° 06.494' S 036° 34.165' W	896.4
IP15	PS124_100-2	10.03.21 07:15	74° 29.426' S 032° 31.736' W	872.9
IP16	PS124_107-7	12.03.21 06:54	75° 01.582' S 026° 54.327' W	860.5
IP17	PS124_111-4	14.03.21 03:45	75° 16.625' S 024° 57.973' W	838.3

Except for one sampling event, where only 273.9 liters were pumped due to unknown reasons, all sampling events were completed successfully and the 1.000 L stainless steel tank (Inox Behälter GmbH, PC1000A4) was completely filled with sea water.

The mobile immersion pump and the 1.000 L tank were connected via a 15 m PTFE hose. All three components were rinsed with seawater from the respective station prior to filling the tank with the final sample.

For rinsing and sampling the immersion pump with the attached PTFE-hose was deployed by the on-board crane. The crane was extended to its maximum and the steel rope of the crane was released long enough to submerge the pump (approximately 30 – 80 cm below the water surface depending on the sea state). During sampling the immersion pump was approximately 5 m away from the side of the hull at starboard side. Sampling was performed when the vessel was standing. The rinsing process took approximately 15 min, while sampling and filling the tank took approximately 2 min.

After the tank was filled, it was transported to the working alley with a pallet wagon, where the seawater was filtered. By means of a pneumatic pump (Almatec, E15TTT-F4) water was led and filtered through a 500 µm cartridge filter (Wolftechnik, 01WTGD05) to remove bigger particles, followed by a stainless-steel pressure filter holder (Pieper Filter GmbH, H293SSI) with a 10 µm stainless-steel filter (diameter: 293 mm; Körner, 1076420) to collect particles between 10 µm and 500 µm in size. The tank and the filter holders were connected in series via ½" PTFE-hoses. Before the 10 µm filter was inserted, 100 L of the sampled seawater were pumped through the filtration setup to rinse the system and to avoid cross contamination.

The 10 µm filters with the suspended solids were folded, wrapped in Milli-Q rinsed aluminum foil and stored in Milli-Q rinsed aluminum boxes at -20 °C.

Surface water sampled by Manta Trawl

Two trawls were performed from a rubber boat during PS124 with a target sampling duration of 20 min (Fig. 12.2 and Table 12.2).

Tab. 12.2: Samples taken with the Manta-Trawl

Sample ID	Date Time	Time [min]	RV Position	Av. Distance to RV	Filtered Vol. [m^3]
MTZ01	18.02.21 11:29	16	74° 41.429'S 032°41.062'W	~600m	70.956
MTZ02	24.02.21 14:39	20	74° 04.974'S 032°21.630'W	~500m	75.000

Even though the first sample was still taken successfully, it was aborted after 16 min due to ice accumulation in the mesh. The Manta Trawl (MT; aperture: 30 cm x 15 cm) was equipped with a mechanical flowmeter and a 300 µm mesh with a removable cod end. The MT was deployed from a pole that was attached to the rubber boat making it possible to deploy the trawl from the starboard side, approximately 1.5 m away from the rubber boat, to avoid contamination due to

turbulence generated by the boat. Prior to sampling the trawl was pulled through the water without the attached cod end sampler for 1 min to remove possibly adhered particles from the mesh. After rinsing, the cod end was attached to the mesh and the sample was collected. The tows resulted in a filtered volume of 71 m^3 and 75 m^3, respectively. The samples were screened for putative MP immediately after sampling in the onboard laboratory. To do so, the content of the cod end was rinsed into a glass beaker by means of Milli-Q water. For visual screening, samples were transferred portion wise to a Bogorov counting chamber and inspected under a stereo microscope (Olympus SZ61) equipped with a camera (Olympus SC50). Putative MP particles were sorted, imaged and measured (CellSense, Version 2.1). Afterwards the particles were transferred to glass petri dishes and dried at 40 °C, ATR-FTIR measurements to evaluate the chemical composition of these putative MP will be conducted in the laboratories at AWI in Heligoland.

Fig. 12.2: Manta Trawl pulled by the rubber boat

Fig.12.3: Installation of the geological sieve with protection by a wooden box to sample sub-surface water by the Klaus pump on board

Sub-surface water sampled by on-board seawater pump

A Klaus Union Sealex Centrifugal Pump (Bochum, Germany) delivered seawater from approximately 11.2 m depth to the laboratory via stainless steel pipes (first described by Lusher et al. 2014). The water was filtered twice a day for approximately one hour on to a geological sieve with 20 µm stainless steel meshes, protected by a dimension-tailored solid wooden construction (Fig. 12.3 and Table 12.3).

One sample was taken by a Teflon membrane pump in cooperation with the biochemical cycling group (Chapter 8) from a depth of 25 m (Table 12.3). Samples were transferred to pre-rinsed glass jars by means of a PTFE squirt bottle and Milli-Q water and were stored at -20 °C.

Tab. 12.3: Samples taken by pumped seawater (Klaus pump, Teflon pump)

Sample ID	Date	Time Start	Time [min]	Filtered Vol. [L]	Coord. Start	Coord. End
SWP01	05.02.21	09:58	53	242.0	54° 25.322' S 056° 22.870' W	54° 37.348' S 056° 17.796' W
SWP02	06.02.21	09:59	58	158.0	63° 38.289' S 048° 24.496' W	63° 46.127' S 048° 05.882' W
SWP03	06.02.21	19:58	61	174.0	64° 59.905' S 045° 06.297' W	65° 08.402' S 044° 45.087' W
SWP04	07.02.21	08:58	58	96.0	66° 46.886' S 040° 30.184' W	66° 53.738' S 040° 06.059' W
SWP05	07.02.21	21:46	60	139.0	68° 33.853' S 035° 34.105' W	68° 42.197' S 035° 10.063' W
SWP06	08.02.21	08:07	59	161.0	70° 00.759' S 031° 16.141' W	70° 07.494' S 030° 48.257' W
Teflon pump01	08.02.21	22:36	48	223.2	70° 25.157' S 030° 00.276' W	70° 25.115' S 030° 00.156' W
SWP07	10.02.21	08:07	60	168.0	72° 40.596' S 022° 09.864' W	72° 47.450' S 022° 03.094' W
SWP08	10.02.21	19:02	63	152.0	73° 31.418' S 023° 18.637' W	73° 32.934' S 023° 55.585' W
SWP09	11.02.21	09:10	60	175.0	73° 46.802' S 026° 09.981' W	73° 52.039' S 026° 39.313' W
SWP10	11.02.21	20:10	61	177.0	74° 01.825' S 028° 04.715' W	74° 01.891' S 028° 04.897' W
SWP11	12.02.21	08:20	75	193.0	74° 54.423' S 029° 24.634' W	74° 54.774' S 029° 24.957' W
SWP12	12.02.21	19:50	80	236.0	74° 55.213' S 029° 25.395' W	74° 55.218' S 029° 25.456' W
SWP13	13.02.21	08:15	60	176.0	74° 00.397' S 030° 30.120' W	74° 00.706' S 030° 40.049' W
SWP14	13.02.21	20:08	58	163.0	74° 15.890' S 030° 18.241' W	74° 15.870' S 030° 18.165' W
SWP15	14.02.21	09:18	67	186.0	74° 35.144' S 030° 00.157' W	74° 35.799' S 029° 55.067' W
SWP16	14.02.21	20:27	64	190.0	75° 08.553' S 030° 26.658' W	75° 08.558' S 030° 26.707' W
SWP17	15.02.21	08:26	65	180.0	74° 54.554' S 029° 25.202' W	74° 55.322' S 029° 30.634' W
SWP18	15.02.21	20:19	60	133.0	74° 51.007' S 030° 23.089' W	74° 50.957' S 030° 25.886' W

Seal scats sampled

In total, 22 Weddell Seal scats and one scat of a Crabeater Seal were collected (Fig. 12.4 and Table 12.4). Samples were collected by the SEAROSE and Sea Ice team during their work on ice and on an extra flight for seal scats sampling.

Fig. 12.4 Sampling of seal scats

Tab. 12.4: Seal scats (1 – 22: from Weddell seals, taken by the SEAROSE team, 23: from Crabeater Seal, taken by the Sea Ice team)

Sample no	Date	Latitude	Longitude	Comment (tag no)
1	14.02.21	75° 40.030'S	034° 25.805'W	Seal 1
2	17.02.21	74° 39.350'S	035° 53.630'W	Seal 2
3	19.02.21	74° 38.750'S	035° 50.730'W	Seal 3
4	22.02.21	74° 24.000'S	037° 02.720'W	Seal 5
5	24.02.21	74° 14.000'S	033° 22.000'W	
6	25.02.21	74° 30.600'S	035° 21.000'W	
7	27.02.21	75° 00.000'S	035° 40.000' W	
8	27.02.21	75° 02.355'S	035° 40.611'W	Seal 6
9	04.03.21	75° 17.527'S	031° 09.921'W	
10	04.03.21	75° 17.527'S	031° 09.211'W	Seal 7
11	04.03.21	74° 42.305'S	029° 16.929'W	
12	11.03.21	74° 42.305'S	025° 16.929'W	
13	11.03.21	74°42.305'S	025° 16.929'W	Seal 8
14	14.03.21	74° 42.020'S	025° 07.030'W	
15	14.03.21	74° 42.020'S	025° 07.030'W	
16	14.03.21	74° 42.020'S	025° 07.030'W	Two jars
17	18.03.21	70° 34.055'S	008° 00.941'W	

Sample no	Date	Latitude	Longitude	Comment (tag no)
18	18.03.21	70° 37.746'S	008° 06.166'W	Two jars (1 & 2)
19	18.03.21	70° 37.746'S	008° 06.166'W	
20	18.03.21	70° 37.746'S	008° 06.166'W	
21	18.03.21	70° 37.746'S	008° 06.166'W	
22	18.03.21	70° 37.746'S	008° 06.166'W	
23	18.02.21	74° 59.886'S	023° 36.831'W	

Samples were taken with a stainless-steel spoon that was cleaned with snow prior to sampling and between sampling different scats. The samples were transferred to Milli-Q rinsed glass jars and stored at -20 °C. In our home laboratory the scat samples will be prepared for MP analyses according to Bravo Rebolledo et al. (2013) and machine washed in gauze bags (mesh size: 300 µm) with enzymatic detergent prior to visual sorting and ATR-FTIR measurements

Fig.12.5: Box core form the multi grab, sampling of the upper sediment layer

Sediments sampled by multi grab

The Benthic Fauna group provided one box core from 14 sampling events with the Multi Grab (Table 12.5). From these sediment cores the upper 6 – 12 cm were transferred to aluminum boxes and stored frozen at -20 °C (Fig. 12.5). Sediment samples will be analyzed in our home laboratories according to Abel et al. (2021). Previous to FPA based µ-FT-IR, organic residues will be removed by an oxidation treatment (Fenton's reagent) while remaining inorganic material will be removed by density-separation (modified from Abel et al. 2021 with sodium bromide, density: 1.4 – 1.6 g/cm^3).

MP sampled by drifting sediment traps

Drifting sediment traps were deployed by the Particle Flux group at 6 stations (Table 12.6 and Chapter 7, Fig. 7.1). At each depth of the drifting sediment trap (100, 200 and 300 m) a viscous gel was deployed in the collection cylinders. These gels were and will further be screened for sinking MP.

Tab. 12.5: Samples taken from the Multi Grab (*= total sediment length 7 cm)

Sample ID	Station ID	Date and Time	Position	Average cm sampled	Depth [m]
MG01	PS124_8-10	12.02.21 20:31	74° 55.211' S 029° 25.240' W	11.03	404.6
MG02	PS124_16-7	14.02.21 21:23	75° 08.559' S 030° 26.664' W	10.33	454.7
MG03	PS124_21-6	16.02.21 02:00	74° 52.079' S 030° 39.767' W	8.00	495.5

Sample ID	Station ID	Date and Time	Position	Average cm sampled	Depth [m]
MG04	PS124_26-8	17.02.21 05:20	74° 50.880‘ S 031° 51.050‘ W	6.07	636.1
MG05	PS124_33-6	19.02.21 07:52	74° 43.377‘ S 035° 09.574‘ W	9.83	498.3
MG06	PS124_37-4	20.02.21 21:29	74° 35.855‘ S 036° 25.995‘ W	9.00	411.5
MG07*	PS124_52-2	22.02.21 11:28	74° 20.434‘ S 036° 03.692‘ W	9.47	1542
MG08	PS124_45-7	24.02.21 20:52	74° 15.612‘ S 032° 20.289‘ W	10.00	928.5
MG09	PS124_68-6	01.03.21 05:26	76° 03.968‘ S 030° 16.746‘ W	9.77	467.8
MG10	PS124_88-4	06.03.21 01:57	77° 06.505‘ S 036° 33.932‘ W	10.27	1101.8
MG11	PS124_92-1	07.03.21 11:27	77° 09.961‘ S 033° 41.647‘ W	7.00	269.2
MG12	PS124_100-6	10.03.21 14:24	74° 33.548‘ S 032° 40.005‘ W	10.97	663.6
MG13	PS124_111-6	14.03.21 05:35	75° 16.649‘ S 024° 57.935‘ W	11.67	638.9
MG14	PS124_112-3	14.03.21 22:05	75° 22.331‘ S 025° 43.625‘ W	12.33	790.6

Tab. 12.6: Samples from the sediment drift traps with blanks

Sample ID	Station ID deployment	Date and Time deployment	Position deployment	Depth [m]
DT01	PS124_8-4	12.02.21 11:45	74° 57.191‘ S 029° 26.654‘ W	100 200 300
DT02	PS124_26-1	16.02.21 17:29	74° 51.113‘ S 031° 54.038‘ W	100 200 300
DT03	PS124_54-8	25.02.21 12:01	74° 40.961‘ S 033° 34.277‘ W	100 200 300
DT04	PS124_71-1	01.03.21 15:59	75° 58.599‘ S 031° 22.128‘ W	100 200 300
DT04 - BLANK	PS124_71-1	01.03.21 15:59	75° 58.599‘ S 031° 22.128‘ W	BLANK - 200

Sample ID	Station ID deployment	Date and Time deployment	Position deployment	Depth [m]
DT05	PS124_79-1	04.03.21 08:58	76° 05.540‘ S 030° 25.282‘ W	100 200 300
DT05 - BLANK	PS124_79-1	04.03.21 08:58	76° 05.540‘ S 030° 25.282‘ W	BLANK - 100
DT06	PS124_90-1	06.03.21 14:29	77° 02.413‘ S 033° 39.062‘ W	100 200 300
DT06 - BLANK	PS124_90-1	06.03.21 14:29	77° 02.413‘ S 033° 39.062‘ W	BLANK - 300

After recovery, the collection cylinders were set for approximately 4 hours before the gels were removed. The gels were screened for putative MP under the stereo microscope (Olympus SZ61) equipped with a camera (Olympus SC50). Putative MP particles were imaged, measured and the position of the particles in the gel was mapped. After the gels have been imaged at AWI Bremerhaven by the Particle Flux group, we will be able to recover putative MP from the gels and conduct FT-IR measurements to evaluate the chemical composition.

Quality control and contamination protection measures on board

Quality control and contamination protection is a crucial aspect and we tackled this issue very seriously, applying all possible precautionary measures. Cotton clothes and cotton laboratory coats were worn during all procedures in the laboratory and on the deck, whenever possible. When weather conditions required synthetic clothes to be worn, precautionary measures (such as keeping distance to the samples and the devices) and taking reference samples of the clothes and synthetic equipment (such as ropes etc.) were taken. All instruments and material (such as sampling jars, spoons, tweezers, aluminum foil and any other utensils) were rinsed with Milli-Q water before use on board, or, when off board, at least cleaned with uncontaminated snow (see scat samples). In the onboard laboratory all work (e.g. visual screening) was performed under a cotton mosquito net (Bosshart et al. 2020). Additional specific measures were applied according to the following:

The Manta Trawl aperture was sealed with a cotton cloth for transport to the rubber boat and only removed just before releasing the Manta Trawl to the water. As long as stored in the lab, the Manta Trawl was protected by a cotton cover.

Sediment samples: To avoid airborne contamination of the box cores from the sediment samples, the box cores were immediately covered by aluminum foil, as soon as they were on board and transported to the laboratory for further analysis.

Drift sediment sampling: To avoid contamination of the gels prior to sampling, the gels were poured under a cotton mosquito net, visually screened for MP and microfibers under the stereo microscope after pouring and potential contamination was removed with forceps before sealing and storing the gels till the deployment. Before the deployment, the gels were transferred to weighted dishes under the cotton mosquito net and screened a last time to check that the gels were free of MP.

Use of blanks: During visual screening of the samples retrieved by the manta trawl and after recovery of the gels off the sediment traps, glass petri dishes with Milli-Q water were placed next to the stereo microscope during visual screening and screened afterwards to test for airborne contamination during the screening processes.

To test for contamination during the deployment and recovery of the drift trap sediment samples on the working deck, three blank samples were taken by preparing a gel in a collection cylinder in the same way as the gels deployed with the drift trap. The blanks were opened simultaneously to the collecting cylinders on the drift trap and covered again when the cylinders were submerged with seawater. The same blank was opened when the cylinders were recovered from the sea and sealed simultaneously to the cylinders on the drift trap.

Preliminary (expected) results

Surface water sampled with the *in-situ immersion pump*

An average (± SD) 873.9 ± 21.4 L of seawater were filtered per successful sample and a total of 13382.2 L were filtered. We expect microplastic particles in the size range 10 µm – 500 µm.

S*urface* water *sampled by Manta Trawl*

By visual inspection, we found some putative microplastic particles, namely 4 microplastic particles, one of those obviously ship paint and 4 microfibres in the first manta trawl sample. In the second manta trawl sample, we recovered 2 putative microplastic particles and 3 microfibres (Fig 12.6).

Photos were taken for ease of retrieval in the home laboratory. A thorough ATR-FTIR analysis in the home laboratory has to be conducted for further analysis.

In the gels of the drift sediment trap samples, we visually identified putative microplastic particles (Fig. 12.7), some of those ship paint particles presumably.

We expect to find microplastic particles in the other samples, such as sub-surface water samples, seal scats and sediments samples. All particles and microfibers under suspect will be analysed in the home laboratory, as described above.

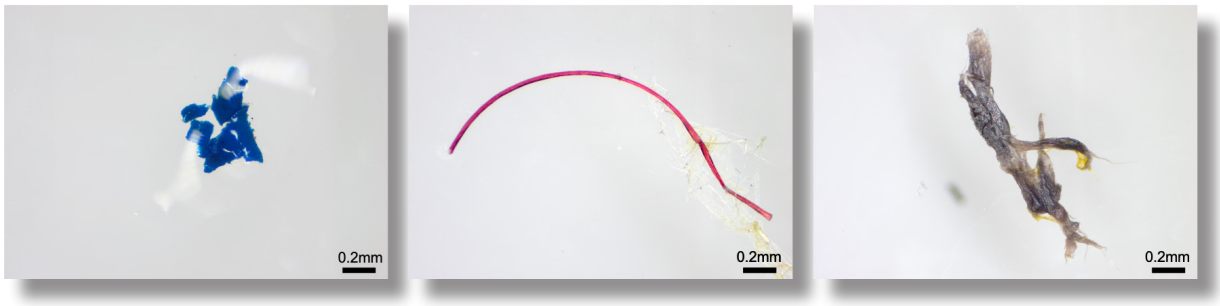

Fig. 12.6: Putative blue ship paint, MP fiber and fragment recovered from Manta Trawl samples

Tab. 12.7: Putative microplastic particles in gels of the sediment drift trap samples

Sample ID	Potential MP	Potential ship paint	Depth [m]
DT01	-	2	100
	-	2	200
	-	-	300
DT02	1	8	100
	-	-	200
	-	9	300
DT03	2	2	100
	-	2	200
	2	5	300
DT04	1	3	100
	-	6	200
	-	3	300
DT04 - BLANK	5 (2 x clear spherules)	4	200*
DT05	-	1	100
	-	13	200
	-	3	300
DT05 - BLANK	1	18	100*
DT06	1	4	100
	-	5	200
	-	8	300
DT06 - BLANK	-	11	300*

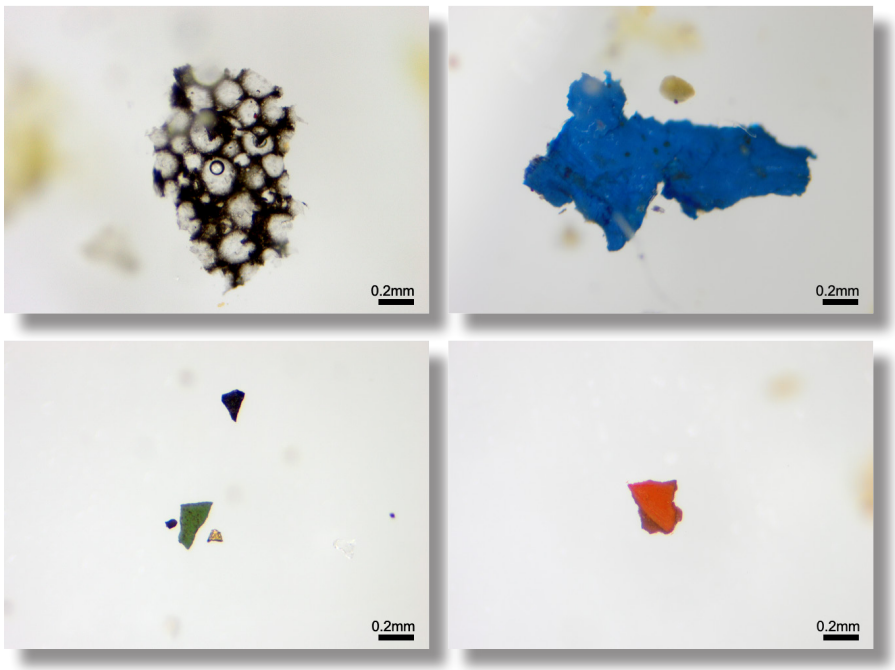

Fig. 12.7: Putative MP foam/fragment and ship paint of blue, green and red/orange color found in the gels of the drifting sediment traps

Data management

Microplastic samples will either be destroyed by analysis or, those not analyzed, will be stored at the home laboratory at University of Basel. Environmental data will be archived, published and disseminated according to international standards by the World Data Center PANGAEA Data Publisher for Earth & Environmental Science (www.pangaea.de) within two years after the end of the cruise at the latest. By default the CC-BY license will be applied.

Any other data will be submitted to an appropriate long-term archive that provides unique and stable identifiers for the datasets and allows open online access to the data.

In all publications, based on this cruise, the Grant No. AWI_PS124_10 will be quoted and the following *Polarstern*-article will be cited:

Alfred-Wegener-Institut Helmholtz-Zentrum für Polar- und Meeresforschung (2017). Polar Research and Supply Vessel *POLARSTERN* Operated by the Alfred-Wegener-Institute. Journal of large-scale research facilities, 3, A119. http://dx.doi.org/10.17815/jlsrf-3-163.

References

Abel SM, Primpke S, Int-Veen, Brandt A. Gerdts G (2021) Systematic identification of microplastics in abyssal and hadal sediments of the Kuril Kamchatka trench. Environmental Pollution, 269, 116095.

Bosshart S, Erni-Cassola G, Burkhardt-Holm P (2020) Independence of microplastic ingestion from environmental load in the round goby (Neogobius melanostomus) from the Rhine river using high quality standards. Environmental Pollution, 267, 115664.

Bravo Rebolledo EL, Van Franeker JA, Jansen OE, Brasseur SMJM (2013) Plastic ingestion by harbour seals (Phoca vitulina) in The Netherlands. Marine Pollution Bulletin, 67, 200-202.

Lusher AL, Burke A, O'Connor, I. Officer,w R (2014) Microplastic pollution in the Northeast Atlantic Ocean: validated and opportunistic sampling. Marine Pollution Bulletin 88 (1-2), 325-333.

13. AD HOC EXPLORATIONS

All teams involved: Weather (Chapter 2), Oceanography (Chapter 3), Seals and Oceanography (Chapter 4), Bathymetry (Chapter 5), Sea ice physics and Biology (Chapter 6), Particle transport (Chapter 7), Biogeochemistry (Chapter 8), Geochemistry (Chapter 9), C-Pump and Benthic Fauna (Chapter 10), Benthic Fluxes (Chapter 11), Microplastic (Chapter 12)

Outline

During PS124, the scientific party onboard *Polarstern* conducted several joint ad hoc explorations, initiated by three remarkable observations:

1. On 16 February 2021, the Ocean Floor Observation and Bathymetry System (OFOBS) recorded an unprecedented breeding colony of nesting icefish on the seafloor.
2. On 28 February 2021, *Polarstern* sailed through extensive patches of pancake ice with a unique bright-yellow colour.
3. On 13 March 2021, the weather conditions allowed a circumnavigation of the large A74 iceberg (area ~1,270 km^2), which had calved two weeks earlier from the nearby Brunt Ice Shelf, to sample the newly exposed water column and seafloor,

each of these opportunities initiated an ad hoc planning of joint measurements to further investigate the observed phenomena. In the following, the objectives, work at sea, and preliminary results are presented for each of the three explorations. Most of the method description and sample treatment have already been described in the previous chapters. Here, we focus on the additional work for the ad hoc investigations.

13.1 Ice Fish Nesting

Objectives

During the third deployment of the OFOBS on 16 February 2021 (PS124_21-7) a novel ecosystem was imaged. The entire seafloor, throughout several hours of OFOBS transect time, was populated by nesting ice fish, at the exclusion of other seafloor fauna. The great majority of nests contained brooding ice fish and high abundances of eggs (Fig. 13.1).

This unexpected finding drove a multidisciplinary investigation of these nests, and the decision was made to determine various aspects of the distribution and development of this ecosystem. The ad hoc interdisciplinary approach investigating:

- the spatial extent of the active nesting area,
- the spatial extent of the old nesting areas,
- the correlation between nest abundance and bottom water characteristics such as temperature and oxygen,

- and the deployment of an ad hoc mooring, equipped with cameras and sensors to track fish behaviour and nest use over the next two years.

To conduct this work, the OFOBS team (Chapter 11) was joined by the teams for oceanography and seals (Chapters 3 and 4), biogeochemistry and benthic ecology (Chapters 7, 8, 10), and bathymetry (Chapter 5).

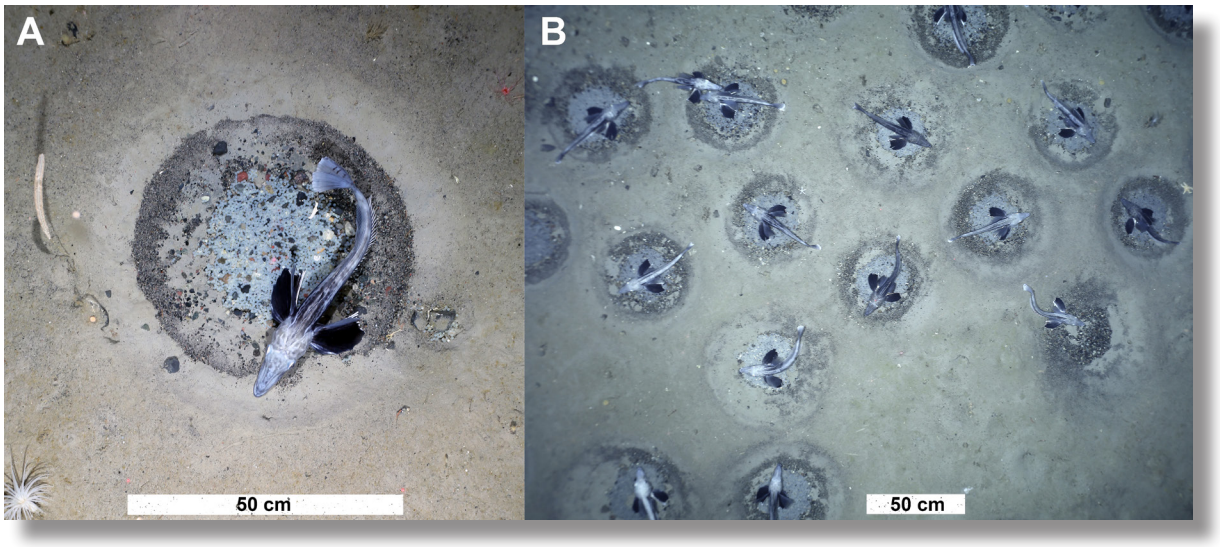

Fig. 13.1: a) Notothenioid ice fish brooding > 2000 eggs in an active fish nest on the Filcher Trough eastern flank b) Dense array of active fish nests; overlap between individual nests was observed to be very uncommon. The seafloor across a region of 6 x 40 km exhibited a comparable density of fish nests and sparsity of other fauna.

Work at sea

Four dives in total were conducted with OFOBS at the fish nest site (Fig. 13.2): dive PS124_21-7, _63-1, _67-1, and _101-1 (see Table 11.1). After the initial find, the dives were made at an altitude of 3 m above seafloor, and a CTD sensor was mounted on the OFOBS for the subsequent investigative dives. Throughout all dives, seafloor coverage of nests was apparent in the forward sonar (Fig. 13.3) and side scan sonar systems (Fig. 13.4).

On short notice, one mooring was equipped with devices from several groups, including two stills cameras, a CTD, and a current meter. The “WetCam-Fish” mooring was deployed at station PS124_67-2 (see Chapter 3), a site with highest nest densities, to observe and record the development of the nesting site over the forthcoming two years.

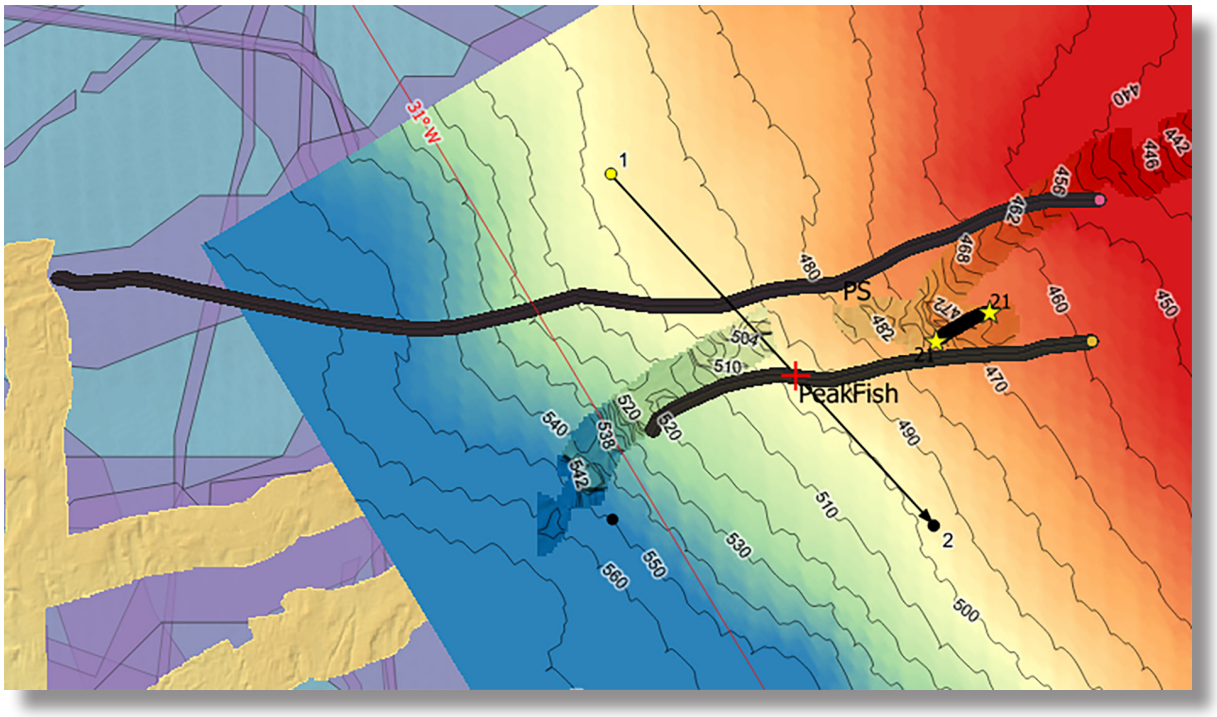

Fig. 13.2: OFOBS transects (black lines) to monitor fish nests during PS124; the blue-to-red colours show the bathymetry with depth isolines. The red cross indicates peak densities of fish nests.

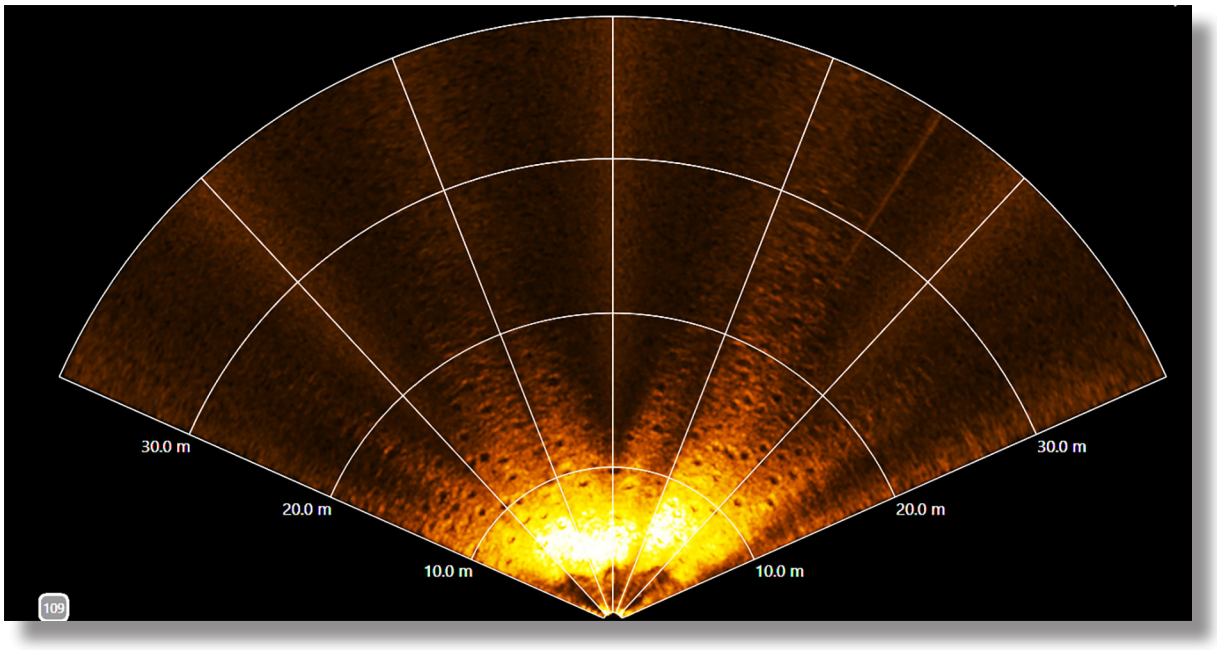

Fig. 13.3: Forward acoustic camera image of the small-scale topography during a typical deployment in the fish nest area; depressions from fish nests in front of OFOBS are clearly visible.

Preliminary results

Visual and acoustic investigations quantify fish nest abundances across an area of ~6 x 40 km of the eastern flank of the Filcher Trough. In total, 12,020 nests in active use were photographed, with more than 100,000 nests mapped with a side scan system (Fig. 13.4). Based on the collected images, an average density of 0.26 nests per square meter was estimated across the surveyed region. Active nest use was observed between depths of 535 and 420 m, with a peak density of 1.47 nests per square meter at 497-m depth. Subsequent surveys at comparable depths on the sill of the Filcher Trough observed similar densities of unoccupied, partially filled fish nests covering the entire seafloor up to 60 km from the active nesting area.

The CTD probe measuring temperature, pressure, and salinity indicated that the benthic waters intercepting the sea floor had a temperature of ~ –1.0 to 0.0° C, characteristic of the modified Warm Deep Water (mWDW, see Chapter 3) onshore flow originating from the deeper Weddell Sea, which fluctuates in flow course from season to season. Bottom water temperatures measured in areas with high nest abundance but no active ongoing nesting behavior were cooler, at –1.5 to –2.0° C. This observation may indicate that nest location selection is determined by the course of the warmer, oxygen depleted mWDW during a particular breeding season.

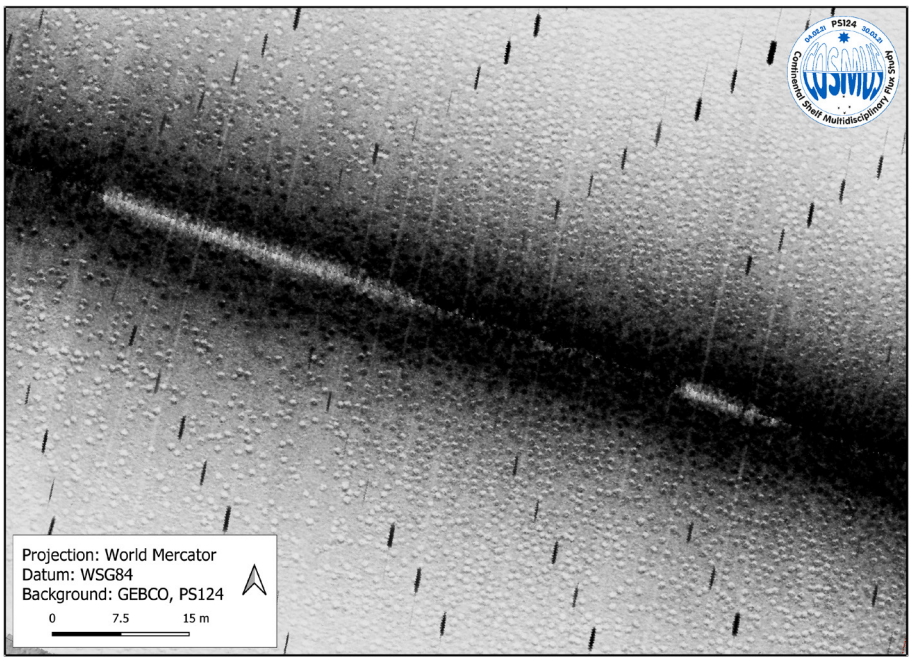

Fig. 13.4: Georeferenced side scan map showing the high fish nest abundance found throughout the surveyed region; the array of regularly spaced black lines are acoustic interference caused by the OFOBS positioning system.

Data management

For the data management we refer to the respective sections of the previous chapters.

13.2 Yellow Pancake Ice and New Ice Formation

Objectives

New ice formation is a particular process during austral fall in the Antarctic marginal seas. Various types of ice occur from slush ice accumulating in band-like structures at the surface of the ocean: under calm conditions they grow into Nilas ice, under turbulent conditions they evolve into pancake ice. Frazil ice growth is known to entrap organisms from the water column and enrich them in the newly forming sea ice. Since this process usually occurs in a period of rapid environmental change with declining solar elevations, reducing the incoming photo synthetically active radiation (PAR) and limiting algae growth, it was assumed that this enrichment would not result in any increasing primary production and biomass development and, thus, might be neglected in the overall carbon budget of the Southern Ocean.

On 28 February 2021 *Polarstern* sailed from approximately 75° S to 76° S, mostly through a 100 % coverage of thin, newly formed Nilas ice. In the afternoon at about 5 pm UTC, first occurrences of thicker pancake ice was found at approximately 76° S, 30.3° W with a distinct yellow colouring (Fig. 13.5). In the following days, high concentrations of these pancakes were observed with increasing intensities of yellow and amber, to the point almost 100 % of the surface were covered by such ice. The increasing colouration of the pancake ice suggested an active growth of algae in and under the new developing sea ice cover. In order to study the role of this unexpected fall bloom for the carbon cycle of the eastern Weddell Sea, we developed an ad hoc interdisciplinary approach investigating

- the aerial extent of this bloom,
- the development and species composition of this bloom,
- its potential primary production,
- its potential for vertical particle flux,
- the occurrence of micronutrients sustaining the bloom,
- the potential source region of this bloom.

Work at sea

The first round of observations directly focused on the occurrence of this pancake bloom and included sampling pancake ice with a rubber boat right next to the ship. During the first station, PS124_68-11_IF_1, large chunks of ice were sawed from the pancake ice and studied for physical and biogeochemical parameters (see also Chapters 6, 8, 9 and Table 13.1). In addition, melted samples of the pancake ice algae assemblages were transferred to roller tanks to test their aggregation capacity and their potential contribution to vertical carbon flux (see Chapter 7). During PS124_77-1_IF_2, the sampling was conducted with a 9-cm Kovacs ice corer. Here, individual ice cores were collected, both from the pancake and the adjacent Nilas ice. Primary and bacterial production experiments were carried out in additon to the analysis of physical and biogeochemical parameters (see Chapter 8 and Table 13.1). Strong easterly winds exceeding 10 m/s on 2 and 3 March shifted the yellow ice zone westwards. On 4 March, we were passing an area with large yellow stripes of slush ice farther east, which was sampled with buckets from the ship. These *in-situ* observations of the bloom were accompanied by an extensive sea ice characterisation via helicopter, which also gave insights to the extent of the bloom.

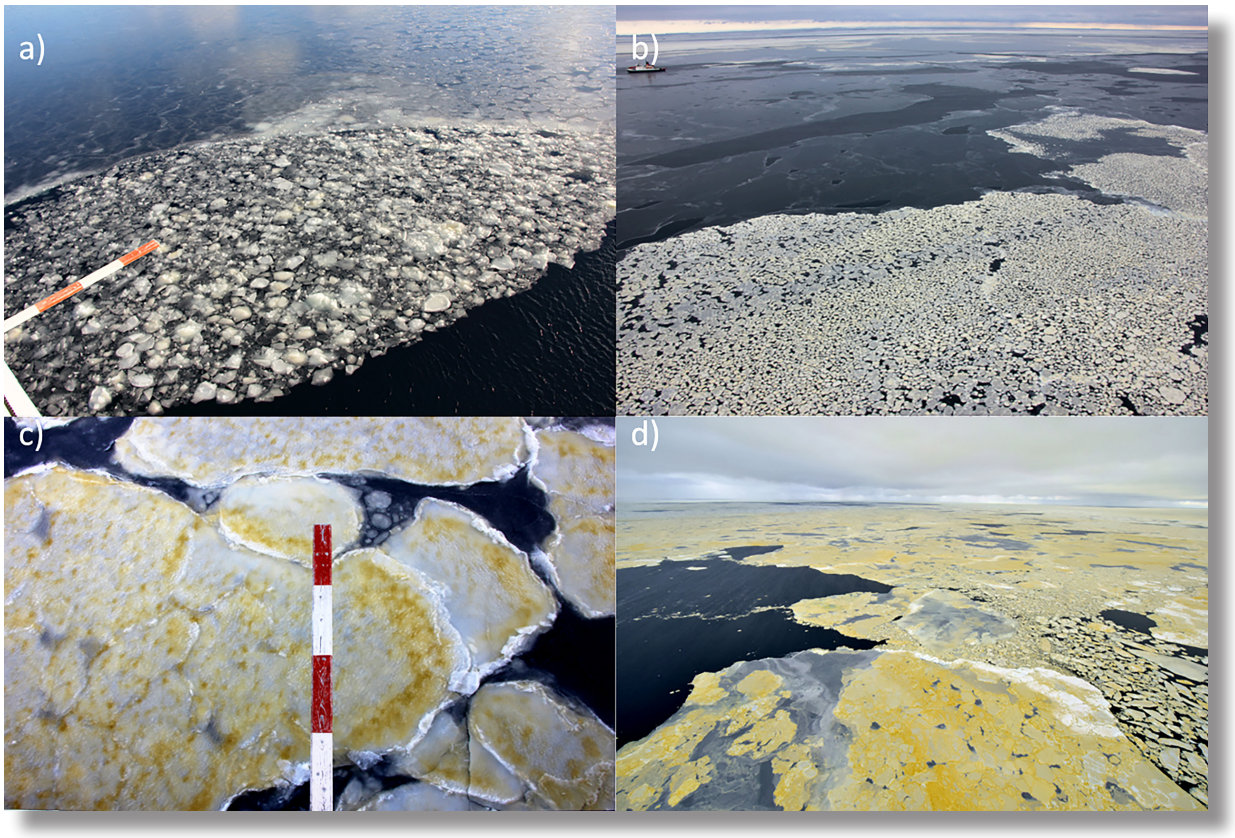

Fig. 13:5: Colouration change of the pancake ice over a period of five days; 28.02.2021 (a), 01.03.2021 (b), 02.03.2021 (c), and 03.03.2021 (d)
Fig. a) and c) were made from the Polarstern and b) and d) from the helicopter.

Fig. 13.6: Different views of the colouration of a chunk of pancake ice directly after sawing it during station PS124_77-1_IF_2; views are from the top (a), the bottom (b), and the side (c).

Tab. 13.1: Overview of all samples collected during the young-ice sampling.
Abbreviations for the parameters and details of the obtained parameters can be found in Table 6.1.

In addition, * PP/BP stands for primary and bacterial production incubations as well as for the collection of vitamins. IRON involves DFe (dissolved Fe) and TDFe (total dissolvable Fe, see also Table 9.1). During PS124_77-1_IF_2, additional Si-isotopes were collected from UIW and ice.

Station	Date	Time [UTC], start	Latitude, [°S] start	Longitude [°W] start	Ice							Water		
					BIO	DNA_1	*PP/ BP	Iron	IP-25	NEO	TEX	UIW	NEO-UIW	IRON_UIW
PS124_68-11_IF_1	03/01/2021	10:57	-76.1034	-30.3401	9				1	1	3	1	1	1
PS124_77-1_IF_2	03/03/2021	09:04	-75.9704	-31.7567	12	2	3	3			2	1		1
PS124_77-1_IF_3	03/04/2021	14:44	-76.1009	-30.4012	2		1							
PS124_98-4_IF_4	03/09/2021	09:27	-75.3953	-28.6521	3				1	1	3	1	1	
PS124_108-1_IF_5	03/12/2021	09:06	-75.0326	-26.8664	3							3		
PS124_111-10_IF_6	03/14/2021	17:13	-75.2549	-24.9181	3							3		

Thereafter, *Polarstern* moved south and left the region of this bloom. After returning back into the bloom region on 8 March, again stripes with coloured pancakes were present (Fig. 13.7). Since the ice was more mobile, it was only possible to get different chunks of freshly broken pancake ice during station PS124_98-4_IF_4, which only allowed a limited sampling approach (Table. 13.1). Coloured slush ice was further collected in front of the Brunt Ice Shelf (PS124_108-1_IF_5). New ice, which turned out to be mainly platelet ice, was also collected in the crack behind the recently detached iceberg A74 (PS124_111-10_IF_6).

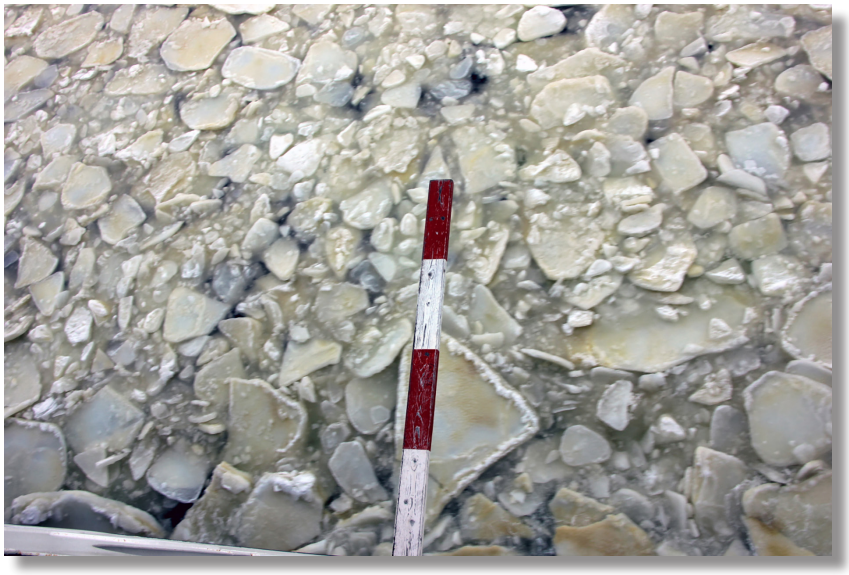

Fig. 13.7: New brown pancake ice observed from Polarstern on 8 March 2021

Preliminary results

The aim of this study is to understand the development of this unusual austral fall bloom in Antarctic new ice by taking advantage of the diverse interdisciplinary expertise on board. This will allow reconstructing the bloom formation, its magnitude as well as investigating the driving key species for this bloom. It also allows to distinguish the physical processes maintaining the bloom and to elucidate whether, e.g., enhanced micronutrient supply may have steered up this bloom, and what contribution these findings make to the overall carbon export of the eastern Weddell Sea.

Compared to water column and older sea ice, extremely high biomasses had accumulated in the pancake ice, which still need to be measured quantitatively in the home labs. Preliminary nutrient analyses via Lab-on-Chip sensors (see Chapter 10) reveal a total depletion of nitrate in the ice, except for the bottom ice sections, which still had nutrient concentrations comparable to the underlying water.

From the first pancake sampling, the surface and bottom sections showed a clear separation of the dominating algae species. Phaeocystis spp. was almost exclusively present in the surface communities (Fig. 13.8a), which might explain the yellow appearance of the ice floes due to the high production of the sulphur-containing compound dimethylsulphoniopropionate (DMSP), which in high concentrations has been reported for this species in the Weddell Sea. In contrast, the more brownish looking underside of the ice was dominated by various Fragilariopsis species (Fig. 13.8b), which were also found in other sea-ice cores (see Chapter 6).

The additional under ice water sampling performed during PS124_77-1_IF_2 revealed a clear separation between the pancake communities and those of the underlying water. Here,

various Chaetoceros species and particular spores of these species were dominating the phytoplankton. During the second sampling, the Phaeocystis and Fragilariopsis species were dominating the ice cores, but the clear separation between surface and bottom communities was less pronounced. This tendency of having both species mixed throughout the ice core was even more pronounced at the last thin-ice sampling PS124_98-4_IF_4. Both slush ice samplings at the beginning and towards the end of the observation again showed the dominance of the already mentioned species. The last sampling of the supercooled water in the crack behind iceberg A74 was characterized by very low occurrences of a few *Fragilariopsis* and *Thalassiosira* species with slightly higher abundance in the platelet ice.

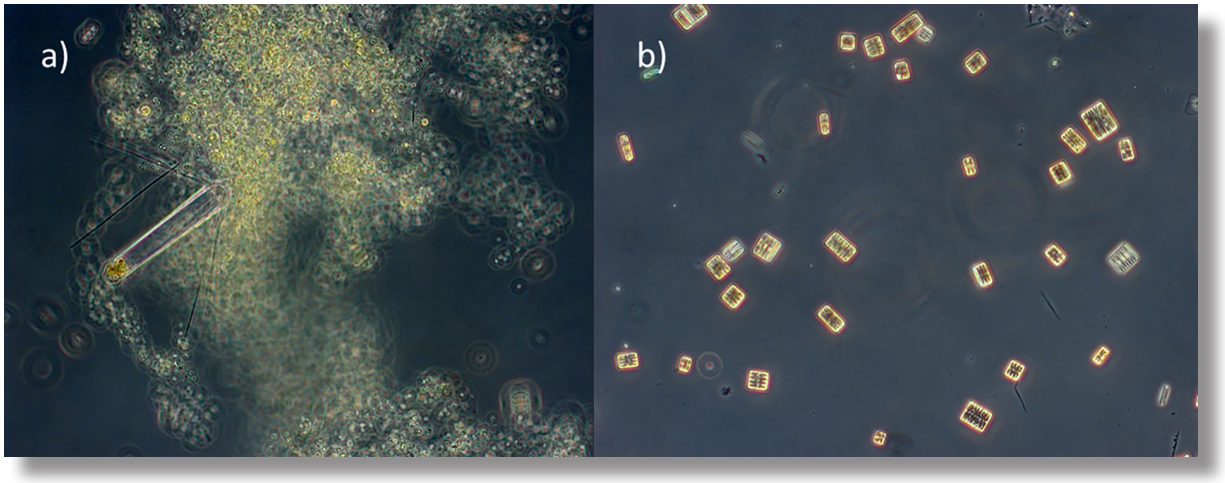

Fig. 13.8: Representative microscopic photos of (a) Phaeocystis spp. situated at the surface and (b) Fragilariopsis spp. communities from the bottom of the ice core; samples were collected during PS124_68-11_IF_1.

The formation history of the pancake ice was reconstructed by means of Sentinel-1 SAR imagery received on board. Fig. 13.9 shows the first occurrences of grease ice, slush, and pancake ice on 22 February in the polynya west of the northern Brunt Ice Shelf. That region of new ice formation expanded to the south of the western tip of the Brunt Ice Shelf by 24 February, either by advection or by new ice formation farther south, or by both. It should be noted that on 22 February, the air temperatures at the location of *Polarstern* began to drop from approximately –3° C to below –7° C on 27 February, and remained between –7° C and –5° C until 2 March. Temperatures were likely lower just west of the Brunt Ice Shelf and suggest an enhanced new ice formation during this period. Between 2 to 4 March, air temperatures rose to values above –4° C.

By 25 February, the complete polynya west of the Brunt Ice Shelf appeared to be covered by new ice. Due to persistent easterly/north-easterly winds, the region of pancake ice continued to move west and southwest. Thus, it was likely that the western edge was crossed by *Polarstern* on 28 February when the first occurrences of yellow pancake ice were noted. Continued easterly winds shifted the ice further west, and on 4 March, when air temperatures had risen to around –3° C, the eastern edge of the region had already drifted to west of 30° W. To the east, open water extended to the coast, covered by occasional bands of yellow/amber slush, sampled during PS124_77-1_IF_3 (Fig. 13.10). Those slush bands can also be identified in the SAR image of 4 March as narrow dark lines (Fig. 13.9).

On 3 and 4 March, we carried out an airborne, visual ice observation survey to map the spatial extent of the plume of yellow ice (Fig. 13.11). The ice was observed by oblique and nadir photography with a handheld and mounted GoPro camera, respectively. The observers noted

subjectively the occurrence of white/clear, bright, medium, and dark yellow ice as well as the ice type (Nilas, pancake, or grease ice). Results are shown in Fig. 13.11, and are in good agreement with the interpretation of the SAR images in terms of the western, southern, and eastern extent of the region. The surveys could not reach the end of the region in the northeast.

In Fig. 13.11, the results are overlaid with a “true-colour” MODIS image acquired on 2 March, one to two days before the survey, when the yellow ice was still farther east. Despite the cloud cover, green ice can be seen particularly in the upper right quadrant of the image, in good agreement with the results of the surveys and the interpretation of the SAR images. Unfortunately, persistent cloud cover prevented us from mapping the yellow pancake ice more systematically with the MODIS imagery, but occasionally green ice appears in the images before 4 March.

On 1, 3, and 9 March, ice cores and slab samples of the yellow pancakes were taken for physical properties (Table 13.1), ranging from 4 to 14 cm in thickness. Figs. 13.12 and 13.13 show the texture and salinities of these samples. In general, most ice consisted of fine-grained orbicular granular ice. Some of the samples comprised two or three layers indicative of rafting experienced by the pancake or Nilas ice prior to sampling. Ice core PS124_20210303_IF_2_TEX2 consisted almost exclusively of columnar ice as it was taken from dark Nilas, located between and firmly frozen to 5 to 20 m large yellow pancake floes. The salinity of all samples ranged between 5 and 15 ppt, with prominent C-shaped vertical profiles typical for thin, young ice.

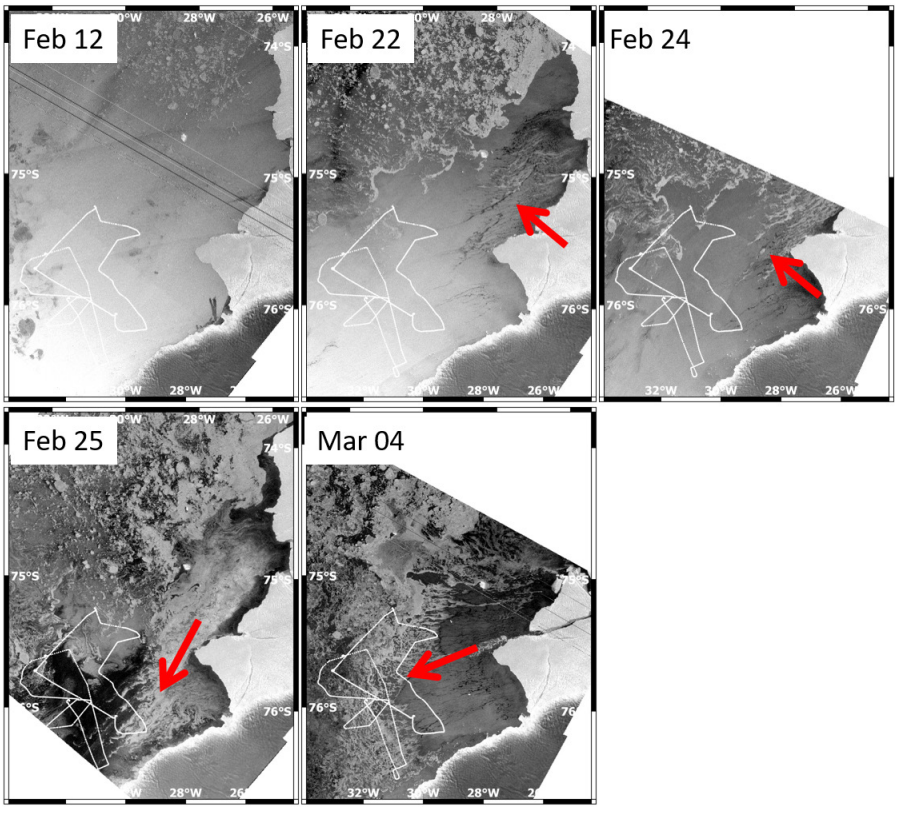

Fig. 13.9: Sentinel-1 SAR images showing the formation history of the pancake ice sampled and surveyed from 1 to 4 March 2021; white, wiggly lines near bottom show flight track of airborne pancake ice observations on 3 and 4 March 2021 (Fig. 13.11). Red arrows point to regions of forming slush and pancakes (top row), and to the location and approximate drift direction of the pancake-ice band.

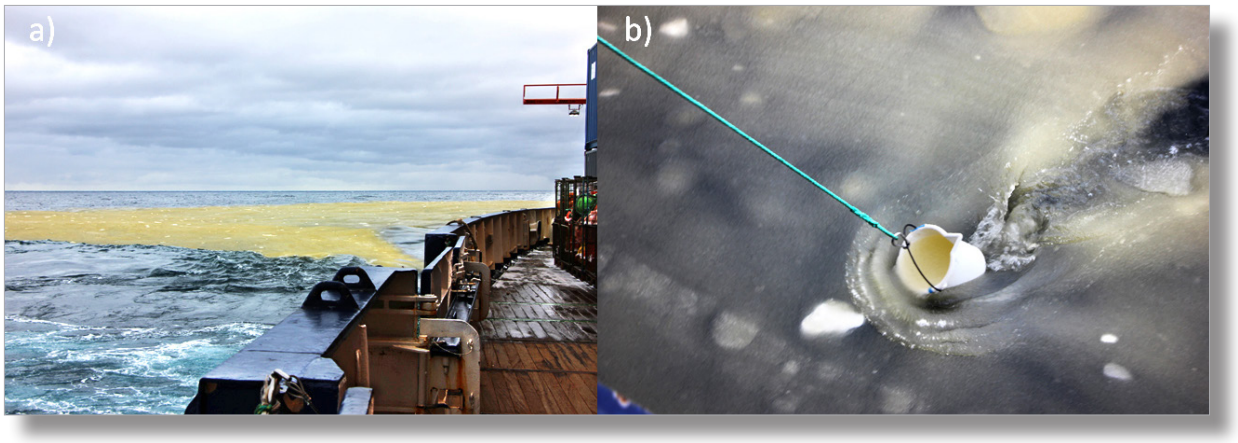

Fig. 13.10: Yellow/amber band close to Polarstern on 4 March 2021 (a), which was bucket sampled during station PS124_77-1_IF_3 (b)

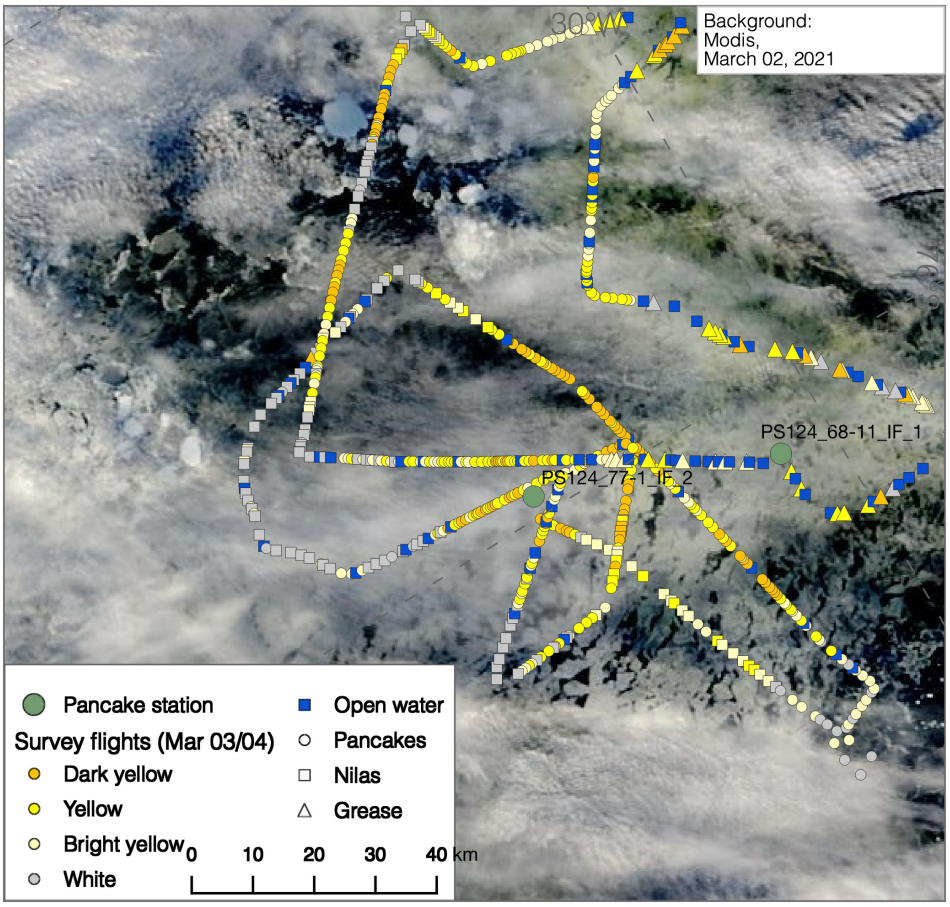

Fig. 13.11: Results of airborne, visual ice observation surveys carried out on 3 and 4 March 2021, overlaid on MODIS "true-colour" image acquired on 2 March 2021

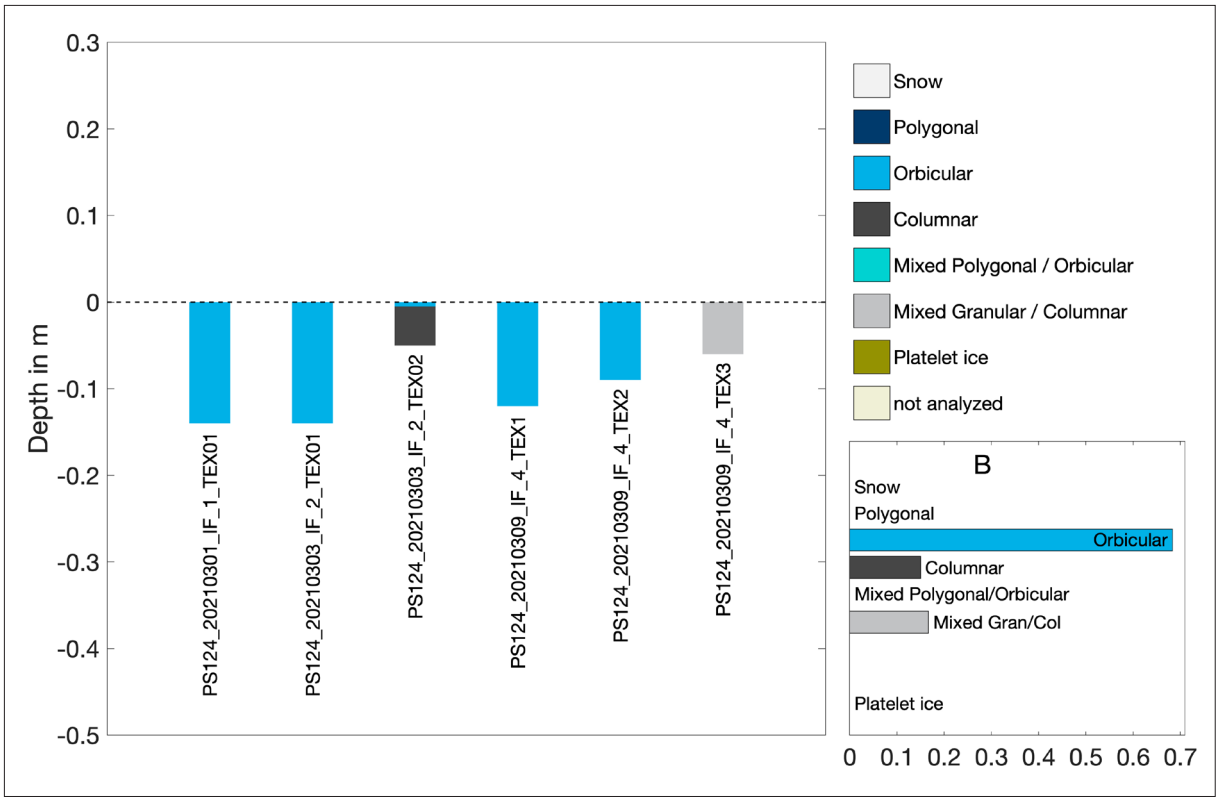

Fig. 13.12: (A) Texture of pancake ice samples (cf. Fig. 6.9); (B) Relative frequency distribution of ice texture classes

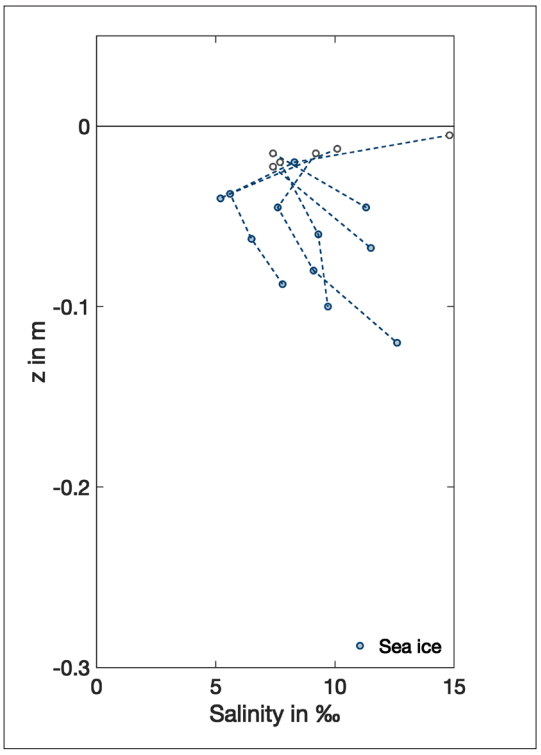

Fig. 13.13: Salinity profiles of all pancake ice samples

Data management

For the data management we refer to the respective sections of the previous chapters.

13.3 Iceberg A74

Objectives

On 26 February 2021, the large iceberg A74 with an area of 1,270 km², calved from the nearby Brunt Ice Shelf. A gap of the length of approx. 100 km was formed, which was initially filled with smaller ice shelf fragments in the North and, thus, too narrow for a passage. The following days, A74 was observed via satellite (TSX from DLR, Fig. 13.14) while moving further away from the Brunt Ice Shelf under prevailing easterly winds. Two weeks after the calving event, favorable weather conditions allowed the circumnavigation of A74 from late afternoon on 13 March until early morning 15 March 2021. It should be noted that *Polarstern* passed this area in 1987/88 during ANT-VI/3. With the opportunity to access a previously ice shelf covered area, we jointly developed an ad hoc approach to study

- the newly exposed seafloor and investigate benthic life and sediment geochemistry underneath the ice shelf,
- the physical and chemical parameters of the exposed water column,
- the sea ice formation processes in the wake of the calving process.

To conduct this work, the team was joined by the oceanography- (Chapter 3), bathymetry- (Chapter 5), sea ice physics- and biology- (Chapter 6), and all biogeochemical and biological groups (Chapters 7 – 12).

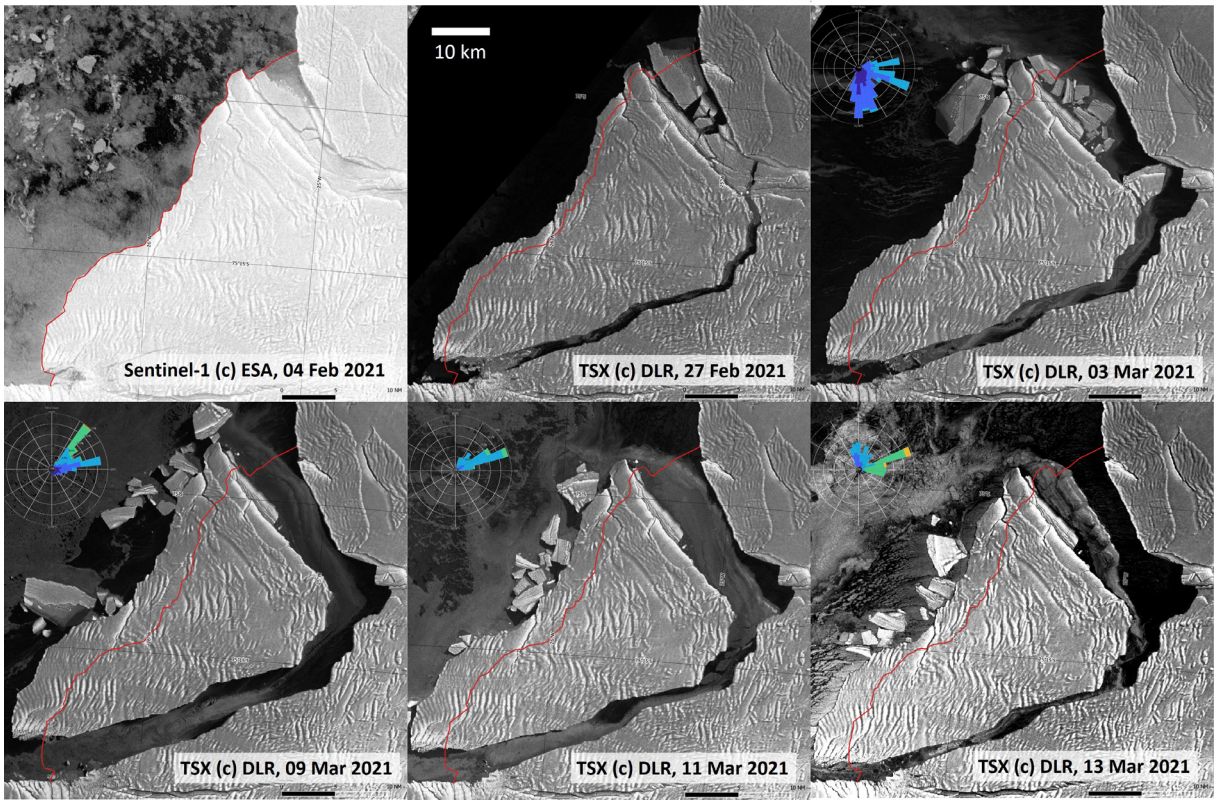

Fig. 13.14: Calving of iceberg A74 from the Brunt Ice Shelf. The circumnavigation took place on 13 – 14 March 2021. The red line denotes the ice shelf front before calving. A wind rose is inserted after the initial break up to correlate direction of A74 drift and prevailing wind (weak to strong wind speeds marked by dark blue to green/yellow colours, respectively).

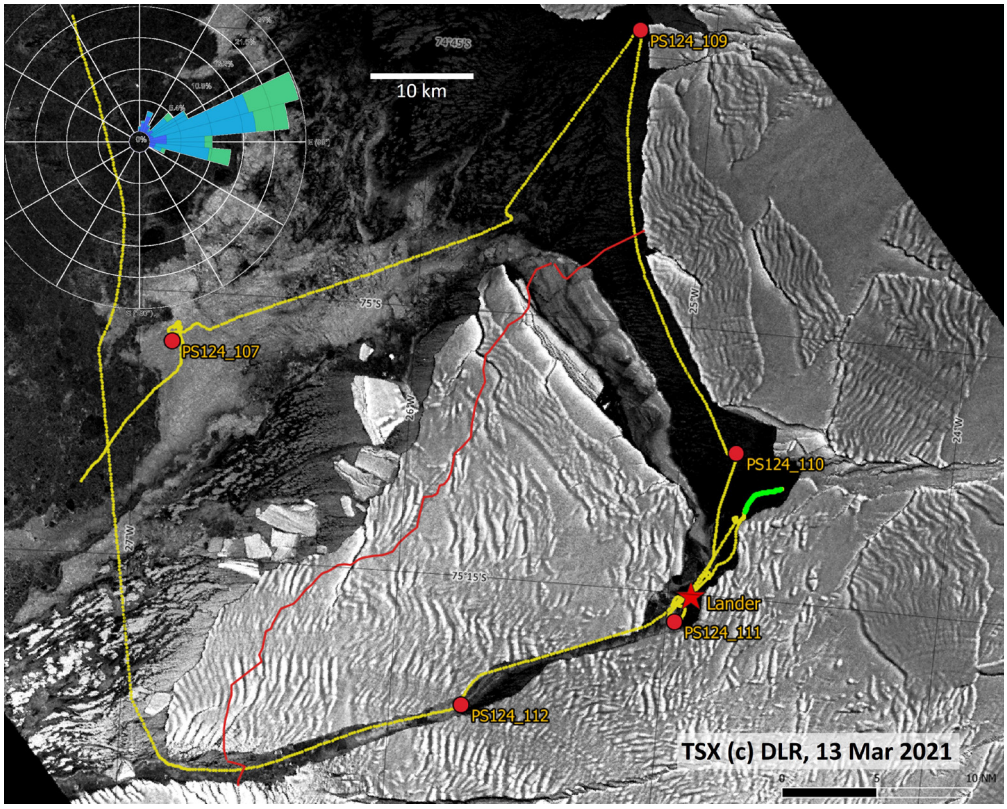

Fig. 13.15: Map with cruise track (yellow line) and stations (red circles) of the circumnavigation of A74. The position of the benthic Lander (red star) and the OFOBS transect (green line) are marked separately. The wind rose shows the wind directions during the circumnavigation. The red line denotes the ice shelf boundary before calving.

Tab. 13.2: Stations sampled during the circumnavigation of A74

Station	Date	Time	Lat [°S]	Lon [°W]	Depth [m]	Gear
PS124_109-1	2021-03-13	15:07	-74.726	-25.275	650	CTD-Rosette-Niskin
PS124_110-1	2021-03-13	19:27	-75.114	-24.796	557	CTD-Rosette-Niskin
PS124_110-2	2021-03-13	20:27	-75.113	-24.797	576	(Clean) CTD-Rosette-GoFlo
PS124_110-3	2021-03-13	21:14	-75.113	-24.798	576	Multi Box Corer
PS124_110-4	2021-03-13	22:25	-75.114	-24.799	572	Multi Corer
PS124_111-1	2021-03-14	00:49	-75.277	-24.965	615	CTD-Rosette-Niskin
PS124_111-2	2021-03-14	01:25	-75.277	-24.967	637	CTD-Rosette-Niskin
PS124_111-3	2021-03-14	02:22	-75.277	-24.967	635	(Clean) CTD-Rosette-GoFlo
PS124_111-4	2021-03-14	03:11	-75.277	-24.966	635	*In-situ* Immersion Pump
PS124_111-5	2021-03-14	04:02	-75.277	-24.966	638	Multi Corer
PS124_111-6	2021-03-14	05:05	-75.277	-24.966	638	Multi Box Corer
PS124_111-7	2021-03-14	08:08	-75.253	-24.915	587	Lander deployment
PS124_111-8	2021-03-14	09:54	-75.174	-24.748	570	OFOBS
PS124_111-9	2021-03-14	16:50	-75.253	-24.911	587	Lander recovery

Station	Date	Time	Lat [°S]	Lon [°W]	Depth [m]	Gear
PS124_111-10	2021-03-14	17:13	-75.255	-24.918	591	Ice Bucket
PS124_112-1	2021-03-14	19:24	-75.370	-25.724	771	CTD-Rosette-Niskin
PS124_112-2	2021-03-14	20:33	-75.370	-25.725	790	(Clean) CTD-Rosette-GoFlo
PS124_112-3	2021-03-14	21:37	-75.372	-25.730	784	Multi Box Corer
PS124_112-4	2021-03-14	22:38	-75.372	-25.724	795	Multi Corer

Preliminary results

Water column

The newly exposed water column was thoroughly mixed without the typical stratification in the upper water column (Fig. 13.16). Temperatures were well below the surface freezing temperature of –1.88° C. Oxygen concentrations were at 85 % air saturation even at the very surface, without any signs of primary production or O_2 accumulation from atmospheric influx. This agrees with extremely low fluorescence values that do not show any peaks in surface waters. Compared to the Ice Shelf Water in the Filchner Trough, the ice shelf waters underneath A74 were significantly less saline (~34.3 psu) and thus formed a specific signature in the T-S diagram (Fig. 13.17).

The water temperature down to depths of 32 m (PS124_110), 84 m (PS124_111), and 66 m (PS124_112) was below the *in-situ* freezing temperature (Fig. 13.18). Ice formation in the surface layers was indicated by increased scatter in the beam transmission profiles of the CTD, but also by pictures of frazil ice particles made by the Underwater Vision Profiler (UVP, see Chapter 7) during the CTD casts (Fig. 13.19).

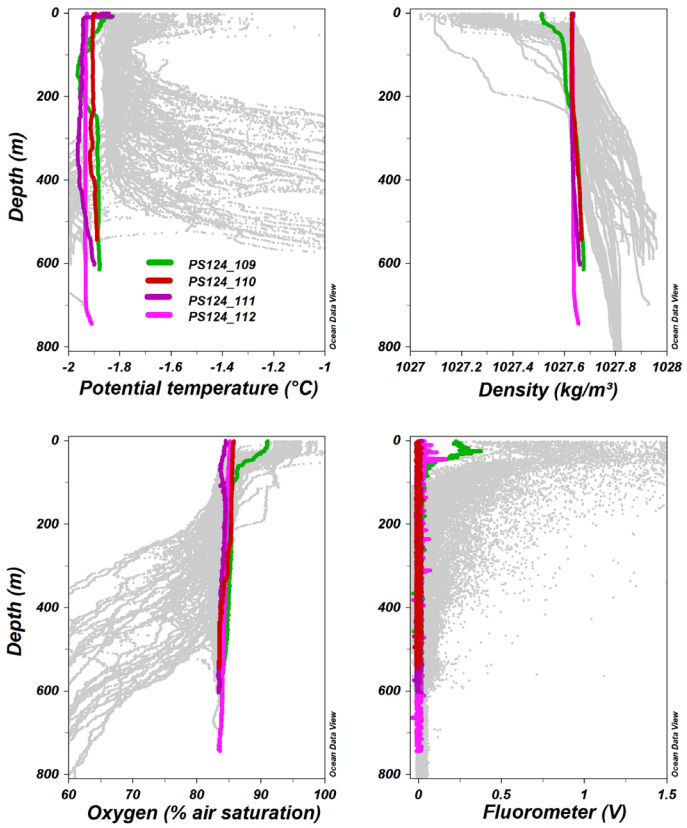

Fig. 13.16. Water column profiles of temperature, density, oxygen, and fluorescence for the three stations formerly covered by A74 (red, purple, pink) and for the reference station (green); all other PS124 stations in grey.

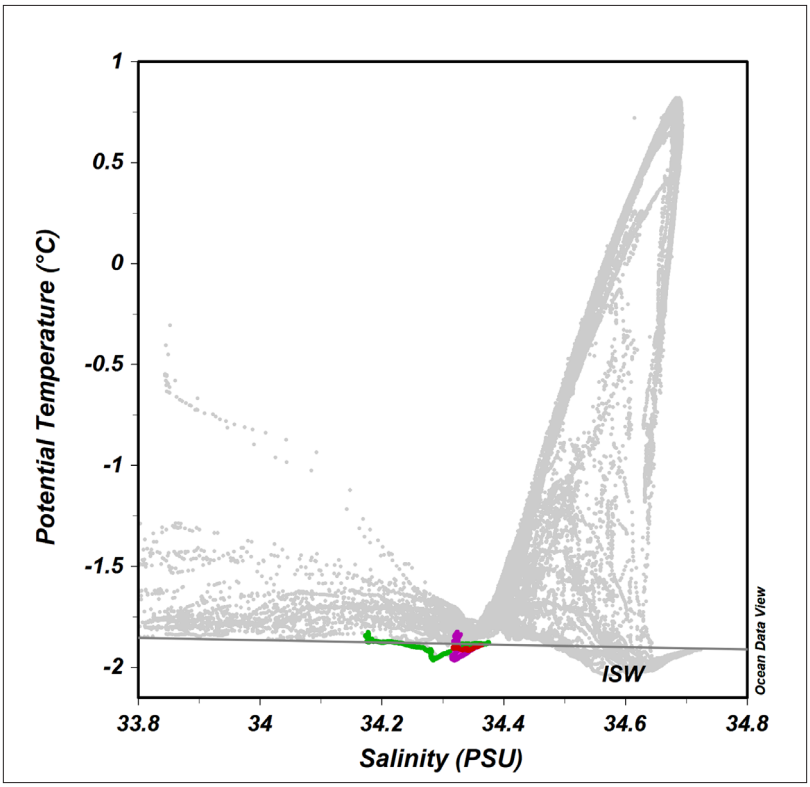

Fig. 13.17: T-S diagram marking the three stations formerly covered by A74 (red, purple, pink) and the reference station (green); all other PS124 stations in grey; ‘ classical’ Ice Shelf Water is indicated for comparison.

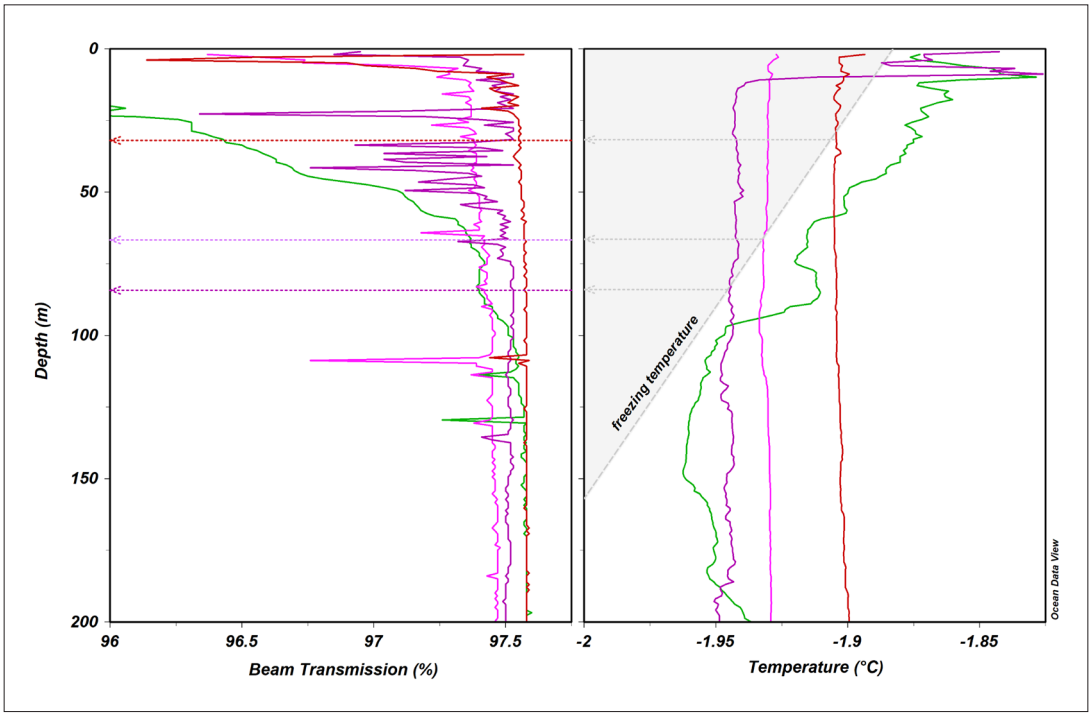

Fig. 13.18: Beam transmission and temperature profiles of the upper 200 m; the depth dependent freezing temperatures are indicated by the grey area; the horizontal lines mark the depths where in-situ temperatures of the three stations match the in-situ freezing point.

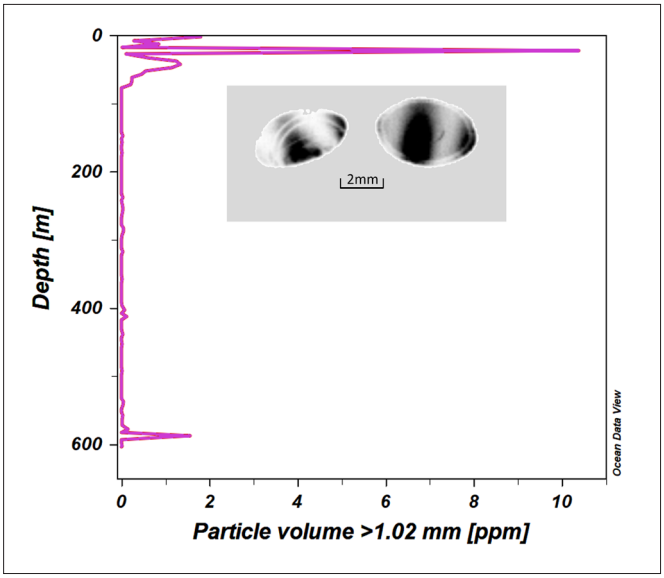

Fig: 13.19: Particle profile based on UVP5 (Underwater Vision Profiler 5hd) of station PS124_111; the distribution of the particle size class >1 mm was characterized by a limited number of outliers reaching values of up to 2 ppm and even 10 ppm in surface waters.Those outliers potentially represent frazil ice.
Insert: Images of frazil ice particles acquired by UVP5 at station _111 at 5.5 m and 34.9 m depth; see Chapter 7 for further details about the UVP.

Sea ice formation

At station PS124_111-10 (Table 13.2), new ice on the water surface was sampled with a bucket and studied for physical and biogeochemical parameters. The ice turned out to be mainly platelet ice and was immediately separated from the under-ice water, and both were filtered for the various biogeochemical variables (see also Chapter 6). First life microscopic observations indicated a very low autotrophic biomass as already indicated by the low values of the fluorescence profile (Fig. 13.16). Only a few *Fragilariopsis* and *Thalassiosira* species were observed with slightly higher abundance in the platelet ice. The enrichment from water to platelet ice is further corroborated by pigment measurements with high pressure liquid chromatography, indicating extreme low biomass of algae in the water < 0,01 µg Chl*a* L^{-1} and < 0,03 µg Chl*a* L^{1} in the platelet ice. The occurrence of fucoxanthin, the main marker for diatoms, indicated this group as the most prominent in the environmental setting, while in one of the samples a marker for prymnesiophytes, 19'-hexanoyloxy-fucoxanthin, was also present. Future Illumina sequencing analysis will give further insights into the biodiversity found in the newly exposed waters after the calving of A 74.

On 14 March 2021, a helicopter-borne sea ice thickness and roughness survey was carried out with the EM-Bird (see Chapter 6) to investigate the new ice in the crack that had formed in the northeast of A74 since 28 February, when the iceberg started to detach from the ice shelf. Ice conditions in the crack were relatively well observed by TerraSAR-X imagery (e.g., Fig. 13.14), which were showing a band of new ice successively forming on the side of the iceberg. The image of 13 March shows that the new ice was structured with bands parallel to the iceberg edge, probably due to alternating opening and partial closing of the crack and the addition of new ice in the open water, which was then pushed into the older ice by strong winds (Fig. 13.20).

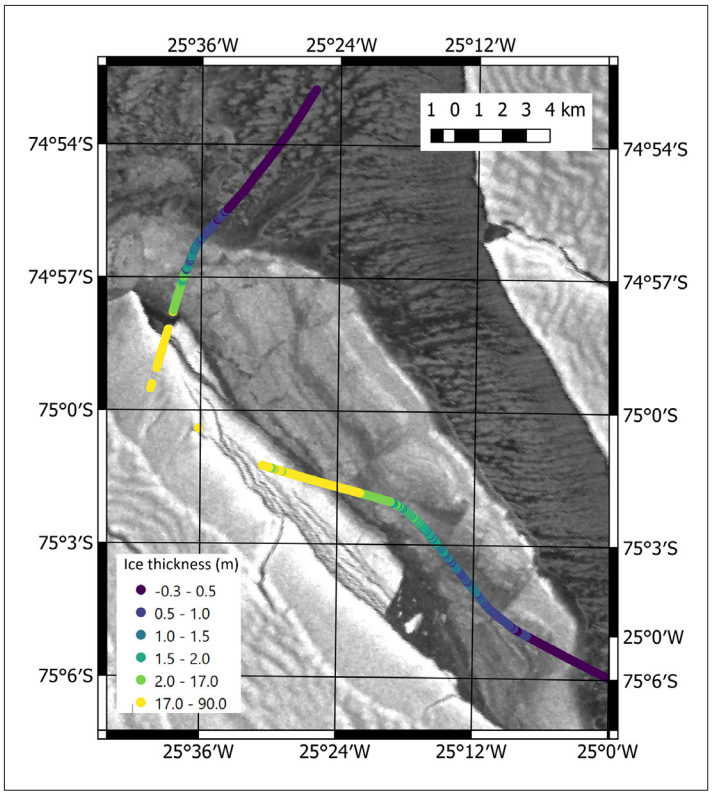

Fig. 13.20: TerraSAR-X image of 13 March 2021 showing the crack between A74 (bottom left) and the Brunt Ice Shelf (top right); the western part of the crack is covered by new ice with a banded structure extending parallel to the iceberg edge. Coloured symbols show ice thickness obtained along a helicopter flight track on 14 March 2021 by means of electromagnetic sounding.

Fig. 13.21 shows the corresponding thickness profile, extending from the open water in the southeast across the banded ice and onto the iceberg (*cf.* Fig. 13.20). The data show the strong thickening of the less than 2-week-old ice towards the iceberg, with thicknesses of the oldest ice larger than 2 m. It can also be seen that different bands correspond to different roughness regimes potentially caused by different ice deformation events. Reconstruction of the deformational history of the new ice and the interpretation of the X-band radar backscatter signatures will be the objective of following work.

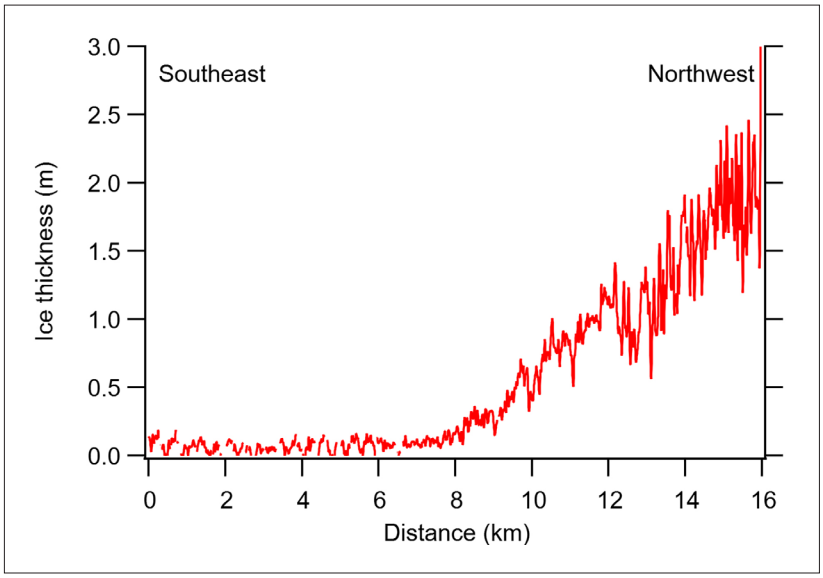

Fig. 13.21: Ice thickness profile across the banded new ice visible in Fig. 13.20; profile shows the southern part, from the open water in the southeast to the thick ice in the northwest. Note strong thickness gradient across banded ice and different roughness regimes indicative of different deformation histories

Sediment Geochemistry

Sediments for geochemical analysis were sampled with the MUC and processed as described in Chapter 9. Preliminary results of the porewater analysis (Fig. 13.22) indicate that sediments formerly covered by A74 are non-typical shelf sediments. Shelves usually receive high amounts of organic matter which drive microbially mediated degradation processes. Microbes oxidize organic matter through the successive reduction of oxygen, nitrate, manganese oxides, iron oxides, and sulfate. In typical shelf sediments, the iron reduction zone is reached in a few millimeters to centimeters sediment depth. At site PS124/111-5 (Fig. 13.22) and PS124/110-4 (not shown), however, nitrate is present until 35-cm depth at a concentration of 40 to 50 µmol/L. The $NH4^+$ concentration is < 1 µmol/L throughout the cores. Nitrite is present at low concentrations of < 0.2 µmol/L at site 111-5 and up to 2 µmol/L at site 110-4. Dissolved Fe^{2+} was not detected in the top 15 cm at site 111-5. Further below and at site 110-4, the extracted pore water volume was not sufficient for the photometric analysis. Phosphate, released during organic matter degradation and by desorption from iron oxides during dissimilatory iron reduction, only shows a very slight increase from 2 to 6 µmol/L at both locations. In summary, the sediments behind A74 appear to be microbially inactive, which indicates very low levels of TOC. Only $Si(OH)^4$ increases significantly from ~ 60 µmol/L in the bottom water to ~ 400 µmol/L at ~ 5 cm depth indicating that some biogenic opal reaches the seafloor and undergoes rapid dissolution.

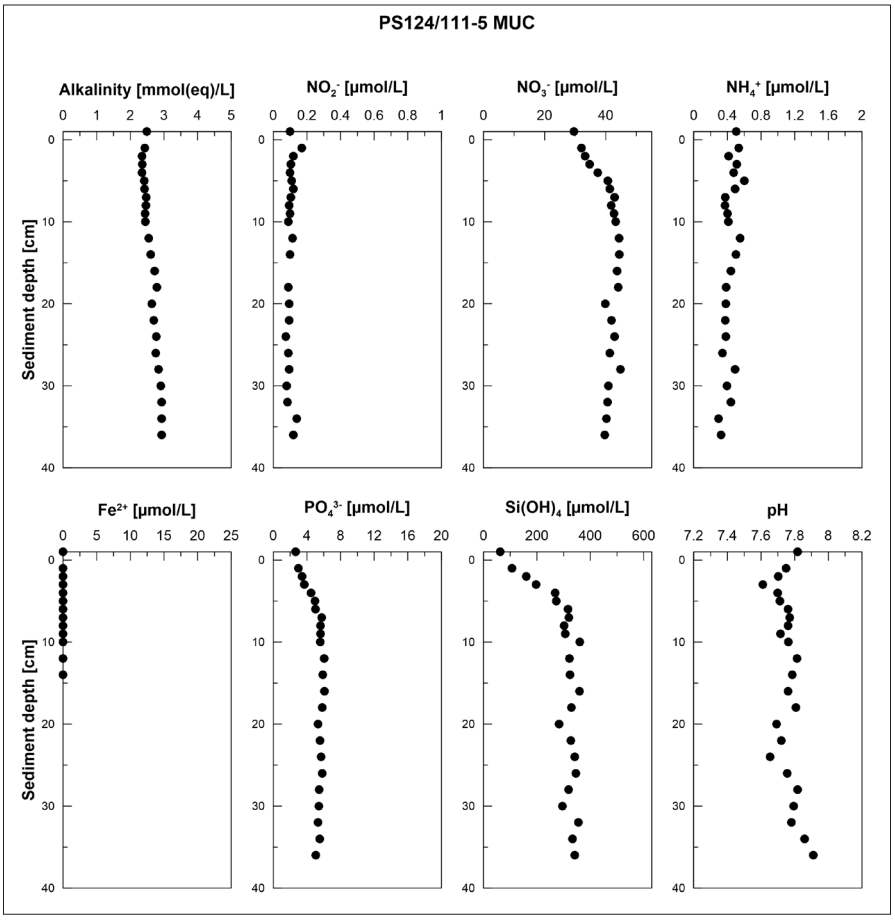

Fig. 13.22: Porewater concentrations of alkalinity, pH, and nutrients at station PS124_111

Benthic fauna

The seafloor was photographed, filmed and acoustically mapped using the Ocean Floor Observation and Bathymetry System (OFOBS, see Chapter 11) throughout the deployment at PS124_111_10. About 800 images were collected from an altitude of 1.5 to 2 m above the seafloor. Furthermore, sediment samples for makro fauna were taken by the Multi-Box-Corer (MG, see Chapter 10) at station PS124_110, PS124_111, and PS124_112.

The region surveyed by OFOBS was fairly uniform in appearance, with the seafloor comprising primarily of fine grained sediments scattered with occasional small dropstones (Fig. 13.23-A). The dropstones varied in maximum diameter from a few centimeters to over a meter across, with the majority of ~15 – 25 cm in diameter.

Virtually every imaged dropstone supported a diverse community of sessile and mobile filter feeders as well as occasional scavengers. In Fig. 13.23-B a rich community of sessile bryzoans, corals, sponges, and encrusting worms are using the dropstone as a substrate. Though small in size, these fauna are clearly of numerous years age, and one large sponge probably of several decades age at least. As with all dropstones encountered on the A74 transect, a developed community was evident on each dropstone, not indicative of recently colonising individuals and, therefore, representative of a stable community present prior to the calving of A74. The majority of the sessile fauna were clearly filter feeders. Several mobile fauna are also evident in Fig. 13.23-B, including a shrimp and several ophiuroids. Ophiuroids and holothurians (Fig. 13.23-C) were found across the seafloor sediment, with holothurians, seafloor deposit feeders, actually being more abundant during the A74 transect than at any other station surveyed during the expedition. At least four species of fish and occasional echinoids were found during the A74 survey.

There was very little indication of infauna recorded during the transect. OFOBS deployments conducted outside of the former ice shelf area during PS124 tended to have a higher abundance of surface burrow exits and piles of deeper material brought to the surface during burrowing than was evident in images recorded during the A74 survey. This would perhaps indicate that much of the more labile material transported by benthic currents under the ice shelf are utilized by the filter and deposit feeders before being incorporated into seafloor sediments.

Based on in- and epifaunal surveys, the benthos resembles that of the ISW related community (see Chapter 10). The presence of fauna, especially of suspension feeders on top of dropstones, suggests the transport of material from adjacent basins. Based on the direction of water circulation, it is possible that benthos below the Brunt Ice Shelf has been supported by advection of food particles from the shallower continental shelf in west/northwest direction. As of now, the observations during PS124 depict only a single point in time right after the break-off of A74. It would be highly interesting to revisit the area in the future to understand if the situation observed at the Brunt Ice Shelf matches that of the areas formerly covered by the Larsen A and B ice shelves, and use this as a reference study on Antarctic benthos recolonization and development.

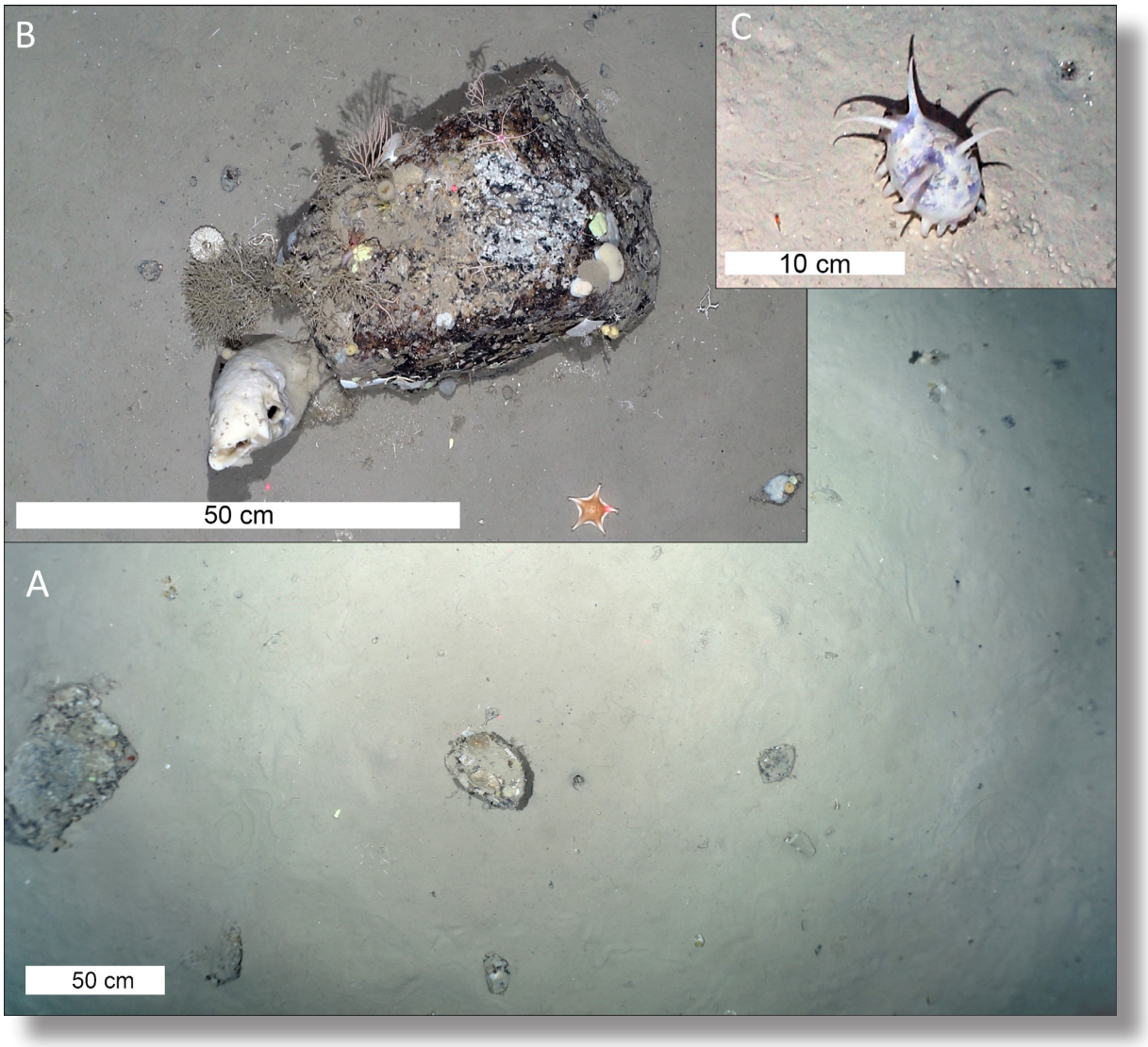

Fig. 13.23: Images taken by OFOBS along the transect (Fig. 13.15) at station PS124_111-8

Data management

For the data management we refer to the respective sections of the previous chapters.

Danksagung

PS124 hätte nicht stattfinden können ohne die bedingungslose Unterstützung vieler Hände. Dieses sind die Mitarbeiter*innen der Logistik des Alfred-Wegener-Instituts (AWI), die Kapitäne und Besatzungsmitglieder der Lufthansa Flüge, der Kapitän und die gesamte Besatzung der *Polarstern*, die Piloten und Techniker der Hubschrauber an Bord und das Team des Deutschen Wetterdienstes.

Wir danken allen für ihre engagierte und enthusiastische Unterstützung während der Vorbereitung und Durchführung der erfolgreichen COSMUS Expedition.

Acknowledgements

PS124 would not have taken place without the unconditional support of various parties. These are the members of the Logistic Department of the Alfred Wegener Institute (AWI), captains and crew members of the Lufthansa flights, captain and entire crew of *Polarstern*, the pilots and technicians of the onboard helicopters, and the team of the Deutscher Wetterdienst.

We thank all for their dedicated and enthusiastic support prior and during the successful COSMUS expedition.

APPENDIX

A.1 TEILNEHMENDE INSTITUTE / PARTICIPATING INSTITUTIONS

Institution	Address
CH.UNIBAS	Universität Basel, MGU Vesalgasse 1 4051 Basel Switzerland
DE.AWI	Alfred-Wegener-Institut Helmholtz-Zentrum für Polar- und Meeresforschung Am Handelshafen 12 27570 Bremerhaven Germany
DE.CAU	Christian-Albrechts-Universität zu Kiel Olshausenstraße 75 24118 Kiel Germany
DE.DWD	Deutscher Wetterdienst Bernhard-Nocht-Straße 76 20359 Hamburg Germany
DE.MPIMM	Max-Plank-Institut für Marine Mikrobiologie Celsiusstraße 1 28359 Bremen Germany
DE.UNI-Bremen	Universität Bremen Institut für Umweltphysik Otto-Hahn-Allee 1 28359 Bremen Germany
DE.UNI-GREIFSWALD	Universität Greifswald Domstraße 11 17489 Greifswald Germany
DE.UNI-Oldenburg	Carl von Ossietzky Universität Oldenburg Carl-von-Ossietzky-Straße 9-13 26132 Oldenburg Germany
FR.LOCEAN.UPMC	LEOCEAN-IPSL Sorbonnes Université (UPMC) 4 Pl. Jussieu 75005 Paris France

Institution	Address
NO.NORCE	Norwegian Research Centre AS Nygårdsgaten 112 5008 Bergen Norway
NO.UIB	Geophysical Institute Bjerknes Centre for Climate Research P.O. Box 7803 5020 Bergen Norway
UK.NOC	NOC Southampton National Oceanography Centre European Way Southampton SO14 3ZH United Kingdom

A.2 FAHRTTEILNEHMER / CRUISE PARTICIPANTS

Name/ Last name	Vorname/ First name	Institut/ Institute	Beruf/ Profession	Fachrichtung/ Discipline
Arndt	Stefanie	DE.AWI	Scientist	Sea Ice Physics
Balaguer	Jenna	DE.AWI	Student	Pelagic Production
Böhringer	Lillian	DE.AWI	Student	Bathymetry
Bornemann	Horst	DE.AWI	Scientist	Biology
Brenneis	Georg	DE.UNI-GREIFSWALD	Scientist	Biology
Burkhardt-Holm	Patricia	CH.UNIBAS	Scientist	Ecology
Darelius	Elin	NO.UIB	Scientist	Phys. Oceangr.
Dürwald	Alexandra	DE.UNI-GREIFSWALD	Student	Biology
Eggers	Sarah L.	DE.AWI	Scientist	Sea Ice Physics
Ehlert	Claudia	DE.UNI-Oldenburg	Scientist	Geochemistry
Flintrop	Clara	DE.AWI	Scientist	Biology
Glemser	Barbara	DE.MPIMM	Student	Biology
Haas	Christian	DE.AWI	Scientist	Sea Ice Physics
Hargesheimer	Theresa	DE.AWI	Technician	Biology
Hehemann	Laura	DE.AWI	Data Manager	Bathymetry
Hellmer	Hartmut H.	DE.AWI	Chief Scientist	Phys. Oceanogr.
Hellmer	Henning	DE.AWI	Student	Pelagic Production
Henkel	Susann	DE.AWI	Scientist	Geochemistry
Hinse	Yannik	DE.UNI-Bremen	Student	Phys. Oceanogr.
Holtappels	Moritz	DE.AWI	Scientist	Biology
Janout	Markus	DE.AWI	Scientist	Phys. Oceanogr.
Kalvelage	Tim			
Koch	Florian	DE.AWI	Scientist	Pelagic Production
LeGoff	Herve	FR.LOCEAN. UPMC	Scientist	Phys. Oceanogr.
Leistenschneider	Clara	CH.UNIBAS	Student	Ecology
Monsees	Matthias	DE.AWI	Technician	Phys. Oceanogr.
Nordhausen	Axel	DE.MPIMM	Technician	Deep Sea Ecology
Neudert	Mara	DE.UNI-Bremen	Student	Sea Ice Physics
Østerhus	Svein	NO.NORCE	Scientist	Phys. Oceanogr.
Peeken	Ilka	DE.AWI	Scientist	Sea Ice Physics

Name/ Last name	**Vorname/ First name**	**Institut/ Institute**	**Beruf/ Profession**	**Fachrichtung/ Discipline**
Pineda-Metz	Santiago E.A.	DE.AWI	Scientist	Biology
Purser	Autun	DE.AWI	Scientist	Deep Sea Ecology
Rogge	Andreas	DE.CAU	Scientist	Biology
Schaap	Allison	UK.NOC	Scientist	Biology
Schall	Elena	DE.AWI	Student	Phys. Oceanogr.
Spiesecke	Stefanie	DE.AWI	Technician	Phys. Oceanogr.
Schröder	Henning	DE.AWI	Engineer	Biology
Stimac	Ingrid	DE.AWI	Technician	Geochemistry
Tippenhauer	Sandra	DE.AWI	Technician	Phys. Oceanogr.
Timmermann	Ralph	DE.AWI	Scientist	Phys. Oceanogr.
van Caspel	Mathias	DE.AWI	Scientist	Phys. Oceanogr.
Vignes	Lucie	FR.LOCEAN. UPMC	Student	Phys. Oceanogr.
Voelkner	Christian	DE.AWI	Technician	Pelagic Production
Wege	Mia	DE.AWI	Scientist	Biology
Wenzhoefer	Frank	DE.AWI	Scientist	Deep Sea Ecology
Werner	Ellen	DE.AWI	Scientist	Bathymetry
DWD				
Otte	Frank	DE.DWD	Scientist	Meteorology
Rohleder	Christian	DE.DWD	Technician	Meteorology
Schröter	Steffen	DE.DWD	Scientist	Meteorology
Heli-Service				
Drach	Sebastian	DE.HeliService	Pilot	Aviation
Prieto Turienzo	Elena Maria	DE.HeliService	Technician	Aviation
Stenssen	Willem A.	DE.HeliService	Technician	Aviation
Zillgen	Carsten	DE.HeliService	Chief Pilot	Aviation
Rückkehrer von *Neumayer III* / Return staff from *Neumayer III* (*NM III*)				
Ackle	Roman	DE.RFL	Engineer	Wintering team (WT)
Bähler	Stefanie	DE.RFL	Engineer	Technics *NM III*
Beyer	Mario	DE.RFL	Engineer	Wintering team
De Almeida Santos	Wanderson	DE.RFL	Cook	Wintering team
Eder	Pitt	DE.RFL	Technician	Technics *NM III*

Name/ Last name	**Vorname/ First name**	**Institut/ Institute**	**Beruf/ Profession**	**Fachrichtung/ Discipline**
Fromm	Tanja	DE.AWI	Scientist	Geophysics
Geis	Peter	COM.Kässbohrer	Technician	Technics *NM III*
Guba	Klaus	DE.RFL	Physician	WT Medicine
Heitland	Tim	DE.AWI	Physician	Summer staff *NM III*
Jörss	Anna-Marie	DE.AWI	Scientist	WT Meteorology
Laubach	Hannes	DE.RFL	Technician	Summer staff *NM III*
Lemm	René	DE.RFL	Steward	Summer staff *NM III*
Loftfield	Julia	DE.AWI	Scientist	WT Air Chemistry
Oblender	Andreas	DE.RFL	Engineer	Summer staff *NM III*
Preis	Loretta	DE.AWI	Engineer	Summer staff *NM III*
Riess	Felix	DE.RFL	Technician	Summer staff *NM III*
Schmithüsen	Holger	DE.AWI	Scientist	Meteorology
Schubert	Holger	DE.RFL	Technician	Summer staff *NM III*
Schütt	Philipp	DE.RFL	Technician	Summer staff *NM III*
Sterbenz	Thomas	DE.RFL	Engineer	Summer staff *NM III*
Trumpik	Noah	DE.AWI	Scientist	WT Geophysics
Vrakking	Vincent	DE.DLR	Engineer	Summer staff *NM III*
Wehner	Ina	DE.AWI	Scientist	WT Geophysics
Weller	Rolf	DE.AWI	Scientist	Chemistry

A.3 SCHIFFSBESATZUNG / SHIP'S CREW

Name/Last name	Vorname/First name	Rang/Rank
Schwarze	Stefan	Master
Grundmann	Uwe	Chief Mate
Heuck	Hinnerk Sören	Chief Engineer
Kentges	Felix	1st Mate
Lauber	Felix	1st Mate
Fischer	Tibor	2nd Mate
Müller	Andreas	Comm Officer
Gößmann-Lange	Petra	Ships Doctor
Brose	Thomas Christian Gerhard	2nd. Engineer
Haack	Michael Detlev	2nd. Engineer
Kästner	Manfred Andre	2nd. Engineer
Redmer	Jens Dirk	E-Engineer
Frank	Gerhard	Electician/Engineer
Hüttebräucker	Olaf	Electician/Engineer
Krüger	Lars	Electician/Engineer
Nasis	Ilias	Electician/Engineer
Brück	Sebastian	Bosun
Reise	Lutz	Carpenter
Decker	Jens	MP Rating
Klee	Philipp	MP Rating
Köpnick	Ulrich	MP Rating
Lello	Ants	MP Rating
Möller	Falko	MP Rating
Bäcker	Andreas	AB
Burzan	Gerd-Ekkehard	AB
Wende	Uwe	AB
Preußner	Jörg	Storekeeper
Gebhardt	Norman	MP Rating
Rhau	Lars-Peter	MP Rating
Sautmann	David	MP Rating
Schwarz	Uwe	MP Rating
Teichert	Uwe	MP Rating

Name/Last name	Vorname/First name	Rang/Rank
Schnieder	Sven	Cook
Silinski	Frank	Cooksmate
Zahn	Maren	Cooksmate
Czyborra	Bärbel	Chief Stewart
Braun	Maja	Nurse / Stewart
Arendt	Rene	2nd Stewart
Bachmann	Julia Maria	2nd Stewart
Chen	Danheng	2nd Stewart
Dibenau	Torsten Karl	2nd Stewart
Silinski	Carmen Viola	2nd Stewart
Sun	Yong Sheng	Laundrymate
Krumrei	Benni	App.MP
Stellamanns	Thies Christian	App.MP

A.4 STATIONSLISTE / STATION LIST PS124

Tab. A.4: Station list of expedition PS124 from Stanley to Stanley; the list details the action log for all stations along the cruise track.

See https://www.pangaea.de/expeditions/events/PS124 to display the station (event) list for expedition PS124.
This version contains Uniform Resource Identifiers for all sensors listed under https://sensor.awi.de.
See https://www.awi.de/en/about-us/service/computing-centre/data-flow-framework.html for further information about AWI's data flow framework from sensor observations to archives (O2A).

Event label	Optional label	Date/Time	Latitude	Longitude	Depth [m]	Gear	Action	Comment
PS124_0_ Underway-28		2021-02-04T16:00:00	-51.66604	-57.76930		SWEAS	Station start	
PS124_0_ Underway-28		2021-02-04T16:00:00	-51.66604	-57.76930		SWEAS	Station end	
PS124_0_ Underway-27		2021-02-04T16:00:00	-51.66391	-57.76913		W-RADAR	Station start	
PS124_0_ Underway-27		2021-02-04T16:00:00	-54.22980	-53.99986		W-RADAR	Station end	
PS124_0_ Underway-22		2021-02-04T16:00:00	-51.66381	-57.76906		SVP	Station start	
PS124_0_ Underway-22		2021-02-04T16:00:00	-54.22899	-54.00102		SVP	Station end	
PS124_1-1		2021-02-04T16:25:31	-55.93560	-55.72571		ARGOFL	Station start	BSH Float; Responsible: M. Janout
PS124_1-1		2021-02-04T16:25:31	-55.93651	-55.73292		ARGOFL	Station end	BSH Float; Responsible: M. Janout
PS124_0_ Underway-24		2021-02-04T16:36:09	-55.95138	-55.73226	4079.7	TSG	Station start	
PS124_0_ Underway-24		2021-02-04T16:36:09	-54.23188	-53.99675	2085.4	TSG	Station end	

Event label	Optional label	Date/Time	Latitude	Longitude	Depth [m]	Gear	Action	Comment
PS124_0_ Underway-23		2021-02-04T16:36:29	-55.95260	-55.73137	4075.2	TSG	Station start	
PS124_0_ Underway-23		2021-02-04T16:36:29	-54.23288	-53.99522	2085.4	TSG	Station end	
PS124_0_ Underway-20		2021-02-04T16:36:56	-55.95419	-55.73020	4065.1	PS	Station start	
PS124_0_ Underway-20		2021-02-04T16:36:56	-54.23348	-53.99428	2085.4	PS	Station end	
PS124_0_ Underway-13		2021-02-04T16:40:56	-55.96906	-55.72020	4062.0	HS	Station start	
PS124_0_ Underway-13		2021-02-04T16:40:56	-54.23414	-53.99329	2085.4	HS	Station end	
PS124_0_ Underway-11		2021-02-04T16:41:18	-55.97041	-55.71923	4063.3	MAG	Station start	
PS124_0_ Underway-11		2021-02-04T16:41:18	-54.23501	-53.99201	2103.3	MAG	Station end	
PS124_0_ Underway-9		2021-02-04T16:42:15	-55.97391	-55.71671	4069.5	HVAIR	Station start	
PS124_0_ Underway-9		2021-02-04T16:42:15	-54.23675	-53.98933	2148.3	HVAIR	Station end	
PS124_0_ Underway-6		2021-02-04T16:43:40	-55.97917	-55.71314	4141.7	MYON	Station start	
PS124_0_ Underway-6		2021-02-04T16:43:40	-54.23727	-53.98847	2165.3	MYON	Station end	
PS124_0_ Underway-5		2021-02-04T16:44:21	-55.98168	-55.71135	4182.1	CCAM	Station start	
PS124_0_ Underway-5		2021-02-04T16:44:21	-54.23943	-53.98523	2215.3	CCAM	Station end	
PS124_0_ Underway-2		2021-02-04T16:44:53	-55.98365	-55.70984	4187.9	AFIM	Station start	

Event label	Optional label	Date/Time	Latitude	Longitude	Depth [m]	Gear	Action	Comment
PS124_0_ Underway-2		2021-02-04T16:44:53	-54.24055	-53.98361	2237.3	AFIM	Station end	
PS124_0_ Underway-1		2021-02-04T16:45:27	-55.98574	-55.70832	4180.6	ADCP	Station start	
PS124_0_ Underway-1		2021-02-04T16:45:27	-54.24263	-53.98063	2263.3	ADCP	Station end	
PS124_0_ Underway-7		2021-02-04T16:46:13	-55.98859	-55.70645	4167.5	FBOX	Station start	
PS124_0_ Underway-7		2021-02-04T16:46:13	-54.24301	-53.98006	2270.7	FBOX	Station end	
PS124_2-1		2021-02-04T20:30:00	-56.80935	-55.31519	3302.4	ARGOFL	Station start	BSH Float; Responsible: M. Janout
PS124_2-1		2021-02-04T20:30:00	-56.80959	-55.32642	3010.2	ARGOFL	Station end	BSH Float; Responsible: M. Janout
PS124_3-1		2021-02-04T23:21:03	-57.44298	-55.04797	4116.7	ARGOFL	Station start	BSH Float; Responsible: M. Janout; BSH Float
PS124_3-1		2021-02-04T23:21:03	-57.49888	-55.01937	4359.1	ARGOFL	Station end	BSH Float; Responsible: M. Janout; BSH Float
PS124_4-1		2021-02-05T18:31:36	-61.30810	-52.66902	1187.1	ARGOFL	Station start	AWI Float; O. Boebel; Responsible: M. Janout
PS124_4-1		2021-02-05T18:31:36	-61.30858	-52.66378	1188.3	ARGOFL	Station end	AWI Float; O. Boebel; Responsible: M. Janout
PS124_0_ Underway-18		2021-02-08T09:56:07	-70.26027	-30.49041	4470.6	UWPCO2	Station start	
PS124_0_ Underway-18		2021-02-08T09:56:07	-54.24408	-53.97855	2279.8	UWPCO2	Station end	
PS124_5-1		2021-02-08T11:20:03	-70.41854	-29.99995		CTD-RO	max depth	Responsible: C. Völkner; TCTD Ultra Clean; SL = 100 m AWI 030

Event label	Optional label	Date/Time	Latitude	Longitude	Depth [m]	Gear	Action	Comment
PS124_5-2		2021-02-08T11:54:27	-70.41781	-30.00190	4487.3	CTD-RO	max depth	Responsible: S. Tippenhauer; SL= 52; SL=4.416 m; EL31
PS124_5-3		2021-02-08T17:32:12	-70.41621	-29.99969	4488.1	CTD-RO	max depth	Responsible: C. Völkner; SL= 4.004 m
PS124_5-4		2021-02-08T20:14:39	-70.41794	-29.99860	4488.9	CTD-RO	max depth	Responsible: S. Tippenhauer; SL= 1.005 m
PS124_5-5		2021-02-08T21:18:57	-70.41961	-30.00196	4488.8	ISP	Station start	Responsible: C. Voelkner
PS124_5-5		2021-02-08T21:18:57	-70.41772	-30.01135	4487.3	ISP	Station end	Responsible: C. Voelkner
PS124_5-6		2021-02-09T02:57:18	-70.41772	-30.01138	4487.3	OFOBS	Station start	Responsible: A. Purser
PS124_5-6		2021-02-09T02:57:18	-70.41853	-30.01864	4486.5	OFOBS	Station end	Responsible: A. Purser
PS124_5-7		2021-02-09T05:51:43	-70.41983	-30.02265	4486.8	MSC	max depth	Responsible: C. Flintrop; SL= 20 m; SE32.1; SL= 75m
PS124_5-8		2021-02-09T06:55:33	-70.41777	-30.02023	4487.1	ISP	Station start	Responsible: P. Holm
PS124_5-8		2021-02-09T06:55:33	-70.41823	-30.01920	4486.5	ISP	Station end	Responsible: P. Holm
PS124_0_ Underway-29		2021-02-09T16:00:00	-71.05921	-27.98370	4226.3	ICEOBS	Station start	
PS124_0_ Underway-29		2021-02-09T16:00:00	-54.24553	-53.97651	2291.1	ICEOBS	Station end	
PS124_6-1		2021-02-11T00:56:47	-73.71846	-25.72268	3221.1	CTD-RO	max depth	Responsible: C. Völkner; Clean CTD; SE32.1; SL=1523m
PS124_6-2		2021-02-11T03:24:30	-73.72358	-25.69847	3204.2	CTD-RO	max depth	Responsible: S. Tippenhauer; EL31; SL=3210m
PS124_6-3	AWI255-2	2021-02-11T05:40:00	-73.72151	-25.77915	3211.1	MOOR	Station start	Responsible: M. Monsees. recovery
PS124_6-3	AWI255-2	2021-02-11T05:40:00	-73.72495	-25.76176	3212.3	MOOR	Station end	Responsible: M. Monsees. recovery

Event label	Optional label	Date/Time	Latitude	Longitude	Depth [m]	Gear	Action	Comment
PS124_7-1	P6/SWS 06-01	2021-02-11T13:02:35	-74.01997	-28.09147	2480.1	MOOR	Station start	Recovery mooring P6/SWS 06-01
PS124_7-1	P6/SWS 06-01	2021-02-11T13:02:35	-74.02543	-28.09015	2526.5	MOOR	Station end	Recovery mooring P6/SWS 06-01
PS124_7-2	SWS 06-01 (W18)	2021-02-11T15:50:14	-74.01351	-28.09861	2538.0	MOOR	max depth	Deployment mooring SWS 06-01 (W18)
PS124_7-3		2021-02-11T18:35:00	-74.02520	-28.06576	2528.9	ISP	Station start	Responsible: P. Holm
PS124_7-3		2021-02-11T18:35:00	-74.02654	-28.07430	2526.4	ISP	Station end	Responsible: P. Holm
PS124_7-4		2021-02-11T20:32:23	-74.03028	-28.08005	2520.1	CTD-RO	max depth	Responsible: S. Tippenhauer; SL= 2501m
PS124_8-1		2021-02-12T03:27:02	-74.90691	-29.41029	390.7	OFOBS	Station start	Responsible: A. Purser
PS124_8-1		2021-02-12T03:27:02	-74.92565	-29.42784	406.2	OFOBS	Station end	Responsible: A. Purser
PS124_8-2		2021-02-12T07:00:00	-74.90741	-29.41053	407.2	B_LANDER	Station start	Responsible: M. Holtappels; Eddy Lander
PS124_8-2		2021-02-12T07:00:00	-74.90721	-29.40969	408.0	B_LANDER	Station end	Responsible: M. Holtappels; Eddy Lander
PS124_8-3		2021-02-12T08:39:46	-74.91249	-29.41725	403.0	B_LANDER	Station start	Responsible: F. Wenzhöfer; Lander/KUM
PS124_8-3		2021-02-12T08:39:46	-74.91275	-29.41655	402.8	B_LANDER	Station end	Responsible: F. Wenzhöfer; Lander/KUM
PS124_8-4		2021-02-12T11:45:08	-74.95319	-29.44423	399.0	DRIFT	max depth	Responsible: C. Flintrop; D-Trap/D
PS124_8-5		2021-02-12T12:35:45	-74.92035	-29.42207	401.9	CTD-RO	max depth	Responsible: S. Tippenhauer; EL31; SL=379m
PS124_8-6		2021-02-12T13:33:39	-74.92033	-29.42304	402.2	MSC	max depth	Responsible: C. Flintrop; 1.; SE32.1; SL=55m; surface
PS124_8-7		2021-02-12T14:03:07	-74.92051	-29.42322	400.3	ISP	Station start	Responsible: P. Holm
PS124_8-7		2021-02-12T14:03:07	-74.92083	-29.42404	398.4	ISP	Station end	Responsible: P. Holm

Event label	Optional label	Date/Time	Latitude	Longitude	Depth [m]	Gear	Action	Comment
PS124_8-8		2021-02-12T17:21:24	-74.92046	-29.42452	401.0	CTD-RO	max depth	Responsible: C. Völkner; Clean CTD; SL=375m
PS124_8-9		2021-02-12T17:58:19	-74.92042	-29.42427	401.1	CTD-RO	max depth	Responsible: S. Tippenhauer; SL=201m
PS124_8-10		2021-02-12T18:15:00	-74.92068	-29.42391	400.2	GRAB	Station start	SL= 381m
PS124_8-10		2021-02-12T18:15:00	-74.92021	-29.42322	405.3	GRAB	Station end	SL= 381m
PS124_8-11		2021-02-12T21:25:24	-74.91968	-29.42000	405.7	MUC	max depth	Responsible: F. Wenzhöfer; SL= 384m
PS124_9-1		2021-02-13T07:27:47	-74.00481	-30.50403	2189.8	CTD-RO	max depth	Responsible: S. Tippenhauer; SL=2169m
PS124_9-2	SWS05-01 (W17)	2021-02-13T09:28:32	-74.00494	-30.69397	2145.5	MOOR	Station start	Responsible: M . Moonsses; SWS05-01 (W17)
PS124_9-2	SWS05-01 (W17)	2021-02-13T09:28:32	-74.00499	-30.69920	2142.0	MOOR	Station end	Responsible: M . Moonsses; SWS05-01 (W17)
PS124_10-1		2021-02-13T13:41:47	-74.08622	-30.54237	1952.8	CTD-RO	max depth	Responsible: S. Tippenhauer; EL31; SL=1928m
PS124_11-1		2021-02-13T17:10:51	-74.26465	-30.30381	1544.1	CTD-RO	max depth	Responsible: S. Tippenhauer; SL=1519m
PS124_11-2		2021-02-13T19:07:49	-74.26468	-30.30445	1545.2	CTD-RO	max depth	Responsible: Ch. Völkner; SL=1494m
PS124_11-3		2021-02-13T20:45:39	-74.26459	-30.30285	1547.0	MUC	max depth	Responsible: F. Wenzhöfer; SL= 1477m
PS124_12-1		2021-02-13T23:31:15	-74.36495	-30.22488	1253.2	CTD-RO	max depth	Responsible: S Tippenhauer; SL= 1228m
PS124_13-1		2021-02-14T02:03:29	-74.50729	-29.94123	905.0	CTD-RO	max depth	Responsible: S. Tippenhauer; EL31; SL=880m
PS124_14-1	M3	2021-02-14T07:01:00	-74.55000	-29.91734	754.9	MOOR	Station start	Mooring M3. Responsible: M. Monsees

Event label	Optional label	Date/Time	Latitude	Longitude	Depth [m]	Gear	Action	Comment
PS124_14-1	M3	2021-02-14T07:01:00	-74.55903	-29.98506	640.4	MOOR	Station end	Mooring M3. Responsible: M. Monsees
PS124_15-1	M6	2021-02-14T10:00:07	-74.59725	-29.92732	530.9	MOOR	max depth	Responsible: Monsses; Recovery M6 (swedish Mooring)
PS124_16-1		2021-02-14T14:43:24	-75.13504	-30.44789	436.3	DRIFT	max depth	Responsible: C. Flintrop
PS124_16-2		2021-02-14T16:05:02	-75.14233	-30.44619	451.6	CTD-RO	max depth	Responsible: S. Tippenhauer; SL=431m
PS124_16-3		2021-02-14T17:04:33	-75.14274	-30.44609	452.7	CTD-RO	max depth	Responsible: Ch. Völkner; SL=389m
PS124_16-4		2021-02-14T17:36:20	-75.14269	-30.44567	452.8	MSC	max depth	Responsible: C. Flintrop; SL100m
PS124_16-5		2021-02-14T18:32:49	-75.14239	-30.44422	452.2	ISP	Station start	Responsible: P. Holm
PS124_16-5		2021-02-14T18:32:49	-75.14284	-30.44700	453.6	ISP	Station end	Responsible: P. Holm
PS124_16-6		2021-02-14T20:16:10	-75.14287	-30.44703	454.3	MUC	max depth	Responsible: F. Wenzhöfer; SL= 433m
PS124_16-7		2021-02-14T21:00:51	-75.14282	-30.44521	454.0	GRAB	Station start	S. Metz; SL= 435m
PS124_16-7		2021-02-14T21:00:51	-75.14561	-30.44863	455.6	GRAB	Station end	S. Metz; SL= 435m
PS124_16-8		2021-02-14T22:36:26	-75.14564	-30.44874	455.5	OFOBS	Station start	Responsible: A. Purser
PS124_16-8		2021-02-14T22:36:26	-75.14133	-30.26953	437.5	OFOBS	Station end	Responsible: A. Purser
PS124_17-1		2021-02-15T06:40:10	-74.92075	-29.42386	400.4	MUC	max depth	Responsible: F. Wenzhöfer; SL=384m
PS124_8-12		2021-02-15T07:57:58	-74.90802	-29.41645	405.0	B_LANDER	Station start	Responsible: M. Holtappels; Eddy Lander; recovered
PS124_8-12		2021-02-15T07:57:58	-74.91581	-29.43101	407.8	B_LANDER	Station end	Responsible: M. Holtappels; Eddy Lander; recovered
PS124_18-1	P4	2021-02-15T11:20:08	-74.84973	-30.39153	448.3	MOOR	Station start	P4. Responsible: M. Monsees

Event label	Optional label	Date/Time	Latitude	Longitude	Depth [m]	Gear	Action	Comment
PS124_18-1	P4	2021-02-15T11:20:08	-74.85205	-30.38287	462.9	MOOR	Station end	P4. Responsible: M. Monsees
PS124_8-13		2021-02-15T14:46:38	-74.91086	-29.43013	392.0	B_LANDER	Station start	Responsible: F. Wenzhöfer. Recovery KUM Lander
PS124_8-13		2021-02-15T14:46:38	-74.91083	-29.41217	399.5	B_LANDER	Station end	Responsible: F. Wenzhöfer. Recovery KUM Lander
PS124_19-1		2021-02-15T16:48:24	-74.90843	-29.41369	403.0	MUC	max depth	Responsible: F. Wenzhöfer; SL=386m
PS124_20-1		2021-02-15T19:32:32	-74.85015	-30.38477	463.2	CTD-RO	max depth	Responsible: S. Tippenhauer; SL=442m
PS124_21-1		2021-02-15T21:13:18	-74.86849	-30.67064	496.5	CTD-RO	max depth	Responsible: S. Tippenhauer; SL= 474m
PS124_21-2		2021-02-15T22:24:15	-74.86814	-30.66731	497.0	CTD-RO	max depth	Responsible: C. Völkner; SL=441m
PS124_21-4		2021-02-15T23:32:27	-74.86814	-30.66810	497.4	ISP	Station start	Responsible: P. Holm
PS124_21-4		2021-02-15T23:32:27	-74.86774	-30.66494	496.6	ISP	Station end	Responsible: P. Holm
PS124_21-3		2021-02-16T00:21:26	-74.86764	-30.66439	496.8	MSC	max depth	Responsible: C. Flintrop; device broke, station cancelled.; SE32.1; SL=100m
PS124_21-5		2021-02-16T01:01:30	-74.86802	-30.66364	496.0	MUC	max depth	Responsible: F. Wenzhöfer; GE72.1; SL=478 m; surface
PS124_21-6		2021-02-16T01:38:09	-74.86804	-30.66363	495.9	GRAB	Station start	Responsible: S. Pineda-Metz; GE72.1; SL=472m; surface
PS124_21-6		2021-02-16T01:38:09	-74.86821	-30.66469	495.3	GRAB	Station end	Responsible: S. Pineda-Metz; GE72.1; SL=472m; surface
PS124_21-7		2021-02-16T02:57:53	-74.86831	-30.66366	495.1	OFOBS	Station start	Responsible: A. Purser
PS124_21-7		2021-02-16T02:57:53	-74.87082	-30.59860	468.2	OFOBS	Station end	Responsible: A. Purser

Event label	Optional label	Date/Time	Latitude	Longitude	Depth [m]	Gear	Action	Comment
PS124_22-1	P3	2021-02-16T07:16:40	-74.85110	-30.71930	484.1	MOOR	Station start	Mooring P3, Responsible: M. Monsees
PS124_22-1	P3	2021-02-16T07:16:40	-74.84993	-30.71601	502.8	MOOR	Station end	Mooring P3, Responsible: M. Monsees
PS124_23-1	P1	2021-02-16T09:39:49	-74.85211	-31.04880	539.6	MOOR	Station start	Responsible: Monsess // P1 Recovery
PS124_23-1	P1	2021-02-16T09:39:49	-74.85270	-31.06037	577.3	MOOR	Station end	Responsible: Monsess // P1 Recovery
PS124_23-2		2021-02-16T10:55:18	-74.85233	-31.06108	574.9	CTD-RO	max depth	Responsible: Tippenhauer; SL= 556m
PS124_24-1		2021-02-16T12:32:36	-74.84160	-31.37919	603.0	CTD-RO	max depth	Responsible: S. Tippenhauer; EL31; SL=580m
PS124_24-2	P2	2021-02-16T13:00:59	-74.83930	-31.38238	608.4	MOOR	Station start	Recovery mooring P2; Responsible: M Monsees
PS124_24-2	P2	2021-02-16T13:00:59	-74.84856	-31.38248	600.9	MOOR	Station end	Recovery mooring P2; Responsible: M Monsees
PS124_25-1	S2-2018_E	2021-02-16T15:09:50	-74.85806	-31.84419	633.9	MOOR	Station start	Responsible: M. Monsees; Recovery mooring S2-2018_E
PS124_25-1	S2-2018_E	2021-02-16T15:09:50	-74.85323	-31.84215	635.5	MOOR	Station end	Responsible: M. Monsees; Recovery mooring S2-2018_E
PS124_26-1		2021-02-16T17:29:45	-74.85188	-31.90064	629.3	DRIFT	max depth	Responsible: C. Flintrop
PS124_26-2		2021-02-16T18:21:06	-74.85551	-31.83047	635.6	CTD-RO	max depth	Responsible: S. Tippenhauer; SL=614m
PS124_26-3		2021-02-16T19:26:28	-74.85542	-31.83039	635.8	MSC	max depth	Responsible: C. Flintrop; SL=90m
PS124_26-4		2021-02-16T19:40:40	-74.85536	-31.83044	636.2	ISP	Station start	Responsible: P. Holm
PS124_26-4		2021-02-16T19:40:40	-74.85557	-31.83139	637.3	ISP	Station end	Responsible: P. Holm

Event label	Optional label	Date/Time	Latitude	Longitude	Depth [m]	Gear	Action	Comment
PS124_26-5		2021-02-16T20:55:48	-74.85490	-31.83251	637.9	CTD-RO	max depth	Responsible: C. Völkner; SL=599m
PS124_26-6		2021-02-16T21:37:03	-74.85455	-31.83305	636.4	CTD-RO	max depth	Responsible: S. Tippenhauer; SL=143m
PS124_26-7		2021-02-16T23:46:36	-74.84988	-31.84162	633.5	OFOBS	Station start	Responsible: A. Purser
PS124_26-7		2021-02-16T23:46:36	-74.84708	-31.95294	612.3	OFOBS	Station end	Responsible: A. Purser
PS124_26-8		2021-02-17T04:30:00	-74.84798	-31.85134	635.9	GRAB	Station start	Responsible: Pineda-Metz; SL=606m
PS124_26-8		2021-02-17T04:30:00	-74.84805	-31.85133	636.1	GRAB	Station end	Responsible: Pineda-Metz; SL=606m
PS124_26-9		2021-02-17T06:26:37	-74.84797	-31.85114	636.2	MUC	max depth	Responsible: F. Wenzhöfer; SL=604m
PS124_26-10		2021-02-17T07:14:16	-74.84807	-31.85101	636.5	MUC	max depth	Responsible: F. Wenzhöfer; SL=603m
PS124_26-11		2021-02-17T08:06:17	-74.84819	-31.85097	636.9	B_LANDER	Station start	Responsible: M. Holtappels; Eddy Lander
PS124_26-11		2021-02-17T08:06:17	-74.84599	-31.87415	635.2	B_LANDER	Station end	Responsible: M. Holtappels; Eddy Lander
PS124_26-12		2021-02-17T09:26:48	-74.84591	-31.87437	635.4	B_LANDER	Station start	Responsible: Wenzhöfer; KUM Lander
PS124_26-12		2021-02-17T09:26:48	-74.84539	-31.87860	633.6	B_LANDER	Station end	Responsible: Wenzhöfer; KUM Lander
PS124_27-1	S2 -2017-E	2021-02-17T11:04:08	-74.85610	-32.09967	593.1	MOOR	Station start	Responsible: S. Osterhus; Recovery S2 -2017-E
PS124_27-1	S2 -2017-E	2021-02-17T11:04:08	-74.85042	-32.11023	615.7	MOOR	Station end	Responsible: S. Osterhus; Recovery S2 -2017-E
PS124_27-2		2021-02-17T12:29:18	-74.84990	-32.11225	615.3	CTD-RO	max depth	Responsible: S. Tippenhauer; EL31; SL=593m

Event label	Optional label	Date/Time	Latitude	Longitude	Depth [m]	Gear	Action	Comment
PS124_28-1	S2-2018-C	2021-02-17T13:51:32	-74.83804	-32.52537	577.9	MOOR	Station start	Recovery mooring S2-2018-C; Responsible: M. Monsees
PS124_28-1	S2-2018-C	2021-02-17T13:51:32	-74.83437	-32.51537	598.6	MOOR	Station end	Recovery mooring S2-2018-C; Responsible: M. Monsees
PS124_29-1	S2-2018_W	2021-02-17T15:27:02	-74.85441	-33.01344	594.3	MOOR	max depth	Recovery mooring S2-2018_W Responsible: M. Monsees
PS124_30-1		2021-02-17T17:36:13	-74.85215	-32.99095	593.6	CTD-RO	max depth	Responsible: S. Tippenhauer; SL=574m
PS124_30-2		2021-02-17T18:46:20	-74.85187	-32.99051	593.3	CTD-RO	max depth	Christian Völkner; SL=570m
PS124_30-3		2021-02-17T19:22:21	-74.85184	-32.99028	593.4	MSC	max depth	Responsible: C. Flintrop; SL=90m
PS124_30-4		2021-02-17T19:37:00	-74.85176	-32.99014	593.6	ISP	Station start	Responsible: P. Holm
PS124_30-4		2021-02-17T19:37:00	-74.85187	-32.99163	594.4	ISP	Station end	Responsible: P. Holm
PS124_30-5		2021-02-17T20:55:01	-74.85241	-32.99169	594.9	MUC	max depth	Responsible: F. Wenzhöfer; SL= 568m
PS124_30-6		2021-02-17T21:40:28	-74.85202	-32.99269	595.3	MUC	max depth	Responsible: F. Wenzhöfer; SL0=571m
PS124_0_ Underway-31		2021-02-17T22:00:00	-74.85204	-32.99045	594.4	HS	Station start	Responsible: Purser
PS124_0_ Underway-31		2021-02-17T22:00:00	-54.24642	-53.97533	2295.6	HS	Station end	Responsible: Purser
PS124_30-8		2021-02-17T22:00:53	-74.85201	-32.99033	594.8	HS	Station start	Responsible: Purser
PS124_30-8		2021-02-17T22:00:53	-74.89179	-32.67263	581.7	HS	Station end	Responsible: Purser
PS124_30-7		2021-02-18T00:03:11	-74.81136	-32.70602	578.2	OFOBS	Station start	Responsible: A. Purser
PS124_30-7		2021-02-18T00:03:11	-74.78096	-32.56393	591.1	OFOBS	Station end	Responsible: A. Purser

Event label	Optional label	Date/Time	Latitude	Longitude	Depth [m]	Gear	Action	Comment
PS124_31-1		2021-02-18T06:49:43	-74.72028	-32.55323	601.7	CTD-RO	max depth	Responsible: S. Tippenhauer; SL=583m
PS124_31-2		2021-02-18T07:21:34	-74.71837	-32.56410	601.1	DRIFT	max depth	Recovery, Responsible: C. Flintrop
PS124_31-3		2021-02-18T11:16:00	-74.69121	-32.67716	599.3	ZODIAK	Station start	Responsible: P. Holm. Mantatrawl for Microplastic
PS124_31-3		2021-02-18T11:16:00	-74.68899	-32.70433	600.2	ZODIAK	Station end	Responsible: P. Holm. Mantatrawl for Microplastic
PS124_26-13		2021-02-18T14:33:25	-74.84539	-31.86803	635.7	B_LANDER	Station start	Recovery KUM Lander Responsible: F. Wenzhöfer
PS124_26-13		2021-02-18T14:33:25	-74.84475	-31.87957	630.2	B_LANDER	Station end	Recovery KUM Lander Responsible: F. Wenzhöfer
PS124_26-14		2021-02-18T15:49:46	-74.84820	-31.84840	637.3	B_LANDER	max depth	Responsible: M. Holtappels; Eddy Lander; recovery
PS124_32-1		2021-02-18T23:41:18	-74.74718	-35.22219	498.5	CTD-RO	max depth	Responsible: Tippenhauer; SL= 89m
PS124_33-1		2021-02-19T00:47:01	-74.74966	-35.18532	500.2	CTD-RO	max depth	Responsible: S. Tippenhauer; EL31; SL=485m
PS124_33-2		2021-02-19T01:50:48	-74.75012	-35.15103	502.9	CTD-RO	max depth	Responsible: C. Völkner; SE32.1; SL=405m
PS124_33-3		2021-02-19T02:20:00	-74.75011	-35.13600	502.3	MSC	max depth	Responsible: C. Flintrop; SE32.1; SL=30m; surface
PS124_33-4		2021-02-19T02:30:19	-74.74771	-35.13783	502.5	OFOBS	Station start	Responsible: A. Purser
PS124_33-4		2021-02-19T02:30:19	-74.71877	-35.11615	504.1	OFOBS	Station end	Responsible: A. Purser
PS124_33-5		2021-02-19T06:47:11	-74.72494	-35.18026	497.0	MUC	max depth	Responsible: F. Wenzhöfer; SL=472m
PS124_33-6		2021-02-19T07:37:05	-74.72362	-35.16423	497.2	GRAB	Station start	Responsible: Pineda-Metz; SL=472m

Event label	Optional label	Date/Time	Latitude	Longitude	Depth [m]	Gear	Action	Comment
PS124_33-6		2021-02-19T07:37:05	-74.72198	-35.15014	499.4	GRAB	Station end	Responsible: Pineda-Metz; SL=472m
PS124_33-7		2021-02-19T08:59:40	-74.68762	-35.14388	484.1	B_LANDER	max depth	Responsible: M. Holtappels; Eddy Lander
PS124_20210219_SB01	WMO7101592	2021-02-19T10:35:00	-75.08600	32.16670		BUOY_SNOW	max depth	deployment of buoy 2021S114; not logged in D-Ship
PS124_33-8		2021-02-19T10:51:20	-74.68080	-35.17850	498.9	B_LANDER	Station start	Responsible: Wenzhöfer; Lander KUM deployed
PS124_33-8		2021-02-19T10:51:20	-74.68283	-35.18209	499.1	B_LANDER	Station end	Responsible: Wenzhöfer. Lander KUM deployed
PS124_0_Underway-17		2021-02-19T15:17:52	-74.75004	-34.87211	506.5	UWPCO2	Station start	
PS124_0_Underway-17		2021-02-19T15:17:52	-54.24761	-53.97378	2304.5	UWPCO2	Station end	
PS124_34-1		2021-02-20T09:49:55	-74.40386	-34.97611	860.5	CTD-RO	max depth	Responsible: S. Tippenhauer; SL=841m
PS124_35-1		2021-02-20T11:49:07	-74.32831	-34.93977		CTD-RO	max depth	Responsible: Tippenhauer; SL=1216m
PS124_36-1		2021-02-20T13:53:21	-74.22925	-34.95142	1601.7	CTD-RO	max depth	EL31; SL=1622m
PS124_37-1		2021-02-20T19:01:15	-74.57999	-36.40273	424.7	CTD-RO	max depth	Responsible: S. Tippenhauer; SL=412m
PS124_37-2		2021-02-20T19:48:46	-74.58116	-36.39624	425.3	MSC	max depth	Responsible: C. Flintrop; SL=50m
PS124_37-3		2021-02-20T20:05:09	-74.58037	-36.39776	424.0	ISP	Station start	Responsible: P. Holm
PS124_37-3		2021-02-20T20:05:09	-74.58099	-36.40054	423.5	ISP	Station end	Responsible: P. Holm
PS124_37-4		2021-02-20T21:05:37	-74.59492	-36.41409	420.5	GRAB	Station start	Responsible: P. Metz; SL= 399m

Event label	Optional label	Date/Time	Latitude	Longitude	Depth [m]	Gear	Action	Comment
PS124_37-4		2021-02-20T21:05:37	-74.59985	-36.44772	412.3	GRAB	Station end	Responsible: P. Metz; SL= 399m
PS124_37-5		2021-02-20T22:20:24	-74.60256	-36.46237	415.3	MUC	max depth	Responsible: F. Wenzhöfer; SL= 396m
PS124_37-6		2021-02-21T00:30:02	-74.58106	-36.40403	421.4	OFOBS	Station start	Responsible: A. Purser
PS124_37-6		2021-02-21T00:30:02	-74.61235	-36.42789	415.0	OFOBS	Station end	Responsible: A. Purser
PS124_33-9		2021-02-21T07:49:22	-74.68453	-35.15648	483.4	B_LANDER	Station start	Responsible: M. Holtappels Eddy Lander; recovery
PS124_33-9		2021-02-21T07:49:22	-74.68079	-35.14676		B_LANDER	Station end	Responsible: M. Holtappels Eddy Lander; recovery
PS124_33-10		2021-02-21T10:01:46	-74.68086	-35.18899		B_LANDER	Station start	Responsible: Wenzhöfer; Kum Lander
PS124_33-10		2021-02-21T10:01:46	-74.68016	-35.17833	497.8	B_LANDER	Station end	Responsible: Wenzhöfer; Kum Lander
PS124_38-1		2021-02-21T14:33:47	-74.50993	-36.37990	849.5	CTD-RO	max depth	Responsible: S. Tippenhauer; EL31; SL=833m
PS124_39-1	P7	2021-02-21T15:29:54	-74.51925	-36.36774	768.3	MOOR	Station start	Deployment mooring P7; Responsible: M. Monsees
PS124_39-1	P7	2021-02-21T15:29:54	-74.51552	-36.38019	819.2	MOOR	Station end	Deployment mooring P7; Responsible: M. Monsees
PS124_40-1		2021-02-21T17:43:00	-74.67159	-36.01654	429.7	CTD-RO	max depth	Responsible: S. Tippenauer; SL=414m
PS124_41-1		2021-02-21T20:09:01	-74.55570	-36.01867	514.4	CTD-RO	max depth	Responsible: S. Tippenhauer SL= 497m
PS124_42-1		2021-02-21T21:45:57	-74.54391	-36.01580	602.4	CTD-RO	max depth	Responsible: Tippenhauer; SL= 588m
PS124_43-1		2021-02-21T23:42:48	-74.45845	-36.00827	1063.8	CTD-RO	max depth	Responsible: Tippenhauer; SL=1049m

Event label	Optional label	Date/Time	Latitude	Longitude	Depth [m]	Gear	Action	Comment
PS124_44-1		2021-02-22T01:32:38	-74.42172	-36.02508	1234.2	CTD-RO	max depth	Responsible: S. Tippenhauer; EL31; SL=1221m
PS124_45-1		2021-02-22T02:59:03	-74.36271	-36.08281	1428.0	OFOBS	Station start	Responsible: A. Purser
PS124_45-1		2021-02-22T02:59:03	-74.36613	-36.02331	1445.5	OFOBS	Station end	Responsible: A. Purser
PS124_45-2		2021-02-22T06:38:23	-74.36614	-36.01985	1445.2	CTD-RO	max depth	Responsible: S. Tippenhauer; SL=1428m
PS124_45-3		2021-02-22T08:24:41	-74.36261	-36.04563	1459.4	CTD-RO	max depth	Responsible: C. Völkner; SL=1397m
PS124_45-4		2021-02-22T09:29:02	-74.35028	-36.04133	1505.5	MSC	max depth	Responsible: Flintrop; SL= 75m
PS124_45-5		2021-02-22T09:57:43	-74.34751	-36.04839	1519.2	ISP	Station start	Responsible: P. Holm
PS124_45-5		2021-02-22T09:57:43	-74.34668	-36.04242	1521.4	ISP	Station end	Responsible: P. Holm
PS124_45-6		2021-02-22T10:55:44	-74.34010	-36.06701	1540.6	GRAB	Station start	Responsible: S. Metz; SL=1482m
PS124_45-6		2021-02-22T10:55:44	-74.34174	-36.05942	1538.8	GRAB	Station end	Responsible: S. Metz; SL=1482m
PS124_45-7	SWS-W2	2021-02-22T12:32:45	-74.36898	-35.94408	1430.9	MOOR	Station start	Responsible: M. Monsees; Deployment mooring SWS-W2
PS124_45-7	SWS-W2	2021-02-22T12:32:45	-74.36445	-35.95295	1445.3	MOOR	Station end	Responsible: M. Monsees; Deployment mooring SWS-W2
PS124_46-1		2021-02-22T15:18:58	-74.41456	-36.37150	1244.5	CTD-RO	max depth	Responsible: S. Tippenhauer; EL31; SL=1222m
PS124_46-2		2021-02-22T16:15:00	-74.41493	-36.36573	1243.8	GRAB	Station start	Responsible: Pineda-Metz; SL=1186m
PS124_46-2		2021-02-22T16:15:00	-74.41653	-36.37654	1237.1	GRAB	Station end	Responsible: Pineda-Metz; SL=1186m
PS124_46-3		2021-02-22T18:26:25	-74.36434	-36.54602	1199.2	OFOBS	Station start	Responsible: A. Purser

Event label	Optional label	Date/Time	Latitude	Longitude	Depth [m]	Gear	Action	Comment
PS124_46-3		2021-02-22T18:26:25	-74.37732	-36.50421	1160.5	OFOBS	Station end	Responsible: A. Purser
PS124_47-1		2021-02-22T23:18:53	-74.28113	-36.06717	1717.8	CTD-RO	max depth	Responsible: Trippenhauer; SL= 1694m
PS124_47-2		2021-02-23T00:48:31	-74.25348	-36.23372	1726.3	OFOBS	Station start	Responsible: A. Purser
PS124_47-2		2021-02-23T00:48:31	-74.25497	-36.09597	1787.1	OFOBS	Station end	Responsible: A. Purser
PS124_47-3		2021-02-23T06:15:05	-74.25498	-36.09622	1786.8	GRAB	Station start	Responsible: S. Pineda-Metz; SL=1710m
PS124_47-3		2021-02-23T06:15:05	-74.24810	-36.07314	1761.2	GRAB	Station end	Responsible: S. Pineda-Metz; SL=1710m
PS124_48-1		2021-02-23T11:02:27	-74.05827	-35.79581	2026.8	CTD-RO	max depth	Responsible: Tippenhauer; SL= 2013m
PS124_48-2	SWS-D1	2021-02-23T13:00:00	-74.05411	-35.77699	2094.4	MOOR	Station start	Deployment mooring SWS-D1; Responsible: M. Monsees
PS124_48-2	SWS-D1	2021-02-23T13:00:00	-74.05182	-35.77433	2097.5	MOOR	Station end	Deployment mooring SWS-D1; Responsible: M. Monsees
PS124_49-1	AWI256-2	2021-02-24T07:06:59	-73.99839	-32.36102	1742.6	MOOR	Station start	Responsible: M. Monsees; Recovery not successful
PS124_49-1	AWI256-2	2021-02-24T07:06:59	-73.99567	-32.36492	1835.2	MOOR	Station end	Responsible: M. Monsees; Recovery not successful
PS124_49-2		2021-02-24T09:58:04	-73.99651	-32.41445	1839.5	CTD-RO	max depth	Responsible: Tippenhauer SL= 1818m
PS124_50-1		2021-02-24T13:04:20	-74.08201	-32.33856	1572.9	CTD-RO	max depth	Responsible: S. Tippenhauer; EL31; SL=1549m
PS124_51-1		2021-02-24T17:41:19	-74.17715	-32.34712	1233.8	CTD-RO	max depth	Responsible: S. Tippenhauer; SL=1208m
PS124_52-1		2021-02-24T19:48:32	-74.25975	-32.33084	930.9	CTD-RO	max depth	Responsible: S. Tippenhauer; SL=905m

Event label	Optional label	Date/Time	Latitude	Longitude	Depth [m]	Gear	Action	Comment
PS124_52-2		2021-02-24T20:19:24	-74.26004	-32.33384	929.5	GRAB	Station start	Responsible: S. Metz; SL0= 880m
PS124_52-2		2021-02-24T20:19:24	-74.25997	-32.34312	931.5	GRAB	Station end	Responsible: S. Metz; SL0= 880m
PS124_53-1		2021-02-24T22:35:30	-74.32154	-32.36076	653.2	CTD-RO	max depth	Responsible: Trippenhauer; SL= 630m
PS124_54-1		2021-02-25T02:10:56	-74.63476	-33.54469	588.0	OFOBS	Station start	Responsible: A. Purser
PS124_54-1		2021-02-25T02:10:56	-74.66598	-33.55783	591.1	OFOBS	Station end	Responsible: A. Purser
PS124_54-2		2021-02-25T06:31:27	-74.66526	-33.56029	592.1	CTD-RO	max depth	Responsible: S. Tippenhauer; SL=83m
PS124_54-3		2021-02-25T07:38:55	-74.66567	-33.56625	593.0	CTD-RO	max depth	Responsible: S. Tippenhauer; SL=574m
PS124_54-4		2021-02-25T08:48:02	-74.66587	-33.57947	591.3	CTD-RO	max depth	C. Völkner; SL= 527m
PS124_54-5		2021-02-25T09:20:21	-74.66671	-33.58703	590.0	MSC	max depth	Responsible: Flintrop; SL=25m
PS124_54-6		2021-02-25T09:42:23	-74.66766	-33.59383	589.6	MSC	max depth	Responsible: Flintrop; SL=60m
PS124_54-7		2021-02-25T10:11:28	-74.66801	-33.59523	589.1	ISP	Station start	Responsible: P. Holm
PS124_54-7		2021-02-25T10:11:28	-74.68625	-33.56971	588.8	ISP	Station end	Responsible: P. Holm
PS124_54-8		2021-02-25T11:57:36	-74.68315	-33.57573	588.9	DRIFT	max depth	Responsible: Flintrop
PS124_54-9		2021-02-25T12:10:55	-74.68346	-33.55079	594.8	B_LANDER	Station start	Deployment KUM Lander; Responsible: F. Wenzhöfer
PS124_54-9		2021-02-25T12:10:55	-74.68741	-33.54756	586.4	B_LANDER	Station end	Deployment KUM Lander. Responsible: F. Wenzhöfer
PS124_54-10		2021-02-25T14:00:25	-74.69882	-33.54895	587.5	B_LANDER	Station start	Responsible: M. Holtappels; Eddy Lander. deployment
PS124_54-10		2021-02-25T14:00:25	-74.69917	-33.55073	588.1	B_LANDER	Station end	Responsible: M. Holtappels; Eddy Lander. deployment

Event label	Optional label	Date/Time	Latitude	Longitude	Depth [m]	Gear	Action	Comment
PS124_54-11		2021-02-25T15:22:30	-74.70706	-33.57086	584.6	GRAB	Station start	Responsible: S. Pineda-Metz; SL=563m
PS124_54-11		2021-02-25T15:22:30	-74.70653	-33.57895	587.4	GRAB	Station end	Responsible: S. Pineda-Metz; SL=563m
PS124_54-12		2021-02-25T16:56:03	-74.70721	-33.57760	588.4	MUC	max depth	Responsible: F. Wenzhöfer; SL=559m
PS124_55-1		2021-02-25T20:37:42	-74.78599	-34.92985	520.0	CTD-RO	max depth	Responsible: Flintrop; SL= 498m
PS124_56-1		2021-02-25T22:25:24	-74.79794	-34.53729	546.8	CTD-RO	max depth	Responsible: Flintrop; SL= 524m
PS124_57-1		2021-02-26T00:08:00	-74.80961	-34.14482	555.2	CTD-RO	max depth	Responsible: S. Tippenhauer; EL31; SL=535m
PS124_58-1		2021-02-26T01:51:33	-74.82471	-33.75804	567.2	CTD-RO	max depth	Responsible: S. Tippenhauer; EL31; SL=549m
PS124_59-1		2021-02-26T03:27:01	-74.84116	-33.38876	581.3	CTD-RO	max depth	Responsible: S. Tippenhauer; EL31; SL=558m
PS124_60-1		2021-02-26T05:13:19	-74.85301	-33.00118	597.5	CTD-RO	max depth	Responsible: S. Tippenhauer; SL=579m
PS124_60-2	S2-2021_W	2021-02-26T05:54:32	-74.85310	-33.00063	597.2	MOOR	max depth	S2-2021_W deployment; Responsible: M. Monsees
PS124_61-1		2021-02-26T08:55:25	-74.83201	-32.52516	593.5	CTD-RO	max depth	Responsible: Tippenhauer; SL=572m
PS124_61-2	S2-2021-C	2021-02-26T09:55:25	-74.83315	-32.55356	597.3	MOOR	max depth	S2-2021-C Mooring deployment; Responsible: M. Monsees
PS124_54-13		2021-02-26T12:51:02	-74.64810	-33.71259	570.7	DRIFT	max depth	Recovery; Responsible: C. Flintrop
PS124_62-1		2021-02-26T14:22:36	-74.64384	-33.71754	589.4	CTD-RO	max depth	Responsible: S. Tippenhauer; EL31; SL=329m

Event label	Optional label	Date/Time	Latitude	Longitude	Depth [m]	Gear	Action	Comment
PS124_54-14		2021-02-26T15:11:03	-74.69860	-33.54878	567.4	B_LANDER	max depth	Responsible: M. Holtappels; Eddy Lander; recovery
PS124_54-15		2021-02-26T16:40:29	-74.68609	-33.56016	589.9	B_LANDER	max depth	KUM Lander recovery. Responsible: F. Wenzhöfer.
PS124_62-2		2021-02-26T18:25:12	-74.70680	-33.57603	589.1	MUC	max depth	Responsible: F. Wenzhöfer; Winde 72.1 SL=562m
PS124_63-1		2021-02-27T00:15:24	-74.85007	-30.96381	536.8	OFOBS	Station start	Responsible: A. Purser
PS124_63-1		2021-02-27T00:15:24	-74.89245	-30.51155	476.2	OFOBS	Station end	Responsible: A. Purser
PS124_64-1		2021-02-27T07:52:59	-74.85082	-31.06317	572.3	CTD-RO	max depth	Responsible: S. Tippenhauer; SL=556m
PS124_64-2	P1	2021-02-27T08:49:45	-74.84304	-31.02156	560.7	MOOR	Station start	Responsible: Monsses / Mooring P1 deployed
PS124_64-2	P1	2021-02-27T08:49:45	-74.84867	-31.02221	561.1	MOOR	Station end	Responsible: Monsses / Mooring P1 deployed
PS124_65-1	P2	2021-02-27T10:54:54	-74.85709	-31.38220	609.1	MOOR	Station start	Responsible: Monsees / Morring P2 deployed
PS124_65-1	P2	2021-02-27T10:54:54	-74.85367	-31.37842	606.4	MOOR	Station end	Responsible: Monsees / Morring P2 deployed
PS124_65-2		2021-02-27T12:06:37	-74.85124	-31.32443	606.5	CTD-RO	max depth	Responsible: Tippenhauer; EL31; SL=585m
PS124_66-1		2021-02-27T14:25:18	-74.85229	-31.83128	631.6	CTD-RO	max depth	Responsible: S. Tippenhauer; EL31; SL=608m
PS124_66-2	S2-2021-E	2021-02-27T14:59:28	-74.85450	-31.83788	635.1	MOOR	Station start	Deployment mooring S2-2021-E; Responsible: M. Monsees
PS124_66-2	S2-2021-E	2021-02-27T14:59:28	-74.85298	-31.83075	631.3	MOOR	Station end	Deployment mooring S2-2021-E; Responsible: M. Monsees
PS124_67-1		2021-02-27T17:34:21	-74.72725	-31.40988	571.2	OFOBS	Station start	Responsible: A. Purser

Event label	Optional label	Date/Time	Latitude	Longitude	Depth [m]	Gear	Action	Comment
PS124_67-1		2021-02-27T17:34:21	-74.86075	-30.42717	467.2	OFOBS	Station end	Responsible: A. Purser
PS124_67-2	WetCam/ FishNests	2021-02-28T07:46:55	-74.85730	-30.80431	515.7	MOOR	Station start	Responsible: M. Monsees
PS124_67-2	WetCam/ FishNests	2021-02-28T07:46:55	-74.86284	-30.81192	522.3	MOOR	Station end	Responsible: M. Monsees
PS124_68-1		2021-02-28T17:55:04	-76.09976	-30.30265	467.1	ISP	Station start	Responsible: Ch. Voelkner; SL=36m
PS124_68-1		2021-02-28T17:55:04	-76.09531	-30.38305	470.9	ISP	Station end	Responsible: Ch. Voelkner; SL=36m
PS124_68-2		2021-02-28T22:27:14	-76.10267	-30.30485	471.7	CTD-RO	max depth	Responsible:: Tippenhauer; SL= 75m
PS124_68-3		2021-02-28T23:26:28	-76.10296	-30.31304	470.7	CTD-RO	max depth	Responsible: Tippenhauer; SL= 448m
PS124_68-4		2021-03-01T00:22:07	-76.10202	-30.31894	468.9	CTD-RO	max depth	Responsible: C. Völkner; SE32.1; SL=412m
PS124_68-5		2021-03-01T01:07:43	-76.08962	-30.33692	475.4	OFOBS	Station start	Responsible: A. Purser
PS124_68-5		2021-03-01T01:07:43	-76.10189	-30.29028	472.2	OFOBS	Station end	Responsible: A. Purser
PS124_68-6		2021-03-01T04:26:23	-76.08945	-30.33715	474.2	MUC	max depth	Responsible: F. Wenzhöfer; SL=450m
PS124_68-7		2021-03-01T05:12:21	-76.06626	-30.27807	466.9	GRAB	Station start	Responsible: F. Wenzhöfer; SL=444m
PS124_68-7		2021-03-01T05:12:21	-76.06647	-30.28495	468.1	GRAB	Station end	Responsible: F. Wenzhöfer; SL=444m
PS124_68-8		2021-03-01T06:44:27	-76.08969	-30.33621	476.2	MUC	max depth	Responsible: F. Wenzhöfer; SL=454m
PS124_68-9		2021-03-01T08:12:41	-76.08544	-30.30377	470.6	B_LANDER	Station start	Responsible: Wenzhöfer; KUM Lander recovery
PS124_68-9		2021-03-01T08:12:41	-76.09352	-30.35260	479.1	B_LANDER	Station end	Responsible: Wenzhöfer; KUM Lander recovery

Event label	Optional label	Date/Time	Latitude	Longitude	Depth [m]	Gear	Action	Comment
PS124_68-10		2021-03-01T09:46:46	-76.08168	-30.30780	470.4	B_LANDER	Station start	Responsible: M. Holtappels; Eddy Lander
PS124_68-10		2021-03-01T09:46:46	-76.08463	-30.33667	471.5	B_LANDER	Station end	Responsible: M. Holtappels; Eddy Lander
PS124_68-11		2021-03-01T10:57:51	-76.10339	-30.34007	474.3	ICE	Station start	Responsible: Haas
PS124_68-11		2021-03-01T10:57:51	-76.10652	-30.36110	478.9	ICE	Station end	Responsible: Haas
PS124_69-1	AWI252-3	2021-03-01T12:01:58	-76.09135	-30.46940		MOOR	Station start	Recovery mooring AWI252-3; Responsible: M. Monsees
PS124_69-1	AWI252-3	2021-03-01T12:01:58	-76.09225	-30.47552		MOOR	Station end	Recovery mooring AWI252-3; Responsible: M. Monsees
PS124_70-1	AWI253-3	2021-03-01T13:43:37	-76.04735	-31.01858	456.0	MOOR	Station start	Recovery mooring AWI253-3; Responsible: M. Monsees
PS124_70-1	AWI253-3	2021-03-01T13:43:37	-76.04564	-31.03810	471.8	MOOR	Station end	Recovery mooring AWI253-3; Responsible: M. Monsees
PS124_71-1		2021-03-01T15:14:35	-75.98066	-31.34618	507.4	DRIFT	max depth	Responsible: C. Flintrop
PS124_72-1		2021-03-01T17:12:31	-75.96258	-31.53263	616.1	CTD-RO	max depth	Responsible: S. Tippenhauer; SL=599m
PS124_72-2		2021-03-01T18:16:22	-75.96608	-31.56456	621.4	CTD-RO	max depth	Responsible: Ch. Völkner; Winde 32.1 486m
PS124_72-3		2021-03-01T18:51:59	-75.96166	-31.54263	616.0	MSC	max depth	Responsible: C. Flintrop; SL=75m
PS124_72-4		2021-03-01T19:06:32	-75.96180	-31.54583	616.1	ISP	Station start	Responsible: P. Holm
PS124_72-4		2021-03-01T19:06:32	-75.96097	-31.55914	616.8	ISP	Station end	Responsible: P. Holm
PS124_72-5		2021-03-01T20:37:16	-75.94986	-31.48865	610.9	MUC	max depth	Responsible: F. Wenzhöfer; SL= 585m
PS124_72-6		2021-03-01T21:19:22	-75.94939	-31.50611	616.6	MUC	max depth	Responsible: F. Wenzhöfer; SL= 592m
PS124_72-7		2021-03-01T22:23:30	-75.94710	-31.66397	681.9	GRAB	Station start	Responsible: S. Metz; SL= 685m

Event label	Optional label	Date/Time	Latitude	Longitude	Depth [m]	Gear	Action	Comment
PS124_72-7		2021-03-01T22:23:30	-75.94575	-31.68438	692.2	GRAB	Station end	Responsible: S. Metz; SL= 685m
PS124_72-8		2021-03-01T23:48:04	-75.94523	-31.67927	689.9	OFOBS	Station start	Responsible: A. Purser
PS124_72-8		2021-03-01T23:48:04	-75.93153	-31.44973	600.1	OFOBS	Station end	Responsible: A. Purser
PS124_72-9	AWI254-3	2021-03-02T07:00:00	-75.96137	-31.48158	596.4	MOOR	Station start	Responsible: M. Monsees; Mit EK60 recovered
PS124_72-9	AWI254-3	2021-03-02T07:00:00	-75.96177	-31.53007	617.0	MOOR	Station end	Responsible: M. Monsees; Mit EK60 recovered
PS124_73-1	AWI263-1	2021-03-02T10:56:59	-75.86774	-31.99164	735.1	MOOR	Station start	Responsible: M. Monsees; AWI 263-1 Deployment
PS124_73-1	AWI263-1	2021-03-02T10:56:59	-75.86569	-31.99459	736.0	MOOR	Station end	Responsible: M. Monsees; AWI 263-1 Deployment
PS124_74-1		2021-03-02T12:39:21	-75.90729	-32.21639	724.7	DRIFT	max depth	Responsible: C. Flintrop; Recovery
PS124_74-2		2021-03-02T14:33:56	-75.89683	-32.26271	762.6	CTD-RO	max depth	Responsible: S. Tippenhauer; EL31. SL=357m
PS124_75-1	AWI253-4	2021-03-02T17:10:41	-76.05461	-30.98967	451.9	MOOR	Station start	Responsible: M. Monsees
PS124_75-1	AWI253-4	2021-03-02T17:10:41	-76.05189	-30.99333		MOOR	Station end	Responsible: M. Monsees
PS124_76-1		2021-03-02T20:27:02	-75.86635	-32.06764	734.7	CTD-RO	max depth	Responsible: Tippenhauer; SL= 712m
PS124_76-2		2021-03-02T22:04:19	-75.86818	-32.11683	739.7	CTD-RO	max depth	Responsible: Völkner; SL= 611m
PS124_76-3		2021-03-02T22:41:09	-75.86630	-32.13443	748.5	MSC	max depth	Responsible: C. Flintrop; SL=50m
PS124_76-4		2021-03-02T23:01:20	-75.86522	-32.14363	746.7	ISP	Station start	Responsible: P. Holm
PS124_76-4		2021-03-02T23:01:20	-75.86371	-32.15424	748.8	ISP	Station end	Responsible: P. Holm
PS124_76-5		2021-03-03T00:21:22	-75.87202	-32.07439	736.8	MUC	max depth	Responsible: F. Wenzhöfer; GE72.1; SL=704m; surface

Event label	Optional label	Date/Time	Latitude	Longitude	Depth [m]	Gear	Action	Comment
PS124_76-6		2021-03-03T01:11:10	-75.87042	-32.06977	735.2	MUC	max depth	Responsible: F. Wenzhöfer; GE72.1; SL=704m; surface
PS124_77-1		2021-03-03T09:04:37	-75.97038	-31.75672	709.0	ICE	Station start	Responsible: Haas
PS124_77-1		2021-03-03T09:04:37	-75.98067	-31.77185	689.5	ICE	Station end	Responsible: Haas
PS124_77-2	AWI254-4R (SWS-03-01)	2021-03-03T12:30:20	-75.96146	-31.51146	606.9	MOOR	Station start	Deployment mooring 254-4R (SWS-03-01)
PS124_77-2	AWI254-4R (SWS-03-01)	2021-03-03T12:30:20	-75.95522	-31.51588	616.7	MOOR	Station end	Deployment mooring 254-4R (SWS-03-01)
PS124_77-3		2021-03-03T14:56:59	-75.96967	-31.56582	619.5	CTD-RO	max depth	Responsible: S. Tippenhauer; EL31; SL=599m
PS124_77-4	AWI254-4	2021-03-03T15:24:46	-75.95975	-31.49426	605.8	MOOR	Station start	Deployment mooring AWI254-4; Responsible: M. Monsees
PS124_77-4	AWI254-4	2021-03-03T15:24:46	-75.96125	-31.50725	605.0	MOOR	Station end	Deployment mooring AWI254-4; Responsible: M. Monsees
PS124_78-1		2021-03-03T18:54:33	-76.04241	-31.02602	472.8	CTD-RO	max depth	Responsible: S. Tippenhauer; SL=453m
PS124_78-2		2021-03-03T19:51:19	-76.03973	-31.04547	473.3	CTD-RO	max depth	Responsible: Ch. Völkner; SL=384m
PS124_78-3		2021-03-03T20:23:49	-76.03906	-31.04937	473.8	MSC	max depth	Responsible: C. Flintrop; SL= 50m
PS124_78-4		2021-03-03T20:39:11	-76.03825	-31.04551	473.8	ISP	Station start	Responsible: P. Holm
PS124_78-4		2021-03-03T20:39:11	-76.04635	-31.02837	474.0	ISP	Station end	Responsible: P. Holm
PS124_78-5		2021-03-03T21:46:39	-76.04709	-31.02811	474.7	MUC	max depth	Responsible: F. Wenzhöfer; SL= 452m

Event label	Optional label	Date/Time	Latitude	Longitude	Depth [m]	Gear	Action	Comment
PS124_78-6		2021-03-03T22:26:30	-76.04680	-31.02106	473.1	MUC	max depth	Responsible: F. Wenzhöfer; SL= 454m
PS124_78-7		2021-03-03T23:05:21	-76.04595	-31.02347	473.5	GRAB	Station start	Responsible: S. Metz; SL= 449m
PS124_78-7		2021-03-03T23:05:21	-76.04658	-31.01292	473.5	GRAB	Station end	Responsible: S. Metz; SL= 449m
PS124_78-8		2021-03-04T00:19:30	-76.05398	-30.94597	466.1	OFOBS	Station start	Responsible: A. Purser
PS124_78-8		2021-03-04T00:19:30	-76.06944	-30.67962	461.3	OFOBS	Station end	Responsible: A. Purser
PS124_79-1		2021-03-04T08:59:06	-76.09235	-30.42165	467.1	DRIFT	max depth	Responsible: Flintrop
PS124_79-2	AWI252-4	2021-03-04T09:41:45	-76.10127	-30.28863	474.5	MOOR	Station start	Responsible: Monsees; AWI 252-4
PS124_79-2	AWI252-4	2021-03-04T09:41:45	-76.10009	-30.30012	468.8	MOOR	Station end	Responsible: Monsees; AWI 252-4
PS124_79-3	AWI252-4R	2021-03-04T12:52:15	-76.10340	-30.37406	478.6	MOOR	Station start	Deployment mooring AWI252-4R
PS124_79-3	AWI252-4R	2021-03-04T12:52:15	-76.10499	-30.37559	477.8	MOOR	Station end	Deployment mooring AWI252-4R
PS124_79-4		2021-03-04T14:44:41	-76.10087	-30.40125	470.6	ICE	Station start	Responsible: F. Koch
PS124_79-4		2021-03-04T14:44:41	-76.10214	-30.40000	472.3	ICE	Station end	Responsible: F. Koch
PS124_68-12		2021-03-04T15:15:34	-76.09138	-30.34721	478.0	B_LANDER	Station start	Recovery KUM Lander. Responsible: F. Wenzhöfer
PS124_68-12		2021-03-04T15:15:34	-76.08061	-30.34912	449.7	B_LANDER	Station end	Recovery KUM Lander. Responsible: F. Wenzhöfer
PS124_80-1		2021-03-04T18:40:52	-75.83357	-30.93710	474.6	CTD-RO	max depth	Responsible: S.Tippenhauer; SL=454m
PS124_81-1		2021-03-04T21:32:47	-75.90881	-29.94517	498.4	CTD-RO	max depth	Responsible: Tippenhauer; SL= 480m
PS124_82-1		2021-03-05T00:18:17	-76.00748	-29.12552	403.3	CTD-RO	max depth	Responsible: S. Tippenhauer; EL31; SL=387m

Event label	Optional label	Date/Time	Latitude	Longitude	Depth [m]	Gear	Action	Comment
PS124_83-1		2021-03-05T02:37:46	-76.11009	-28.30503	359.9	CTD-RO	max depth	Responsible: S. Tippenhauer; EL31; SL=342m
PS124_84-1		2021-03-05T04:42:17	-76.23392	-29.05426	324.0	CTD-RO	max depth	Responsible: S. Tippenhauer; SL=306m
PS124_84-2		2021-03-05T05:07:24	-76.23356	-29.05478	326.0	GRAB	Station start	Responsible: S. Pineda-Metz; SL=304m
PS124_84-2		2021-03-05T05:07:24	-76.23332	-29.05425	327.2	GRAB	Station end	Responsible: S. Pineda-Metz; SL=304m
PS124_68-13		2021-03-05T08:22:23	-76.08437	-30.34978	468.2	B_LANDER	Station start	Responsible: M. Holtappels; Eddy Lander
PS124_68-13		2021-03-05T08:22:23	-76.08328	-30.34500	467.8	B_LANDER	Station end	Responsible: M. Holtappels; Eddy Lander
PS124_85-1		2021-03-05T10:56:33	-76.16705	-30.88340	437.4	DRIFT	max depth	Responsible: Flintrop
PS124_86-1		2021-03-05T12:16:12	-76.16849	-30.88701	453.3	CTD-RO	max depth	Responsible: Tippenhauer; EL31; SL=435m
PS124_87-1		2021-03-05T17:35:00	-76.87924	-33.86096	573.3	ARGOFL	Station start	Lotus buoy. Responsible: E. Darelius
PS124_87-1		2021-03-05T17:35:00	-76.87956	-33.86249	573.6	ARGOFL	Station end	Lotus buoy; Responsible: E. Darelius
PS124_88-1		2021-03-05T22:26:00	-77.10758	-36.58377	1107.6	CTD-RO	max depth	Responsible: Trippenhauer; SL= 1079m
PS124_88-2		2021-03-06T00:04:26	-77.10789	-36.57509	1109.2	CTD-RO	max depth	Responsible: Völkner; SE32.1; SL=1057m
PS124_88-3		2021-03-06T00:33:30	-77.10818	-36.57237	1110.5	ISP	Station start	Responsible: P. Holm
PS124_88-3		2021-03-06T00:33:30	-77.10834	-36.56870	1106.1	ISP	Station end	Responsible: P. Holm
PS124_88-4		2021-03-06T01:22:02	-77.10840	-36.56834	1104.4	GRAB	Station start	Responsible: S. Pineda-Metz; GE72.1; SL = 1052m; surface

Event label	Optional label	Date/Time	Latitude	Longitude	Depth [m]	Gear	Action	Comment
PS124_88-4		2021-03-06T01:22:02	-77.10850	-36.56298	1100.3	GRAB	Station end	Responsible: S. Pineda-Metz; GE72.1; SL=1052m; surface
PS124_88-5		2021-03-06T03:07:13	-77.10837	-36.56017	1100.4	MUC	max depth	Responsible: F. Wenzhöfer; GE72.1; SL=1047m; surface
PS124_88-6		2021-03-06T08:01:39	-77.09887	-36.53741	1097.2	B_LANDER	Station start	Responsible: Wenzhöfer; KUM. deployed
PS124_88-6		2021-03-06T08:01:39	-77.09700	-36.52584	1096.0	B_LANDER	Station end	Responsible: Wenzhöfer KUM. deployed
PS124_ 20210306_ SB02	WMO7101593	2021-03-06T10:51:00	-77.18451	-36.14963		BUOY_ SNOW	Station start	deployment of buoy 2021S115. not logged in D-Ship
PS124_ 20210306_ SB02	WMO7101593	2021-03-06T10:51:00	-77.82900	-38.75080		BUOY_ SNOW	Station end	deployment of buoy 2021S115; not logged in D-Ship
PS124_89-1		2021-03-06T13:08:29	-77.00893	-34.05871	495.1	ARGOFL	Station start	LOTUS Buoy; Responsible: E. Darelius
PS124_89-1		2021-03-06T13:08:29	-77.00808	-34.04649	486.7	ARGOFL	Station end	LOTUS Buoy; Responsible: E. Darelius
PS124_89-2		2021-03-06T13:28:34	-77.01772	-33.83977	443.4	ARGOFL	Station start	LOTUS Buoy; Responsible: E. Darelius
PS124_89-2		2021-03-06T13:28:34	-77.01906	-33.82244	439.0	ARGOFL	Station end	LOTUS Buoy; Responsible: E. Darelius
PS124_89-3		2021-03-06T13:45:20	-77.02784	-33.65969	400.4	ARGOFL	Station start	LOTUS Buoy; Responsible: E. Darelius
PS124_89-3		2021-03-06T13:45:20	-77.03052	-33.64569	394.7	ARGOFL	Station end	LOTUS Buoy; Responsible: E. Darelius
PS124_90-1		2021-03-06T13:55:54	-77.03484	-33.61800	383.8	DRIFT	max depth	Deployment; Responsible: C. Flintrop
PS124_90-2		2021-03-06T14:52:45	-77.02416	-33.54601	374.9	B_LANDER	Station start	Responsible: M. Holtappels; Eddy Lander. deployment

Event label	Optional label	Date/Time	Latitude	Longitude	Depth [m]	Gear	Action	Comment
PS124_90-2		2021-03-06T14:52:45	-77.02996	-33.56979	380.9	B_LANDER	Station end	Responsible: M. Holtappels; Eddy Lander. deployment
PS124_90-3		2021-03-06T16:25:59	-77.03897	-33.59288	382.5	CTD-RO	max depth	Responsible: S. Tippenhauer; SL=130m
PS124_90-4		2021-03-06T16:55:33	-77.04251	-33.60339	378.8	CTD-RO	max depth	Responsible: S. Tippenhauer; SL=358m
PS124_90-5		2021-03-06T17:56:37	-77.03893	-33.57854	378.1	CTD-RO	max depth	Responsible: Ch. Völkner; SL=304m
PS124_90-6		2021-03-06T18:32:46	-77.03907	-33.57961	378.7	MSC	max depth	Responsible: C. Flintrop; SL=60m
PS124_90-7		2021-03-06T19:02:28	-77.03996	-33.57609	374.8	MSC	max depth	SL=40m
PS124_90-8		2021-03-06T19:47:41	-77.03803	-33.43596	276.7	MUC	max depth	Responsible: F. Wenzhöfer; SL=266m
PS124_90-9		2021-03-06T20:12:09	-77.03779	-33.43186	272.1	GRAB	Station start	Responsible: Metz; SL= 260m
PS124_90-9		2021-03-06T20:12:09	-77.03818	-33.43172	272.1	GRAB	Station end	Responsible: Metz; SL= 260m
PS124_90-10		2021-03-06T20:58:20	-77.03821	-33.43174	272.6	GRAB	Station start	Responsible: Metz; SL=265m
PS124_90-10		2021-03-06T20:58:20	-77.03828	-33.42989	271.4	GRAB	Station end	Responsible: Metz; SL=265m
PS124_90-11		2021-03-06T22:07:16	-77.04409	-33.53418	349.1	MUC	max depth	Responsible: F. Wenzhöfer; SL= 335m
PS124_90-12		2021-03-06T22:43:17	-77.03946	-33.50413	338.1	GRAB	Station start	Responsible: Metz; SL=325m
PS124_90-12		2021-03-06T22:43:17	-77.03802	-33.51034	346.3	GRAB	Station end	Responsible: Metz; SL=325m
PS124_90-13		2021-03-07T01:00:00	-77.20176	-33.81745	509.1	OFOBS	Station start	Responsible: A. Purser
PS124_90-13		2021-03-07T01:00:00	-77.17258	-33.61532	259.2	OFOBS	Station end	Responsible: A. Purser
PS124_91-1		2021-03-07T08:31:47	-77.19071	-33.99622	482.0	DRIFT	max depth	Responsible: Flintrop
PS124_91-2		2021-03-07T09:25:16	-77.19196	-34.02367	471.9	CTD-RO	max depth	Responsible: Tippenhauer; SL=451m

Event label	Optional label	Date/Time	Latitude	Longitude	Depth [m]	Gear	Action	Comment
PS124_92-1		2021-03-07T11:06:33	-77.16622	-33.70507	260.8	GRAB	Station start	Responsible: Metz; SL=254m
PS124_92-1		2021-03-07T11:06:33	-77.16581	-33.68206	267.7	GRAB	Station end	Responsible: Metz; SL=254m
PS124_90-14		2021-03-07T12:55:11	-77.02922	-33.57283	369.9	B_LANDER	Station start	Responsible: M. Holtappels; Eddy Lander; recovery
PS124_90-14		2021-03-07T12:55:11	-77.03065	-33.57519	380.0	B_LANDER	Station end	Responsible: M. Holtappels; Eddy Lander; recovery
PS124_93-1		2021-03-07T15:48:37	-77.05115	-34.74140	775.4	CTD-RO	max depth	Responsible: S. Tippenhauer; EL31; SL=87m
PS124_93-2		2021-03-07T16:42:48	-77.05009	-34.73992	778.7	CTD-RO	max depth	Responsible: S. Tippenhauer; SL=752m
PS124_94-1		2021-03-07T17:54:25	-77.04394	-34.72681	794.2	CTD-RO	max depth	Responsible: Ch. Völkner; SL=611m
PS124_94-2		2021-03-07T18:29:00	-77.04546	-34.73659	799.0	MSC	max depth	Responsible: C. Flintrop
PS124_94-3		2021-03-07T19:01:08	-77.05004	-34.74116	779.7	GRAB	Station start	Responsible: S. Pineda-Metz; SL=740m
PS124_94-3		2021-03-07T19:01:08	-77.05023	-34.74138	779.4	GRAB	Station end	Responsible: S. Pineda-Metz; SL=740m
PS124_94-4		2021-03-07T20:43:41	-77.04943	-34.73751	779.5	MUC	max depth	Responsible: F. Wenzhöfer; SL= 741m
PS124_94-5		2021-03-07T21:47:16	-77.04737	-34.73728	788.6	OFOBS	Station start	Responsible: A. Purser
PS124_94-5		2021-03-07T21:47:16	-77.03480	-34.58735	764.6	OFOBS	Station end	Responsible: A. Purser
PS124_95-1		2021-03-08T04:10:07	-77.07475	-35.17126	928.0	CTD-RO	max depth	Responsible: S. Tippenhauer; SL=900m
PS124_96-1		2021-03-08T06:14:09	-77.08014	-35.82775	1060.0	CTD-RO	max depth	Responsible: S. Tippenhauer; SL=1032m
PS124_88-7		2021-03-08T07:54:51	-77.09752	-36.52990	1096.2	B_LANDER	Station start	Responsible: Wenzhöfer. KUM RECOVERY
PS124_88-7		2021-03-08T07:54:51	-77.09763	-36.52479	1099.9	B_LANDER	Station end	Responsible: Wenzhöfer; KUM RECOVERY

Event label	Optional label	Date/Time	Latitude	Longitude	Depth [m]	Gear	Action	Comment
PS124_97-1		2021-03-08T10:22:15	-77.09977	-36.53441	1097.6	MUC	max depth	Responsible: F. Wenzhöfer; SL= 1045m
PS124_98-1		2021-03-09T06:06:36	-75.38675	-28.67738	453.7	CTD-RO	max depth	Responsible: S. Tippenhauer; SL=433m
PS124_98-2		2021-03-09T07:14:00	-75.39436	-28.69038	443.4	MUC	max depth	Responsible: F. Wenzhöfer; SL=421m
PS124_98-3	P5	2021-03-09T07:42:00	-75.39091	-28.64770	448.5	MOOR	Station start	Mooring P5. Recovery; Responsible: M. Monsees
PS124_98-3	P5	2021-03-09T07:42:00	-75.39322	-28.64561	444.0	MOOR	Station end	Mooring P5. Recovery; Responsible: M. Monsees
PS124_98-4		2021-03-09T09:27:47	-75.39533	-28.65208	442.7	ICE	Station start	Responsible: Haas
PS124_98-4		2021-03-09T09:27:47	-75.39677	-28.65716	442.4	ICE	Station end	Responsible: Haas
PS124_98-5		2021-03-09T09:51:29	-75.39691	-28.65704	443.5	GRAB	Station start	Responsible: Metz; SL= 421m
PS124_98-5		2021-03-09T09:51:29	-75.39834	-28.65915	442.4	GRAB	Station end	Responsible: Metz; SL= 421m
PS124_99-1	M6	2021-03-09T16:14:21	-74.59522	-29.91765	542.5	MOOR	Station start	Mooring M6. Responsible: M. Monsees
PS124_99-1	M6	2021-03-09T16:14:21	-74.59481	-29.91687	548.8	MOOR	Station end	Mooring M6. Responsible: M. Monsees
PS124_100-1		2021-03-10T06:16:58	-74.48559	-32.50818	656.1	CTD-RO	max depth	Responsible: S. Tippenhauer; SL=635m
PS124_100-2		2021-03-10T06:53:26	-74.48900	-32.51990	658.1	ISP	Station start	Responsible: P. Holm
PS124_100-2		2021-03-10T06:53:26	-74.49227	-32.53536	660.0	ISP	Station end	Responsible: P. Holm
PS124_100-3		2021-03-10T07:46:03	-74.49587	-32.54886	661.1	MSC	max depth	Responsible: C. Flintrop; SL=50m
PS124_100-4		2021-03-10T08:21:32	-74.50081	-32.56360	660.7	ISP	Station start	Responsible: Koch; SL= 28m
PS124_100-4		2021-03-10T08:21:32	-74.53264	-32.65807	663.7	ISP	Station end	Responsible: Koch; SL= 28m

Event label	Optional label	Date/Time	Latitude	Longitude	Depth [m]	Gear	Action	Comment
PS124_100-5		2021-03-10T13:00:32	-74.54864	-32.66000	661.9	MUC	max depth	Responsible: F. Wenzhöfer; GE72.1; SL=633m
PS124_100-6		2021-03-10T13:30:54	-74.55608	-32.67478	663.9	GRAB	Station start	Responsible: S. Pineda-Metz; GE72.1; SL=634m
PS124_100-6		2021-03-10T13:30:54	-74.56229	-32.66761	662.9	GRAB	Station end	Responsible: S. Pineda-Metz; GE72.1; SL=634m
PS124_100-7		2021-03-10T14:37:59	-74.56300	-32.63668	664.1	MARKII	Station start	Responsible: C. Haas
PS124_100-7		2021-03-10T14:37:59	-74.59808	-32.64822	666.0	MARKII	Station end	Responsible: C. Haas
PS124_101-1		2021-03-10T22:46:42	-74.89173	-30.76771	516.7	OFOBS	Station start	Responsible: A. Purser
PS124_101-1		2021-03-10T22:46:42	-74.85362	-30.68285	497.1	OFOBS	Station end	Responsible: A. Purser
PS124_102-1	M3	2021-03-11T07:17:52	-74.54997	-29.90917	741.3	MOOR	Station start	Mooring M3; Responsible: M. Monsees
PS124_102-1	M3	2021-03-11T07:17:52	-74.55022	-29.91055	760.5	MOOR	Station end	Mooring M3; Responsible: M. Monsees
PS124_103-1		2021-03-11T10:46:09	-74.52781	-29.11892	1310.5	ARGOFL	Station start	APECS / Responsible: M. Janout
PS124_103-1		2021-03-11T10:46:09	-74.52852	-29.11652	1310.7	ARGOFL	Station end	APECS / Responsible: M. Janout
PS124_104-1		2021-03-11T11:14:17	-74.56814	-29.19501	1161.1	ARGOFL	Station start	Responsible: Janout; APECS
PS124_104-1		2021-03-11T11:14:17	-74.56824	-29.19681	1158.2	ARGOFL	Station end	Responsible: Janout; APECS
PS124_105-1		2021-03-11T11:46:23	-74.61894	-29.38016	893.8	ARGOFL	Station start	Responsible:: Janout ; APECS
PS124_105-1		2021-03-11T11:46:23	-74.61960	-29.40477	875.7	ARGOFL	Station end	Responsible:: Janout ; APECS
PS124_202103011_SB03	WMO7101590	2021-03-11T12:46:00	-74.46261	-29.61355		BUOY_SNOW	max depth	deployment of buoy 2021S112. not logged in D-Ship
PS124_106-1	P5	2021-03-11T16:52:11	-75.38979	-28.63707	439.9	MOOR	Station start	Deployment P5; Responsible: M. Monsees

Event label	Optional label	Date/Time	Latitude	Longitude	Depth [m]	Gear	Action	Comment
PS124_106-1	P5	2021-03-11T16:52:11	-75.38976	-28.63673	455.2	MOOR	Station end	Deployment P5; Responsible: M. Monsees
PS124_107-1		2021-03-11T22:13:52	-75.04702	-26.88109	289.5	CTD-RO	max depth	Responsible: Tippenhauer; SL=271m
PS124_107-2		2021-03-11T23:16:59	-75.04570	-26.88857	288.8	CTD-RO	max depth	Responsible: Völkner; SL= 270m
PS124_107-3		2021-03-11T23:58:42	-75.04558	-26.90015	298.0	GRAB	Station start	Responsible: S. Pineda-Metz; GE72.1; SL=283m
PS124_107-3		2021-03-11T23:58:42	-75.04788	-26.90692	294.9	GRAB	Station end	Responsible: S. Pineda-Metz; GE72.1; SL=283m
PS124_107-4		2021-03-12T00:53:43	-75.04837	-26.90863	295.9	MUC	max depth	Responsible: F. Wenzhöfer; GE72.1; SL=286m
PS124_107-5		2021-03-12T01:41:18	-75.05983	-26.74345	299.6	OFOBS	Station start	Responsible: A. Purser
PS124_107-5		2021-03-12T01:41:18	-75.06100	-26.65895	339.7	OFOBS	Station end	Responsible: A. Purser
PS124_107-6		2021-03-12T06:02:42	-75.03594	-26.94211	313.0	MSC	max depth	Responsible: C. Flintrop; SL=70m; surface
PS124_107-7		2021-03-12T06:15:10	-75.03706	-26.94655	311.2	ISP	Station start	Responsible: P. Holm
PS124_107-7		2021-03-12T06:15:10	-75.02638	-26.90568	302.8	ISP	Station end	Responsible: P. Holm
PS124_107-8		2021-03-12T08:00:52	-75.02981	-26.82814	292.7	B_LANDER	Station start	Responsible: M. Holtappels; Eddy Lander; deployment
PS124_107-8		2021-03-12T08:00:52	-75.03217	-26.86232	286.6	B_LANDER	Station end	Responsible: M. Holtappels; Eddy Lander; deployment
PS124_108-1		2021-03-12T09:06:00	-75.03258	-26.86641	286.3	ICE	Station start	Responsible: Peeken
PS124_108-1		2021-03-12T09:06:00	-75.03546	-26.88297	293.3	ICE	Station end	Responsible: Peeken
PS124_107-9		2021-03-13T08:51:30	-75.03406	-26.85801	282.4	B_LANDER	Station start	Responsible: M. Holtappels; recovery
PS124_107-9		2021-03-13T08:51:30	-75.03372	-26.86975	284.7	B_LANDER	Station end	Responsible: M. Holtappels; recovery
PS124_109-1		2021-03-13T15:32:20	-74.72541	-25.27435	648.8	CTD-RO	max depth	EL31; SL=625

Event label	Optional label	Date/Time	Latitude	Longitude	Depth [m]	Gear	Action	Comment
PS124_110-1		2021-03-13T19:47:40	-75.11421	-24.79473	576.2	CTD-RO	max depth	Responsible: S. Tippenhauer; SL=553m
PS124_110-2		2021-03-13T20:51:08	-75.11234	-24.79870	575.3	CTD-RO	max depth	Responsible: Völkner; SL= 551m
PS124_110-3		2021-03-13T21:14:49	-75.11254	-24.79837	575.5	GRAB	Station start	Responsible: Metz; SL= 542m
PS124_110-3		2021-03-13T21:14:49	-75.11296	-24.80236		GRAB	Station end	Responsible: Metz; SL= 542m
PS124_110-4		2021-03-13T22:42:05	-75.11293	-24.79577	578.4	MUC	max depth	Responsible: F. Wenzhöfer; SL= 545m
PS124_111-1		2021-03-14T01:02:58	-75.27723	-24.96629	635.9	CTD-RO	max depth	Responsible: S. Tippenhauer; EL31; SL=59m
PS124_111-2		2021-03-14T01:51:14	-75.27716	-24.96773	635.5	CTD-RO	max depth	Responsible: S. Tippenhauer; EL31; SL=613m
PS124_111-3		2021-03-14T02:51:38	-75.27718	-24.96544	635.9	CTD-RO	max depth	Responsible: C. Völkner; SE32.1; SL=613m
PS124_111-4		2021-03-14T03:11:22	-75.27703	-24.96555	635.3	ISP	Station start	Responsible: P. Holm
PS124_111-4		2021-03-14T03:11:22	-75.27747	-24.96581	637.6	ISP	Station end	Responsible: P. Holm
PS124_111-5		2021-03-14T04:29:49	-75.27715	-24.96629	636.1	MUC	max depth	Responsible: F. Wenzhöfer; SL=605m
PS124_111-6		2021-03-14T05:05:15	-75.27737	-24.96604	637.9	GRAB	Station start	Responsible: S. Pineda-Metz; SL=608m
PS124_111-6		2021-03-14T05:05:15	-75.27707	-24.96585	636.7	GRAB	Station end	Responsible: S. Pineda-Metz; SL=608m
PS124_111-7		2021-03-14T08:08:33	-75.25271	-24.91537	586.5	B_LANDER	Station start	Responsible: F . Wenzhöfer KUM
PS124_111-7		2021-03-14T08:08:33	-75.25298	-24.91559	586.9	B_LANDER	Station end	Responsible: F . Wenzhöfer KUM
PS124_111-8		2021-03-14T09:54:31	-75.17440	-24.74837	569.5	OFOBS	Station start	Responsible: A. Purser
PS124_111-8		2021-03-14T09:54:31	-75.14345	-24.61591	654.5	OFOBS	Station end	Responsible: A. Purser

Event label	Optional label	Date/Time	Latitude	Longitude	Depth [m]	Gear	Action	Comment
PS124_111-9		2021-03-14T16:18:05	-75.25386	-24.92634	569.4	B_LANDER	Station start	KUM Lander Responsible: F. Wenzhöfer
PS124_111-9		2021-03-14T16:18:05	-75.25358	-24.92622	589.3	B_LANDER	Station end	KUM Lander Responsible: F. Wenzhöfer
PS124_111-10		2021-03-14T17:13:43	-75.25495	-24.91809	591.0	ICE	Station start	Responsible: I. Peeken; on deck
PS124_111-10		2021-03-14T17:13:43	-75.25477	-24.91814	590.1	ICE	Station end	Responsible: I. Peeken; on deck
PS124_112-1		2021-03-14T19:48:08	-75.37150	-25.73089	782.5	CTD-RO	max depth	Responsible: S. Tippenhauer; SL=757m
PS124_112-2		2021-03-14T21:04:50	-75.37158	-25.73235	781.9	CTD-RO	max depth	Responsible: Völkner; SL=757m
PS124_112-3		2021-03-14T21:37:16	-75.37161	-25.72991	784.1	GRAB	Station start	Responsible: Metz; SL= 747m
PS124_112-3		2021-03-14T21:37:16	-75.37229	-25.72348	797.0	GRAB	Station end	Responsible: Metz; SL= 747m
PS124_112-4		2021-03-14T23:02:20	-75.37289	-25.72328	793.4	MUC	max depth	Responsible: Janout; SL= 749m
PS124_113-1		2021-03-15T06:27:23	-74.65817	-27.36946	386.1	ARGOFL	Station start	APECS float; Responsible: M. Janout
PS124_113-1		2021-03-15T06:27:23	-74.65613	-27.36992	455.3	ARGOFL	Station end	APECS float; Responsible: M. Janout
PS124_114-1		2021-03-15T06:49:05	-74.61406	-27.28418	1447.4	ARGOFL	Station start	APEX-float; Responsible: M. Janout
PS124_114-1		2021-03-15T06:49:05	-74.61300	-27.27904	1457.4	ARGOFL	Station end	APEX-float; Responsible: M. Janout
PS124_115-1		2021-03-15T12:22:45	-74.01704	-26.13312	2863.3	CTD-RO	max depth	Responsible: Tippenhauer; EL31; SL=2851m
PS124_115-2	SWS07-01	2021-03-15T13:32:50	-74.01628	-26.13161	2864.3	MOOR	Station start	Deployment mooring SWS07-01; Responsible: M. Monsees

Event label	Optional label	Date/Time	Latitude	Longitude	Depth [m]	Gear	Action	Comment
PS124_115-2	SWS07-01	2021-03-15T13:32:50	-74.01549	-26.12983	2864.1	MOOR	Station end	Deployment mooring SWS07-01; Responsible: M. Monsees
PS124_202103017_TB01		2021-03-17T17:45:00	-70.62313	-7.67486		BUOY_SNOW	max depth	deployment of buoy 2021T86; not logged in D-Ship
PS124_202103017_SB04	WMO7101591	2021-03-17T18:15:00	-70.62313	-7.67486		BUOY_SNOW	max depth	deployment of buoy 2021S113 not logged in D-Ship
PS124_116-1	AWI244-6	2021-03-20T15:00:20	-68.99917	-7.03291	2943.5	MOOR	Station start	Recovery mooring AWI 244-6; Responsible: M. Monsees
PS124_116-1	AWI244-6	2021-03-20T15:00:20	-69.00367	-7.03574	2980.8	MOOR	Station end	Recovery mooring AWI 244-6; Responsible: M. Monsees
PS124_117-1		2021-03-24T08:02:04	-68.99912	-26.99789	4717.7	CTD-RO	max depth	Responsible: S. Tippenhauer; SL=4755m
PS124_117-2	BGC-1	2021-03-24T10:02:21	-69.00319	-27.00586	4716.7	MOOR	Station start	Responsible: Monsees; Mooring: BGC-1
PS124_117-2	BGC-1	2021-03-24T10:02:21	-69.00056	-27.00049	4717.0	MOOR	Station end	Responsible: Monsees; Mooring: BGC-1
PS124_118-1		2021-03-28T20:01:43	-57.40011	-49.61532	4262.5	ARGOFL	Station start	Responsible: M. Janout
PS124_118-1		2021-03-28T20:01:43	-57.39972	-49.61583	4279.6	ARGOFL	Station end	Responsible: M. Janout
PS124_119-1		2021-03-29T11:38:13	-55.01734	-53.00641	4053.5	ARGOFL	Station start	Responsible: JANOUT
PS124_119-1		2021-03-29T11:38:13	-55.01986	-53.01082	4052.7	ARGOFL	Station end	Responsible: JANOUT

** Comments are limited to 130 characters. See https://www.pangaea.de/expeditions/events/PS124 to show full comments in conjunction with the station (event) list for expedition PS124*

Abbreviation	Method/Device
ADCP	Acoustic Doppler Current Profiler
AFIM	AutoFim
ARGOFL	Argo float
BUOY_SNOW	Snow buoy
B_LANDER	Bottom lander
CCAM	Cloud camera
CTD-RO	CTD/Rosette
DRIFT	Drifter
FBOX	FerryBox
GRAB	Grab
HS	HydroSweep
HVAIR	High volume air sampler
ICE	Ice station
ICEOBS	Ice observation
ISP	In situ pump
MAG	Magnetometer
MARKII	Mark II motorized coring device, Kovacs Enterprise Inc
MOOR	Mooring
MSC	Marine snow catcher
MUC	MultiCorer
MYON	DESY Myon Detector
OFOBS	Ocean Floor Observation and Bathymetry System
PS	ParaSound
SVP	Sound velocity profiler
SWEAS	Ship Weather Station
TSG	Thermosalinograph
UWPCO2	Underway pCO2 measurements
W-RADAR	Wave Radar System
ZODIAK	Rubber boat, Zodiac

Die **Berichte zur Polar- und Meeresforschung** (ISSN 1866-3192) werden beginnend mit dem Band 569 (2008) als Open-Access-Publikation herausgegeben. Ein Verzeichnis aller Bände einschließlich der Druckausgaben (ISSN 1618-3193, Band 377-568, von 2000 bis 2008) sowie der früheren **Berichte zur Polarforschung** (ISSN 0176-5027, Band 1-376, von 1981 bis 2000) befindet sich im electronic Publication Information Center **(ePIC)** des Alfred-Wegener-Instituts, Helmholtz-Zentrum für Polar- und Meeresforschung (AWI); see https://epic.awi.de. Durch Auswahl “Reports on Polar- and Marine Research“ (via “browse”/”type”) wird eine Liste der Publikationen, sortiert nach Bandnummer, innerhalb der absteigenden chronologischen Reihenfolge der Jahrgänge mit Verweis auf das jeweilige pdf-Symbol zum Herunterladen angezeigt.

The **Reports on Polar and Marine Research** (ISSN 1866-3192) are available as open access publications since 2008. A table of all volumes including the printed issues (ISSN 1618-3193, Vol. 377-568, from 2000 until 2008), as well as the earlier **Reports on Polar Research** (ISSN 0176-5027, Vol. 1-376, from 1981 until 2000) is provided by the electronic Publication Information Center **(ePIC)** of the Alfred Wegener Institute, Helmholtz Centre for Polar and Marine Research (AWI); see URL https://epic.awi.de. To generate a list of all Reports, use the URL http://epic.awi.de and select “browse”/ ”type” to browse ”Reports on Polar and Marine Research”. A chronological list in declining order will be presented, and pdf-icons displayed for downloading.

Zuletzt erschienene Ausgaben:

Recently published issues:

755 (2021) The Expedition PS124 of the Research Vessel POLARSTERN to the southern Weddell Sea in 2021, edited by Hartmut H. Hellmer and Moritz Holtappels with contributions of the participants

754 (2021) MOSAiC Expedition: Airborne Surveys with Research Aircraft POLAR 5 and POLAR 6 in 2020, edited by Andreas Herber, Sebastian Becker, Hans Jakob Belter, Jörg Brauchle, André Ehrlich, Marcus Klingebiel, Thomas Krumpen, Christof Lüpkes, Mario Mech, Manuel Moser, and Manfred Wendisch

753 (2021) The Expedition PS123 of the Research Vessel POLARSTERN to NEUMAYER STATION III in 2020/2021, edited by Tim Heitland with contributions of the participants

752 (2021) Expeditions to Fennoscandia in 2020, edited by Matthias Fuchs, Lona van Delden, Nele Lehmann, and Torben Windirsch

751 (2021) The MOSES Sternfahrt Expeditions of the Research Vessels ALBIS, LITTORINA, LUDWIG PRANDTL, MYA II and UTHÖRN to the Elbe River, Elbe Estuary and German Bight in 2020, edited by Ingeborg Bussmann, Norbert Anselm, Holger Brix, Philipp Fischer, Götz Flöser, Felix Geissler, Norbert Kamjunke

750 (2021) International Online Symposium: Focus Siberian Permafrost – Terrestrial Cryosphere and Climate Change, editorial board: Pfeiffer EM, Vybornova O, Kutzbach L, Fedorova I, Knoblauch C, Tsibizov L & Beer C

749 (2021) Russian-German Cooperation: Expeditions to Siberia in 2019, edited by Matthias Fuchs, Dmitry Bolshiyanov, Mikhail Grigoriev, Anne Morgenstern, Luidmila Pestryakova, Leonid Tsibizov, and Antonia Dill

748 (2020) Das Alfred-Wegener-Institut in der Geschichte der Polarforschung: Einführung und Chronik, 2., erweiterte und überarbeitete Auflage, von Christian R. Salewski, Reinhard A. Krause, Elias Angele

747 (2020) Reconstruction of paleo sea ice and climate dynamics based on highly branched isoprenoids at the Western Antarctic Peninsula, by Maria-Elena Vorrath

ALFRED-WEGENER-INSTITUT
HELMHOLTZ-ZENTRUM FÜR POLAR-
UND MEERESFORSCHUNG

BREMERHAVEN

Am Handelshafen 12
27570 Bremerhaven
Telefon 0471 4831-0
Telefax 0471 4831-1149
www.awi.de

HELMHOLTZ